

Copyright

By

Brooke L. Barnette

2020

**The Dissertation Committee for Brooke Lawson Barnette Certifies that this is the  
approved version of the following dissertation:**

An Integrated Omics Approach to Define the Molecular Mechanisms of Low Dose, High  
Charge, High Energy Irradiation (HZE) in Liver

**Committee:**

---

Mark Emmett, Ph.D. Mentor

---

Rovshan Sadygov, Ph.D. Chair

---

Martin Colman, M.D.

---

Paul Wood, Ph.D.

---

Heidi Spratt, Ph.D.

---

---

Dean, Graduate School

**An Integrated Omics Approach to Define the Molecular Mechanisms of  
Low Dose, High Charge, High Energy (HZE) Irradiation in Liver**

**by**

**Brooke Lawson Barnette, BS, MS**

**Dissertation**

Presented to the Faculty of the Graduate School of

The University of Texas Medical Branch

in Partial Fulfillment

of the Requirements

for the Degree of

**Doctor of Philosophy**

**The University of Texas Medical Branch**

**July 30, 2020**

## **Dedication**

This work is dedicated to some very special people in my life who have always believed in me and encouraged me to chase my dreams-my mom and dad. I can't thank you enough for all your support and everything you have done to help make my dreams come true. You taught me from a young age to always dream big, and that with hard work and dedication there are no limits to what can be achieved. You have been my rock and encouraged me to keep going even when I would start to lose faith in myself. This work is also dedicated in loving memory to my great grandfather, Jack Owens, who always told me that he hoped that he at least lived long enough to see me become a doctor. I wish you could be here today, but I know that you are so proud that this day is finally here and will be smiling down on me.



## **Acknowledgements**

First, I would like to express my deepest gratitude to my supervisor and mentor Mark Emmett for all his help and support through the learning process of this dissertation. I am especially grateful that he recognizes the importance of teaching and mentoring and has allowed me to pursue several opportunities to teach and mentor students throughout my graduate career. A special thanks goes to my committee members for their support and input along this journey. I would also like to acknowledge the UTMB proteomics core and the Next Generation Sequencing Core especially Dr. Bill Russell and Dr. Steve Widen for all their help and expertise with data acquisition for both the proteomics and transcriptomics and their willingness to always answer questions and provide feedback. A very special thank you goes to Dr. Cheryl Litchi for all of her words of wisdom, advice and encouragement along this journey. She was particularly instrumental in helping me towards the end of my dissertation when I was trying to finish interpreting the IPA results and trying to piece them together in the big picture. I would like to thank Dr. Yongjia Yu for his help with tissue collection as well as teaching me how to perform PCR on mitochondria DNA. A special thank you goes to Dr. Evagelia Laiakis for her help in obtaining the metabolomics data set as well for great discussion about the data and other metabolomics findings in regard to irradiation. I also greatly appreciate Dr. Ramkumar Menon and Dr. Casey Wright for allowing us to use some of their lab equipment during some of these experiments. I am very fortunate to have had the opportunity to work around so many wonderful and talented individuals both past and present. Besides all

those previously mentioned, I would also like to thank Dr. Alexander Shavkunov and Dr. Shinji Strain. It was a pleasure working around both of them as they always provided helpful feedback and discussion as well just a friendly face, smile and lighthearted conversation on a rough day. Dr. Shavkunov was also instrumental in helping me learn the proteomics protocols. The beginning of graduate school also brought two very wonderful friends to my life, Dr. Samantha Sheller Miller and Dr. Karryanne Belanger. We all went through the dissertation process together and I could always count on them for scientific advice, a shoulder to lean on or just an ear to listen. I also appreciate Dr. Jonathan Hommel for allowing us to have joint lab meetings with his group and for all their feedback and discussion. Some great ideas came from these meetings and I also gained a close friend, Catherine Sampson, who has been another great support throughout this process. I would like to take this time to thank some very special people in my life. To my mom and dad words cannot express how thankful and blessed I am to have your continuous love and support in my life. To my wonderful husband thank you for following me to Texas to pursue my dream and for supporting me along this journey. I know it hasn't been easy, but I am so glad to have had you by my side through this process. To the rest of my extended family and friends, I can't thank you all individually but you all have played such a huge role in my life as well, and you have all helped make this possible whether it was by your encouraging words, prayers, or support. You all have helped me keep the faith and to continue pursuing my dreams. Most importantly, I would like to thank my Lord and Savior, Jesus Christ. It is through His strength that I have completed this journey and finished the race.

# **An Integrated Omics Approach to Define the Molecular Mechanisms of Low Dose, High Energy, High Charge ions (HZE) in Liver**

Publication No. \_\_\_\_\_

Brooke Lawson Barnette, Ph.D.

The University of Texas Medical Branch, 2020

Supervisor: Mark R. Emmett

Galactic Cosmic Rays are primarily composed of protons (85%), helium (14%), and high charge-high energy ions (HZE) such as  $^{56}\text{Fe}$ ,  $^{28}\text{Si}$ , and  $^{16}\text{O}$ . Humans are normally not exposed to HZE ions but will be exposed during deep space travel such as upcoming missions to Mars and the dark side of the moon. Exposure to HZE is a major risk factor for astronauts due to the possibility of HZE induced cancer as well as other potential health risks. In order to access the risks of HZE irradiation, our approach utilized a multi-omics, systems biology platform encompassing lipidomics, metabolomics, proteomics and deep RNA sequencing as well as molecular techniques to define these changes induced by HZE exposure. C3H/HeNCrL mice (more susceptible to HCC) along with C57BL16 (more of a wild type) were placed into 6 treatment groups and received the following irradiation treatments: 600 MeV/n  $^{56}\text{Fe}$  (0.2 Gy), 1 GeV/n  $^{16}\text{O}$  (0.2 Gy), 350 MeV/n  $^{28}\text{Si}$  (0.2 Gy),  $^{137}\text{Cs}$  (1.0 Gy) gamma rays,  $^{137}\text{Cs}$  (3.0 Gy) gamma rays, and sham irradiation. Left liver lobes were collected at 30, 60, 120, 270 & 360 days post-irradiation. Radiation exposure is known to produce excess reactive oxygen species

(ROS) that can result in functional changes in target cells by interacting with and modifying molecules such as lipids, cellular proteins, and DNA. When comparing data from transcriptomics and proteomics utilizing ingenuity pathway analysis (IPA), several pathways involved in mitochondrial function were altered after HZE irradiation. Lipids and metabolites also exhibited changes that are connected to mitochondrial function. Molecular assays for determining Complex I activity, mitochondria count and cardiolipin levels were also used as validation of these findings. Significant decreases were seen in Complex I activity and while not significant, changes were also seen in the mitochondria number and cardiolipin levels that also support mitochondria dysfunction. These altered pathways indicate an increased risk for astronauts during deep space travel and could potentially lead to possible targets for countermeasures to mitigate the risk.

## TABLE OF CONTENTS

LIST OF TABLES .....	x
LIST OF FIGURES .....	xii
LIST OF ABBREVIATIONS.....	xv
<b>INTRODUCTION .....</b>	<b>17</b>
CHAPTER 1 TO INFINITY AND BEYOND.....	17
HIGH ENERGY, HIGH CHARGE (HZE) IRRADIATION.....	17
CELLULAR CONNECTIVITY .....	19
IONIZING IRRADIATION.....	20
REACTIVE OXYGEN SPECIES (ROS) AND MITOCHONDRIA.....	22
HEPATOCELLULAR CARCINOMA (HCC) .....	26
KNOWN EFFECTS OF HZE .....	28
<b>DESIGN, TECHNIQUES &amp; METHODS .....</b>	<b>30</b>
CHAPTER 2 INTEGRATED OMICS-LIFE AT THE BENCH .....	30
SLICING.....	31
TECHNIQUES .....	32
TRANSCRIPTOMICS .....	33
RNA ISOLATION AND RIBOSOMAL RNA REMOVAL.....	33
RNA SEQUENCING.....	33
DATA ANALYSIS RNA SEQUENCING .....	34
PROTEOMICS.....	34
PROTEOMICS SAMPLE PREPARATION .....	34
SPECTRAL LIBRARY GENERATION.....	35
LC-MS/MS-PROTEOMICS .....	37
MS DATA ANALYSIS-PROTEOMICS.....	38
LIPIDOMICS .....	38
LIPID EXTRACTION .....	38
LC-MS/MS-LIPIDOMICS .....	40
MS DATA ANALYSIS-LIPIDOMICS.....	41

METABOLOMICS .....	42
METABOLITE EXTRACTION.....	42
METABOLITE PROFILING VIA MS .....	43
METABOLITE DATA ANALYSIS .....	43
MITOCHONDRIA ANALYSIS .....	43
MITOCHONDRIA ISOLATION .....	43
COMPLEX I ASSAY .....	44
REAL-TIME QUANTITATIVE PCR ANALYSIS OF MITOCHONDRIAL DNA .....	44
CARDIOLIPIN ASSAY KIT.....	46
<b>RESULTS/DISCUSSION.....</b>	<b>47</b>
CHAPTER 3 FINDINGS FROM OMICS PLATFORMS .....	47
TRANSCRIPTOMICS AND PROTEOMICS .....	47
LIPIDOMICS .....	136
METABOLOMICS .....	150
BIOLOGICAL SIGNIFICANCE OF METABOLITES.....	177
Chapter 4 MITOCHONDRIAL DYSFUNCTION VALIDATION BY BIOLOGICAL ASSAYS .....	182
MITOCHONDRIAL COMPLEX I ASSAY.....	182
MITOCHONDRIA COPY NUMBERS VIA QT-PCR.....	187
CARDIOLIPINS .....	189
WEIGHTS.....	190
<b>CONCLUSIONS AND FUTURE DIRECTIONS .....</b>	<b>194</b>
Chapter 5 WHAT DOES IT ALL MEAN AND WHERE DO WE GO FROM HERE? .....	194
Bibliography/References .....	199
Vita.....	205

## List of Tables

Table 1:	Number of Differentially Expressed Genes and Proteins for Each Condition .....	47
Table 2:	Specific Proteins that are in Common between the Conditions Shown in the Venn Diagrams in Figure 12 .....	53
Table 3:	Specific Proteins that are in Common across the C57 <sup>56</sup> Fe Irradiated Time Course Venn Diagram Found in Figure 13 .....	65
Table 4:	Specific Proteins that are in Common across the C57 <sup>16</sup> O Irradiated Time Course Venn Diagram Found in Figure 13 .....	67
Table 5:	Specific Proteins that are in Common between the Conditions Shown in the Venn Diagrams in Figure 14 .....	69
Table 6:	Specific Proteins that are in Common in C3H <sup>56</sup> Fe Irradiated Time Course from Venn Diagrams found in Figure 15 .....	82
Table 7:	Specific Proteins in Common for C3H <sup>16</sup> O Irradiated Time Course found in Figure 15.....	84
Table 8:	Representative of Dysregulated Proteins in 1 month <sup>16</sup> O Mice Liver that are relevant to Mitochondria Function and Specific Metabolites .....	89
Table 9:	Number of Transcripts and Proteins within Mitochondria Dysfunction Pathway for Each Condition as well as the Names of the Transcripts and Proteins that are Dysregulated .....	91

Table 10:	Top Canonical Pathways and Upstream Regulators from Transcriptomics Data via IPA.....	101
Table 11:	Top Canonical Pathways and Upstream Regulators from Proteomics Data via IPA.....	121
Table 12:	Number of Differentially Expressed Metabolites for Each Condition	150
Table 13:	Description of Metabolite Changes throughout Time Course.....	166



## List of Figures

Figure 1:	HZE Analogy .....	18
Figure 2:	Incidence of HCC in Relation to Radiation by Dose .....	29
Figure 3:	Experimental Conditions and Tissue Collection/Processing .....	31
Figure 4:	Overall Workflow for Multi-omics Experiments.....	32
Figure 5:	Lipidomic Workflow .....	40
Figure 6:	Lipid Data Analysis Workflow .....	42
Figure 7:	Mitochondria Dysfunction Occurs in Transcriptomic 1 month $^{16}\text{O}$ irradiated C57 mice .....	49
Figure 8:	Venn Diagrams Show Differentially Expressed Transcripts in Common for Each Condition in the C57 Mice throughout the Time Course. ....	50
Figure 9:	Venn Diagrams Show Differentially Expressed Transcripts in Common for Each Time in the C57 $^{56}\text{Fe}$ and $^{16}\text{O}$ Irradiated Mice .....	51
Figure 10:	Venn Diagrams Show Differentially Expressed Transcripts in Common for Each Condition in the C3H Mice throughout the Time Course .....	52
Figure 11:	Venn Diagrams Show Differentially Expressed Transcripts in Common for Each Time in the C3H $^{56}\text{Fe}$ and $^{16}\text{O}$ Irradiated Mice.....	52
Figure 12:	Venn Diagrams Show Differentially Expressed Proteins in Common for Each Condition in the C57 Mice throughout the Time Course .....	53

Figure 13:	Venn Diagrams Show Differentially Expressed Proteins in Common for Each Time Point in the C57 <sup>56</sup> Fe and <sup>16</sup> O Irradiated Mice.....	65
Figure 14:	Venn Diagrams Show Differentially Expressed Proteins in Common for Each Condition in the C3H Mice throughout the Time Course. ....	68
Figure 15:	Venn Diagrams Show Differentially Expressed Proteins in Common for Each Time Point in the C3H <sup>56</sup> Fe and <sup>16</sup> O Irradiated Mice .....	82
Figure 16:	Mitochondria Dysfunction Pathway from Entire Proteomics list for 1 Month <sup>16</sup> O irradiated in order to determine the Coverage of Mitochondrial Proteins .....	88
Figure 17:	1 Month Lipids of Interest in C57 Mice .....	140
Figure 18:	2 Month Lipids of Interest in C57 Mice.....	142
Figure 19:	4 Month Lipids of Interest in C57 Mice.....	143
Figure 20:	9 Month Lipids of Interest in C57 Mice.....	146
Figure 21:	12 Month Lipids of Interest in C57 Mice.....	149
Figure 22:	Venn Diagrams Show Differentially Expressed Metabolites in Common for Each Condition in the C57 Mice throughout the Time Course....	151
Figure 23:	1 Month Metabolomics Graphs.....	152
Figure 24:	2 Month Metabolomics Graphs.....	156
Figure 25:	4 Month Metabolomics Graphs .....	159

Figure 26:	9 Month Metabolomics Graphs.....	162
Figure 27:	12 Month Metabolomics Graphs.....	164
Figure 28:	Mitochondria Complex I Activity of C57 Mice.....	184
Figure 29:	Mitochondria Complex I Activity of C3H Mice.....	185
Figure 30:	mtDNA Copy Number Determined via PCR for Each Time Point Post-Irradiation.....	186
Figure 31:	Data from Figure 30 Graphed to Show Each Individual Sample.....	187
Figure 32:	mtDNA Copy Number results from figure 30 and 31 Compared against Mitochondria Complex I Activity for All Time Points.....	187
Figure 33:	Cardiolipin Levels.....	189
Figure 34:	Weights for C57 Mice at Each Time Point.....	191
Figure 35:	Weights for C3H Mice at Each Time Point.....	192

## List of Abbreviations

BHT	Butylated Hydroxytoluene
CPA	Cyclic Phosphatidic Acid
CDKs	Cyclin Dependent Kinases
DNA	Deoxyribonucleic acid
DAG	Diacylglyceride
DAMP	Damage-Associated Molecular Pattern
DHA	Docosahexaenoic Acid
DDA	Data Dependent Acquisition
DIA	Data Independent Acquisition
DSBs	Double Strand Brakes
ER	Endoplasmic Reticulum
EIF2 $\alpha$	Eukaryotic Initiation Factor 2
EDTA	Ethylenediaminetetraacetic acid
FA	Fatty Acid
FT-ICR	Fourier transform ion cyclotron resonance
FXR	Farnesoid X Receptor
GCR	Galactic Cosmic Rays
GM	Ganglioside mannoside
Glc-GP	Phosphatidylglucose
GSK-3	Glycogen Synthase Kinase 3
GST	Glutathione S-transferase
GSBS	Graduate School of Biomedical Science
HCC	Hepatocellular Carcinoma
HZE	High energy, high charge
IPA	Ingenuity Pathway Analysis
IL	Interleukin
ISS	International Space Station
IR	Ionizing Radiation
LC	Liquid Chromatography
LET	Linear Energy Transfer
LPC	Lysophosphatidylcholine
LPE	Lysophosphatidylethanolamine
LPI	Lysophosphatidylinositol
LPS	Lysophosphatidylserine
LXR	Liver X Receptor
m/z	mass/charge
MS	Mass Spectrometry
MAP	Mitogen-activated protein
MEOH	Methanol
mtDNA	Mitochondrial DNA
mRNA	Messenger RNA
Nrf2	Nuclear Factor Erythroid 2
ppb/ppm	Parts per billion/million

PA	Phosphatidic Acid
PAMP	Pathogen-Associated Molecular Pattern
PCM	Pep Cal Mix
PE	Phosphatidylethanolamine
PG	Phosphatidylglycerol
PI	Phosphatidylinositol
PS	Phosphatidylserine
Psd1	Phosphatidylserine decarboxylase
PLA2	Phospholipase A2
PET	Positron Emission Tomography
PPAR $\gamma$	Peroxisome Proliferator-Activated Receptor $\gamma$
PTM	Post Translational Modification
ROS/RNS	Reactive Oxygen/Nitrogen Species
RNA	Ribonucleic acid
rRNA	Ribosomal RNA
RT	Retention Time
SIRT	Sirtuin
STATs	Signal Transducer and Activators of Transcription
TOF	Time of Flight
TAG	Triacylglyceride
TCA	Tricarboxylic Acid
TEAB	Triethylammonium Bicarbonate
TFA	Trifluoroacetic Acid
UTMB	University of Texas Medical Branch

## INTRODUCTION

### Chapter 1 TO INFINITY AND BEYOND

#### HIGH ENERGY, HIGH CHARGE (HZE) IRRADIATION

In 1948, Von Braun wrote the non-fiction scientific book, *The Mars Project*, about a manned mission to Mars which helped sparked the fascination in traveling deeper into our galaxy. It is now hoped that this mission will be possible by the year 2030, but with that hope there are several issues that must first be addressed. Most importantly, the risks associated with deep space travel must be assessed and then determine if there are any countermeasures that can eliminate or mitigate these risks. One of the most eminent risks is exposure to cosmic radiation.

During deep space travel, astronauts are exposed to high energy, high charge ions (HZE) which can be a tremendous health risk due to the possibility of carcinogenesis, cardiac dysfunction, and cognitive dysfunction. Unlike low-linear energy transfer (LET) radiation like gamma rays and x-rays, HZE ions are much more densely ionizing and therefore more damaging to tissues and cells. These types of ions are considered high-LET and include ions such as  $^{56}\text{Fe}$ ,  $^{28}\text{Si}$ , and  $^{16}\text{O}$  that are present in the Galactic Cosmic Rays (GCRs). While GCR's are only comprised of ~1% HZE ions, these ions possess significant higher ionizing power with greater potential for radiation induced damage. These particles are so penetrating that shielding can only partly reduce the doses that are absorbed by the crew. While thick shielding with aluminum could possibly reduce the effective dose to about 25% and polyethylene to about 35%, these types of shielding create problems for spacecraft launches because of their masses. During a mission to Mars, it is

estimated that an astronaut's body will be hit with an HZE ion about once a month. While this may seem like an insufficient amount, these ions are so destructive just a small dose can cause severe damage.<sup>1</sup> Shown in Figure 1 is an illustrative representation of the effect of HZE irradiation compared to gamma irradiation. Damage from low-LET including gamma rays and x-rays can be thought of as a full metal jacket bullet seen in the left-hand melon whereas high-LET such as HZE irradiation can be thought of as more like that of a hollow point bullet on the right-hand side of the figure. While the full metal jacket can travel a farther distance, the damage is much more localized whereas with the hollow point bullet the damage is much more widespread. We believe this is also the case when tissues and cells are hit with HZE irradiation.



Figure 1: HZE analogy: The melon on the left was shot with a full metal jacket bullet to emulate low LET irradiation such as gamma and x-rays whereas the melon on the right was shot with a hollow point to represent high-LET irradiation such as HZE.

Since humans have yet to be exposed to deep space radiation (the international space station (ISS) is protected by the Earth's magnetic field that deflects this type of irradiation), it is difficult to determine the exact effects of HZE. Therefore, animal models irradiated with simulated space radiation were used in this study. These studies are crucial to help elucidate the biological effects of HZE<sup>2-6</sup>. Previous studies conducted by other researchers have focused on the direct effects of HZE on chromosomes: terminal deletions, exchange aberrations, viability and chromosome instability<sup>1,7</sup>. While

some have also emphasized transcripts, proteins, or metabolites on an individual basis,<sup>3,4,8,9</sup> they have yet to look at the system as a whole. While all these components are highly critical, in a biological system all these molecules are linked together which calls for a broader systems approach. This type of approach will produce a more complete systematic characterization to define changes in the microenvironment and determine the role of such changes in carcinogenesis. Thus, this study was the first application of an integrated omics approach to study the effects of deep space irradiation.

#### **CELLULAR CONNECTIVITY**

Cellular signaling is known to be a very complex and eloquent process in which many levels of regulation are orchestrated to elicit the proper response (e.g. proliferation, differentiation, migration, survival, etc.). DNA contains the instructions that make these processes possible, which are transcribed into RNA to relay the message that is ultimately translated into proteins. Proteins can also be further regulated by post translational modifications. Proteins then go on to play key roles in cellular regulation. Although lipids/metabolites are products of proteins (enzymes) regulated by DNA, the lipids/metabolites themselves are not encoded within the DNA making them an excellent target for micro-environmental change. With this much interconnectivity, it is easy to understand why a multi-omics platform would be beneficial in monitoring the effects of deep space radiation especially in relation to the formation and progression of cancer where dysfunction occurs on many levels. Thus, we applied an integrated approach to elucidate information on the interaction between DNA/RNA, lipids/metabolites, and proteins induced by high charge, high energy (HZE) ions.



## IONIZING IRRADIATION

Radiation is classified in two major groups: ionizing and non-ionizing. High frequency, high-energy waves are termed “ionizing” because they contain enough energy to displace an electron from its orbit around a nucleus. Ionizing radiation (IR) is known to result in cellular damage by two different mechanisms known as direct and indirect effect. In direct effect, the radiation interacts with the DNA molecule directly and disrupts the molecular structure of the DNA. This mechanism is responsible for changes in the DNA such as double stranded breaks (DSBs), single stranded breaks, associated base damage or clusters of these damage types. It has been proposed that indirect effects are caused by damage produced from reactive oxygen and nitrogen species acquired from the radiolysis of water <sup>10-12</sup>. In this process, radiation ionizes water molecules, the major constituent of the cell, along with other organic molecules which results in the formation of free radicals such as hydroxyl (HO·) and alkoxy (RO<sub>2</sub>·). Of these, HO· is the most abundant and is particularly destructive to DNA <sup>10,12</sup>. These radicals can attack DNA resulting in several alterations including DNA breaks, base damage, destruction of sugars, crosslinks, and telomere dysfunction <sup>12</sup>. It is thought that most radiation-induced damage results from the indirect action mechanism as water constitutes nearly 70% of the cellular composition <sup>11</sup>. Because of their high linear energy transfer (LET), HZE ions are thought to cause clusters of damage where many molecular bonds are broken in the tissue along their trajectory. The cell’s ability to repair DNA damage becomes impaired as the severity of clustering increases leading to DNA deletions and other forms of mutations<sup>13</sup>. However, the number of free radicals produced by IR depends on the total dose of IR<sup>11</sup>. Since all other studies in the field have dealt

with high total doses of HZE, high levels of DSBs have been observed <sup>1,7-9</sup>, and should be expected due to the direct interaction with DNA and the creation of more free radicals that can produce more drastic clusters of damage. DSBs originate through the coordinated reactivity of two HO· radicals at nearby ribose sites ultimately leading to strand breaks through subsequent radical pathways <sup>12</sup>. Both nucleobases and deoxyribose can be targets for HO· mediated damage. With purine nucleobases, HO· typically adds at C4, C5, and C8, generating reactive adduct radicals that lead to a variety of products, with 8-hydroxypurines being the most common. Specifically, 8-oxo-deoxyguanine (8-oxo-dG) is known for being the hallmark of DNA damage <sup>10,12</sup>. This alteration can result in a mismatch pairing of guanine with adenosine causing a G to T and C to A substitutions in the genome. Guanine is the preferentially attacked base for oxidative DNA damage because it has the lowest oxidation potential of the four bases. The presence of this oxidation product has been known to reduce the methylation efficiency of nearby cytosines in a proximity-dependent manner which exhibits how IR-generated ROS can impact the epigenome. In a study involving low-dose IR given during gestation, an increase in DNA methylation was seen in the offspring <sup>12</sup>. Not only could IR affect the epigenome of future generations, but DNA methylation status is also thought to correlate with the response and resistance to IR. Decreased methylation was found to be linked to decreased apoptosis and increased post-IR survival <sup>12</sup>. Since methylation can alter transcription, it may be possible to tell which genes could be targets of epigenetic changes by the RNA sequencing data. However, RNA sequencing will only provide data for transcripts being up or down regulated, not the mechanism by which this change is occurring. Therefore, it is not possible to distinguish if decreased

gene transcription is occurring due to an epigenetic change like methylation or if the transcript is simply being rapidly degraded. Many enzymes that are involved in epigenetic processes are, however, directly regulated by phosphorylation and oxidative post-translational modifications (PTMs), and thus it may be possible to analyze these enzymes and their respective regulation by proteomic studies. Since our studies are utilizing a low dose HZE (0.2 Gy), the damage was not expected to be clustered as has been seen with higher doses of HZE studies. This may explain why low dose HZE results in infrequent DSBs.

#### **REACTIVE OXYGEN SPECIES (ROS) AND MITOCHONDRIA**

ROS has been suggested to be generated secondarily following IR from biological sources such as mitochondria. These ROS have a variety of biological roles including apoptotic signaling, genomic instability, and radiation-induced bystander effects that ultimately impact cellular integrity and survival. It's unclear exactly how the mitochondria are responsible but it is thought that it is due to leakage of electrons from the electron transport chain that results in the generation of superoxide radicals ( $O_2^{\cdot-}$ ) through their interaction with molecular oxygen.<sup>14-15</sup> Mitochondria just like most other biological systems do not operate at 100% efficiency thus electrons are occasionally lost and ROS is produced. ROS from mitochondria is a normal occurrence, but as the mitochondria are damaged the leakage increases resulting in increased levels of ROS. Mitochondrial DNA (mtDNA) is made up of entirely coding regions and lacks a protective histone coat. It also undergoes limited proof reading and repair when it's copied. These factors along with its rich source of ROS contribute to 10 to 20 fold greater mutation rate compared to that of the nuclear genome. Alterations in the

respiratory system and mtDNA are thought to be a general feature in malignant cells. This damage ultimately leads to dysfunction in the oxidative phosphorylation pathway and causes defects in ATP production and numerous disorders in tissues that have higher demands for energy such as skeletal muscle, cardiac, and the nervous system.<sup>15,16</sup> Studies have shown significant decreases in Complex I activity and it has been suggested this Complex could be the contributor for the initiation of mitochondria biogenesis.<sup>15</sup> Dysfunction of this particular complex is the main cause of several mitochondrial diseases and disorders.<sup>15</sup>

In 2012 and 2013, Datta et al.<sup>3,4</sup> studied 2 Gy and 5 Gy gamma irradiation and 1.6 Gy and 4 Gy <sup>56</sup>Fe irradiation in mice. Activation of  $\beta$ -catenin was observed in both the tumor bearing and non-tumor areas in <sup>56</sup>Fe irradiated animals along with elevated levels of oxidative DNA damage. Results showed that radiation quality affected the level of persistent oxidative stress with higher elevation of intracellular reactive oxygen species (ROS) and mitochondrial superoxide in <sup>56</sup>Fe irradiated compared to non-irradiated and gamma irradiated groups. Additionally, NADPH oxidase activity, mitochondrial membrane damage and loss of membrane potential was greater in <sup>56</sup>Fe irradiated animals. Mitochondria are responsible for producing 90% of the energy our bodies need to function which is why they are known as the “powerhouse of the cell”. Mitochondria are the major source of intracellular ROS and are key players in initiation of apoptosis<sup>17</sup>. They also play many key roles in cell signaling, cell differentiation, senescence, and regulation of cell growth<sup>18</sup>. They are highly dynamic organelles that have the ability to change their function, morphology and number in response to the

physiological conditions and stressors that they are exposed to in their microenvironment<sup>19</sup>.

Recent studies have also identified acylcarnitines as a marker of radiation exposure. Acylcarnitines are small molecule lipid derivatives that range in length from two carbons to twenty six linked to carnitine by an ester bond.<sup>20</sup> The components of this system are involved in the bi-directional transport of acyl moieties from the cytosol to the mitochondria and vice versa. They play an important role in allowing the switching between glucose and fatty acid metabolism which makes them an important mediator in cancer metabolism as cancer cells can easily reprogram their metabolism to satisfy their energy requirements even under harsh and hypoxic conditions.<sup>21</sup> Acylcarnitines have long been identified as markers of inborn errors of metabolism and alteration in their plasma profiles have been seen in type 2 diabetes and obesity. In a metabolomics study looking at urine from patients who received radiation therapy, six carnitines were reduced 6 hours post irradiation and after 24 hours only acetylcarnitine and valerylcarnitine showed recovery.<sup>20</sup>

Cheema et al. monitored metabolite changes in mice exposed to 2 Gy gamma irradiation compared to 1.6 Gy <sup>56</sup>Fe. Results showed decreased adenine and guanosine and increased inosine and uridine which suggests perturbed nucleotide metabolism. <sup>56</sup>Fe irradiation also resulted in upregulation of prostaglandin biosynthesis and eicosanoid signaling.<sup>8</sup> Laiakis et al's<sup>9</sup> metabolic studies identified pathways affected by 0.5 and 2 Gy of 1 GeV/nucleon of protons which also comprise GCRs. Differences were identified in metabolites that map to the TCA cycle and fatty acid metabolism suggesting energy metabolism was severely impacted. Products of purine and pyrimidine metabolism were

upregulated which infers DNA damage or apoptosis. Various amino acid pathways such as tryptophan, tyrosine, arginine, proline and phenylalanine were also affected potentially implicating DNA damage repair<sup>9</sup>. Mitochondria have a central role in amino acid metabolism so these changes could be related to mitochondria dysfunction. Many of the carbon skeletons used in amino acid biosynthesis originate from metabolites of the TCA cycle and carbon backbones of all amino acids may be converted either directly or indirectly into TCA intermediates. Key reactions for the removal of ammonium ions generated from catabolism of amino acids also take place in the mitochondria<sup>22</sup>. Out of 20 amino acids, the metabolic pathways of 17 utilize mitochondrial enzymes and dysfunction of these enzymes is the causative factor for over 40 known mitochondria diseases and disorders in humans<sup>23</sup>.

As discussed in the nature review “Heavy Ion Carcinogenesis and Human Space Exploration”, DNA damage is generally accepted as the initiating event of the multi-step carcinogenic process, but recent evidence has pointed towards non-targeted effects that are independent of DNA lesions<sup>1,7</sup>. However, many of the studies with HZE irradiation have utilized high doses of HZE ( $\geq 0.5\text{Gy}$ ). Our studies aim to focus on lower doses (0.2Gy) which are more similar to what astronauts will be exposed to during deep space travel, and to study a broader range of HZE ions than just  $^{56}\text{Fe}$  as GCRs are comprised of other ions besides iron. It is also theorized that DNA damage is not the cause of carcinogenesis at these low doses. We hypothesize that carcinogenesis occurs because of several minor micro-environmental changes which our approach is designed to identify.

## **HEPATOCELLULAR CARCINOMA (HCC)**

On Earth, HCC is the most common type of liver cancer accounting for approximately 80% of all liver cancers. HCC is the fifth most common cancer in the world and third leading cause of cancer-related deaths<sup>24,25</sup>. Current treatment options can be grouped into three categories: potentially curative, palliative, and symptomatic. Potentially curative treatments include liver resection, liver transplant, and local ablation. These treatments have a promising 75% five year survival rate. However, due to a shortage of livers for transplant purposes, advanced tumor stage, and liver dysfunction, less than 20% of patients are eligible for these treatments. Palliative treatment has approximately a 3 year survival rate whereas symptomatic treatment has a survival rate of less than 3 months. Also, chemotherapeutic choices are very limited for HCC<sup>26</sup>. At present, HCC typically develops as a consequence of underlying liver disease such as hepatitis B (HBV) or C (HCV) infection and is associated with cirrhosis in approximately 90% of HCC. Alcohol consumption is a major contributor in cirrhosis leading to HCC. Hepatocarcinogenesis is known to be a multistep process involving a number of factors such as, activation of Wnt/ $\beta$ -catenin signaling, p53 inactivation, loss of retinoblastoma protein (pRB) activity, mitogen-activated protein (MAP) kinase pathways, and activation of JAK/STAT pathway. Wnt/ $\beta$ -catenin signaling is a highly conserved pathway that is involved in homeostasis, cell proliferation, differentiation, motility and apoptosis. Alterations in this pathway occur early on from HBV/HCV infections, and alcoholic liver cirrhosis. Activation of Wnt signaling produces an inflammatory response. Gain of function mutations in the gene encoding  $\beta$ -catenin results in increased activation of nuclear factor  $\kappa$ B (NF $\kappa$ B) which is a master regulator

of inflammation and cell death. Wnt/ $\beta$ -catenin pathways also controls expression of glutathione S-transferase (GST) which is heavily involved in liver detoxification of xenobiotic compounds and biotransformation. This process plays an important role in the defense against oxidative stress. Altered expression of GSTs due to Wnt/ $\beta$ -catenin signaling has been seen in both humans and rodent models. Normally, p53 levels are low, but in response to stress its level is rapidly upregulated. In about 50% of human tumors, the tumor suppressor gene TP53 is inactivated by a single point mutation. In other tumors, p53 is still expressed at normal levels, however, the signaling pathways that lead to cell cycle arrest and apoptosis are defective. HCC patients with upregulated mutant p53 expression have shorter overall survival compared to those with wild-type p53. pRB is a major tumor suppressor, and it helps to prevent cancer by controlling cell cycle progression through the inhibition of the E2F transcription factor family of proteins. Cyclin-dependent kinases (CDKs) phosphorylate and activate pRb to induce G1/S cell cycle transition. Some studies have also seen a strong correlation between the loss of pRb activity and lack of functional p53 in HCC. The MAP kinase family of proteins are also implemented in a diverse set of cellular processes such as cell survival, differentiation, adhesion, and proliferation, and several studies have shown MAPK signaling to be a factor in HCC. Signal transducer and activators of transcription (STATs) are a family of transcription factors activated by a variety of cytokines, hormones, and growth factors. Their activation occurs through tyrosine phosphorylation by JAKs. JAK activation of STATs stimulates cell proliferation, migration, differentiation and apoptosis, and inactivation of inhibitors in this pathways such as



suppressors of cytokine signaling (SOCS-1), and SSI-1 (a JAK-binding protein) have been noted in HCC<sup>24,25</sup>.

#### **KNOWN EFFECTS OF HZE**

Previous studies by Weil et al. examined the induction of murine acute myeloid leukemia and HCC by HZE compared to gamma rays. They studied <sup>28</sup>Si and <sup>56</sup>Fe ions, and found that these ions were not substantially more effective than gamma rays at producing acute myeloid leukemia. However, when they looked at the induction of HCC, they discovered a much greater incidence of this type of cancer produced by HZE compared to gamma rays. Figure 2<sup>6</sup>, shows an increase (~2.5 fold) in the incidence of HCC at much lower doses of HZE compared to the incidence produced by gamma rays at the same dosage. Due to the unexpected, non-linear, convex shape of the dose response curve for the HZE ions, it has been hypothesized that non-targeted effects could play a major role in the development of HCC. Non-targeted effects include upregulation of inflammatory signaling, cytokine production, and immune responses, all of which have been shown to play a role in cancer development and progression. Therefore, if carcinogenesis is due to these non-targeted effects, it should be exhibited in changes in the microenvironment. Similar results were also seen for induction of Harderian gland tumors following exposure to a variety of HZE ions<sup>2,27</sup>. The data obtained from Harderian gland tumors in mice is one of the most complete data sets for carcinogenesis induced by HZE. However, since humans lack these glands the applicability of studies still remains in question<sup>6</sup>.

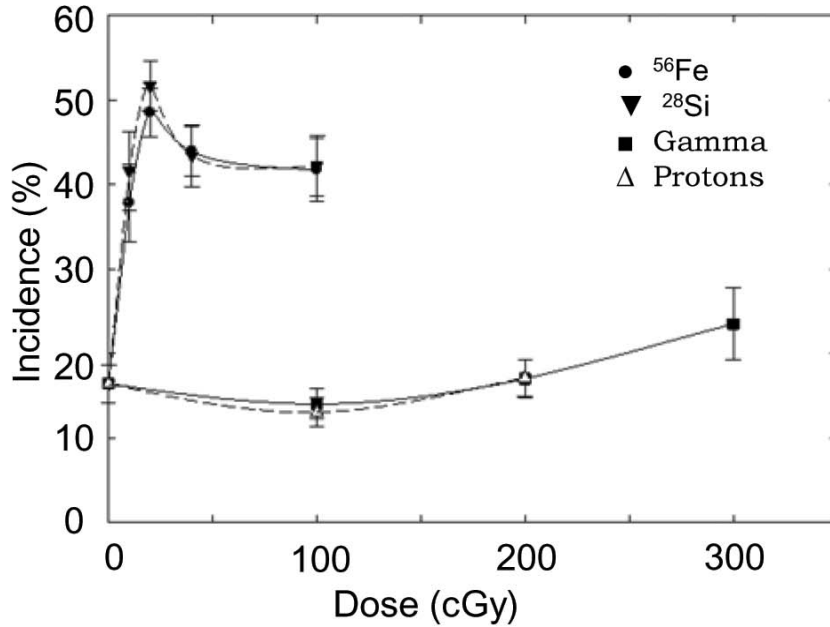


Figure 2: Incidence of HCC in relation to radiation by dose. HZE radiation produces greater incidence at much lower doses than radiation with gamma or protons. Displays the following irradiated treatments: 300 MeV/n  $^{28}\text{Si}$ , 600 MeV/n  $^{56}\text{Fe}$ ,  $^{137}\text{Cs}$  gamma rays, & SPE 1972 protons

In order to access the molecular mechanisms of low dose, HZE irradiation in the liver, the following specific aims will be utilized:

1. Develop and implement an integrated omics platform utilizing transcriptomics, proteomics, lipidomics and metabolomics to identify micro-environmental - bystander responses to low dose HZE exposure in mice
2. The integrated omics data sets will be used to predict alterations in biological/biochemical pathways induced by low dose HZE exposure. Biochemical assays will also be used as validation for the effected pathways.
3. Predictions will be made as to the risk involved for human astronauts during deep space travel who will be exposed to similar doses of HZE and potential countermeasures to combat the HZE induced changes will be discussed.

## DESIGN, TECHNIQUES & METHODS

### Chapter 2 INTEGRATED OMICS-LIFE AT THE BENCH

In this study, we utilized C3H/HeNCrL mice which are more susceptible to HCC induced by HZE along with C57BL16 mice that are more resistant (Ullrich unpublished observations). Under normal conditions, C3H are more prone to spontaneous hepatomas<sup>28</sup> and have approximately 17% occurrence of HCC tumors<sup>6</sup> whereas the C57BL16 do not exhibit this increased induction of liver tumors. Therefore, in this project the C57BL16 served as a wild type for comparison to the irradiated C3H mice. Since we do not know what drives the induction of HCC by HZE irradiation, using both strains will help facilitate identification of changes that may be particularly informative with respect to HCC carcinogenesis.

Twenty-five mice of each strain were placed in each of the 6 groups and received the defined irradiation treatment. All the mice were irradiated at Brookhaven National Laboratory (Upton, New York) and then brought to Galveston, TX where they were housed in the animal care facilities at UTMB until the time point they were euthanized. The 6 treatment groups were: 600 Me V/n <sup>56</sup>Fe (0.2 Gy), 1 Ge V/n <sup>16</sup>O (0.2 Gy), 350 Me V/n <sup>28</sup>Si (0.2 Gy), <sup>137</sup>Cs (1.0 Gy) gamma rays, <sup>137</sup>Cs (3.0 Gy) gamma rays, and no irradiation. Based on data collected from deep space probes, it has been calculated that an astronaut will receive a total dose of HZE of approximately 0.2 Gy on a trip to Mars and back. Thus, 0.2 Gy was used for the dosing of the animals in this study.

Five mice of both strains in each of the 6 groups (determined by a priori analysis using G\* Power Software) were euthanized at the following time points post irradiation:

30, 60, 120, 270 and 360 days via CO<sub>2</sub> asphyxiation (as per current AVMA guidelines). The left liver lobes were excised and flash frozen. Samples were stored at -80°C until analysis was performed.

## SLICING

Extractions for lipidomics, proteomics and RNA sequencing were optimized so that two 40-micron slices could be used. Slicing allows for multiple slices to be taken from a tissue while eliminating multiple freeze/thaw cycles thus helping to preserve the integrity of the tissue. A small droplet of MilliQ water was used to mount tissues to the cryotome mounting plate. Slices were performed on a cryotome at -20°C as seen in Figure 3.

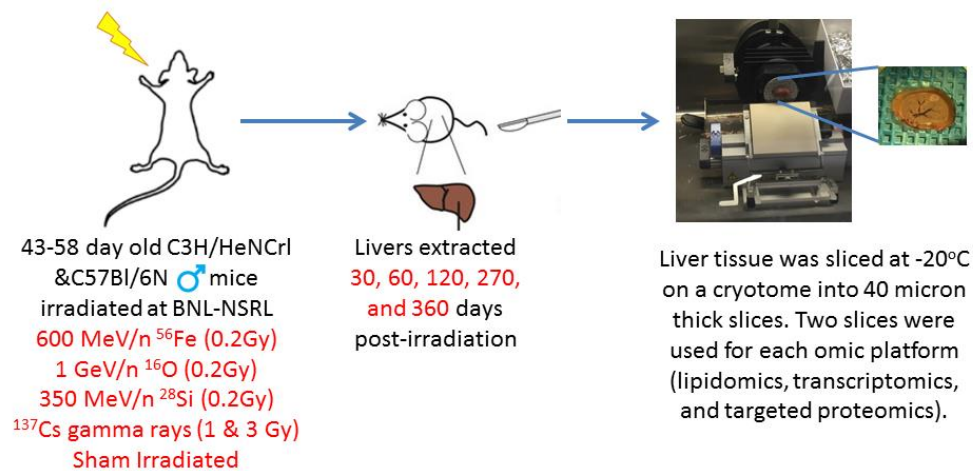


**Figure 3:** Experiential conditions and tissue collection/processing. C3H/HeNcrL mice (more susceptible to HCC) along with C57BL16 (more resistant) were placed into 6 treatment groups and received the following irradiation treatments: 600 Me V/n <sup>56</sup>Fe (0.2 Gy), 1 GeV/n <sup>16</sup>O (0.2 Gy), 350 MeV/n <sup>28</sup>Si (0.2 Gy), <sup>137</sup>Cs (1.0 Gy) gamma rays, <sup>137</sup>Cs (3.0 Gy) gamma rays, and no irradiation. Left liver lobes were collected at 30, 60, 120, 270 & 360 days post-irradiation and two 40 micron slices were taken on cryotome for each respective omics platform.

## TECHNIQUES

Figure 4 shows the overall workflow that was used to conduct the integrated omics experiments. As discussed in the introduction, there is a great deal of communication and interconnectivity within the cell with all the molecules working together for the cell to function properly. Thus, to gain a better understanding of what was occurring and being disturbed on a molecular level from deep space irradiation, this project encompassed transcriptomics, proteomics, lipidomics and metabolomics.

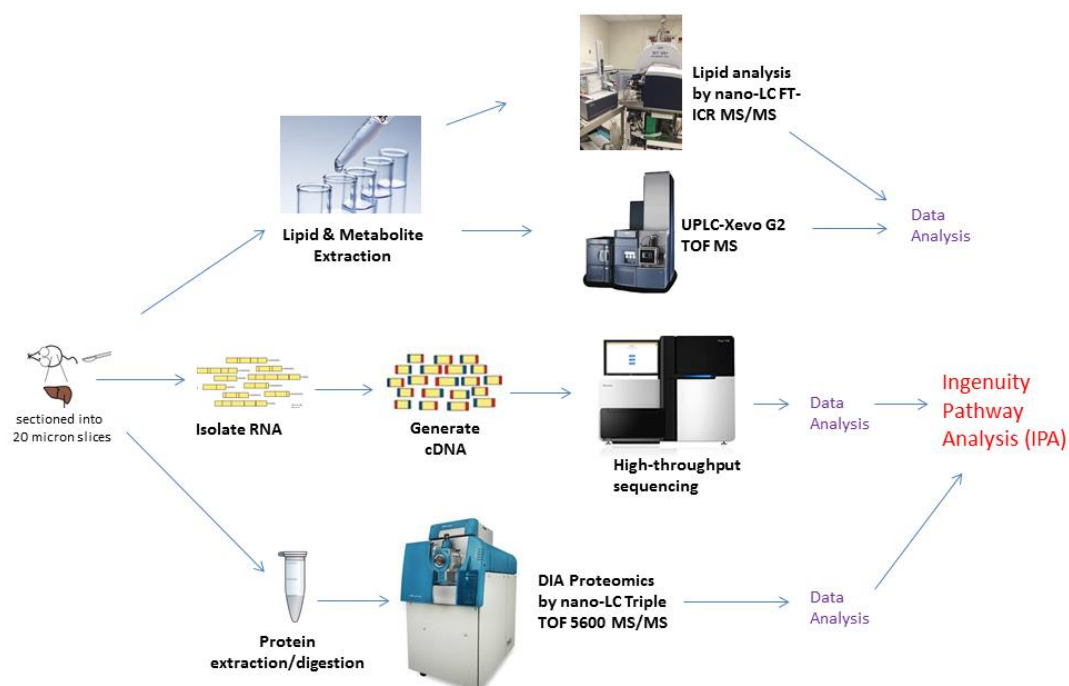


Figure 4: Overall Workflow for Multi-omics Experiments: Lipids extracted via Bligh-Dyer (methanol: chloroform extraction) were analyzed on a 12T Bruker Solarix Fourier transform ion cyclotron resonance mass spectrometer (FT-ICR MS). RNA sequencing was conducted on an Illumina HiSeq 1500 after RNA isolation and removal of rRNA via Ribo-Zero. An untargeted data independent acquisition method using a Sciex 5600 Q-TOF was utilized for proteomics studies. C57 caudate liver for non-irradiated,  $^{56}\text{Fe}$ ,  $^{16}\text{O}$  and 1Gy Gamma was analyzed for metabolites via UPLC-Xevo G2 TOF MS at Georgetown University, Washington D.C.

## **TRANSCRIPTOMICS**

### **RNA ISOLATION AND RIBOSOMAL RNA REMOVAL**

Total RNA was isolated from two 40 micron slices via phenol-free kits from RNAAqueous (Invitrogen, Vilnius, Lithuania). RNA was monitored for yield and quality via Nanodrop spectrophotometer (Thermo Scientific) and an RNA 1000 chip on an Agilent 2100 Bioanalyzer (Agilent Technologies). Ribosomal RNA (rRNA) was removed via Ribo-Zero Gold rRNA removal kits (Human/Mouse/Rat) from Illumina (San Diego, CA).

### **RNA SEQUENCING**

To create cDNA libraries, messenger RNA (mRNA) from samples were selected from total RNA (0.5-2.0 µg) using poly dT primers that recognize the polyA tail. mRNA was fragmented using divalent cations and heat (94°C, 8 minutes). Illumina TruSeq V2 sample preparation kits were used for library construction. Fragmented PolyA<sup>+</sup> samples were converted to cDNA by random primed synthesis using superscript II reverse transcriptase (Invitrogen). Following second strand synthesis, the double strand DNAs were treated with T4DNA polymerase, 5' phosphorylated and an adenine residue was added to the 3' ends. Adapters were then ligated to the ends of the target template DNAs. After ligation, the template DNAs were amplified using primers specific to each of the non-complimentary sequences in the adapter. This created a library of DNA templates that have non-homologous 5' and 3' ends. 50 base pair reads were acquired on an Illumina HiSeq 1500 and fed into the NEB RNA Ultra Library Kit for Illumina to complete the library. Samples were clustered onto the flow cell using the cBot and sequenced on the HiSeq-1500 as a Paired End run with 50x50bp lengths in high output mode.

## **DATA ANALYSIS RNA SEQUENCING**

Reads were aligned with the STAR alignment program using the ENCODE recommended parameters. Reads per gene were counted using the –quant Mode Gene Counts option. PIVOT version 1.0.0 (Junhyong Kim Lab, University of Pennsylvania) was used for differential expression analysis. Within PIVOT, RLE(DeSeq) was used for data normalization and an exact test with false discovery rate (FDR) set to 0.1 was used to compare control groups to treatment groups via experiment design ~condition. Acquired lists were then filtered for a 1.5-fold change or greater and imported into IPA.

## **PROTEOMICS**

### **PROTEOMICS SAMPLE PREPARATION**

Tissue slices were lysed with RIPA buffer mixed with Halt protease inhibitor ethylenediaminetetraacetic acid (EDTA) free, Halt phosphatase inhibitor cocktail and Pierce universal nuclease<sup>29</sup> and homogenized on ice with a polytron equipped with a micro-generator (20s x 1, @10,000 rpm). Samples were incubated on ice for 30 mins with brief vortexing twice during incubation then centrifuged at 15,000 g for 20 min at 4°C. Protein concentration of the supernatant was determined via Pierce BCA Protein Assay Kit, Thermo Scientific (Rockford, IL). 100ug of resulting protein was reduced and alkylated. Ten uL of 200mM tris (2-carboxyethyl) phosphine (TCEP) diluted with 50mM triethylammonium bicarbonate (TEAB) was added to each sample and incubated at 55°C for 1h while mixing. Ten uL of 375mM iodoacetamide was added and incubated in the dark at room temperature for 45 mins while mixing. Proteins were precipitated

overnight at -20°C with 880uL of ice-cold acetone. Samples were centrifuged at 15,000 g for 20 min at 4°C. Supernatant was decanted and samples were de-lipidated by adding 1mL of ice cold (tri-n-butylphosphate/acetone/methanol, 1:12:1)<sup>30</sup> and incubated for 90 mins on ice. Samples were centrifuged at 2,800g for 15 min at 4°C. Supernatant was removed and 1 mL ice cold tri-n-butylphosphate was added. Samples were centrifuged again under the same conditions as previously stated. Supernatant was removed, and 1 mL ice cold acetone was added. Centrifugation was repeated, and supernatant removed. One mL of ice-cold methanol was added, and samples were centrifuged for a final time. Upon removing supernatant, sample pellets were air dried then resuspended in 12.5uL of 8M urea. Four mg of trypsin in 50mM triethyl ammonium bicarbonate (TEAB) was added to each sample and incubated for 24 hours at 37°C. Samples were desalted using C18 Sep-Pak Vac 1cc cartridges attached to a vacuum manifold. Cartridges were equilibrated using three 1ml aliquots of acetonitrile at a flow rate of ~2ml/min. Cartridges were then washed with three 1 mL aliquots of 0.25% trifluoroacetic acid (TFA). TFA acid was added to samples to bring them to a final concentration of 1%. Samples were loaded on to Sep-Pak cartridges and allowed to pass via gravity flow. Cartridges were then washed with four 1mL aliquots of 0.25% TFA. Peptides were then eluted in 1mL of 80% acetonitrile/0.1% formic acid by gravity flow. Eluted peptides were lyophilized in a LabConco CentriVamp Concentrator.

#### **SPECTRAL LIBRARY GENERATION**

Forty µg of protein was taken from all proteomic samples and pooled together. A 400 µg aliquot was then taken for fractionation (Agilent Technologies 1260 Infinity). The



pooled peptides were lyophilized to dryness and reconstituted in 125 $\mu$ L of 85% acetonitrile/56 mM formic acid (aqueous). The peptides were fractionated using a hydrophilic interaction chromatography column (HILIC, PolyLC PolyHydroxyethyl A, PolyLC Inc., Columbia, MD, 200 x 4.6mm, particle size 5  $\mu$ m). Buffer A was 85% acetonitrile/56 mM formic acid, pH 3.0 and Buffer B was 8.5 mM ammonium formate/56 mM formic acid, pH 3.0. Fifty three 1 mL fractions were collected at a flow rate of 1 mL/min under the following gradient: column was equilibrated with ten column volumes of 100% A, sample loaded on the column, column was washed with four column volumes of 100% A, sample collection was initiated with 3.5 column volumes to 15% B, four column volumes to 40% B and finished with 10 column volumes to 100% B. All fractions were lyophilized to dryness and fractions 21-40 were reconstituted in 25 $\mu$ L of 98% H<sub>2</sub>O, 2% acetonitrile and 0.1% formic acid. These fractions were then pooled with a corresponding fraction 1-20. For example, fraction 1 and 40, 2 and 39, 3 and 38, etc. Fractions 41-53 were taken up into 12.5 $\mu$ L individually. Peptide concentrations of all samples whether individual or pooled were determined on a 2 $\mu$ L aliquot from each sample on the nanodrop spectrophotometer (Thermo). Fraction pairs 4 and 37, 5 and 36, 6 and 35, 7 and 34, and 8 and 33 were spun down at 12,000g for 5 mins. Eighteen  $\mu$ L of the remaining 23 $\mu$ L were added to auto sampler vials for proteomic analysis by LC/MS/MS data dependent acquisition (DDA) MS on a Thermo Fusion mass spectrometer. Six  $\mu$ L of each pooled samples was injected for LC separation and MS analysis. Other fractions were further pooled to achieve desired peptide concentrations that were at least 0.1mg/mL or greater. Pooled groups were as follows:

Fraction 1, 40, 19, 22, 9 & 32; 20, 21, 17, 24, 15 & 26; 14, 27, 10, 31, 2, 39, 12 & 29; 16, 25, 18, 23, 13, 28, 11 & 30; and finally 41-53. These combined fractions were then also analyzed by DDA MS. Samples were injected onto a ChromXP nanoLC trap column 350  $\mu$ m id x 0.5 mm, ChromXP C18 3  $\mu$ m 120 $\text{\AA}$  (Sciex, Inc., Redwood City, CA) and separated over a ChromXP nanoLC column 75  $\mu$ m id x 15 cm, ChromXP C18 3 $\mu$ m 120 $\text{\AA}$

(Sciex, Inc., Redwood City, CA) prior to DDA analysis on the Thermo Fusion. Once collected, data from all 10 fractions were combined to search mouse UKB DB. These files were then used to create the spectral/ion library.

#### **LC-MS/MS-PROTEOMICS**

For data independent acquisition (DIA) proteomic analysis, chromatographic separation and mass spectrometric analysis was performed with a nano-LC chromatography system (Thermo Dionex Ultimate 3000 RSLC nano system) interfaced to a ABSciex Triple Time of Flight (TOF) 5600 mass spectrometer. Samples were analyzed by LC-MS/MS at a flow rate of 300 nL/min. Samples were separated over an Acclaim PepMap 100 C18 LC column 0.075mm diameter and 250mm in length (Thermo). One  $\mu$ g of protein from each sample was injected onto the column. The gradient started at 97%/3% A/B ramping to 20%/80% A/B over 72 mins. 20%/80% A/B was held for 6 mins then re-equilibrated to 97%/3% A/B and held for 25 mins. Solvent compositions were: Solvent A: 100% H<sub>2</sub>O with 0.1% formic acid. Solvent B: 100% acetonitrile with 0.1% formic acid. The total gradient profile lasted for a total of 105 mins. DIA was used to enhance sequence coverage. A custom isolation scheme was used over the mass range of 400-1200 m/z so that smaller isolation windows could be applied in mass ranges that are known to have the highest concentration of peptides. A rolling collision energy was used for MS/MS acquisition. All samples were run in block randomized order.

## **MS DATA ANALYSIS-PROTEOMICS**

The ion library was imported in PeakView (Sciex) followed by individual samples for all conditions. Retention Time (RT) alignment process settings were as follows:

Peptide Filter:

Number of Peptides per protein: 15

Number of Transitions per Peptide: 5

Peptide Confidence Threshold %: 95

False Discovery Rate Threshold %: 1.0

XIC Options:

XIC Extraction Window (min): 8.0

XIC width (ppm): 30

RT standards were selected from Pep Cal Mix (PCM) spike in and carbamoyl-phosphate for approximately every 5-10 mins during the duration of the run for RT calibration. Once selected, RT fit was calculated and points were deleted and added as necessary so that best fit was achieved. After RT calibration was complete, processing was continued. Areas were then exported to MarkerView (Sciex) where statistical analysis was conducted by pairwise comparisons between control and treated groups. Lists were then filtered to contain peptides with p values  $\leq 0.05$  and a fold change  $> 1.5$ . Filtered lists were imported into IPA for analysis.

## **LIPIDOMICS**

### **LIPID EXTRACTION**

As shown in Figure 5, two 40 micron mouse liver tissue slices were homogenized in 400 uL of 155mM ammonium acetate<sup>31</sup> solution on ice using a Polytron equipped with a micro-generator (10s x 2, @15,000rpm). A 2uL volume was removed

from homogenate and diluted in 155mM ammonium acetate (typically 2uL of sample in total volume of 4.5uL) for BCA total protein determination. For BCA, 2uL of diluted sample was combined with 20uL of working reagent and read on the Nanodrop. Volume corresponding to 200ug of total protein was transferred to a 2mL screw cap (Teflon lined) glass vial and 1:1 MeOH:CHCl<sub>3</sub> (400 uL of each solvent) was added. The MeOH solution contained 2mM butylated hydroxytoluene (BHT) to prevent lipid oxidation<sup>32</sup>. Samples were placed in a sonicating water bath for 30 minutes then transferred to a shaking heat block at 48°C where they remained overnight. After removing from heating block, samples were placed in a sonicating water bath for 10 minutes. Sample was centrifuged at 5,000g for 15 minutes at room temperature. Supernatant was transferred to a 30mL glass Corex tube, capped with a piece of aluminum foil and saved for later (can be stored at room temp). One to one MeOH:CHCl<sub>3</sub> (400 uL of each solvent) was added to the pellet in the vial, and the 10 minute sonication step and 15 minute centrifugation step was repeated. Supernatant was combined with the previous aliquot in the 30 mL Corex tube. One to one MeOH:CHCl<sub>3</sub> was added to pellet once more and process was repeated. To the combined supernatants in the Corex tube, 3.3mL of H<sub>2</sub>O & 1.2mL of CHCl<sub>3</sub> was added. The mixture was vortexed and mixed well with aid of a glass pipet. Corex tubes with combined aliquots were centrifuged at 5,000g for 20 minutes at room temperature to produce 2 phases with clear separation. Polar lipids are in the aqueous layer (top layer). This layer was transferred to 2mL screw cap glass vials and lyophilized in a CentriVamp. The non-polar layer was transferred to 4mL screw cap glass vial and stored at -80°C for future

use. Once dried, samples were taken up in 100 $\mu$ L of 80% MeOH, 20% H<sub>2</sub>O with 10mM NH<sub>4</sub>OAc to be analyzed by mass spectrometry<sup>33</sup>.

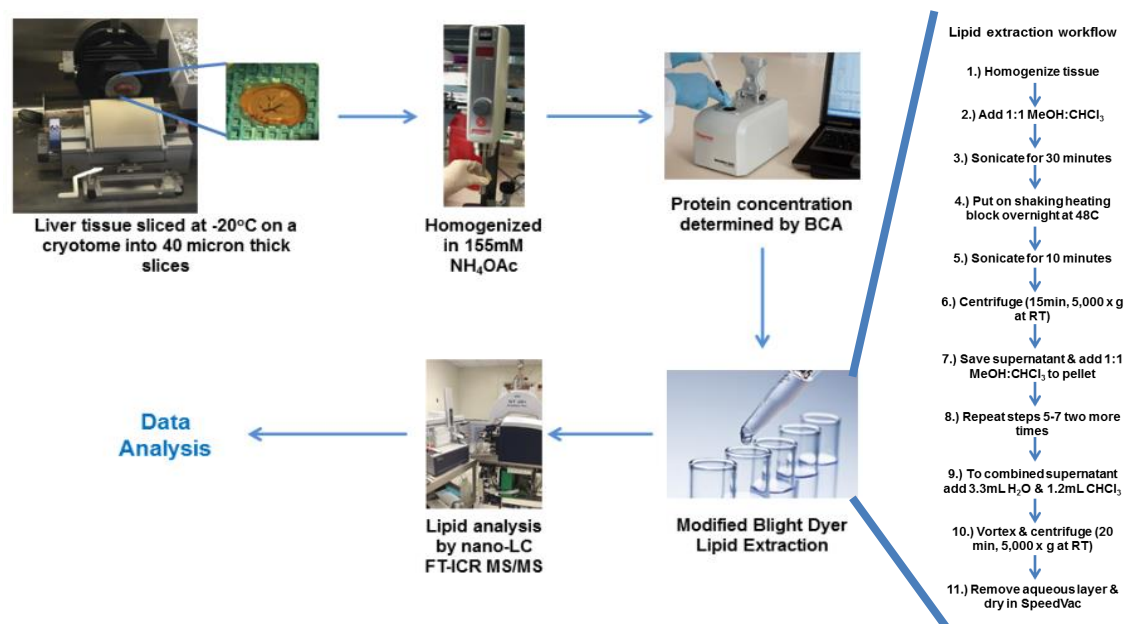


Figure 5: Lipidomic Workflow: Two 40 micron slices of liver were homogenized in 155mM ammonium acetate solution before BCA analysis. Volume corresponding to 200ug of total protein was used for lipid extraction via a modified Blight Dyer before analysis by nano-LC FT-ICR MS/MS.

## LC-MS/MS-LIPIDOMICS

For lipid analysis, chromatographic separation and mass spectrometric analysis were performed with a nano-LC chromatography system (Eksigent nanoLC 2D system) interfaced to a 12T Bruker Solarix Fourier Transform ion cyclotron resonance (FT-ICR MS) mass spectrometer. Samples were analyzed by nano-LC-MS/MS at a flow rate of 400nL/min. Samples were separated over an in-house packed 75 micron i.d. nano-LC column packed with 8 cm of Phenyl hexal resin. Five  $\mu$ L of sample was injected onto the nano-LC column (syringe fill volume is 7 $\mu$ L) and washed for 5 min with 20%/80% A/B solvent. The sample was eluted with a gradient starting at 20%/80% A/B solvent and

ramping to 1%/99% A/B solvent over 10 min. 1%/99% A/B solvent was held for 5 min to elute everything off of the column. The solvent was then stepped down immediately to 20%/80% A/B solvent and held there for 10 min to re-equilibrate the column for the next sample. The total gradient profile (load/sample wash/gradient elute/column wash/column re-equilibrate) lasted for a total of 30 mins. Solvent compositions were: Solvent A: 98% H<sub>2</sub>O, 2% MeOH, with 10mM NH<sub>4</sub>OAc. Solvent B: 98% MeOH, 2% H<sub>2</sub>O with 10mM NH<sub>4</sub>OAc)<sup>33</sup>. MS/MS was conducted at 20V collision energy. All samples were run in a block randomized order.

#### **MS DATA ANALYSIS-LIPIDOMICS**

Lipidomics data was processed via Bruker's Data Analysis 4.0. The SNAP algorithm was implemented for peak picking and charge state determination. Lipid identification was conducted by searching neutral state in the lipid maps structural database (LMSD) as well as the computationally-generated databased of 'bulk' lipid species (COMP\_DB)<sup>34</sup>. This workflow can be seen in Figure 6. Lipids of interest were then targeted for statistical analysis using a t-test to compare the respective non-irradiated control (strain & time matched) to each irradiated condition using PRISM 8 version 8.4.2.

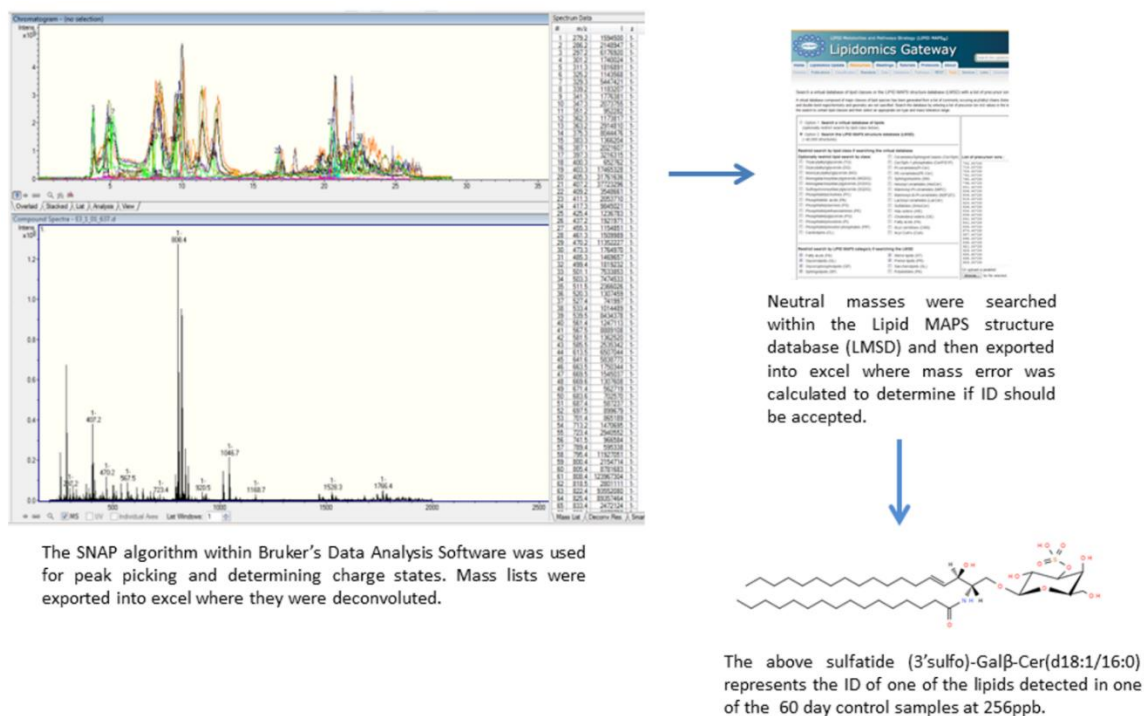


Figure 6: Lipidomic Data Analysis Workflow: The SNAP algorithm within Bruker's Data Analysis Software was used for peak picking and determining charge states. Once mass lists were deconvoluted in excel they were searched within the Lipid MAPS database to make identifications.

## METABOLOMICS

### METABOLITE EXTRACTION

Caudate livers were cut into pieces corresponding to ~10mg and placed in 1.5mL Eppendorf tubes on ice. Prior to beginning the experiment, samples were removed from ice. Three hundred  $\mu\text{L}$  of chilled 50% methanol with 30  $\mu\text{M}$  4-NBA and 4 $\mu\text{M}$  Debrisoquine sulfate was added to each sample. Samples were homogenized on ice until suspended using PowerGen-125 (Fisher Scientific, Hampton, NH). Three hundred  $\mu\text{L}$  of chilled 100% acetonitrile was added to each sample and vortexed for 10 seconds. Samples were then incubated on ice for 15 minutes before being centrifuged at 13,000

rpm for 15 minutes at 4°C. Supernatant was transferred to new tubes and dried by speed vac Vacufuge™ (Eppendorf, New York) with no heat. The pellet was resuspended in 100µL of 50% methanol for metabolomics profiling.

#### **METABOLITE PROFILING VIA MS**

Samples were analyzed on a UPLC-Xevo G2 TOFMS at a flow rate of .5mL/min. Gradient started with 95%/5% A/B and ramped to 5%/95% A/B over 8 minutes. Solvents used were A: water +0.1% formic acid B: acetonitrile+0.1% formic acid.

#### **METABOLITE DATA ANALYSIS**

Data deconvolution and normalization was completed using Progenesis Q1. Statistical analysis was completed within MetaboLyzer software. <sup>56</sup>Fe, <sup>16</sup>O and 1Gy gamma were all compared against the non-irradiated control. Metabolites were then filtered based on a FDR ≤0.1 and a fold change of 1.5 or greater. Abundance values for the metabolites of interest were then obtained from the raw data files and were graphed using PRISM 8 version 8.4.2 and t-tests were performed to compare the respective non-irradiated control (strain & time matched) to each irradiated condition.

#### **MITOCHONDRIA ANALYSIS**

##### **MITOCHONDRIA ISOLATION**

Mitochondria were isolated from four 40 micron liver slices via mitochondrial isolation kits (abcam, Cambridge, MA). Protease inhibitor was added to the isolation buffer (1:100). One mL of isolation buffer was added to each sample and homogenized on ice using a Polytron equipped with a micro-generator (10s x 1, @15,000 rpm). Homogenates were transferred to a 2mL centrifuge tube and spun at 1,000 G for 10 min at 4°C. Supernatant was transferred to a fresh tube and spun at 12,000 G for 15 min at 4°C.



Supernatant was decanted, and pellet was washed and resuspended in 500 $\mu$ L of isolation buffer. Samples were again spun at 12,000 G for 15 min at 4°C and previous step was repeated. Once pellet was resuspended in 500 $\mu$ L of isolation buffer, the process was repeated once more. The final pellet was resuspended in 200 $\mu$ L of isolation buffer and BCA was used to determine protein concentration.

#### **COMPLEX I ASSAY**

Eighty  $\mu$ g of protein was taken from each sample and brought up to a final volume of 405 $\mu$ L with isolation buffer. Two hundred  $\mu$ L was loaded on the assay plates from the Complex I Enzyme Activity Microplate Assay Kit (Colorimetric) (abcam, Cambridge, MA). Samples were run in duplicate. Plates were incubated for 3 hours at room temperature then washed with 300 $\mu$ L of 1X buffer three times. Two hundred  $\mu$ L of assay solution was added to each well and optical density was measured on a Synergy H4 Hybrid Multi-Mode Microplate Reader (BioTek) in kinetic mode at room temperature for 30mins with a reading taken every 30 seconds. Using Microsoft excel, replicates were averaged and plotted using the scatter with straight lines and markers function. Slopes were compared using analysis of covariance in R Studio<sup>35</sup> version 1.1.456. Since the results indicated that all the slopes were different the emmeans package<sup>36</sup> was then used to determine where the differences lie.

#### **REAL-TIME QUANTITATIVE PCR ANALYSIS OF MITOCHONDRIAL DNA**

Pieces of tissue about the size of a grain of rice were taken to isolate DNA from all of the samples. DNeasy Blood and Tissue Kits from Qiagen (Germantown, MD) were used to isolate DNA. One hundred eight  $\mu$ L of Buffer ATL and 20 $\mu$ L of proteinase K were added and the samples were incubated overnight at 56°C to complete tissue lysis. The following day isolation was completed following the kit protocol. Samples were then analyzed on the nanodrop spectrophotometer (Thermo Scientific) to determine

concentration and purity. Samples were ultimately diluted to a final concentration of .1ng/μl. The DNA primers used were:

The Mt CO1 primers:

Forward: 5-TGC TAG CCG CAG GCA TTA C-3

Reverse: 5-GGG TGC CCA AAG AAT CAG AAC-3

TheNDUFV1primers

Forward: 5-CTTCCCCACTGGCCTCAA G-3

Reverse: 5-CCA AAA CCC AGT GAT CCA GC-3<sup>37</sup>

A master mix of each primer was made for each plate using 250μl of H<sub>2</sub>O, 100 μl of primer, and 500 μl of iTaq Universal SYBR Green Supermix (BioRad, Hercules, CA). Samples were run in triplicate. Fifty one μl of master mix and 9μl of DNA was placed in the first well and thoroughly mixed. Twenty μl of the solution was then transferred into a second and third well. This was repeated for each sample with both sets of primers. The PCR cycle was as follows:

94<sup>0</sup>C x 10 min to initiate

40 cycles of:

94<sup>0</sup>C x 10 sec

60<sup>0</sup>C x 30 sec<sup>38</sup>

Analysis was completed using a CFX96 Real time system (BioRad) with a C1000 Touch Thermal Cycler. Replicates for each primer was averaged and the ΔCt was calculated which is equal to the counts via the nuclear primer minus the counts from the mitochondria specific primer. The ratio mtDNA/nDNA was calculated using the formula  $2^{x\Delta C_t}$ . The calculated values were graphed in Prism 6.07 and were analyzed via One-Way ANOVA at each time point for both strains. The ratio values determined by PCR were also grouped with their corresponding values from the Complex I Assay (Slope from Complex I assay/PCR ratio). These values were also graphed in Prism 6.07 and were analyzed via one-way ANOVA at each time point for both strains.

## CARDIOLIPIN ASSAY KIT

Cardiolipin Assay Kits (Fluorometric) (BioVision, Milpitas, CA) were used to determine the amount of cardiolipin present in the samples. The volume corresponding to 5µg of protein from mitochondria samples previously isolated was loaded into a well on the plate to be used as the “sample” and another aliquot containing the same amount was used as the “sample background control”. The “sample” wells were brought up to a final volume of 50µL using the reaction mix which contains 2:50 cardiolipin probe to cardiolipin buffer. The “sample background control” wells were brought up to a final volume of 100µL using the cardiolipin buffer. Plates were incubated for 10 mins and the optical density was measured on a Synergy H4 Hybrid Multi-Mode Microplate Reader (BioTek) Ex/Em 340/480nm. The “sample background control” was not higher than the 0mM reading for any of the samples, so only the 0mM reading was subtracted from the readings. Cardiolipin concentration was calculated for each sample using the equation  $C=B/V \times D$  where B is the amount of cardiolipin in the sample well from the standard curve, V is the volume of sample added into the well, and D is the dilution factor. Since our samples were not diluted, the equation used was simply  $C=B/V$ . Values were graphed in Prism 6.07 and were analyzed via one-way ANOVA at each time point for both strains.

## RESULTS/DISCUSSION

### Chapter 3 FINDINGS FROM OMICS PLATFORMS

#### TRANSCRIPTOMICS AND PROTEOMICS

The results in Table 1 represent the number of genes and proteins for each condition that were imported into IPA after undergoing differentially expression analysis and filtering as mentioned in chapter two. Results from IPA in regards to the transcriptomic dataset showed early mitochondrial effects by HZE irradiation in particularly C57 1 month  $^{16}\text{O}$  irradiated (Figure 7).

Condition	Total # of Significant Genes	Genes ↑	Genes ↓	Total # of Significant Proteins	Proteins ↑	Proteins ↓
1 mo 1 Gy C3H	135	44	91	70	31	39
1 mo 1 Gy C57	57	31	26	54	29	25
1 mo 3 Gy C3H	170	71	99	87	23	64
1 mo 3 Gy C57	89	51	38	79	24	55
1 mo Fe C3H	370	145	225	87	32	55
1 mo Fe C57	709	367	342	70	34	42
1 mo O C3H	449	228	221	64	24	40
1 mo O C57	1156	390	766	68	19	49
1 mo Si C3H	213	127	86	54	22	32
1 mo Si C57	63	48	15	48	24	24
2 mo 1 Gy C3H	397	220	177	57	28	29
2 mo 1 Gy C57	3283	2010	1273	70	25	45
2 mo 3 Gy C3H	331	146	185	47	24	23
2 mo 3 Gy C57	1903	965	938	80	20	60
2 mo Fe C3H	85	44	41	51	21	30
2 mo Fe C57	1920	1292	628	81	24	57
2 mo O C3H	90	65	25	44	19	25
2 mo O C57	1672	913	759	61	14	47
2 mo Si C3H	154	98	56	56	21	35
2 mo Si C57	113	81	32	67	19	48
4 mo 1 Gy C3H	353	150	203	64	33	31
4 mo 1 Gy C57	267	102	165	50	25	25

4 mo 3 Gy C3H	5	2	3	61	28	33
4 mo 3 Gy C57	93	34	59	44	24	20
4 mo Fe C3H	277	135	142	65	28	37
4 mo Fe C57	974	588	386	54	32	22
4 mo O C3H	18	13	5	48	15	33
4 mo O C57	787	416	371	43	24	19
4 mo Si C3H	906	629	277	89	45	44
4 mo Si C57	87	49	38	50	24	26
9 mo 1 Gy C3H	121	87	34	46	29	17
9 mo 1 Gy C57	89	64	25	50	19	31
9 mo 3 Gy C3H	509	483	26	105	66	39
9 mo 3 Gy C57	100	64	36	129	50	79
9 mo Fe C3H	984	577	407	79	35	44
9 mo Fe C57	191	163	28	76	55	21
9 mo O C3H	504	246	258	117	53	64
9 mo O C57	387	243	144	69	23	46
9 mo Si C3H	248	137	111	54	39	15
9 mo Si C57	129	79	50	63	28	35
12 mo 1 Gy C3H	21	6	15	76	32	44
12 mo 1 Gy C57	732	192	540	62	28	34
12 mo 3 Gy C3H	5	0	5	50	20	30
12 mo 3 Gy C57	223	54	169	52	30	22
12 mo Fe C3H	6	6	0	69	39	30
12 mo Fe C57	20	12	8	48	28	20
12 mo O C3H	5	5	0	73	36	37
12 mo O C57	55	42	13	46	24	22
12 mo Si C3H	67	24	43	57	24	33
12 mo Si C57	1	1	0	60	27	33

Table 1: Number of differentially expressed genes and proteins for each condition.

Gene mutations associated with mitochondrial dysfunction

- Complex I (NADH dehydrogenase)
  - NDUYF1, NDUFS1, NDUF7A, NDUF83
  - NDUFA1, NDUFB5, NDUF98
  - NDA4, NDUFA1, NDUF6A3
  - NDUFA8, NDUFAP1, NDUFB9, NDUFV2, ND1
- Complex II (Succinate dehydrogenase)
  - SQHA, SDHB, SDHC, SDHD
- Complex III (Cytochrome bc<sub>1</sub>)
  - UCOA, CY1B
- Complex IV (Cytochrome c oxidase)
  - CX3
- Other genes:
  - APP, PINK1, PRKN-1, LRRK2
  - prenatal-1, Leucodyst., DJ-1

Figure 7: Mitochondria Dysfunction occurs in transcriptomic 1 month  $^{16}\text{O}$  irradiated C57 mice. There were 46 transcripts in this pathway that were dysregulated compared to the non-irradiated control. Although this pathway did not show up in the proteomics data there are several dysregulated proteins that were relevant to mitochondria function that can be seen in the table below.

While evaluating the results from IPA, differences were noted in the pathways based on treatment at the individual time points. Venn diagrams were generated to determine how much similarity there was between the differentially expressed transcripts (Figures 8-11) and proteins (Figures 12-15). Changes in the transcriptomic data demonstrated a tighter commonality between HZE treatments than seen in the proteomics data. Figure 8, shows a fair amount of overlap for the C57 mice especially for months 1 & 2 in regards to  $^{56}\text{Fe}$  and  $^{16}\text{O}$  with 334 and 174 transcripts in common. There was also overlap between gamma irradiated and  $^{56}\text{Fe}$  and  $^{16}\text{O}$  at 2 months. Although  $^{28}\text{Si}$  is also a type of HZE irradiation, it shows very little in common with the other two HZE irradiations throughout the time course.

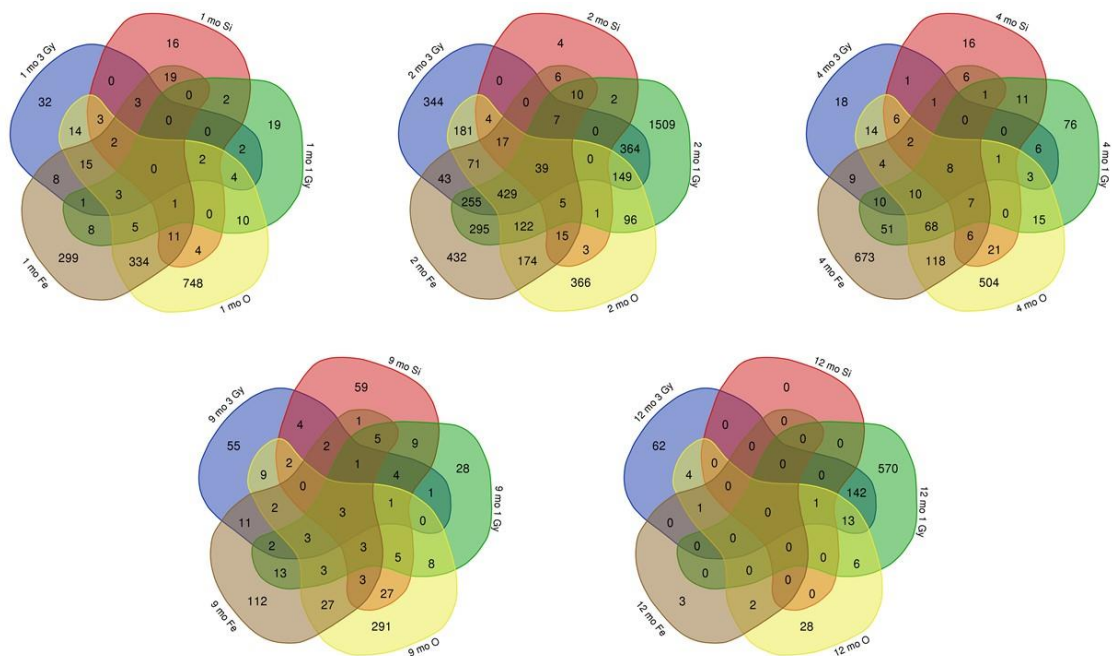


Figure 8: Venn diagrams show differentially expressed transcripts in common for each condition in the C57 mice throughout the time course.

Since  $^{56}\text{Fe}$  and  $^{16}\text{O}$  seem to be the most similar and based on the IPA results seem to have the greatest impact, further comparison of these treatments was conducted within their time points. These analysis shows that in both  $^{56}\text{Fe}$  and  $^{16}\text{O}$  there is a much greater amount of similarity in the transcripts that are being dysregulated between months 1 & 2 and months 2 & 4 as shown in Figure 9.

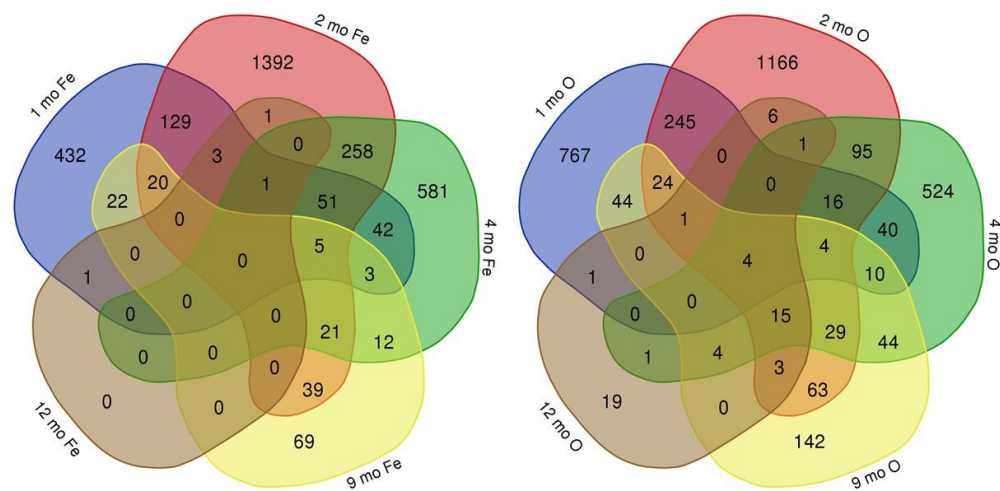


Figure 9: Venn diagrams show differentially expressed transcripts in common for each time point in the C57  $^{56}\text{Fe}$  and  $^{16}\text{O}$  irradiated mice.

Analysis of the transcriptomic data from the C3H mice (Figure 10) show similarity between  $^{56}\text{Fe}$  and  $^{16}\text{O}$  at 1 month, but very little similarity at 2 months. However, an even greater similarity is apparent between them at month 12. The gamma irradiated animals show little similarity with HZE irradiated. The analysis of how the differentially expressed transcripts were changing overtime in the  $^{56}\text{Fe}$  and  $^{16}\text{O}$  irradiated animals (Figure 11) showed different trends for these animals such as similarities between months 1 & 9 and also in months 4 & 9 for the  $^{56}\text{Fe}$  irradiated.



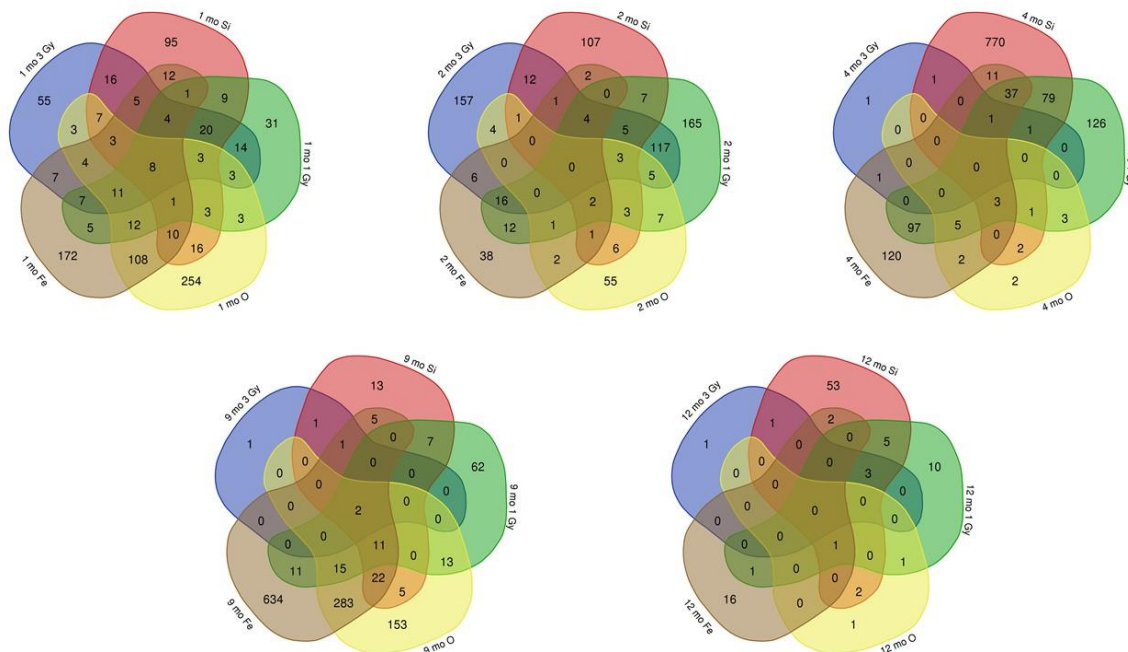


Figure 10: Venn diagrams show differentially expressed transcripts in common for each condition in the C3H mice throughout the time course.

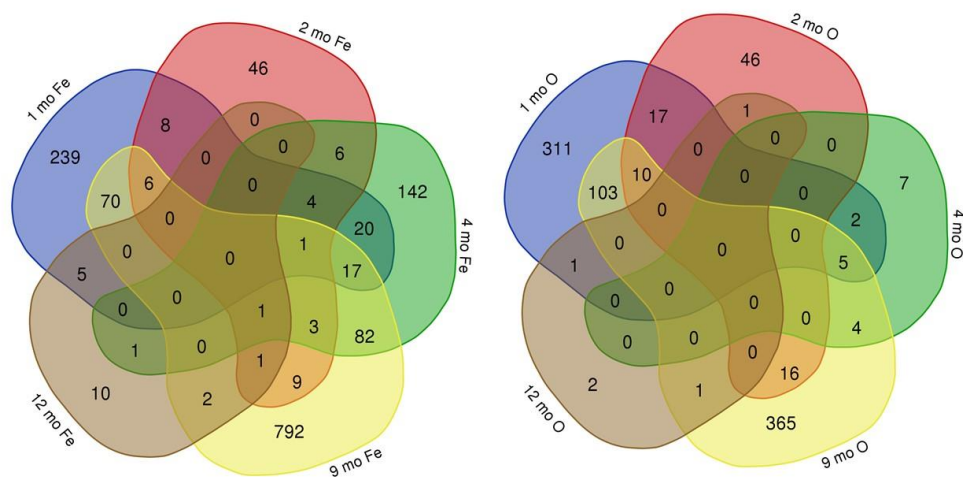


Figure 11: Venn diagrams show differentially expressed transcripts in common for each time point in the C3H  $^{56}\text{Fe}$  and  $^{16}\text{O}$  irradiated mice.

As mentioned previously, the same analysis method was used with the proteomics dataset. However, unlike the transcriptomic dataset few proteins were in common among the treatments in the C57 animals (Figure 12). Thus, focus was placed on the proteins that were in common. Table 2 shows that proteins that were in common for the different treatment groups across the different time points. **Proteins that were**

known to be involved in the mitochondria are highlighted in yellow in Tables 2-7. The elaborated descriptions found within Tables 2-7 were obtained from Uniprot. For C57, fourteen of the in common proteins were mitochondria related proteins.

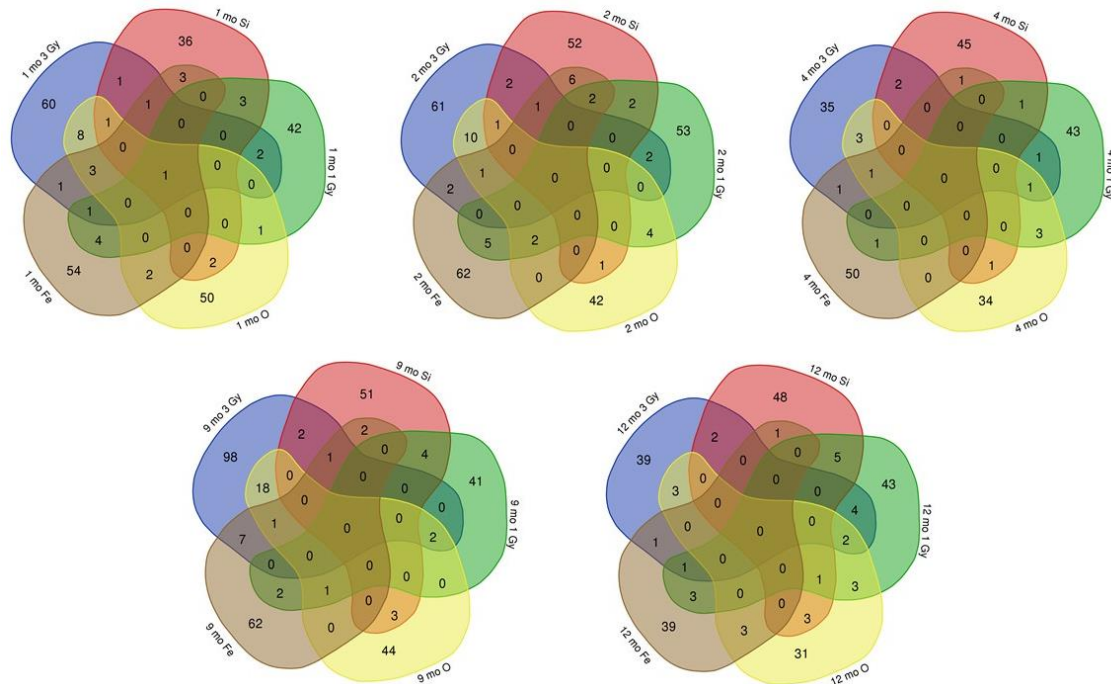


Figure 12: Venn diagrams show differentially expressed proteins in common for each condition in the C57 mice throughout the time course.

Specific Proteins that are in Common between the Conditions for C57 Mice throughout Time Course			
Conditions with proteins in common	# of proteins in common	Protein	Description
1 mo 1 Gy 1 mo 3 Gy 1 mo Fe 1 mo O 1 mo Si	1	Q3U487	E3 ubiquitin-protein ligase HECTD3
1 mo 3 Gy 1 mo O 1 mo Si	1	Q3TBY6	Uncharacterized protein
1 mo 3 Gy 1 mo Fe 1 mo Si	1	Q0VG99	Ank1 protein
1 mo 1 Gy 1 mo 3 Gy 1 mo Fe	1	D3YU39	Cholinephosphotransferase
1 mo 3 Gy 1 mo Fe 1 mo O	3	A0A125T908	Light chain kappa
		Q9CPZ6	ORM1-like protein 3-negative regulator of sphingolipid synthesis & may indirectly regulate ER-mediated Ca <sup>2+</sup> signaling

Specific Proteins that are in Common between the Conditions for C57 Mice throughout Time Course			
Conditions with proteins in common	# of proteins in common	Protein	Description
		Q8BYK6	YTH domain-containing family protein 3
1 mo 3 Gy 1 mo Si	1	Q9JHE7	Protein TSSC4
1 mo 1 Gy 1 mo 3 Gy	2	Q8JZV7	N-acetylglucosamine-6-phosphate deacetylase- Hydrolyzes the N-glycolyl group from N-glycolylglucosamine 6-phosphate (GlcNGc-6-P) in the N-glycolylneuraminic acid (Neu5Gc) degradation pathway
		Q61160	FAS-associated death domain protein-involved in initiating apoptosis & plays a role in positive regulation of interferon signaling
1 mo 3 Gy 1 mo O	8	Q61268	Apolipoprotein C-IV –may participate in lipoprotein metabolism
		Q3UKQ5	Mannose-6-phosphate receptor, cation dependent, isoform CRA_a
		Q9R0Q6	Actin-related protein 2/3 complex subunit 1A
		Q99JF8	PC4 and SFRS1-interacting protein
		Q3TCI2	Uncharacterized protein
		P62322	U6 snRNA-associated Sm-like protein LSM5-plays a role in pre-mRNA splicing
		P43406	Integrin alpha-V
		Q9D8H7	Metalloendopeptidase OMA1, mitochondrial-part of quality control system in inner membrane
1 mo 3 Gy 1 mo Fe	1	Q3TCF4	Uncharacterized protein
1 mo 1 Gy 1 mo Si	3	Q3UWG7	Uncharacterized protein
		Q8BW84	Glutamyl-tRNA(Gln) amidotransferase subunit B, mitochondrial- Allows the formation of correctly charged Gln-tRNA(Gln) through the

Specific Proteins that are in Common between the Conditions for C57 Mice throughout Time Course			
Conditions with proteins in common	# of proteins in common	Protein	Description
			transamidation of misacylated Glu-tRNA(Gln)
		Q3UCF2	MCG18249, isoform CRA_a
1 mo O 1 mo Si	2	O88876	Short-chain dehydrogenase/reductase 3
		Q3US15	NAD(P) dependent steroid dehydrogenase-like
1 mo Fe 1 mo Si	3	P56389	Cytidine deaminase
		F8VPN4	Amylo-1,6-glucosidase, 4-alpha-glucanotransferase
		Q9CX86	Heterogeneous nuclear ribonucleoprotein A0
1 mo 1 Gy 1 mo O	1	Q58EU1	Probable tRNA N6-adenosine threonylcarbamoyltransferase
1 mo 1 Gy 1 mo Fe	4	Q9JI39	ATP-binding cassette sub-family B member 10, mitochondrial-may mediate critical mito transport functions related to heme biosynthesis
		G5E823	Histidyl-tRNA synthetase-like, isoform CRA_a
		Q9WTU6	Mitogen-activated protein kinase 9
		Q8C2E7	WASH complex subunit 5
1 mo Fe 1 mo O	2	B6VGH4	Cytochrome P450
		Q5U5M8	Biogenesis of lysosome-related organelles complex 1 subunit 3
2 mo 3 Gy 2 mo O 2 mo Si	1	O89079	Coatomer subunit epsilon
2 mo 3 Gy 2 mo Fe 2 mo Si	1	A0A0R4J1H2	Glycerate kinase
2 mo 3 Gy 2 mo Fe 2 mo O	1	Q3U706	Death-associated protein
2 mo 1 Gy 2 mo Fe 2 mo Si	2	A0A0B4J1G1	Fc receptor, IgG, low affinity IIb
		Q3UBS3	Haptoglobin
2 mo 1 Gy 2 mo Fe 2 mo O	2	Q91X72	Hemopexin-binds heme and transports it to the liver for breakdown and iron recovery
		Q91Z05	Ighg protein
2 mo 3 Gy 2 mo Si	2	Q3U234	Uncharacterized protein

Specific Proteins that are in Common between the Conditions for C57 Mice throughout Time Course			
Conditions with proteins in common	# of proteins in common	Protein	Description
		Q545H3	Mitochondrial import inner membrane translocase subunit TIM17-essential component of the TIM23 complex that mediates the translocation of transit peptide-containing proteins across the inner membrane
2 mo 1 Gy 2 mo 3 Gy	2	B1AVZ0	Uracil phosphoribosyltransferase homolog
		Q3TD71	Secretory carrier-associated membrane protein
2 mo 3 Gy 2 mo O	10	Q8CGK3	Lon protease homolog, mitochondrial-ATP-dependent serine protease that mediates the selective degradation of misfolded, unassembled or oxidatively damaged polypeptides. Participates in the regulation of mito gene expression and maintenance of the integrity of the mito genome
		P00687	Alpha-amylase 1
		G3X8T2	RIKEN cDNA 5830416A07, isoform CRA_c
		A2BIN1	Major urinary protein 10
		Q543N3	LIM and SH3 protein 1, isoform CRA_b
		Q61074	Protein phosphatase 1G
		Q9D071	MMS19 nucleotide excision repair protein homolog
		Q8BXV2	BRI3-binding protein
		Q2M2Q8	Msi2h protein
		P06801	NADP-dependent malic enzyme
2 mo 3 Gy 2 mo Fe	2	P70304	Phosphoinositide 3-kinase p85alpha
		Q9CXS4	Centromere protein V
2 mo 1 Gy 2 mo Si	2	G5E8J9	SCY1-like protein 2
		Q9D2R0	Acetoacetyl-CoA synthetase
2 mo O 2 mo Si	1	Q9D8W4	MCG141777

Specific Proteins that are in Common between the Conditions for C57 Mice throughout Time Course			
Conditions with proteins in common	# of proteins in common	Protein	Description
2 mo Fe 2 mo Si	6	Q8QZR1	Tyrosine aminotransferase-involved in tyrosine breakdown. Converts tyrosine to p-hydroxyphenylpyruvate. Can catalyze the reverse reaction, using glutamic acid, with 2-oxoglutarate as cosubstrate
		Q64337	Sequestosome-1
		B7ZMP1	Probable Xaa-Pro aminopeptidase 3
		K9J7B2	UDP-glucuronosyltransferase
		E9PWG2	Trafficking protein particle complex 8
		B2RWX2	Complement component 4B (Chido blood group)
2 mo 1 Gy 2 mo O	4	A0A140LHA2	Mitotic checkpoint protein BUB3
		Q8R0J8	Probable gluconokinase
		Q8BFZ9	Erlin-2-involved in regulation of cellular cholesterol homeostasis by regulation of the SREBP signaling pathway
		Q8BQ99	Uncharacterized protein
2 mo 1 Gy 2 mo Fe	5	Q9WTX6	Cullin-1-involved in mediating the ubiquitination of proteins in cell cycle progression, signal transduction & transcription
		Q3UN47	Endonuclease G
		O55137	Acyl-coenzyme A thioesterase 1-catalyze the hydrolysis of acyl-CoAs into free fatty acids and coenzyme A
		Q58E54	Igh protein
		Q3UCJ0	Tyrosine-protein phosphatase non-receptor type
4 mo 1 Gy 4 mo 3 Gy 4 mo O	1	Q8C1E7	Transmembrane protein 120A – necessary for efficient adipogenesis
4 mo 3 Gy 4 mo Fe 4 mo O	1	Q8QZY9	Splicing factor 3B subunit 4-involved in pre-mRNA splicing

Specific Proteins that are in Common between the Conditions for C57 Mice throughout Time Course			
Conditions with proteins in common	# of proteins in common	Protein	Description
4 mo 3 Gy 4 mo Si	2	E9PZS8	Cytochrome c oxidase subunit 7A-related protein, mitochondrial
		Q925N0	Sideroflexin-5-mitochondrial amino-acid transporter. Transports citrate
4 mo 1 Gy 4 mo 3 Gy	1	Q4FK14	Translocating chain-associated membrane protein
4 mo 3 Gy 4 mo O	3	P84084	ADP-ribosylation factor 5-GTP-binding protein involved in protein trafficking; may modulate vesicle budding & uncoating within Golgi
		P49443	Protein phosphatase 1A
		O35744	Chitinase-like protein 3-lectin that binds saccharides with a free amino group (ex. Glucosamine or galactosamine). May play a role in inflammation
4 mo 3 Gy 4 mo Fe	1	Q99JX6	Annexin
4 mo 1 Gy 4 mo Si	1	B2RUC7	Serine/threonine kinase receptor associated protein
4 mo O 4 mo Si	1	P08607	C4b-binding protein
4 mo Fe 4 mo Si	1	B1AUZ1	N-alpha-acetyltransferase 10
4 mo 1 Gy 4 mo O	3	Q3TI08	Uncharacterized protein (Fragment)
		Q9CWW6	Peptidyl-prolyl cis-trans isomerase NIMA-interacting 4-involved as a ribosomal RNA processing factor in ribosome biogenesis
		Q9JIX0	Transcription and mRNA export factor ENY2
4 mo 1 Gy 4 mo Fe	1	P51885	Lumican
9 mo 3 Gy 9 mo Fe 9 mo Si	1	Q91Z05	Ighg protein
9 mo 1 Gy 9 mo 3 Gy 9 mo O	2	Q8C1E7	Transmembrane protein 120A- Necessary for efficient adipogenesis
		Q3TEA8	Heterochromatin protein 1-binding protein 3-component of heterochromatin that maintains heterochromatin integrity during

Specific Proteins that are in Common between the Conditions for C57 Mice throughout Time Course			
Conditions with proteins in common	# of proteins in common	Protein	Description
			G1/S progression & regulates duration of G1 phase. May play a role in hypoxia-induced oncogenesis
9 mo 3 Gy 9 mo Fe 9 mo O	1	E9Q0J5	Kinesin-like protein KIF21A
9 mo 1 Gy 9 mo Fe 9 mo O	1	Q9D281	Protein Noxp20
9 mo 3 Gy 9 mo Si	2	Q3TUF3	Calumenin, isoform CRA_a
		Q78HW2	RIKEN cDNA 4432406C05
9 mo 3 Gy 9 mo O	18	Q3TH57	MCG127945, isoform CRA_a
		Q9D0Q7	39S ribosomal protein L45, mitochondrial
		P63085	Mitogen-activated protein kinase 1
		Q9DAS9	Guanine nucleotide-binding protein G(I)/G(S)/G(O) subunit gamma-12
		Q8BZB2	Phosphopantothenoylecysteine decarboxylase-necessary for the biosynthesis of coenzyme A
		Q7TMB8	Cytoplasmic FMR1-interacting protein 1-may act as an invasion suppressor in cancers
		Q8R123	FAD synthase-catalyzes the adenylation of Flavin mononucleotide (FMN) to form Flavin adenine dinucleotide (FAD)
		O88325	Alpha-N-acetylglucosaminidase
		A0A1L1SRY8	39S ribosomal protein L4, mitochondrial (Fragment)
		Q811S7	Upstream-binding protein 1
		Q7TN25	Sf3a2 protein
		A0A075B5M4	Immunoglobulin kappa variable 4-57-1 (Fragment)-involved in immune response
		O88351	Inhibitor of nuclear factor kappa-B kinase subunit beta
		Q6NSU0	Fam3c protein (Fragment)-negative regulation of gluconeogenesis



Specific Proteins that are in Common between the Conditions for C57 Mice throughout Time Course			
Conditions with proteins in common	# of proteins in common	Protein	Description
		Q5M9P7	Calcium regulated heat stable protein 1
		O08915	AH receptor-interacting protein-may play a positive role in AHR-mediated (aromatic hydrocarbon receptor) signaling
		Q99J29	Carboxypeptidase
		Q78XF5	Oligosaccharyltransferase complex subunit OSTC- Subunit of the oligosaccharyl transferase (OST) complex that catalyzes the initial transfer of a defined glycan (Glc3Man9GlcNAc2 in eukaryotes) from the lipid carrier dolichol-pyrophosphate to an asparagine residue within an Asn-X-Ser/Thr consensus motif in nascent polypeptide chains, the first step in protein N-glycosylation
9 mo 3 Gy 9 mo Fe	7	Q3TPC7	Phytanoyl-CoA hydroxylase, isoform CRA_a
		Q5SWN9	Uncharacterized protein
		A0A0R4J079	Acyl-Coenzyme A binding domain containing 3, isoform CRA_b
		Q3UMR5	Calcium uniporter protein, mitochondrial-inner membrane calcium uniporter that mediates calcium uptake into the mitochondria
		Q6P6M5	Peroxisomal membrane protein 11C-promotes membrane protrusion & elongation on the peroxisomal surface
		P47856	Glutamine--fructose-6-phosphate aminotransferase [isomerizing] 1-controls the flux of glucose into the hexosamine pathway
		Q58E49	Histone deacetylase
9 mo 1 Gy 9 mo Si	4	Z4YKT6	Dehydrogenase/reductase SDR family member 7B

Specific Proteins that are in Common between the Conditions for C57 Mice throughout Time Course			
Conditions with proteins in common	# of proteins in common	Protein	Description
		Q3UPD0	Uncharacterized protein
		Q53YL1	Acyl-CoA thioesterase 3
		A1L3S6	Cytochrome P450, family 7, subfamily a, polypeptide 1
9 mo O 9 mo Si	3	Q8VDQ1	Prostaglandin reductase 2- Functions as 15-oxo-prostaglandin 13-reductase and acts on 15-keto-PGE1, 15-keto-PGE2, 15-keto-PGE1-alpha and 15-keto-PGE2-alpha with highest activity towards 15-keto-PGE2
		Q6PIP8	Igh protein
		Q4FK54	Proteaseome (Prosome, macropain) 28 subunit, 3
9 mo Fe 9 mo Si	2	Q8R1S0	Ubiquinone biosynthesis monooxygenase COQ6, mitochondrial-involved in the ubiquinone biosynthesis pathway
		Q99MZ3	Carbohydrate-responsive element-binding protein-transcriptional repressor
9 mo 1 Gy 9 mo Fe	2	O35490	Betaine--homocysteine S-methyltransferase 1-involved in regulation of homocysteine metabolism
		Q69ZX8	Actin-binding LIM protein 3
12 mo 1 Gy 12 mo 3 Gy 12 mo O	2	Q8K0G8	Epithelial splicing regulatory protein 2
		Q3UND0	Src kinase-associated phosphoprotein 2-may be involved in B-cell & macrophage adhesion processes
12 mo 1 Gy 12 mo 3 Gy 12 mo Fe	1	Q547C4	MCG131749
12 mo 1 Gy 12 mo O 12 mo Si	1	Q9D071	MMS19 nucleotide excision repair protein homolog- Key component of the cytosolic iron-sulfur protein assembly (CIA) complex, a multiprotein complex that

Specific Proteins that are in Common between the Conditions for C57 Mice throughout Time Course			
Conditions with proteins in common	# of proteins in common	Protein	Description
			mediates the incorporation of iron-sulfur cluster into apoproteins specifically involved in DNA metabolism and genomic integrity
12 mo 3 Gy 12 mo Si	2	Q921G9	Tight junction protein
		Q8BU88	39S ribosomal protein L22, mitochondrial
12 mo 1 Gy 12 mo 3 Gy	4	Q3TFA9	Uncharacterized protein
		B9EKP5	Filamin, alpha
		Q9D154	Leukocyte elastase inhibitor A-Neutrophil serine protease inhibitor that plays an essential role in the regulation of the innate immune response, inflammation and cellular homeostasis
		Q6PGC1	ATP-dependent RNA helicase DHX29-ATP-binding RNA helicase involved in translation initiation
12 mo 3 Gy 12 mo O	3	Q91X95	Guanine nucleotide binding protein, alpha 11
		Q561N4	MCG1032217
		Q60967	Bifunctional 3'-phosphoadenosine 5'-phosphosulfate synthase 1
12 mo 3 Gy 12 mo Fe	1	O08997	Copper transport protein ATOX1-Binds and deliver cytosolic copper to the copper ATPase proteins. May be important in cellular antioxidant defense
12 mo 1 Gy 12 mo Si	5	A2A977	Cytochrome P450 4A10
		O35728	Cytochrome P450 4A14-involved in metabolism of fatty acids
		Q9CPZ6	ORM1-like protein 3- Negative regulator of sphingolipid synthesis. May indirectly regulate endoplasmic reticulum-mediated Ca <sup>2+</sup> signaling
		F6TCF9	BAG family molecular chaperone regulator 1

Specific Proteins that are in Common between the Conditions for C57 Mice throughout Time Course			
Conditions with proteins in common	# of proteins in common	Protein	Description
		Q9D1M7	Peptidyl-prolyl cis-trans isomerase FKBP11-accelerate the folding of proteins during protein synthesis
12 mo O 12 mo Si	3	Q5FW60	Major urinary protein 20-male pheromone. Promotes male aggressive behavior
		Q9DBD0	Inhibitor of carbonic anhydrase
		Q8C7H1	Methylmalonic aciduria type A homolog, mitochondrial-mediates the transport of cobalamin into mitochondria for the final steps of adenosylcobalamin synthesis
12 mo Fe 12 mo Si	1	Q91ZW3	SWI/SNF-related matrix-associated actin-dependent regulator of chromatin subfamily A member 5-helicase that possesses intrinsic ATP-dependent nucleosome-remodeling activity
12 mo 1 Gy 12 mo O	3	Q925P3	CEA-related cell adhesion molecule 1
		Q91YE3	Egl nine homolog 1- Cellular oxygen sensor that catalyzes, under normoxic conditions, the post-translational formation of 4-hydroxyproline in hypoxia-inducible factor (HIF) alpha proteins. Under hypoxic conditions, the hydroxylation reaction is attenuated allowing HIFs to escape degradation resulting in their translocation to the nucleus, heterodimerization with HIF1B, and increased expression of hypoxia-inducible genes.
		Q8BFP9	[Pyruvate dehydrogenase (acetyl-transferring)] kinase isozyme 1, mitochondrial-plays key role in regulation of glucose & fatty acid

Specific Proteins that are in Common between the Conditions for C57 Mice throughout Time Course			
Conditions with proteins in common	# of proteins in common	Protein	Description
			metabolism & homeostasis via phosphorylation of the pyruvate dehydrogenase subunits PDHA1 & PDHA2. This inhibits pyruvate dehydrogenase activity, and thereby regulates metabolite flux through the tricarboxylic acid cycle, down-regulates aerobic respiration and inhibits the formation of acetyl-coenzyme A from pyruvate. Plays an important role in cellular responses to hypoxia and is important for cell proliferation under hypoxia. Protects cells against apoptosis in response to hypoxia and oxidative stress
12 mo 1 Gy 12 mo Fe	3	Q64446	Copper-transporting ATPase 2- Copper ion transmembrane transporter involved in the export of copper out of the cells, such as the efflux of hepatic copper into the bile
		Q8R1N0	Zinc finger protein 830-may play a role in pre-mRNA splicing
		D3Z0M9	DEAD (Asp-Glu-Ala-Asp) box polypeptide 23
12 mo Fe 12 mo O	3	Q80X50	Ubiquitin-associated protein 2-like- Plays an important role in the activity of long-term repopulating hematopoietic stem cells
		E9PZS8	Cytochrome c oxidase subunit 7A-related protein, mitochondrial
		B3DFI8	Cisd3 protein (Fragment)

Table 2: Shows the specific proteins that are in common between the conditions shown in the Venn Diagrams in Figure 12

When comparing C57  $^{56}\text{Fe}$  and  $^{16}\text{O}$  across their time course there was also very little similarity. For  $^{56}\text{Fe}$  there were 4 mitochondrial proteins (Table 3) in common at different time points and only one for  $^{16}\text{O}$  (Table 4).

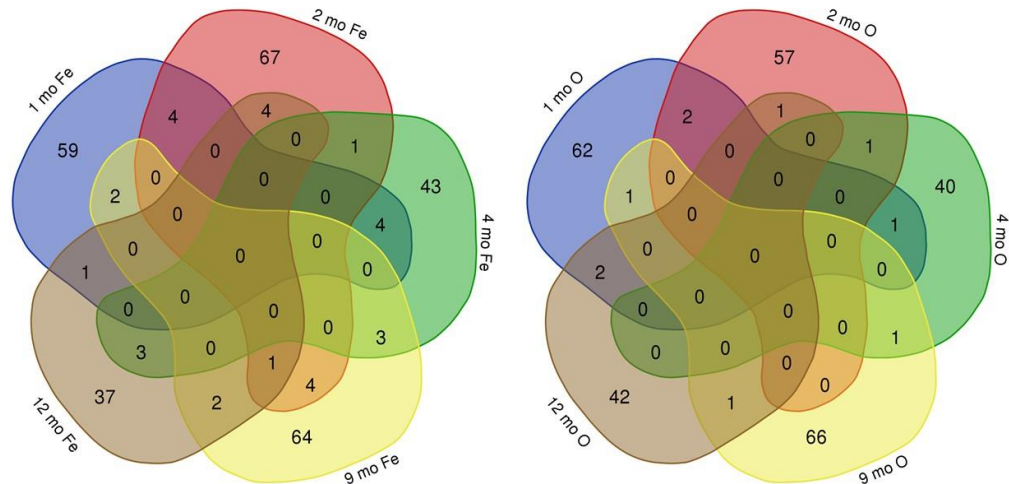


Figure 13: Venn diagrams show differentially expressed proteins in common for each time point in the C57  $^{56}\text{Fe}$  and  $^{16}\text{O}$  irradiated mice.

Proteins in Common throughout Time Course for $^{56}\text{Fe}$ Irradiated C57 Mice			
Time points with proteins in common	# of proteins in common	Protein	Description
12 mo Fe 2 mo Fe 9 mo Fe	1	Q3UMR5	Calcium uniporter protein, mitochondrial-inner membrane calcium uniporter that mediates calcium uptake into mitochondria
1 mo Fe 2 mo Fe	4	Q9WUD0	Cytochrome P450 2B10
		Q496S1	Alcohol dehydrogenase 4 (Class II), pi polypeptide
		E9PVM7	Glutathione S-transferase (Fragment)
		Q9CQM2	ER lumen protein-retaining receptor 2
1 mo Fe 4 mo Fe	4	G5E823	Histidyl-tRNA synthetase-like, isoform CRA_a mitochondrial
		Q8BYK6	YTH domain-containing family protein 3
		Q0VGY9	Ank1 protein
		Q8BZY0	Uncharacterized protein (Fragment)
1 mo Fe 9 mo Fe	2	B2RY27	MCG125789, isoform CRA_a
		Q4VAI2	Acid phosphatase 1, soluble

Proteins in Common throughout Time Course for <sup>56</sup> Fe Irradiated C57 Mice			
Time points with proteins in common	# of proteins in common	Protein	Description
1 mo Fe 12 mo Fe	1	Q9CQB2	MAPK regulated corepressor interacting protein 2
2 mo Fe 4 mo Fe	1	Q8QZR1	Tyrosine aminotransferase-transaminase involved in tyrosine breakdown. Converts tyrosine to p-hydroxyphenylpyruvate. Can catalyze the reverse reaction, using glutamic acid, with 2-oxoglutarate as cosubstrate
2 mo Fe 9 mo Fe	4	Q3U0M8	Uncharacterized protein-mitochondrial tRNA 3'-trailer cleavage
		Q5SWN9	Uncharacterized protein
		Q9QY93	dCTP pyrophosphatase 1- Hydrolyzes deoxynucleoside triphosphates (dNTPs) to the corresponding nucleoside monophosphates
		Q91Z05	Ighg protein
12 mo Fe 2 mo Fe	4	P51830	Adenylate cyclase type 9
		Q8BGG9	Acyl-coenzyme A amino acid N-acyltransferase 2-efficiently conjugates very long-chain and long-chain fatty acids to taurine
		Q58E54	Igh protein
		Q9JI78	Peptide-N(4)-(N-acetyl-beta-glucosaminyl)asparagine amidase-Specifically deglycosylates the denatured form of N-linked glycoproteins in the cytoplasm and assists their proteasome-mediated degradation
4 mo Fe 9 mo Fe	3	A2AM56	ATP-binding cassette, sub-family A (ABC1), member 8b
		O54724	Caveolae-associated protein 1
		Q5SV85	Synergism gamma-may play a role in endocytosis &/or membrane trafficking at the trans-Golgi network
12 mo Fe 4 mo Fe	3	A2ALW5	DnaJ homolog subfamily C member 25
		Q4KL81	Actin, gamma, cytoplasmic 1
		Q8QZY9	Splicing factor 3B subunit 4-involved in pre-mRNA splicing
12 mo Fe 9 mo Fe	2	G3X983	T cell activation inhibitor, mitochondrial

Proteins in Common throughout Time Course for <sup>56</sup> Fe Irradiated C57 Mice			
Time points with proteins in common	# of proteins in common	Protein	Description
		Q8CIM8	Integrator complex subunit 4

Table 3: Shows the specific proteins that are in common across the C57 <sup>56</sup>Fe irradiated time course Venn diagram found in Figure 13.

Proteins in Common throughout Time Course for <sup>16</sup> O Irradiated C57 Mice			
Time points with proteins in common	# of proteins in common	Protein	Description
1 mo O 2 mo O	2	Q4FJX4	Csrp1 protein
		O88876	Short-chain dehydrogenase/reductase 3-catalyzes the reduction of all-trans-retinal to all-trans-retinol in the presence of NADPH
1 mo O 4 mo O	1	Q3UD01	Putative ataxin-7-like protein 3B
1 mo O 9 mo O	1	Q9D1K2	V-type proton ATPase subunit F
1 mo O 12 mo O	2	Q5FWA0	Ribonuclease T2B
		Q8K0G8	Epithelial splicing regulatory protein 2-mRNA splicing factor that regulates the formation of epithelial cell-specific isoforms
2 mo O 4 mo O	1	Q3UCW0	MCG123182
12 mo O 2 mo O	1	Q9D071	MMS19 nucleotide excision repair protein homolog- Key component of the cytosolic iron-sulfur protein assembly (CIA) complex, a multiprotein complex that mediates the incorporation of iron-sulfur cluster into apoproteins specifically involved in DNA metabolism and genomic integrity.
4 mo O 9 mo O	1	Q8C1E7	Transmembrane protein 120A-necessary for efficient adipogenesis
12 mo O 9 mo O	1	Q8BFP9	[Pyruvate dehydrogenase (acetyl-transferring)] kinase isozyme 1, mitochondrial- Kinase that plays a key role in regulation of glucose and fatty acid metabolism & homeostasis via phosphorylation of the pyruvate dehydrogenase subunits PDHA1 & PDHA2. This inhibits pyruvate dehydrogenase activity, and thereby regulates metabolite flux through the tricarboxylic acid cycle, down-regulates aerobic respiration and inhibits the formation of acetyl-coenzyme A from pyruvate. Plays an important role in cellular responses to hypoxia and is important



Proteins in Common throughout Time Course for $^{16}\text{O}$ Irradiated C57 Mice			
Time points with proteins in common	# of proteins in common	Protein	Description
			for cell proliferation under hypoxia. Protects cells against apoptosis in response to hypoxia and oxidative stress

Table 4: Shows the specific proteins in common across the C57  $^{16}\text{O}$  irradiated time course shown in Figure 13.

For C3H, there is a lot more similarity especially in regards to  $^{56}\text{Fe}$  and  $^{16}\text{O}$  at 9 months (Figure 14). Of the proteins that are in common among the treatments, 19 are mitochondria related proteins (Table 5).

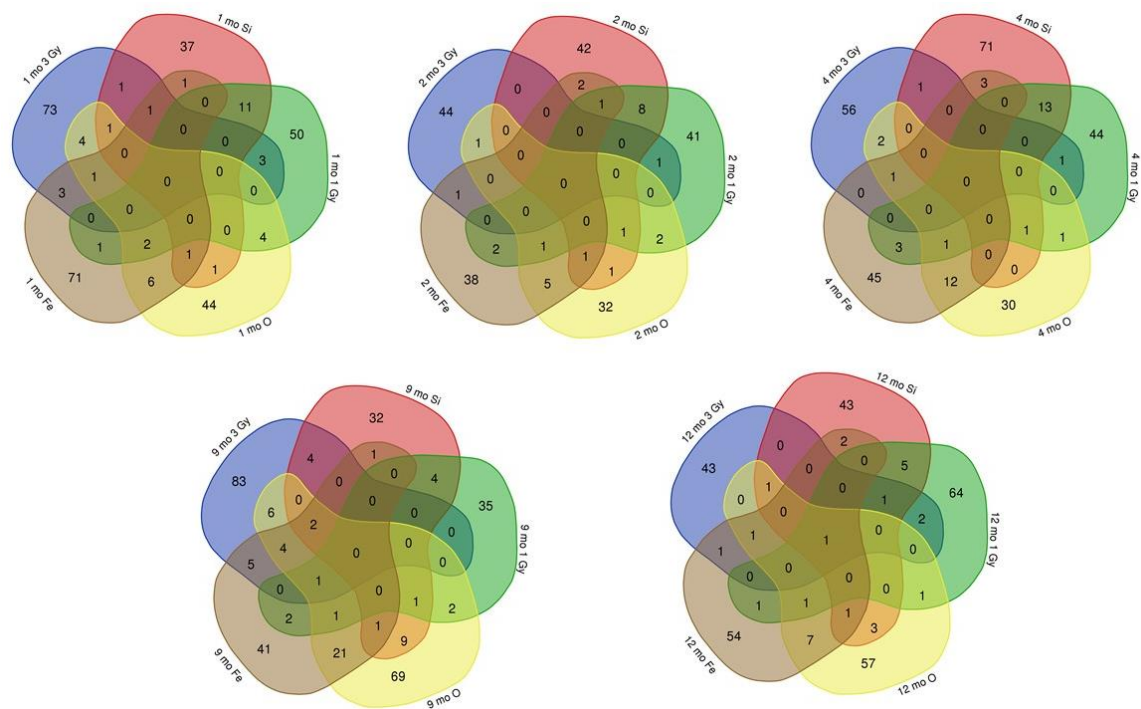


Figure 14: Venn diagrams show differentially expressed proteins in common for each condition in the C3H mice throughout the time course.

Specific Proteins that are in Common between the Conditions for C3H Mice throughout Time Course			
Conditions with proteins in common	# of proteins in common	Protein	Description
1 mo 3 Gy 1 mo O 1 mo Si	1	Q9QWG7	Sulfotransferase family cytosolic 1B member 1
1 mo 3 Gy 1 mo Fe 1 mo Si	1	Q8R1S0	Ubiquinone biosynthesis monooxygenase COQ6, mitochondrial-involved in ubiquinone biosynthesis pathway
1 mo 3 Gy 1 mo Fe 1 mo O	1	Q8QZR1	Tyrosine aminotransferase-involved in tyrosine breakdown. Converts tyrosine to p-hydroxyphenylpyruvate. Can catalyze the reverse reaction, using glutamic acid, with 2-oxoglutarate as cosubstrate
1 mo Fe 1 mo O 1 mo Si	1	Q547C4	MCG131749
1 mo 1 Gy 1 mo Fe 1 mo O	2	Q9EQI8	39S ribosomal protein L46, mitochondrial
		B6VGH4	Cytochrome P450
1 mo 3 Gy 1 mo Si	1	Q3UZZ6	Sulfotransferase 1 family member D1- Sulfotransferase with broad substrate specificity that utilizes 3'-phospho-5'-adenylyl sulfate (PAPS) as sulfonate donor to catalyze the sulfate conjugation of catecholamines, such as dopamine, prostaglandins, leukotriene E4, drugs and xenobiotic compounds
1 mo 1 Gy 1 mo 3 Gy	3	Q80TX4	MKIAA0577 protein (Fragment)
		P62869	Elongin-B
		Q8VE88	Protein FAM114A2
1 mo 3 Gy 1 mo O	4	Q9JIG7	Coiled-coil domain-containing protein 22- involved in regulation of NF-kappa-B signaling
		Q9EQ06	Estradiol 17-beta-dehydrogenase 11
		Q3TJE3	Uncharacterized protein- This protein is involved in step 1 of the subpathway that synthesizes D-glyceraldehyde 3-phosphate and glyceraldehyde phosphate from D-glucose
		Q8R1Q9	Ribokinase- Catalyzes the phosphorylation of ribose at O-5 in a reaction requiring ATP and magnesium. The resulting D-ribose-5-phosphate can then be used either for synthesis of nucleotides, histidine, and

Specific Proteins that are in Common between the Conditions for C3H Mice throughout Time Course			
Conditions with proteins in common	# of proteins in common	Protein	Description
			tryptophan, or as a component of the pentose phosphate pathway
1 mo 3 Gy 1 mo Fe	3	P56183	Ribosomal RNA processing protein 1 homolog A-plays a critical role in generation of 28S rRNA
		Q9DAC7	Tetratricopeptide repeat protein 32
		E0CZ27	Histone H3 (Fragment)
1 mo 1 Gy 1 mo Si	11	Q78IK4	MICOS complex subunit Mic27- Component of the MICOS complex, a large protein complex of the mitochondrial inner membrane that plays crucial roles in the maintenance of crista junctions, inner membrane architecture, and formation of contact sites to the outer membrane. Specifically binds to cardiolipin (in vitro) but not to the precursor lipid phosphatidylglycerol. Plays a crucial role in crista junction formation and mitochondrial function
		Q792Z1	MCG140784
		B2RRC5	RAB GTPase activating protein 1
		Q3TGG2	Ataxin-2-like protein
		Q9D0C4	tRNA (guanine(37)-N1)-methyltransferase
		E9Q4M2	Hormone-sensitive lipase
		Q3UVL4	Vacuolar protein sorting-associated protein 51 homolog
		Q3V3M3	Uncharacterized protein (Fragment)
		Q9CWV6	PRKR-interacting protein 1
		Q6YJU2	GUGU alpha
		F8WJI3	Coiled-coil domain-containing protein 58
1 mo O 1 mo Si	1	Q8BFP9	[Pyruvate dehydrogenase (acetyl-transferring)] kinase isozyme 1, mitochondrial plays key role in regulation of glucose & fatty acid metabolism & homeostasis via phosphorylation of the pyruvate dehydrogenase subunits PDHA1 & PDHA2. This inhibits pyruvate dehydrogenase activity, and thereby regulates metabolite flux through the

Specific Proteins that are in Common between the Conditions for C3H Mice throughout Time Course			
Conditions with proteins in common	# of proteins in common	Protein	Description
			tricarboxylic acid cycle, down-regulates aerobic respiration and inhibits the formation of acetyl-coenzyme A from pyruvate. Plays an important role in cellular responses to hypoxia and is important for cell proliferation under hypoxia. Protects cells against apoptosis in response to hypoxia and oxidative stress
1 mo Fe 1 mo Si	1	Q9JM13	Rab5 GDP/GTP exchange factor
1 mo 1 Gy 1 mo O	4	Q9ES74	Serine/threonine-protein kinase Nek7
		Q9DAV9	Trimeric intracellular cation channel type B- Monovalent cation channel required for maintenance of rapid intracellular calcium release
		O35295	Transcriptional activator protein Pur-beta-Has capacity to bind repeated elements in single-stranded DNA such as the purine-rich single strand of the PUR element located upstream of the MYC gene
		Q9EQ32	Phosphoinositide 3-kinase adapter protein 1- Signaling adapter that contributes to B-cell development by linking B-cell receptor (BCR) signaling to the phosphoinositide 3-kinase (PI3K)-Akt signaling pathway
1 mo 1 Gy 1 mo Fe	1	Q91Y47	Coagulation factor XI
1 mo Fe 1 mo O	6	P33587	Vitamin K-dependent protein C-regulates blood coagulation
		Q14DI6	Acyl-CoA thioesterase 4
		P60334	Cysteine dioxygenase type 1- This protein is involved in step 1 of the subpathway that synthesizes hypotaurine from L-cysteine
		Q9D323	Signal transducer and activator of transcription
		Q3UKM0	MCG21883, isoform CRA_e
		Q8CI33	CWF19-like protein 1
2 mo 1 Gy 2 mo O 2 mo Si	1	A2AS98	Nck-associated protein 1
2 mo 1 Gy 2 mo Fe 2 mo Si	1	Q3UUK3	Uncharacterized protein

Specific Proteins that are in Common between the Conditions for C3H Mice throughout Time Course			
Conditions with proteins in common	# of proteins in common	Protein	Description
2 mo Fe 2 mo O 2 mo Si	1	Q4VAA2	Protein CDV3
2 mo 1 Gy 2 mo Fe 2 mo O	1	Q8VCE7	Transmembrane emp24 protein transport domain containing 5
2 mo 1 Gy 2 mo 3 Gy	1	Q8CF02	Protein FAM25C
2 mo 3 Gy 2 mo O	1	A0A1S6GWG5	Mitochondrial ribosomal protein S9, isoform CRA_b
2 mo 3 Gy 2 mo Fe	1	Q544A1	WW domain binding protein 2
2 mo 1 Gy 2 mo Si	8	Q3U4K3	Uncharacterized protein (Fragment)
		Q52L97	Importin subunit alpha-functions in nuclear pore import
		Q6A0E4	MKIAA0025 protein (Fragment)
		Q9QYI3	DnaJ homolog subfamily C member 7- Acts as co-chaperone regulating the molecular chaperones HSP70 and HSP90 in folding of steroid receptors, such as the glucocorticoid receptor and the progesterone receptor
		A0A1B0GT81	Apoptosis regulator BAX-positive regulation of apoptotic process
		Q9JJV2	Profilin-2-binds to actin and affects the structure of the cytoskeleton
		E9PW39	Putative helicase MOV-10
		Q9D8Y1	Transmembrane protein 126A
2 mo O 2 mo Si	1	Q9D964	Glycine amidinotransferase, mitochondrial- Catalyzes the biosynthesis of guanidinoacetate, the immediate precursor of creatine
2 mo Fe 2 mo Si	2	Q99JY4	TraB domain-containing protein
		Q8CEX1	Uncharacterized protein (Fragment)-CHCH domain-containing protein-involved in mitochondrial translation
2 mo 1 Gy 2 mo O	2	Q4FK14	Translocating chain-associated membrane protein
		P14733	Lamin-B1-component of nuclear lamina, a fibrous layer on the nucleoplasmic side of the inner nuclear membrane, which is thought to provide a framework for the

Specific Proteins that are in Common between the Conditions for C3H Mice throughout Time Course			
Conditions with proteins in common	# of proteins in common	Protein	Description
			nuclear envelope & may also interact with chromatin
2 mo 1 Gy 2 mo Fe	2	F7BGR7	Predicted gene 21992
		Q8QZR1	Tyrosine aminotransferase-involved in tyrosine breakdown. Converts tyrosine to p-hydroxyphenylpyruvate. Can catalyze the reverse reaction, using glutamic acid, with 2-oxoglutarate as cosubstrate
2 mo Fe 2 mo O	5	Q9JL35	High mobility group nucleosome-binding domain-containing protein 5-preferentially binds euchromatin & modulates cellular transcription by counteracting linker histone-mediated chromatin compaction
		P47857	ATP-dependent 6-phosphofructokinase, muscle type- Catalyzes the phosphorylation of D-fructose 6-phosphate to fructose 1,6-bisphosphate by ATP, the first committing step of glycolysis.
		E9Q0J5	Kinesin-like protein KIF21A
		Q5KU03	Glycogen synthase kinase 3 beta
		A2BDX3	Adenylyltransferase and sulfurtransferase MOCS3- Plays a central role in 2-thiolation of mcm5S2U at tRNA wobble positions of cytosolic tRNA(Lys), tRNA(Glu) and tRNA(Gln)
4 mo 3 Gy 4 mo Fe 4 mo O	1	Q3UK02	39S ribosomal protein L9, mitochondrial
4 mo 1 Gy 4 mo O 4 mo Si	1	A0A0B4J1G1	Fc receptor, IgG, low affinity IIb
4 mo 1 Gy 4 mo Fe 4 mo O	1	B6VGH4	Cytochrome P450
4 mo 3 Gy 4 mo Si	1	Q3UIT2	COP9 (Constitutive photomorphogenic) homolog, subunit 6 (Arabidopsis thaliana), isoform CRA_b- Component of the COP9 signalosome complex (CSN), a complex involved in various cellular and developmental processes
4 mo 1 Gy 4 mo 3 Gy	1	Q3TQL4	MICOS complex subunit MIC60 (Fragment)- Component of the MICOS

Specific Proteins that are in Common between the Conditions for C3H Mice throughout Time Course			
Conditions with proteins in common	# of proteins in common	Protein	Description
			complex, a large protein complex of the mitochondrial inner membrane that plays crucial roles in the maintenance of crista junctions, inner membrane architecture, and formation of contact sites to the outer membrane
4 mo 3 Gy 4 mo O	2	F8WIK0	Anamorsin
		E9QQ10	A-kinase anchor protein 9
4 mo 1 Gy 4 mo Si	13	Q3TNY9	Biglycan-may be involved in collagen fiber assembly
		Q4FK25	Proteasome subunit beta type
		Q3UCW0	MCG123182
		A2RTH5	Leucine carboxyl methyltransferase 1
		Q91YR5	Methyltransferase-like protein 13
		Q14DH7	Acyl-CoA synthetase short-chain family member 3, mitochondrial-catalyzes the synthesis of acetyl-CoA from short-chain fatty acids
		Q9D7I5	Phospholysine phosphohistidine inorganic pyrophosphate phosphatase- Phosphatase that hydrolyzes imidodiphosphate, 3-phosphohistidine and 6-phospholysine
		Q6Q899	Probable ATP-dependent RNA helicase DDX58
		Q91Z05	Ighg protein
		Q8BXV2	BRI3-binding protein- Involved in tumorigenesis and may function by stabilizing p53/TP53
		A2AHQ7	Phosphorylase b kinase regulatory subunit alpha, liver isoform- catalyzes the phosphorylation of serine in certain substrates, including troponin & part of glycan biosynthesis
		A2RTI3	Legumain
		Q9CQ22	Ragulator complex protein LAMTOR1- As part of the Ragulator complex it is involved in amino acid sensing and activation of mTORC1, a signaling complex promoting cell growth in response to

Specific Proteins that are in Common between the Conditions for C3H Mice throughout Time Course			
Conditions with proteins in common	# of proteins in common	Protein	Description
			growth factors, energy levels, and amino acids
4 mo Fe 4 mo Si	3	O35841	Apoptosis inhibitor 5-antiapoptotic factor
		Q9CRA5	Golgi phosphoprotein 3-Phosphatidylinositol-4-phosphate-binding protein that links Golgi membranes to the cytoskeleton and may participate in the tensile force required for vesicle budding from the Golgi.
		O88792	Junctional adhesion molecule A-seems to play a role in epithelial tight junction formation
4 mo 1 Gy 4 mo O	1	Q6P9Q4	FH1/FH2 domain-containing protein 1-required for the assembly of F-actin structures, such as stress fibers
4 mo 1 Gy 4 mo Fe	3	E9QMC1	Cingulin
		P47857	ATP-dependent 6-phosphofructokinase, muscle type- Catalyzes the phosphorylation of D-fructose 6-phosphate to fructose 1,6-bisphosphate by ATP, the first committing step of glycolysis.
		Q8BQ99	Uncharacterized protein
4 mo Fe 4 mo O	12	Q8CDP6	Uncharacterized protein
		Q80X71	Transmembrane protein 106B- Involved in dendrite morphogenesis and maintenance by regulating lysosomal trafficking via its interaction with MAP6
		Q8R519	2-amino-3-carboxymuconate-6-semialdehyde decarboxylase- Converts alpha-amino-beta-carboxymuconate-epsilon-semialdehyde (ACMS) to alpha-aminomuconate semialdehyde (AMS). ACMS can be converted non-enzymatically to quinolate (QA), a key precursor of NAD. In the presence of ACMSD, ACMS is converted to AMS, a benign catabolite. ACMSD ultimately controls the metabolic fate of tryptophan catabolism along the kynurenine pathway



Specific Proteins that are in Common between the Conditions for C3H Mice throughout Time Course			
Conditions with proteins in common	# of proteins in common	Protein	Description
		Q60855	Receptor-interacting serine/threonine-protein kinase 1-serine-threonine kinase which is a key regulator of both cell death and cell survival
		Q9MD68	Cytochrome c oxidase subunit 1- Component of the cytochrome c oxidase, the last enzyme in the mitochondrial electron transport chain which drives oxidative phosphorylation
		Q91YM4	Protein TBRG4- Plays a role in processing of mitochondrial RNA precursors and in stabilization of a subset of mature mitochondrial RNA species, such as MT-CO1, MT-CO2, MT-CYB, MT-CO3, MT-ND3, MT-ND5 and MT-ATP8/6. May play a role in cell cycle progression
		A0ZVB6	TBP-associated factor 170
		Q9JKF7	39S ribosomal protein L39, mitochondrial
		A2AKK5	Acyl-coenzyme A amino acid N-acyltransferase 1-efficiently conjugates very long-chain and long-chain fatty acids to taurine
		A2AN08	E3 ubiquitin-protein ligase UBR4-involved in protein ubiquitination
		Q9DC71	28S ribosomal protein S15, mitochondrial
		Q9R1Z7	6-pyruvoyl tetrahydrobiopterin synthase- Involved in the biosynthesis of tetrahydrobiopterin, an essential cofactor of aromatic amino acid hydroxylases
9 mo 3 Gy 9 mo Fe 9 mo O 9 mo Si	2	Q3U711	Perilipin
		P06801	NADP-dependent malic enzyme
9 mo 1 Gy 9 mo 3 Gy 9 mo Fe 9 mo O	1	Q8C2Q3	RNA-binding protein 14
9 mo 3 Gy 9 mo Fe 9 mo O	4	Q8BT09	40S ribosomal protein S6
		Q9DBM2	Peroxisomal bifunctional enzyme-involved in fatty acid beta-oxidation pathway, which is part of lipid metabolism
		O54909	Cis-retinol androgen dehydrogenase 1- oxidoreductase with a preference for NAD

Specific Proteins that are in Common between the Conditions for C3H Mice throughout Time Course			
Conditions with proteins in common	# of proteins in common	Protein	Description
		Q3US73	Uncharacterized protein
9 mo 1 Gy 9 mo O 9 mo Si	1	Q69ZG4	MKIAA1560 protein (Fragment)
9 mo Fe 9 mo O 9 mo Si	1	Q3UKZ1	Syndecan-cell surface proteoglycan
9 mo 1 Gy 9 mo Fe 9 mo O	1	A0A075B5Y3	Immunoglobulin heavy variable 1-80 (Fragment)
9 mo 3 Gy 9 mo Si	4	Q91YM4	Protein TBRG4- Plays a role in processing of mitochondrial RNA precursors and in stabilization of a subset of mature mitochondrial RNA species, such as MT-CO1, MT-CO2, MT-CYB, MT-CO3, MT-ND3, MT-ND5 and MT-ATP8/6. May play a role in cell cycle progression
		Q3UJB0	Splicing factor 3b, subunit 2
		O55137	Acyl-coenzyme A thioesterase 1-catalyzes the hydrolysis of acyl-CoAs into free fatty acids and coenzyme A
		Q9CW79	Golgin subfamily A member 1- Involved in vesicular trafficking at the Golgi apparatus level. Involved in endosome-to-Golgi trafficking
9 mo 3 Gy 9 mo O	6	Q91XC9	Peroxisomal membrane protein PEX16- required for peroxisome membrane biogenesis
		Q8VC30	Triokinase/FMN cyclase- Catalyzes both the phosphorylation of dihydroxyacetone and of glyceraldehyde, and the splitting of ribonucleoside diphosphate-X compounds among which FAD is the best substrate
		A0A0J9YU79	Ketohexokinase
		Q8C3C9	Aldehyde dehydrogenase
		E9Q509	Pyruvate kinase- This protein is involved in step 5 of the subpathway that synthesizes pyruvate from D-glyceraldehyde 3-phosphate
		Q91VS8	FERM, RhoGEF and pleckstrin domain-containing protein 2-Functions as guanine nucleotide exchange factor that activates RAC1

Specific Proteins that are in Common between the Conditions for C3H Mice throughout Time Course			
Conditions with proteins in common	# of proteins in common	Protein	Description
9 mo 3 Gy 9 mo Fe	5	Q9D6Y9	1,4-alpha-glucan-branching enzyme- required for normal glycogen accumulation
		Q99L20	Glutathione S-transferase theta
		Q9WUD0	Cytochrome P450 2B10
		Q3UID0	SWI/SNF complex subunit SMARCC2
		Q53YP5	Fatty acid binding protein 2, intestinal
9 mo 1 Gy 9 mo Si	4	Q3UHG5	Tetraspanin
		A2AFQ0	E3 ubiquitin-protein ligase HUWE1
		Q99KI3	ER membrane protein complex subunit 3
		A0A0R4J0U2	Serine/threonine-protein phosphatase 4 regulatory subunit 2
9 mo O 9 mo Si	9	Q9JI39	ATP-binding cassette sub-family B member 10, mitochondrial-may mediate critical mitochondrial transport functions related to heme biosynthesis
		P19096	Fatty acid synthase- catalyzes the formation of long-chain fatty acids from acetyl-CoA, malonyl-CoA and NADPH
		A0A0R4J138	Arylsulfatase B
		Q91Y47	Coagulation factor XI
		E9Q0F0	Keratin 78
		Q9ET22	Dipeptidyl peptidase 2- Plays an important role in the degradation of some oligopeptides
		Q543X6	Uncharacterized protein
		Q545C7	Cysteine and glycine-rich protein 3
		Q6NSU0	Fam3c protein (Fragment)-negative regulation of gluconeogenesis
		Q00898	Alpha-1-antitrypsin 1-5
9 mo Fe 9 mo Si	1	Q00898	Alpha-1-antitrypsin 1-5
9 mo 1 Gy 9 mo O	2	Q80U95	Ubiquitin-protein ligase E3C-involved in protein ubiquitination
		Q9Z1Q2	Protein ABHD16A- mediates the hydrolysis of phosphatidylserine to generate lysophosphatidylserine (LPS). LPS constitutes a class of signaling lipids that regulates immunological and neurological processes
9 mo 1 Gy 9 mo Fe	2	Q8C3Q0	Uncharacterized protein (Fragment)
		Q9DCV1	Uncharacterized protein

Specific Proteins that are in Common between the Conditions for C3H Mice throughout Time Course			
Conditions with proteins in common	# of proteins in common	Protein	Description
9 mo Fe 9 mo O	21	Q3UP75	UDP-glucuronosyltransferase 3A1- UDP-glucuronosyltransferases catalyze phase II biotransformation reactions in which lipophilic substrates are conjugated with glucuronic acid to increase water solubility and enhance excretion
		Q3TIQ3	Uncharacterized protein (Fragment)
		A0A075B5P5	Immunoglobulin heavy constant gamma 3 (Fragment)
		A0A0U1RPV8	Thioredoxin reductase 2, mitochondrial
		P40936	Indolethylamine N-methyltransferase- plays an important role in the detoxification of selenium compounds
		Q6PIP5	NudC domain-containing protein 1
		P46425	Glutathione S-transferase P 2
		J7NNX8	Interferon-gamma-inducible GTPase Ifgga1 protein
		Q76K67	UDP-glucuronosyltransferase
		Q542V3	Serine/arginine-rich-splicing factor 4
		Q8VCU1	Carboxylesterase 3B- Involved in the detoxification of xenobiotics and in the activation of ester and amide prodrugs
		Q3UIT2	COP9 (Constitutive photomorphogenic) homolog, subunit 6 (Arabidopsis thaliana), isoform CRA_b- Component of the COP9 signalosome complex (CSN), a complex involved in various cellular and developmental processes
		Q14DI6	Acyl-CoA thioesterase 4
		P19157	Glutathione S-transferase P 1
		Q91X77	Cytochrome P450 2C50- Metabolizes arachidonic acid to several midchain and omega-terminal hydroxyeicosatetraenoic acids (HETE)
		Q5SVI6	Phosphotransferase- This protein is involved in step 1 of the subpathway that synthesizes D-glyceraldehyde 3-phosphate and glyceraldehyde phosphate from D-glucose
		Q8BV13	COP9 signalosome complex subunit 7b
		Q543J4	Thyroid hormone responsive SPOT14 homolog (Rattus), isoform CRA_c

Specific Proteins that are in Common between the Conditions for C3H Mice throughout Time Course			
Conditions with proteins in common	# of proteins in common	Protein	Description
		E9PUM4	Talin-2
		E9PYD1	Family with sequence similarity 98, member C
		Q99KV1	DnaJ homolog subfamily B member 11- As a co-chaperone for HSPA5 it is required for proper folding, trafficking or degradation of proteins
12 mo 1 Gy 12 mo 3 Gy 12 mo Fe 12 mo O 12 mo Si	1	E9PUM4	Talin-2
12 mo 1 Gy 12 mo 3 Gy 12 mo Si	1	E0CX20	Protein BUD31 homolog 1-involved in pre-mRNA splicing process
12 mo 3 Gy 12 mo O 12 mo Si	1	Q14C26	RIKEN cDNA 2900064A13, isoform CRA_b
12 mo 3 Gy 12 mo Fe 12 mo O	1	Q99MZ3	Carbohydrate-responsive element-binding-transcriptional repressor
12 mo Fe 12 mo O 12 mo Si	1	Q9BCZ4	Selenoprotein S- Involved in the degradation process of misfolded endoplasmic reticulum (ER) luminal proteins. Participates in the transfer of misfolded proteins from the ER to the cytosol, where they are destroyed by the proteasome in a ubiquitin-dependent manner
12 mo 1 Gy 12 mo Fe 12 mo O	1	A0A1B0GRA5	Stromal interaction molecule 1
12 mo 1 Gy 12 mo 3 Gy	2	Q4PJX1	Protein odr-4 homolog-may play a role in trafficking of a subset of G-protein coupled receptors
		D3YTR6	Protein spinster homolog 1
12 mo 3 Gy 12 mo Fe	1	Q9DBA6	Peroxisomal leader peptide-processing protease- Catalyzes the processing of PTS1-proteins involved in the peroxisomal beta-oxidation of fatty acids
12 mo 1 Gy 12 mo Si	5	Q3UP74	Aminopeptidase
		Q6PB44	Tyrosine-protein phosphatase non-receptor type 23- Plays a role in sorting of endocytic ubiquitinated cargos into multivesicular bodies (MVBs) via its

Specific Proteins that are in Common between the Conditions for C3H Mice throughout Time Course			
Conditions with proteins in common	# of proteins in common	Protein	Description
			interaction with the ESCRT-I complex (endosomal sorting complex required for transport I), and possibly also other ESCRT complexes
		Q5BLK4	Terminal uridylyltransferase 7
		Q8K223	Ercc2 protein
		Q5DU67	MFLJ00088 protein (Fragment)
12 mo O 12 mo Si	3	A0A1S6GWG9	Alpha-mannosidase
		Q8BIG7	Catechol O-methyltransferase domain-containing protein 1
		D3Z7Q5	Programmed cell death protein 5
12 mo Fe 12 mo Si	2	P31532	Serum amyloid A-4 protein-Apolipoprotein of the HDL complex
		Q99N87	28S ribosomal protein S5, mitochondrial
12 mo 1 Gy 12 mo O	1	A0A1Y7VJM4	ERO1-like beta (S. cerevisiae)
12 mo 1 Gy 12 mo Fe	1	Q9D964	Glycine amidinotransferase, mitochondrial- Catalyzes the biosynthesis of guanidinoacetate, the immediate precursor of creatine
12 mo Fe 12 mo O	7	C7G3P2	MKIAA0536 protein (Fragment)
		Q541E3	Peripheral-type benzodiazepine receptor (Fragment)- Can bind protoporphyrin IX and may play a role in the transport of porphyrins and heme
		F8VQ28	Paxillin-cytoskeletal protein involved in actin-membrane attachment at sites of cell adhesion to the extracellular matrix
		B2RUM8	RNA helicase
		Q5U458	DnaJ homolog subfamily C member 11- Required for mitochondrial inner membrane organization. Seems to function through its association with the MICOS complex and the mitochondrial outer membrane sorting assembly machinery (SAM) complex
		Q9EQ06	Estradiol 17-beta-dehydrogenase 11
		A0A0G2JFT8	Protein RUFY3

Table 5: Shows the specific proteins that are in common in the C3H Venn Diagrams found in figure 14.

Analysis of the similarities across the time course for  $^{56}\text{Fe}$  and  $^{16}\text{O}$  (Figure 15) showed a low number of proteins in common across the time points. Of those that were in common only one was mitochondria related in  $^{56}\text{Fe}$  and four were mitochondria related in  $^{16}\text{O}$ .

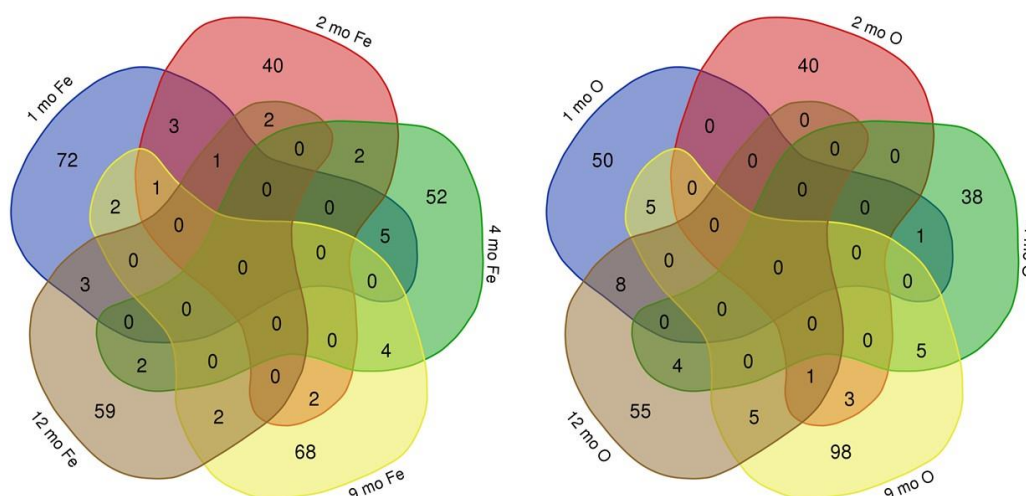


Figure 15: Venn diagrams show differentially expressed proteins in common for each time point in the C3H  $^{56}\text{Fe}$  and  $^{16}\text{O}$  irradiated mice.

Proteins in Common throughout Time Course for $^{56}\text{Fe}$ Irradiated C3H Mice			
Time points with proteins in common	# of proteins in common	Protein	Description
1 mo Fe 2 mo Fe 9 mo Fe	1	Q8BV13	COP9 signalosome complex subunit 7b-involved in ubiquitin conjugation pathway
1 mo Fe 12 mo Fe 2 mo Fe	1	Q8R155	cDNA sequence BC025446
1 mo Fe 2 mo Fe	3	Q80TM9	Nischarin
		Q8QZR1	Tyrosine aminotransferase-involved in tyrosine breakdown. Converts tyrosine to p-hydroxyphenylpyruvate. Can catalyze the reverse reaction, using glutamic acid, with 2-oxoglutarate as cosubstrate
		Q4VAA2	Protein CDV3
1 mo Fe 4 mo Fe	5	Q3TFA9	Uncharacterized protein
		Q3UFP6	Eif4ebp2 protein

Proteins in Common throughout Time Course for <sup>56</sup> Fe Irradiated C3H Mice			
Time points with proteins in common	# of proteins in common	Protein	Description
		B7ZWC4	Insulin-like growth factor 2 receptor
		G5E823	Histidyl-tRNA synthetase-like, isoform CRA_a, mitochondrial
		B6VGH4	Cytochrome P450
1 mo Fe 9 mo Fe	2	Q14DI6	Acyl-CoA thioesterase 4
		Q9JJV2	Profilin-2-binds to actin & affects the structure of the cytoskeleton
1 mo Fe 12 mo Fe	3	P41233	ATP-binding cassette sub-family A member 1
		A0A0R4J065	Cysteine protease-required for the cytoplasm to vacuole transport & autophagy
		Q99PC9	Protein phosphatase 2 regulatory subunit B56 delta isoform
2 mo Fe 4 mo Fe	2	Q8K4F5	Protein ABHD11
		P47857	ATP-dependent 6-phosphofructokinase, muscle type- Catalyzes the phosphorylation of D-fructose 6-phosphate to fructose 1,6-bisphosphate by ATP, the first committing step of glycolysis
2 mo Fe 9 mo Fe	2	Q3TWW4	AP-2 complex subunit mu
		Q3US15	NAD(P) dependent steroid dehydrogenase-like
12 mo Fe 2 mo Fe	2	Q0PD39	Rab17
		P31532	Serum amyloid A-4 protein-apolipoprotein of the HDL complex
4 mo Fe 9 mo Fe	4	Q3U711	Perilipin
		Q3TV38	Uncharacterized protein
		Q8VDK4	Cadherin 13
		A0A087WNZ7	E3 ubiquitin-protein ligase TRIP12
12 mo Fe 4 mo Fe	2	Q8CH18	Cell division cycle and apoptosis regulator protein 1
		E9QP99	Golgin subfamily A member 3
12 mo Fe 9 mo Fe	2	E9PUM4	Talin-2
		A0A1B0GRA5	Stromal interaction molecule 1

Table 6: Shows the specific proteins that are in common in C3H <sup>56</sup>Fe irradiated time course from Venn Diagrams found in Figure 15.



Proteins in Common throughout Time Course for <sup>16</sup> O Irradiated C3H Mice			
Time points with proteins in common	# of proteins in common	Protein	Description
12 mo O 2 mo O 9 mo O	1	Q3UYX6	Uncharacterized protein
1 mo O 4 mo O	1	B6VGH4	Cytochrome P450
1 mo O 9 mo O	5	Q9DBM2	Peroxisomal bifunctional enzyme-involved in the fatty acid beta-oxidation pathway, which is part of lipid metabolism
		A0A075B5P5	Immunoglobulin heavy constant gamma 3 (Fragment)
		Q8BI72	CDKN2A-interacting protein-regulates DNA damage response & cell proliferation in a dose-dependent manner through a number of signaling pathways involved in cell proliferation, apoptosis & senescence
		Q14DI6	Acyl-CoA thioesterase 4
		Q547C4	MCG131749
1 mo O 12 mo O	8	Q5U458	DnaJ homolog subfamily C member 11- Required for mitochondrial inner membrane organization. Seems to function through its association with the MICOS complex and the mitochondrial outer membrane sorting assembly machinery (SAM) complex
		Q6P6M5	Peroxisomal membrane protein 11C- promotes membrane protrusion & elongation on the peroxisomal surface
		Q9DAV9	Trimeric intracellular cation channel type B- monovalent cation channel required for maintenance of rapid intracellular calcium release
		A0A1S6GWG9	Alpha-mannosidase
		B1AU75	Nuclear autoantigenic sperm protein
		Q9EQ06	Estradiol 17-beta-dehydrogenase 11
		E9QMC1	Cingulin
		P59266	Fat storage-inducing transmembrane protein 2- Plays an important role in the formation of lipid droplets (LDs) which are storage organelles at the center of lipid and energy homeostasis
2 mo O 9 mo O	3	Q3UKZ1	Syndecan-cell surface proteoglycan
		Q99LZ4	Mrps23 protein (Fragment)

Proteins in Common throughout Time Course for <sup>16</sup> O Irradiated C3H Mice			
Time points with proteins in common	# of proteins in common	Protein	Description
		Q4FK14	Translocating chain-associated membrane protein
4 mo O 9 mo O	5	Q3UK02	39S ribosomal protein L9, mitochondrial
		F8WIK0	Anamorsin
		A2AKK5	Acyl-coenzyme A amino acid N-acyltransferase 1- efficiently conjugates very long-chain and long-chain fatty acids to taurine
		A0A0B4J1G1	Fc receptor, IgG, low affinity IIb
		Q6A029	MKIAA0639 protein (Fragment)
12 mo O 4 mo O	4	Q91YM4	Protein TBRG4- Plays a role in processing of mitochondrial RNA precursors and in stabilization of a subset of mature mitochondrial RNA species, such as MT-CO1, MT-CO2, MT-CYB, MT-CO3, MT-ND3, MT-ND5 and MT-ATP8/6. May play a role in cell cycle progression
		Q9D967	Magnesium-dependent phosphatase 1
		A0A1Y7VM56	NAD-dependent protein deacylase sirtuin-5, mitochondrial- NAD-dependent lysine demalonylase, desuccinylase and deglutarylase that specifically removes malonyl, succinyl and glutaryl groups on target proteins.
		A0A0G2JFT8	Protein RUFY3
12 mo O 9 mo O	5	B2RY19	Cgnl1 protein
		A0A0R4J0S1	Cdc42 effector protein 1
		B2RVQ1	Transmembrane protein 147
		E9PUM4	Talin-2
		Q71FD5	E3 ubiquitin-protein ligase ZNRF2-involved in protein ubiquitination pathway

Table 7: Shows the specific proteins in common for C3H <sup>16</sup>O irradiated time course found in Figure 15.

Although the data showed solid mitochondrial effects in the transcriptomic data in IPA, the proteomics did not demonstrate a strong correlation with these findings. Based on previous studies in the literature utilizing SWATH, the proteomic data was on par with other published studies. Aebersold's lab<sup>39</sup> quantified over 2,000 proteins in the liver using

this technique while Gao et al.<sup>40</sup> quantified 4,216 proteins with 338 being differentially expressed in HCC tissue compared to adjacent non-tumorous tissue. Our study quantified ~3,200 proteins.

The advancements in technology over the last couple decades have made it possible to track and monitor the inner workings of the cell by accessing their mRNA and proteins levels.<sup>41</sup> Originally, it was believed that there would be direct correlation between mRNA transcripts and generated protein expression and that they would mirror one another. However, studies have shown that correlation can be low due to factors such as different half-lives and post transcription machinery. Physical properties of a transcript can also have a great impact on the translational efficiency and thus will affect the correlation between transcripts and proteins. A good example of this is the Shine-Dalgarno sequence found in prokaryotic transcripts. Those that have a weak sequence are translated much less efficiently whereas those with a strong sequence are translated much more efficiently. Mutations can also affect the efficiencies of these types of sequences. Also, mRNA that has entered the ribosome for translation has much better correlation with the protein expression than those that have not. If a cell is in the process of going through the cell cycle, it can also result in variable mRNA levels that could affect correlation. In this case, the correlation is actually higher. As far as half-lives are concerned, the average half-life of eukaryotic mRNA is reported to be 10-20 hours whereas in eukaryotic proteins the average is reported to be 48-72 hours. Post-translational modifications such as phosphorylation and ubiquitination as well as protein localization also create variability of half-lives in proteins.<sup>42</sup> The protein may also have to interact with other proteins in order to become effective. Thus, because of all the complexities involved with proteins, they will lag behind the mRNA data. Some studies have shown that only the most abundant proteins have good correlation with mRNA levels.<sup>43</sup> Thus, while the data sets do not mirror the same in the transcriptomics and proteomics due to the lag time that is known to exist, similar mitochondria affects are still expected at later time points

especially since mitochondrial dysfunction was one of the most prominent pathways identified.

After discovering that mitochondria dysfunction was one of the prominent effects caused by HZE irradiation, the proteomic coverage was evaluated to see how good it was in regards to collecting data on membrane bound proteins, specifically mitochondria proteins since a vast majority of these proteins are membrane bound. Thus, the entire proteomic dataset without any filtering for some of the conditions was imported into IPA to evaluate what types of proteins were in the data set. For the datasets examined, mitochondria dysfunction was found to be one of the most prevalent pathways ranking as the second top pathway. As seen in Figure 16, 98 proteins were found out of 171 that are within the mitochondria dysfunction pathway. The same was found at 1 month  $^{56}\text{Fe}$  irradiated as well as 2 month  $^{56}\text{Fe}$  and  $^{16}\text{O}$  irradiated. The proteomics data contained numerous mitochondria proteins as seen in Figure 16 and identified multiple mitochondria proteins in common among treatments in Tables 2-7.

Further analysis of the differentially expressed proteins were performed manually and showed dysregulation of mitochondria related proteins. Table 8 gives an example of some of the mitochondria related proteins that were found in C57 1month  $^{16}\text{O}$  irradiated.



Figure 16: The entire proteomics list for 1 month <sup>16</sup>O irradiated in order to determine the coverage of mitochondrial proteins.

It was proposed, filters could have simply been too stringent to witness some of the changes that were occurring within the mitochondrial proteins as up until this point a fold change filter of 1.5 or greater had been used. Using the full proteomic data files that had been imported into IPA for coverage analysis, we tried filtering within IPA using less stringent fold change conditions including 1.2, 1.15, and 1.1. After evaluation, a fold change of  $\geq 1.15$  was selected for the proteomics data set. From here on, the proteomics data discussed will be with the 1.15 applied fold change instead of the original 1.5 fold change. Table 9 shows the number of proteins found within the mitochondria dysfunction pathway after utilizing these new conditions along with the number of differentially expressed transcripts still using the original conditions. The table also includes the names of proteins and transcripts that were dysregulated within this pathway. It is important to note that conditions were only included in this table if the mitochondria dysfunction pathway was detected in either the transcriptomic or proteomic data set for the specific condition.

Dysregulated Proteins in 1 month <sup>16</sup> O irradiated C57 Mice liver Relevant to Mitochondria Function and Specific Metabolites			
ID	Group	Function	Directionality vs non-irradiated
Q9D8H7	Metalloendopeptidase OMA1, mitochondrial	Metalloprotease essential to quality control system in the inner membrane of mitochondria. Essential for regulating lipid metabolism.	down; also down in 3 Gy
B6VGH4	Cytochrome P450	Iron binding, heme binding, oxidoreductase activity, transfer electrons from NADPH to P450.	down; also down in Fe
Q9CXI0	2-methoxy-6-polyprenyl-1,4-benzoquinol methylase, mitochondrial	Protein involved in ubiquinone biosynthesis, which is a redox-active lipid that participates in several cellular	down

Dysregulated Proteins in 1 month <sup>16</sup> O irradiated C57 Mice liver Relevant to Mitochondria Function and Specific Metabolites			
ID	Group	Function	Directionality vs non-irradiated
		processes. It has a central role in mitochondrial electron transport and the production of ROS. Reduced ubiquinone (ubiquinol) is a potent antioxidant.	
Q9JKF7	39S ribosomal protein L39, mitochondrial	Component of the mitochondrial ribosome large subunit (39S).	down
Q8C5Q4	G-rich sequence factor 1	Regulator of post-transcriptional mitochondrial gene expression, required for assembly of the mitochondrial ribosome and for recruitment of mRNA and lncRNA.	down
Q4FJX4	Csrp1 protein	Metal ion binding	down
Q91WS0	CDGSH iron-sulfur domain-containing protein 1	Plays a key role in regulating maximal capacity for electron transport and oxidative phosphorylation.	down
Q9WTL7	Acyl-protein thioesterase 2	Converts oxidized 2-AG to prostaglandins	up
Q8VDP4	Cell cycle and apoptosis regulator protein	Protein critical for maintaining mitochondrial homeostasis in response to stress. Inhibits SIRT1 deacetylase activity leading to increasing levels of p53/TP53 acetylation and p53-mediated apoptosis	up
Q9JL8	Serine--tRNA ligase, mitochondrial	Catalyzes the attachment of serine to tRNA(Ser). Is also probably able to aminoacylate tRNA(Sec) with serine, to form the misacylated tRNA L-seryl-tRNA(Sec), which will be further converted into selenocysteinyl-tRNA(Sec)	up
G3UVW1	Mpv17 transgene, kidney disease mutant, isoform	Mitochondrial genome maintenance	up
P62073	Mitochondrial import inner membrane translocase subunit Tim10	Mitochondrial intermembrane chaperone that participates in the import and insertion of multi-pass transmembrane proteins into the mitochondrial inner membrane.	up

Table 8: This table is representative of dysregulated proteins in 1 month <sup>16</sup>O irradiated mice liver that are relevant to mitochondria function and specific metabolites. All but two of these proteins are unique to <sup>16</sup>O irradiated. One is also seen in <sup>56</sup>Fe irradiated and the other in 3 Gy gamma irradiated mice.

Number of Transcripts/Proteins within the Mitochondria Dysfunction Pathway for each Condition and Names of Dysregulated Transcripts/Proteins				
Conditions with Mitochondria Dysfunction Pathway Effected	Number of transcripts in the pathway	Dysregulated transcripts within pathway	Number of proteins in the pathway	Dysregulated proteins within pathway
1 mo O C57	46	aconitase 2, ATP synthase (H <sup>+</sup> transporting mito F1 complex epsilon subunit, F1 subunit alpha beta & gamma, membrane subunit F, & peripheral stalk subunit OSCP), cytochrome c oxidase (subunit411, 6C, 7A2 like), carnitine palmitoyltransferase 1A, cytochrome c1, glutathione peroxidase 4, glutathione-disulfide reductase, cytochrome b, MTND2, NADH dehydrogenase subunits 4, 5 & 6 (complex I), NADH:ubiquinone oxidoreductase subunits A9, A10, A11, A13, B3, B4, B9, core subunit V1 & V2, pyruvate dehydrogenase E1 alpha 1 subunit, PTEN induced putative kinase 1, peroxiredoxin 3 & 5, succinate dehydrogenase complex iron sulfur subunit B, subunit C, & subunit D, superoxide dismutase 2, ubiquinol-cytochrome c reductase complex III subunit X, core protein 1, core protein 2 & Rieske iron-sulfur polypeptide 1, voltage dependent anion channel 1 & 2	8	ATP synthase membrane subunit f, catalase, NADH dehydrogenase subunit 1 (complex I), NADH:ubiquinone oxidoreductase subunit V3, peroxiredoxin 3, synuclein alpha, SURF1 cytochrome c oxidase assembly factor, xanthine dehydrogenase
1 mo Fe C57	9	ATP synthase F1 subunit gamma, carnitine palmitoyltransferase 1A, cytochrome b, NADH dehydrogenase subunit 1, 4, 5 & 6 (complex I), MTND2, NADH:ubiquinone oxidoreductase subunit B4	0	



Number of Transcripts/Proteins within the Mitochondria Dysfunction Pathway for each Condition and Names of Dysregulated Transcripts/Proteins				
Conditions with Mitochondria Dysfunction Pathway Effected	Number of transcripts in the pathway	Dysregulated transcripts within pathway	Number of proteins in the pathway	Dysregulated proteins within pathway
1 mo Si C57	3	cytochrome b, MTND2, NADH dehydrogenase subunit 6 (complex I)	6	ATP synthase F1 subunit delta, catalase, mitogen-activated protein kinase 9, NADH dehydrogenase subunit 4(complex I), nicastrin, ras homolog family member T2
1 mo 3Gy C57	0		7	ATP synthase membrane subunit f, catalase, NADH dehydrogenase subunit 1 (complex I), MTND2, NADH dehydrogenase subunit 4 (complex I), peroxiredoxin 3, synuclein alpha
1 mo 3Gy C3H	5	cytochrome b, MTND2, NADH dehydrogenase subunit 4, 5 & 6 (complex I)	0	
1 mo 1Gy C3H	7	cytochrome c oxidase subunit 1, cytochrome b, NADH dehydrogenase subunit 1, 4, 5 & 6 (complex I) MTND2	7	ATP synthase membrane subunit f, catalase, cytochrome c oxidase subunit 7A2 like, monoamine oxidase A, NADH

Number of Transcripts/Proteins within the Mitochondria Dysfunction Pathway for each Condition and Names of Dysregulated Transcripts/Proteins				
Conditions with Mitochondria Dysfunction Pathway Effected	Number of transcripts in the pathway	Dysregulated transcripts within pathway	Number of proteins in the pathway	Dysregulated proteins within pathway
				dehydrogenase subunit 4 (complex I), nicastrin, SURF1 cytochrome c oxidase assembly factor
2 mo O C57	37	ATP synthase (H <sup>+</sup> transporting mito F1 complex epsilon subunit, F1 subunit alpha beta, gamma & delta, membrane subunit c locus 1 membrane subunit F & G, & peripheral stalk subunit OSCP & D), cytochrome c oxidase (subunit4I1, 6B1, 6C, 7B, & 8A), carnitine palmitoyltransferase 1A, cytochrome c1, glutathione peroxidase 4, glutathione-disulfide reductase, leucine rich repeat kinase 2, NADH dehydrogenase subunits 4 (complex I), NADH:ubiquinone oxidoreductase subunits A1, A2, A6, A8, A9, A10, A12, A13, B4, B7, B9, B11, S4, V3 core subunit S2 V1 & V2, oxoglutarate dehydrogenase, PTEN induced putative kinase 1, peroxiredoxin 3 & 5, parkin RBR E3 ubiquitin protein ligase, succinate dehydrogenase complex iron sulfur subunit B, subunit C, & subunit D, ubiquinol-cytochrome c reductase complex III subunit X, core protein 2 & Rieske iron-sulfur polypeptide 1, voltage dependent anion channel 1	10	ATP synthase membrane subunit f, catalase, cytochrome c oxidase subunit 7A2 like, mitogen-activated protein kinase 4, mitogen-activated protein kinase 9, NADH:ubiquinone oxidoreductase subunit A11, NADH:ubiquinone oxidoreductase complex assembly factor 1, NADH:ubiquinone oxidoreductase subunit B6, peroxiredoxin 3, thioredoxin reductase 2

Number of Transcripts/Proteins within the Mitochondria Dysfunction Pathway for each Condition and Names of Dysregulated Transcripts/Proteins				
Conditions with Mitochondria Dysfunction Pathway Effected	Number of transcripts in the pathway	Dysregulated transcripts within pathway	Number of proteins in the pathway	Dysregulated proteins within pathway
2 mo Fe C57	19	aph-1 homolog B gamma-secretase subunit, ATP synthase F1 subunit gamma, ATP synthase membrane subunit g, ATP synthase peripheral stalk subunit OSCP, cytochrome c oxidase copper chaperone COX17, cytochrome c oxidase subunit 4I1, cytochrome c oxidase subunit 6C, glutathione peroxidase 4, leucine rich repeat kinase 2, cytochrome b, NADH dehydrogenase subunit 4 (complex I), NADH:ubiquinone oxidoreductase subunits A1, A2, B2, B4, B9, & core subunit V2, synuclein alpha & ubiquinol-cytochrome c reductase binding protein	0	
2 mo O C3H	6	Cytochrome b, NADH dehydrogenase subunit 1, 4, 5 & 6 (complex I) MTND2	0	
2 mo Si C3H	4	NADH dehydrogenase subunit 1, 4 & 6 (complex I), MTND2	0	

Number of Transcripts/Proteins within the Mitochondria Dysfunction Pathway for each Condition and Names of Dysregulated Transcripts/Proteins				
Conditions with Mitochondria Dysfunction Pathway Effected	Number of transcripts in the pathway	Dysregulated transcripts within pathway	Number of proteins in the pathway	Dysregulated proteins within pathway
2 mo 3Gy C57	26	ATP synthase (H <sup>+</sup> transporting mito F1 complex epsilon subunit, F1 subunit gamma & delta, membrane subunit F & G, & peripheral stalk subunit OSCP), cytochrome c oxidase (subunit4I1, 6C, 7A2 like, & 8A), carnitine palmitoyltransferase 1A, cytochrome c1, glutathione peroxidase 4, glutathione-disulfide reductase, cytochrome b, NADH dehydrogenase subunits 1,4,5 & 6 (complex I), MTND2, NADH:ubiquinone oxidoreductase subunits A2, A6, A9, A13, B2, B9, core subunit S2, S7 & V1, PTEN induced putative kinase 1, peroxiredoxin 5, parkin RBR E3 ubiquitin protein ligase, succinate dehydrogenase complex subunit C & D, ubiquinol-cytochrome c reductase complex III subunit X & XI & Rieske iron-sulfur polypeptide 1	0	
4 mo O C57	11	ATP synthase membrane subunit f, ATP synthase peripheral stalk subunit OSCP, cytochrome c oxidase subunit 5A & 6B1, NADH:ubiquinone oxidoreductase subunit A3, A7, A11, A12 & S6, thioredoxin 2, ubiquinol-cytochrome c reductase complex III subunit X	0	
4 mo 3Gy C57	6	cytochrome c oxidase subunit 5A & I, cytochrome b, MTND2, NADH dehydrogenase subunit 4 & 5 (complex I)	0	

Number of Transcripts/Proteins within the Mitochondria Dysfunction Pathway for each Condition and Names of Dysregulated Transcripts/Proteins				
Conditions with Mitochondria Dysfunction Pathway Effected	Number of transcripts in the pathway	Dysregulated transcripts within pathway	Number of proteins in the pathway	Dysregulated proteins within pathway
4 mo 1Gy C57	0		6	caspase 8, NADH dehydrogenase subunit 4 (complex I), nicastrin, NADH:ubiquinone oxidoreductase subunit B6, NADH:ubiquinone oxidoreductase core subunit S3, thioredoxin reductase 2
9 mo O C57	12	ATP synthase membrane subunit c locus 2, cytochrome c oxidase copper chaperone COX11, cytochrome c oxidase subunit 5A, glutathione peroxidase 4, cytochrome b, MTND2, NADH dehydrogenase subunit 4 & 5 (complex I), NADH:ubiquinone oxidoreductase subunit A8, A11, & S6, thioredoxin 2	0	
9 mo 3Gy C57	7	cytochrome c oxidase copper chaperon COX11, cytochrome c oxidase subunit 1, MTND2, NADH dehydrogenase subunit 4 & 6 (complex 1), NADH:ubiquinone oxidoreductase subunit B4, ubiquinol-cytochrome c reductase binding protein	0	

Number of Transcripts/Proteins within the Mitochondria Dysfunction Pathway for each Condition and Names of Dysregulated Transcripts/Proteins				
Conditions with Mitochondria Dysfunction Pathway Effected	Number of transcripts in the pathway	Dysregulated transcripts within pathway	Number of proteins in the pathway	Dysregulated proteins within pathway
9 mo Fe C3H	0		8	caspase 8, caspase 9, catalase, NADH:ubiquinone oxidoreductase subunit B11, NADH:ubiquinone oxidoreductase core subunit S3, presenilin 1, SURF1 cytochrome c oxidase assembly factor, thioredoxin reductase 2
9 mo O C3H	7	aph-1 homolog B gamma-secretase subunit, glutathione peroxidase 7, monoamine oxidase B, cytochrome b, NADH dehydrogenase subunit 1 & 4 (complex I), MTND2	7	catalase, mitogen-activated protein kinase kinase 4, mitogen-activated protein kinase 9, NADH:ubiquinone oxidoreductase core subunit S3, presenilin 1, SURF1 cytochrome c oxidase assembly factor, thioredoxin reductase 2

Number of Transcripts/Proteins within the Mitochondria Dysfunction Pathway for each Condition and Names of Dysregulated Transcripts/Proteins				
Conditions with Mitochondria Dysfunction Pathway Effected	Number of transcripts in the pathway	Dysregulated transcripts within pathway	Number of proteins in the pathway	Dysregulated proteins within pathway
9mo Si C3H	4	monoamine oxidase B, NADH dehydrogenase subunit 1 & 6 (complex 1), thioredoxin 2	7	ATP synthase membrane subunit f, caspase 9, mitogen-activated protein kinase kinase 4, mitogen-activated protein kinase 9, NADH:ubiquinone oxidoreductase subunit A9, NADH:ubiquinone oxidoreductase subunit B6, NADH:ubiquinone oxidoreductase subunit V3
9 mo 1Gy C3H	0		7	ATP synthase membrane subunit f, caspase 9, NADH dehydrogenase subunit (complex 1), MTND2, NADH dehydrogenase subunit 4 (complex I), NADH:ubiquinone oxidoreductase subunit A9, NADH:ubiquinone

Number of Transcripts/Proteins within the Mitochondria Dysfunction Pathway for each Condition and Names of Dysregulated Transcripts/Proteins				
Conditions with Mitochondria Dysfunction Pathway Effected	Number of transcripts in the pathway	Dysregulated transcripts within pathway	Number of proteins in the pathway	Dysregulated proteins within pathway
				ne oxidoreductase subunit B6
9 mo Si C57	0		7	caspase 3, cytochrome c oxidase subunit 7A2 like, mitogen-activated protein kinase 9, MTND2, NADH dehydrogenase subunit 4 (complex I), NADH:ubiquion one oxidoreductase core subunit S3, ras homolog family member T2
12 mo Si C57	0		6	ATP synthase F1 subunit delta, catalase, cytochrome c oxidase subunit 6A1, MTND2, NADH:ubiquino ne oxidoreductase complex assembly factor 2, ras homolog family member T2
12 mo 1Gy C57	9	cytochrome c oxidase subunit 7A2, 7A2 like, & 8A, fission mitochondrial 1, furin paired basic amino acid cleaving	11	ATP synthase F1 subunit delta, catalase, cytochrome c



Number of Transcripts/Proteins within the Mitochondria Dysfunction Pathway for each Condition and Names of Dysregulated Transcripts/Proteins				
Conditions with Mitochondria Dysfunction Pathway Effected	Number of transcripts in the pathway	Dysregulated transcripts within pathway	Number of proteins in the pathway	Dysregulated proteins within pathway
		enzyme, NADH:ubiquinone oxidoreductase subunit B9, S6 & core subunit S2		oxidase assembly homolog COX15, cytochrome c oxidase subunit 7A2 like, mitogen-activated protein kinase 9, MTND2, NADH:ubiquinone oxidoreductase subunit A9, NADH:ubiquinone oxidoreductase complex assembly factor 1, NADH:ubiquinone oxidoreductase subunit B6, ras homolog family member T2, SURF1 cytochrome c oxidase assembly factor

Table 9: Shows the number of transcripts and proteins within the mitochondria dysfunction pathway for each condition as well as the names of the transcripts and proteins that are dysregulated. If a condition is not listed no molecules were found within this pathway.

## TRANSCRIPTOMIC CANONICAL PATHWAY IMPORTANCE AFTER HZE

Mitochondrial stress accompanies not only ROS production and ATP decline, but accumulation of unfolded protein, decrease in Ca<sup>2+</sup> buffering, and alteration in metabolites of TCA cycle, Oxidative Phosphorylation, fatty acid oxidation, etc.<sup>44</sup> As shown in Table 10, the transcriptomic data shows many pathways within the early HZE irradiated C57 mice besides mitochondria dysfunction or oxidative phosphorylation that are also linked to the mitochondria in some form or fashion. These include sirtuin signaling, ER stress, unfolded protein response, L-carnitine shuttle, TCA cycle, ubiquinol-10 biosynthesis, acute phase response, EIF2 signaling, NRF2-mediated oxidative stress response, and amino acid metabolism (ex. Asparagine biosynthesis). The FXR/RXR and LXR/RXR pathways are also altered after exposure to low-dose HZE. Although these pathways are also altered in the C57 gamma irradiated mice the changes occur later as does mitochondrial dysfunction.

Top Canonical Pathways and Upstream Regulators from Transcriptomic Data via IPA			
Condition	Top 5 Canonical Pathways	Top Upstream Regulators	Other interesting dysregulated transcripts and pathways
1 mo O C57	Mitochondrial dysfunction Oxidative phosphorylation Sirtuin Signaling pathway FXR/RXR activation Fatty Acid beta oxidation I	PPARA Pirinixic acid POR TO-901317 Mono-(2-ethylhexyl) phthalate	TCA Cycle II, Gluconeogenesis I (aldolase, fructose-biosphosphate C; enolase 1; malate dehydrogenase 1 & 2, phosphoglycerate kinase 1 all down), ubiquinol-10 biosynthesis, mitochondrial L-carnitine shuttle pathway (acyl-coA synthetase long chain family member 1, carnitine palmitoyltransfease 1A & solute carrier family 27 member 5 all down), ceramide signaling

Top Canonical Pathways and Upstream Regulators from Transcriptomic Data via IPA			
Condition	Top 5 Canonical Pathways	Top Upstream Regulators	Other interesting dysregulated transcripts and pathways
2 mo O C57	<p>EIF2 signaling</p> <p>Oxidative phosphorylation</p> <p>Regulation of eIF4 and p70S6K signaling</p> <p>Mitochondrial dysfunction</p> <p>Sirtuin signaling pathway</p>	<p>MLXIPL</p> <p>RICTOR</p> <p>YAP1</p> <p>MYC</p> <p>MYCN</p>	<p>mTOR signaling, Protein Ubiquitination Pathway, NRF2-mediated oxidative stress response, Unfolded protein response, TCA cycle II (fumarate hydratase, succinate dehydrogenase complex (iron sulfur subunit B, C &amp; D all down)</p>
4 mo O C57	<p>EIF2 signaling</p> <p>Unfolded protein response</p> <p>Regulation of eIF4 and p70S6K signaling</p> <p>Protein Ubiquitination Pathway</p> <p>ER stress pathway-CALR (calreticulin) down, DDIT3 (DNA damage inducible transcript 3) down , EIF2AK3 down, HSP90B1 down, HSPA5 down</p>	<p>XBP1</p> <p>ERN1</p> <p>Tunicamycin</p> <p>RICTOR</p> <p>ATF6</p>	<p>mTOR signaling, sirtuin signaling pathway</p>
9 mo O C57	<p>EIF2 signaling</p> <p>Mitochondrial dysfunction</p> <p>Oxidative phosphorylation</p> <p>Regulation of eIF4 and p70S6K signaling</p> <p>Sirtuin signaling pathway</p>	<p>MLXIPL</p> <p>RICTOR</p> <p>MYC</p> <p>YAP1</p> <p>CTNNB1</p>	<p>mTOR signaling</p>
12 mo O C57	<p>Mouse Embryonic Stem Cell Pluripotency-ID1 (inhibitor of DNA binding), ID2 down</p> <p>Trans, trans-farnesyl diphosphate biosynthesis-FDPS (farnesyl diphosphate synthase) up</p> <p>Pregnenolone biosynthesis-CYP26A1 up</p> <p>Histidine Degradation VI-same</p> <p>Superpathway of Geranylgeranyldiphosphat</p>	<p>ACVR2A</p> <p>LTBP4</p> <p>SMAD1/5</p> <p>Notch</p> <p>BMP10</p>	<p>Ubiquinol-10 biosynthesis-CYP26A1 up, Role of lipids/lipid rafts in the pathogenesis of influenza-FDPS up</p>

Top Canonical Pathways and Upstream Regulators from Transcriptomic Data via IPA			
Condition	Top 5 Canonical Pathways	Top Upstream Regulators	Other interesting dysregulated transcripts and pathways
	e biosynthesis I (via Mevalonate)-FDPS up		
1 mo Fe C57	PXR/RXR activation LPS/IL-1 mediated inhibition of RXR Function Sirtuin Signaling Pathway Nicotine Degradation II Circadian Rhythm Signaling-ARNTL (aryl hydrocarbon receptor nuclear translocator) up, BHLHE40 (basic helix-loop-helix family member e40) down; CLOCK (clock circadian regulator) up; CRY1 (cryptochrome circadian regulator 1) up; PER1 (period circadian regulator 1) down; PER2 down; PER3 down	RORC RORA PPARA Methylpredni solone NR1I2	Ubiquinol-10 biosynthesis, acyl-CoA hydrolysis
2 mo Fe C57	EIF2 Signaling Acute phase response signaling-exported Regulation of eIF4 and p70S6K signaling-exported list mTOR signaling-exported Production of nitric oxide and ROS in macrophages	Lipopolysacc haride MLXIPL IL1B YAP1 IFNG	Sirtuin signaling pathway, FXR/RXR, NRF2-mediated oxidative stress response
4 mo Fe C57	Unfolded protein response Aldosterone signaling in Epithelial cells Endoplasmic reticulum stress pathway Protein ubiquitination pathway NRF2-mediated oxidative stress response	XBP1 Tunicamycin ERN1 ATF6 1,2-dithiol-3-thione	EIF2 signaling, Regulation of eIF4 and p70S6K signaling mTOR, Glucocorticoid receptor signaling, Sirtuin signaling pathway, insulin receptor signaling

Top Canonical Pathways and Upstream Regulators from Transcriptomic Data via IPA			
Condition	Top 5 Canonical Pathways	Top Upstream Regulators	Other interesting dysregulated transcripts and pathways
9 mo Fe C57	<p>Unfolded protein response-CEBPE down, all up ERN1, HSPA8, Hspa1b, HSPH1, MAP3K5</p> <p>NRF2-mediated oxidative stress response-ACTG1, BACH1, DNAJA1, DNAJB1, FKBP5, GSTP1, MAP3K5 all up</p> <p>Aldosterone signaling in epithelial cells-DNAJA1, DNAJB1, HSP90AA1, HSPA8, HSPA4L, HSPH1 all up</p> <p>Protein Ubiquitination pathway same as above</p> <p>Agranulocyte-adhesion and diapedesis-ACTG1 up, CLDN3 down, CXCL2 (C-X-C chemokine ligand) up, CXCL13 up, IL1R1 (interleukin 1 receptor type 1) up</p>	<p>NR5A2</p> <p>Lipopolysaccharide</p> <p>Cisplatin</p> <p>Thapsigargin</p> <p>NR1I3</p>	<p>GADD45 signaling-CDKN1A (cyclin dependent kinase inhibitor 1A) up, GADD45G (growth arrest and DNA damage inducible gamma) up</p> <p>LXR/RXR signaling-C4A/C4B (complement C4B), CYP7A1, HMGCR (3-hydroxy-3-methylglutaryl-CoA reductase), IL1R1 (interleukin 1 receptor type 1) all up</p> <p>Asparagine biosynthesis I-ASNS(asparagine synthetase glutamine-hydrolyzing) up, FXR/RXR-C4A/C4B, CYP7A1, FOXA3, SLC10A2 all up, PXR/RXR ER stress pathway-ALAS1, CYP7A1, IGFBP1 all up, PI3K/AKT signaling-CDKN1A up, GDF15 (growth differentiation factor 15) down, HSP90AA1 up, MAP3K5 up, Sirtuin signaling pathway-BCL2L11, GADD45G, MT-ND2, MT-ND4, MT-ND6, PFKFB3 (6-phosphofructo-2 kinase/fructose 2,6-biphosphatase 3) all up</p> <p>Apoptosis signaling-BCL2L11 up, ENDOG down, MAP3K5 up</p>
12 mo Fe C57	only 6 genes dysregulated all up		<p>Gm23442</p> <p>Gm25394</p> <p>Gm25835</p> <p>Gm26397</p> <p>Snora78</p> <p>Snord13 (small nucleolar RNA)</p>

Top Canonical Pathways and Upstream Regulators from Transcriptomic Data via IPA			
Condition	Top 5 Canonical Pathways	Top Upstream Regulators	Other interesting dysregulated transcripts and pathways
1 mo Si C57	<p>Mitochondrial Dysfunction</p> <p>Asparagine Biosynthesis I-ASNS (asparagine synthetase (glutamine-hydrolyzing) down</p> <p>Sirtuin Signaling Pathway-MT-CYB; MT-ND2; MT-ND6</p> <p>Alpha tocopherol degradation-CYP4A11</p> <p>Oxidative phosphorylation</p>	<p>Actinonin</p> <p>MRPL12</p> <p>DAP3</p> <p>MT-TM</p> <p>SIRT3</p>	Ubiquinol-10 biosynthesis
2 mo Si C57	<p>FXR/RXR activation-FOXA2 up, HPX down, RARA down, SAA1* down</p> <p>Role of Oct4 in Mammalian Embryonic stem cell pluripotency-FOXA2 up, RARA down</p> <p>Acute phase response signaling-HP, HPX (hemopexin), SAA1* all down</p> <p>TR/RXR activation-HP (haptoglobin) and THRSP (thyroid hormone responsive)</p>	<p>Lipopolysaccharide</p> <p>TNF</p> <p>RORC</p> <p>IL1B</p> <p>NR1H4</p>	
4 mo Si C57	<p>Unfolded protein response-DNAJB9, HSPA5, Hspa1b, SYVN1 (synoviolin 1) all down</p> <p>IL-7 signaling pathway-IGHG1, Ighg2b, Ighg2c all up</p> <p>Phagosome formation-IGHG1, Ighg2b, MARCO (macrophage receptor with collagenous structure) all up</p> <p>Autoimmune thyroid disease signaling-IGHG1, Ighg2b both up</p> <p>Hematopoiesis from</p>	<p>CLOCK</p> <p>ATF6</p> <p>Thapsigargin</p> <p>HTT</p> <p>tunicamycin</p>	Phosphatidylethanolamine biosynthesis II (choline kinase alpha up), ER stress pathway (heat shock protein A(HSP70) member 5 down)

Top Canonical Pathways and Upstream Regulators from Transcriptomic Data via IPA			
Condition	Top 5 Canonical Pathways	Top Upstream Regulators	Other interesting dysregulated transcripts and pathways
	pluripotent stem cells- same as above		
9 mo Si C57	Acetone Degradation I (to Methylglyoxal)-CYP2A6 down, CYP2C8 down, CYP4A22 up Stearate biosynthesis I (animals)-ACOT1 down, CYP4A22 up, ELOVL6(ELOVL fatty acid elongase 6) down Nicotine Degradation III-CYP2A6, CYP2C8, UGT1A4 all down Melatonin Degradation I-same as above Nicotine Degradation II-same	STAT5B Pirinixic acid RORC L-triiodothyronine PPARA	Acyl-CoA hydrolysis, ubiquinol-10 biosynthesis
12 mo Si C57	only 1 gene upregulated		Gm22154
1 mo 1Gy C57	Stearate Biosynthesis I (animals)-ACOT1 (acyl-CoA thioesterase 1) down; ACOT4 down; CYP4A11 down; FASN (fatty acid synthase) up Superpathway of cholesterol biosynthesis-FDPS (farnesyl diphosphate synthase) up; MVD (mevalonate diphosphate decarboxylase) up; SQLE (squalene epoxidase) up Acyl-CoA hydrolysis-ACOT1; ACOT4 Superpathway of geranylgeranyl diphosphate biosynthesis I (via Mevalonate) TR/RXR activation-BCL3 (B cell CLL/lymphoma 3) up;	FGR19 PPARA SCAP CFTR SREBF1	Palmitate biosynthesis I, ubiquinol-10 biosynthesis

Top Canonical Pathways and Upstream Regulators from Transcriptomic Data via IPA			
Condition	Top 5 Canonical Pathways	Top Upstream Regulators	Other interesting dysregulated transcripts and pathways
	FASN up; HP (haptoglobin) up		
2 mo 1Gy C57	EIF2 signaling mTOR signaling Regulation of eIF4 and p70S6K signaling Unfolded protein response Complement system	MLXIPL Lipopolysaccharide YAP1 IL6 CTNNB1	Ubiquinol-10 biosynthesis, sphingosine-1-phosphate signaling
4 mo 1Gy C57	Unfolded protein response ER stress pathway-CALR, DDIT3, DNAJC3, EIF2AK3, HSP90B1, HSPA5, XBP1 all down LXR/RXR activation FXR/RXR activation Acute phase response signaling	XBP1 Tunicamycin ERN1 RORC RORA	NRF2-mediated oxidative stress response, acyl-coA hydrolysis, ubiquinol-10 biosynthesis, palmitate biosynthesis I (fatty acid synthase up), fatty acid biosynthesis Initiation II(same from palmitate pathway)
9 mo 1Gy C57	Role of JAK2 in hormone-like cytokine signaling-IRS2 (insulin receptor substrate 2), SOCS2 (suppressor of cytokine signaling), SOCS3 all up Acute phase response signaling-IL1R1, SAA1*(serum amyloid A1), SOCS2, SOCS3, all up TF (transferrin) down Sirtuin signaling pathway-ARNTL, CDH1, GADD45G, MT-ND4, MT-ND5 all up, MYCN (MYCN proto-oncogene, bHLH TF) down IGF-1 signaling-IGFBP1, IRS2, SOCS2, SOCS3 all up IL-9 signaling-IRS2, SOCS2, SOCS3 all up	RORC Dexamethasone IL1B RORA tretinoin	PXR/RXR signaling-CYP2A6 down, CYP2B6 down, IGFBP1 up, LXR/RXR-IL1R1 up, SAA1* up, TF down, FXR/RXR-SAA1* up, SLC22A7 up, TF down Phosphatidylethanolamine biosynthesis II (choline kinase alpha up)



Top Canonical Pathways and Upstream Regulators from Transcriptomic Data via IPA			
Condition	Top 5 Canonical Pathways	Top Upstream Regulators	Other interesting dysregulated transcripts and pathways
12 mo 1Gy C57	<p>Mitochondrial dysfunction VDR/RXR activation- EP300, FOXO1, GADD45A, NCOR2, and PPARG all down, HR up</p> <p>B cell receptor signaling-9 molecules exported</p> <p>Estrogen receptor signaling-EP300, HNRNPB, NCOR2, RRAS, SPEN, TAF15, TAF4B all down</p> <p>Acute phase response signaling-IL1R1, IL6R, MAP3K5, RRAS, SAA1*, SAA2-SAA4, SERPINA3, SOCS3 all down</p>	<p>ST1926 IL3 EPOR Lipopolysacc haride IL1B</p>	Sirtuin signaling, mTOR

Top Canonical Pathways and Upstream Regulators from Transcriptomic Data via IPA			
Condition	Top 5 Canonical Pathways	Top Upstream Regulators	Other interesting dysregulated transcripts and pathways
1 mo 3Gy C57	<p>IL-17A signaling in fibroblasts-CEBPB (CCAAT enhancer binding protein beta) up; CEBPD (delta) up; JUN (Jun proto-oncogene) up; LCN2 (lipocalin 2) down</p> <p>Glucocorticoid receptor signaling-AR (androgen receptor) up; CDKN1A (cyclin dependent kinase inhibitor 1A) up; CEBPB up; DUSP1 (dual specificity phosphatase 1) up; FKBP5 (FK506 binding protein 5) up; JUN up; TSC22D3 (TSC22 domain family member 3) up</p> <p>Acute phase response signaling-APCS (amyloid P component, serum) down; CEBPB up; IL6R (interleukin 6 receptor) up; JUN up; SAA1 (serum amyloid A1) down</p> <p>JAK/Stat Signaling-CDKN1A (cyclin dependent kinase inhibitor 1A) up; CEBPB up; Jun up</p> <p>Hepatic Fibrosis/Hepatic Stellate Cell Activation-COL15A1 (collagen type XV alpha 1 chain) down; COL25A1 (collagen type XXV alpha chain) down; CTGF (connective tissue growth factor) up, IL6R up</p>	<p>TNF</p> <p>IL1B</p> <p>IFNG</p> <p>Glucocorticoid dexamethasone</p>	<p>Sumoylation pathway</p>

Top Canonical Pathways and Upstream Regulators from Transcriptomic Data via IPA			
Condition	Top 5 Canonical Pathways	Top Upstream Regulators	Other interesting dysregulated transcripts and pathways
2 mo 3Gy C57	<p>EIF2 signaling</p> <p>Regulation of eIF4 and p70S6K signaling</p> <p>mTOR signaling</p> <p>Unfolded protein response</p> <p>NRF2-mediated oxidative stress response</p>	<p>MLXIPL</p> <p>YAP1</p> <p>Tunicamycin</p> <p>XBP1</p> <p>MYCN</p>	<p>Sirtuin signaling pathway, ceramide signaling, ER stress pathway</p>
4 mo 3Gy C57	<p>Oxidative phosphorylation</p> <p>Mito dysfunction</p> <p>Sirtuin signaling pathway-FOXO1, MT-CYB, MT-ND2, MT-ND4, MT-ND5, PPARGC1A all up, RRP9 down</p> <p>Unfolded protein response-HSPA5, Hspa1b, SYVN1 all down</p> <p>Granzyme B signaling-ENDOG (endonuclease G), LMNB2 (lamin B2) both down</p> <p>PXR/RXR activation-CYP2C8, FOXO1, PPARGC1A all up</p> <p>FXR/RXR activation-FOXO1 up, PPARGC1A up, SAA1* down</p>	<p>IL1B</p> <p>THBS4</p> <p>STAT3</p> <p>ALKBH1</p> <p>NSUN3</p>	
9 mo 3Gy C57	<p>Mito dysfunction</p> <p>Oxidative phosphorylation</p> <p>IL-7 signaling pathway-IGHG1, Ighg2b, Ighg2c, MYC all up, JUN down</p> <p>Sirtuin signaling pathway-HIST1H4J &amp; JUN down, MT-ND2, MT-ND4, MT-ND6, MYC, NDUFB4 all up</p> <p>LPS/IL-1 mediated inhibition of RXR function-ALAS1, CYP2A6, CYP7A1, GSTA5, Sult1d1 all up and JUN down</p>	<p>Lipopolysaccharide</p> <p>RORC</p> <p>NR1I2</p> <p>RORA</p> <p>Cadmium chloride</p>	

Top Canonical Pathways and Upstream Regulators from Transcriptomic Data via IPA			
Condition	Top 5 Canonical Pathways	Top Upstream Regulators	Other interesting dysregulated transcripts and pathways
12 mo 3Gy C57	<p>Aryl hydrocarbon receptor signaling-DCT (dopachrome tautomerase) up, EP300, NCROR2, NFIA, NFIC, TP53 all down</p> <p>RAR activation-CYP26A1 up, ARID1A, EP300, NCOR2, ZBTB16 all down</p> <p>Iron homeostasis signaling pathway-ATP6V0C, EPAS1, IL6R all down, TFRC up</p> <p>Superpathway of cholesterol biosynthesis-DHCR7 down, FDPS up</p> <p>Hereditary breast cancer signaling-ARID1A, EP300, TP53 all down, UBC (ubiquitin) up</p>	<p>Diethyl nitrosamine</p> <p>ACOX1</p> <p>Hydrogen peroxide</p> <p>Pirinixic acid</p> <p>TAS-103</p>	<p>PPARalpha/RXRalpha-BCL3, EP300, NCOR2 all down, Cyp2c54 up, sumoylation pathway</p>
1 mo O C3H	<p>Superpathway of Cholesterol Biosynthesis-exported</p> <p>Cholesterol Biosynthesis I-FDFT1; HSD17B7; LBR; LSS; MSMO1; SC5D; SQLE; TM7SF2 all down</p> <p>Cholesterol Biosynthesis II</p> <p>Cholesterol Biosynthesis III</p> <p>Mevalonate Pathway-ACAT2 (acetyl-CoA acetyltransferase 2), HMGCR (3-hydroxy-3-methylglutaryl-CoA reductase), HMGCS1 (3-hydroxy-3-methylglutaryl-CoA synthase 1), MVD (mevalonate diphosphate decarboxylase), MVK (mevalonate kinase), PMVK (phosphomevalonate kinase) all down</p>	<p>POR</p> <p>PPARA</p> <p>RORC</p> <p>GPD1</p>	<p>ubiquinol-10 biosynthesis, sirtuin signaling, leukotriene biosynthesis</p>

Top Canonical Pathways and Upstream Regulators from Transcriptomic Data via IPA			
Condition	Top 5 Canonical Pathways	Top Upstream Regulators	Other interesting dysregulated transcripts and pathways
2 mo O C3H	Sirtuin signaling pathway Mito dysfunction Oxidative phosphorylation PXR/RXR activation Aryl hydrocarbon receptor signaling (cytochrome P450 family 1 subfamily A member, nuclear receptor subfamily 0 group B member 2, prostaglandin E synthase 3 all down)	DAP3 MT-TE Actinonin MRPL12 MT-TM	
4 mo O C3H	TR/RXR activation Thyroid cancer signaling PXR/RXR activation (fatty acid synthase up) Palmitate biosynthesis I Fatty acid biosynthesis Initiation II	Thyroid hormone Carbohydrate NCOR1 THRB MED13	Gluconeogenesis I (malic enzyme I up)
9 mo O C3H	LPS/IL-1 mediated inhibition of RXR function PXR/RXR activation Nicotine degradation II Superpathway of melatonin degradation Acetone degradation I (to methylglyoxal)	PPARA STAT5B RORA RORC POR	Ubiquinol-10 biosynthesis, sirtuin signaling pathway
12 mo O C3H	no pathway data	MALAT1 Rxr JAK2 PTEN	

Top Canonical Pathways and Upstream Regulators from Transcriptomic Data via IPA			
Condition	Top 5 Canonical Pathways	Top Upstream Regulators	Other interesting dysregulated transcripts and pathways
1 mo Fe C3H	<p>Superpathway of Cholesterol Biosynthesis- ACAT2, FDFT1, FDPS, HMGCR, HMGCS1, HSD17B7, IDI1, LSS, MSMO1, MVD, MVK, NSDHL, PMVK, SC5D, SQLE all down</p> <p>Superpathway of Geranylgeranyl diphosphate Biosynthesis I (via Mevalonate)</p> <p>Cholesterol Biosynthesis I- FDFT1; HSD17B7; LSS; MSMO1; NSDHL; SC5D; SQLE all down</p> <p>Cholesterol Biosynthesis II</p> <p>Cholesterol Biosynthesis III</p> <p>Mevalonate Pathway- ACAT2 (acetyl-CoA acetyltransferase 2), HMGCR (3-hydroxy-3-methylglutaryl-CoA reductase), HMGCS1 (3-hydroxy-3-methylglutaryl-CoA synthase 1), IDI1 (isopentenyl-diphosphate delta isomerase 1) MVD (mevalonate diphosphate decarboxylase), MVK (mevalonate kinase), PMVK (phosphomevalonate kinase) all down</p>	<p>POR</p> <p>PPARA</p> <p>SCAP</p> <p>SREBF1</p> <p>SREBF2</p>	<p>sirtuin signaling, fatty acid beta oxidation, unfolded protein response, ubiquinol-10 biosynthesis, mito L-carnitine shuttle pathway acyl-CoA synthetase long chain family member 3 &amp; 4 (both down)</p>
2 mo Fe C3H	<p>Adipogenesis pathway</p> <p>Unfolded protein response</p> <p>Glucocorticoid receptor signaling</p> <p>4-hydroxybenzoate biosynthesis</p> <p>4-hydroxyphenylpyruvate biosynthesis</p>	<p>Lipopolysaccharide</p> <p>Sobetirome</p> <p>IL10</p> <p>IFNG</p> <p>Ethanol</p>	<p>Acyl-co hydrolysis, ubiquinol-10 biosynthesis</p>

Top Canonical Pathways and Upstream Regulators from Transcriptomic Data via IPA			
Condition	Top 5 Canonical Pathways	Top Upstream Regulators	Other interesting dysregulated transcripts and pathways
4 mo Fe C3H	Circadian Rhythm signaling PXR/RXR activation Spermidine biosynthesis I Molecular mechanisms of cancer Adipogenesis pathway	L-triiodothyronine Growth hormone Pirinixic acid STAT5B POR	Sphingosine-1-phosphate signaling
9 mo Fe C3H	LPS/IL-1 mediated inhibition of RXR function Aryl hydrocarbon receptor signaling Nicotine degradation II Superpathway of melatonin degradation Acetone degradation I (to Methylglyoxal)	PPARA Pirinixic acid RORC RORA STAT5B	Acyl-CoA hydrolysis, glucose and glucose 1-phosphate degradation, ubiquinol-10 biosynthesis, sirtuin signaling, phosphatidylcholine biosynthesis I (choline/ethanolamine phosphotransferase 1 & choline phosphotransferase 1 down)
12 mo Fe C3H	Pregnenolone Biosynthesis Histidine Degradation VI Ubiquinol-10 biosynthesis GADD45 signaling tRNA charging	CLOCK Bexarotene 9,10-dimethyl-1,2-benzanthracene POU5F1 iron	
1 mo Si C3H	Nicotine Degradation III Circadian Rhythm Signaling Melatonin Degradation I Nicotine Degradation II Superpathway of Melatonin Degradation	RORA CLOCK Pirinixic acid RORC PPARA	Acyl-CoA hydrolysis, palmitate biosynthesis
2 mo Si C3H	nNOS signaling in skeletal muscle cells Netrin signaling Calcium signaling Opioid signaling pathway GNRH	MRPL12 DAP3 Actinonin SIRT3 MALSU1	

Top Canonical Pathways and Upstream Regulators from Transcriptomic Data via IPA			
Condition	Top 5 Canonical Pathways	Top Upstream Regulators	Other interesting dysregulated transcripts and pathways
4 mo Si C3H	Acute phase response signaling LXR/RXR activation Netrin signaling Complement system nNOS signaling in skeletal muscle cells	IL6 TCL1A STAT3 IFNG lipopolysa	Palmitate biosynthesis I
9 mo Si C3H	Stearate biosynthesis I LXR/RXR activation LPS/IL-1 mediated inhibition of RXR function Glutathione-mediated detoxification Acyl-CoA hydrolysis	Pirinixic acid GPD1 PPARA SLC25A13 ACOX1	Ubiquinol-10 biosynthesis
12 mo Si C3H	LXR/RXR activation FXR/RXR activation Asparagine Biosynthesis I Atherosclerosis Signaling Thyroid cancer signaling	GPD1 SLC25A13 CEBPA IL6 Cipro fibrate	
1 mo 1Gy C3H	Superpathway of Cholesterol Biosynthesis- FDPS, HMGCR, LSS, MVD all down Oxidative Phosphorylation Mitochondrial Dysfunction Pregnenolone Biosynthesis-CYP26A1 down, CYP26B1 down, CYP4A11 up Histidine Degradation VI- same as pregnenolone	SCAP INSIG2 SREBF2 SREBF1 DAP3	Sirtuin signaling pathway, ubiquinol-10 biosynthesis
2 mo 1Gy C3H	LPS/IL-1 mediated inhibition of RXR function Fatty Acid beta oxidation I stearate biosynthesis I TR/RXR activation PXR/RXR activation	Pirinixic acid L- triiodothyron ine PPARA RORA POR	Mito L-carnitine shuttle pathway acyl CoA synthetase long chain family member 1 down & solute carrier family 27 member 2 down, sirtuin signaling



Top Canonical Pathways and Upstream Regulators from Transcriptomic Data via IPA			
Condition	Top 5 Canonical Pathways	Top Upstream Regulators	Other interesting dysregulated transcripts and pathways
4 mo 1Gy C3H	Acute phase response signaling Superpathway of cholesterol biosynthesis LXR/RXR activation Osteoarthritis pathway Superpathway of Geranylgeranyl diphosphate biosynthesis I (via Mevalonate)	PPARA Lipopolysacc haride IFNG FGF19 IL6	
9 mo 1Gy C3H	stearate biosynthesis I Acetone degradation I (to methylglyoxal) Acyl-Co hydrolysis Pregnenolone biosynthesis Histidine degradation VI	L- triiodothyron ine RORC HRH3 CEBPA dexamethaso ne	Ubiquinol-10 biosynthesis, sphingomyelin metabolism (sphingomyelin phosphodiesterase 3 (up))
12 mo 1Gy C3H	Retinoate biosynthesis II The visual cycle Retinoate biosynthesis I Retinol Biosynthesis Semaphorin signaling in neurons	GATA6 LTBR RBP7 DPF2 ADGRV1	SPINK1 pancreatic cancer pathway (carboxypeptidase D down) those are the only pathways
1 mo 3Gy C3H	TXR/RXR activation- ACACA, CYP7A1, FASN, FGFR3, SREBF1 (sterol regulatory element binding transcription factor 1), THRSP (thyroid hormone responsive) all down Circadian rhythm signaling Biotin-carboxyl carrier protein assembly AMPK signaling Sirtuin Signaling pathway	ARNTL FGF19 CLOCK SREBF1 Pirinixic acid	palmitate biosynthesis I
2 mo 3Gy C3H	AMPK signaling TR/RXR activation Fatty acid beta oxidation I IL-9 signaling Type II diabetes mellitus signaling	Pirinixic acid PPARA Ins1 FOXO1 POR	Insulin signaling, ubiquinol-10 biosynthesis, mito L-carnitine shuttle pathway acyl coA synthetase long chain family member 1 down & solute carrier family 27 member 2 down

Top Canonical Pathways and Upstream Regulators from Transcriptomic Data via IPA			
Condition	Top 5 Canonical Pathways	Top Upstream Regulators	Other interesting dysregulated transcripts and pathways
4 mo 3Gy C3H	No pathway data	IFIH1 Propylthiouracil BRCA1 BCL2A1 SLC19A1	
9 mo 3Gy C3H	Leukocyte extravasation signaling Phagosome formation Granulocyte adhesion and diapedesis Fcγ Receptor-mediated phagocytosis in macrophages and monocytes Natural killer cell signaling	Lipopolysaccharide TCL1A TNF IFNG IL6	Eicosanoid signaling, thrombopoietin signaling, sphingosine-1-phosphate signaling, ceramide signaling
12 mo 3Gy C3H	Differential Regulation of cytokine production in intestinal epithelial cells by IL-17A and IL-17F IL-17A signaling in fibroblasts Altered T cell and B cell signaling in rheumatoid arthritis Phagosome formation Granulocyte adhesion & Diapedesis	INSIG1 Pro-inflammatory Cytokine TCL1A DPF2 IL22	Also agranulocyte adhesion and diapedesis. These are the only pathways

Table 10: Top canonical pathways and upstream regulators from transcriptomic data via IPA

With sirtuin signaling there are 7 sirtuins found in mammals that are involved in distinct metabolic and stress response pathways. Three of these sirtuins are found directly in the mitochondria which include SIRT 3, 4 & 5. These sirtuins are known to participate in the regulation of ATP production, metabolism, apoptosis, and cell signaling.<sup>19</sup> While these specific sirtuins were not dysregulated in the transcriptomic data, they were in the proteomic data (SIRT 3 and 5). The sirtuin signaling pathway as a

whole is rather large and is involved in many processes including cell proliferation, tumor growth, glycolysis, cholesterol efflux, inflammation, ROS production, autophagy, oxidative stress, apoptosis, fatty acid oxidation, liver gluconeogenesis, etc.

The mitochondria are also in close connection to the endoplasmic reticulum (ER). While their membranes are not directly fused so they can retain their individuality, they do have contact points known as mitochondria-associated ER membranes (MAMs) that make relatively stable connection between the organelles. This allows the ER and mitochondria to coordinate cellular functions such as calcium signaling, apoptosis, ER stress response, phospholipid synthesis as well as translocation of phospholipid from the ER to the mitochondria membrane.<sup>45</sup> Most phospholipids such as PE, PS and PC must be synthesized in the ER and have to be imported into the mitochondria. PE can be produced within the mitochondria but it requires the import of PS which can then be decarboxylated.<sup>46</sup> Mitochondria and ER are also both important storage vessels of calcium and the transfer of calcium between them is crucial for both cell life and death. Calcium transfer between the organelles can be halted by simply increasing the distance of the MAMs. The ER is also responsible for the secretion and synthesis of membrane proteins. Once the proteins are properly folded they are then passed on to the Golgi apparatus. Unfolded or misfolded proteins, however, are retained in the ER where they are degraded. If these unfolded and misfolded proteins build up, the expression of ER chaperons and components of the machinery to degrade them are upregulated. This process is referred to as ER stress response.<sup>47</sup> Organelle crosstalk is very important in relation to tumorigenesis as they constitute a complicated network with one another. Thus, the dysregulation of one of the downstream pathways may lead to severe

mitochondrial dysfunction that would ultimately result in failure to properly regulate energy metabolism and ion buffering.<sup>45</sup> As mitochondria are able to synthesize some of their own proteins, they also have an auto-regulatory mechanism that is similar to the ER stress response that is induced when there is an accumulation of unfolded proteins which is known as the unfolded protein response.<sup>47</sup> Mitochondrial proteostasis is also regulated by other stress responsive signaling mechanisms. When eukaryotic initiation factor 2 (eIF2 $\alpha$ ) is phosphorylated it induces attenuation of protein synthesis and activates other stress-responsive transcription factors.<sup>48</sup> Nuclear factor erythroid (Nrf2) also helps govern the expression of endogenous antioxidant synthesis and ROS-eliminating enzymes. Accumulating evidence shows that mitochondria ROS activates Nrf2 which ultimately induces the expression of antioxidant genes as well as genes that are involved in mitochondrial quality and quantity control.<sup>44</sup> The mitochondria are also required to synthesize uridine which is used to produce UTP for RNA synthesis as well as UTP glucose that is needed for both the synthesis of glycogen and complex carbohydrates. In non-dividing cells, the nucleotides for RNA synthesis mostly come from a pre-existing recycled pool acquired from salvage pathways. However, in times of proliferation or enhanced transcription such as during acute phase response, the mitochondria are necessary to provide the essential nucleic acid building blocks.<sup>49</sup>

The L-carnitine shuttle is critical because the inner mitochondrial membrane is impermeable to fatty acyl-CoA thioesters. Thus, in order for fatty acids to be transported across the inner mitochondrial membrane, the carnitine shuttle is required.<sup>21</sup> The mitochondria matrix is the site of the TCA cycle, and as previously mentioned,

mitochondria also have a central role in amino acid metabolism via deamination and transamination<sup>49</sup>.

CoenzymeQ10 (CoQ<sub>10</sub>) is an essential electron transporter in Complexes I, II and III. Ubiquinone-10 is its oxidized form and it is enzymatically reduced to ubiquinol-10 which acts as a fat-soluble antioxidant that effectively helps protect lipid membranes and lipoproteins from oxidative damage and helps prevent DNA damage. With normal aging, ubiquinol-10 levels and its biosynthesis have been observed to decrease. Thus, ubiquinone-10 is hypothesized to have anti-aging effects. Ubiquinol-10 is also believed to induce pathways that activate SIRT1, SIRT3, peroxisome proliferator-activated receptor gamma coactivator 1 $\alpha$ , and increase mitochondria function.<sup>50</sup>

Farnesoid X receptor (FXR) plays an important role in the maintenance of energy homeostasis as well as the integrity of organs like the liver. It helps regulate bile acid, lipid and glucose metabolism. Liver cancers have been shown to spontaneously develop in mice in the absence of FXR.<sup>51</sup> Liver X receptors (LXRs) are nuclear receptors that are involved in transcriptional control of lipid metabolism as well as function as nuclear cholesterol sensors that are activated in response to elevated intracellular cholesterol levels. LXRs have been found to modulate immune and inflammatory responses in macrophages.<sup>52</sup>

#### **PROTEOMIC CANONICAL PATHWAY IMPORTANCE AFTER HZE**

Table 11 shows the pathways that were found to be dysregulated in the proteomic data set. There are some similarities in the C57 transcriptomics such as sirtuin signaling, acute phase response, L-carnitine shuttle, unfolded protein response, and

amino acid biosynthesis (ex. L-glutamine biosynthesis). The data shows disruption of calcium transport which both the ER and mitochondria are highly involved in as well as, immune related pathways such as NFκB and JAK family kinases which are involved in interleukin 6 (IL-6) type cytokine signaling. When ROS is elevated it can activate NF-κB which ultimately produces pro-inflammatory cytokines such as IL-6<sup>53</sup>. FXR/RXR and LXR/RXR pathways are also altered in both datasets. Unique to the proteomic data is leukocyte extravasation signaling, glycogen degradation, endocytosis signaling, ILK signaling and phagosome maturation.

Top Canonical Pathways and Upstream Regulators from Proteomic Data via IPA			
Condition	Top 5 Canonical Pathways	Top Upstream Regulators	Other interesting dysregulated proteins & pathways
1 mo O C57	Sirtuin Signaling Pathway RhoA Signaling (cytoskeleton organization) Clathrin-mediated Endocytosis signaling LXR/RXR activation Actin Cytoskeleton Signaling	HNF4A-hepatocyte nuclear factor 4 alpha Insulin D-glucose Methylprednisolone ABCB6	PI3K (down) mTOR (up) cyclin dependent kinase 2(up) cyclin dependent kinase inhibitor 1B (down) glycogen synthase kinase 3 beta (down) insulin signaling receptor (down) mannose-6-phosphate receptor (down)
2 mo O C57	Huntington's Disease Signaling (HIP1 down) (HSP40 up) Iron homeostasis signaling pathway ILK signaling Tight Junction Signaling Glycogen Degradation III	HNF4A CST5 Maslinic acid miR-30c-5p (and other miRNAs w/ seed GUAAACA) desmopressin	Also see sirtuin signaling and ceramide signaling (SMPD (sphingomyelin phosphodiesterase 4) up)
4 mo O C57	Acute phase response signaling Clathrin-mediated endocytosis signaling Phagosome maturation Role of JAK family kinases in IL-6 type cytokine signaling FXR/RXR activation	HNF4A CST5 TP53 Methylprednisolone D-glucose	Also see B cell receptor signaling, production of nitric oxide & ROS macrophages, cellular senescence (predicted inhabitation), CDKN1B cyclin dependent kinase inhibitor (down), CDK2 cyclin dependent kinase 2-activation of s-phase

Top Canonical Pathways and Upstream Regulators from Proteomic Data via IPA			
Condition	Top 5 Canonical Pathways	Top Upstream Regulators	Other interesting dysregulated proteins & pathways
			progression, sumoylation pathway-SAE1(SUMO1 activating enzyme subunit 1), LXR/RXR activation, insulin receptor signaling
9 mo O C57	Clathrin-mediated endocytosis signaling RhoA signaling Acute phase response signaling Huntington's disease signaling Signaling by Rho family GTPases	NHF4A RHOJ XBP1 Bvr Sirolimus	Coenzyme A biosynthesis, Sirtuin signaling, heme oxygenase 1 & 2 (down)
12 mo O C57	Acute phase response signaling Tight junction signaling IL-8 signaling LXR/RXR activation L-glutamine Biosynthesis II(tRNA-dependent)	HNF4A CST5 Tetrachlorodibenzodioxin GPD1 SLC25A13	L-carnitine shuttle pathway (acyl-CoA synthetase long chain family member 3 (down)) & member 4 (up), phospholipase c signaling, type II diabetes signaling, role of NFAT in regulation of the immune response, CDK2 (down), Unfolded protein response
1 mo Fe C57	Acute phase response signaling Glycogen degradation III Phagosome maturation Huntington's Disease signaling Clathrin-mediated endocytosis signaling	TO-901317 Cipro fibrate Nitrofurantoin SCAP ACOX1	Calcium transport I (ATPase sarcoplasmic/ER Ca2+ transporting 2 (down) & ATPase plasma membrane Ca2+ transporting 1 (up)), LXR/RXR (apolipoprotein A5-activates cholesterol efflux), Death receptor signaling (CASP7 inhibits DNA repair (down))

Top Canonical Pathways and Upstream Regulators from Proteomic Data via IPA			
Condition	Top 5 Canonical Pathways	Top Upstream Regulators	Other interesting dysregulated proteins & pathways
2 mo Fe C57	Acute phase response signaling Xenobiotic metabolism signaling NAD salvage pathway II UVB-induced MAPK signaling NF-kB activation by viruses	HNF4A Pregnenolone carbonitrile Pirinixic acid Estrone RAB1B	ceramide signaling (sphingosine kinase 2 (up))
4 mo Fe C57	Cell cycle regulation by BTG family proteins Inhibition of ARE-mediated mRNA degradation pathway 5-aminoimidazole ribonucleotide biosynthesis I Dopamine receptor signaling Breast cancer regulation by Stathmin1	HNF4A Camptothecin (+-)-2-hydroxyoleic acid FAS HNRNPH1	Cyclins and cell cycle regulation, regulation of eIF4 & p70S6K signaling, ceramide signaling (different protein that O) sphingosine kinase 2, role of CHK proteins in cell cycle checkpoint, mitochondrial L-carnitine shuttle pathway (acyl-CoA synthetase long chain family member 4 down & solute carrier family 27 member 4 (down), thrombin signaling, mTOR signaling
9 mo Fe C57	Purine nucleotides de novo biosynthesis II 5-aminoimidazole ribonucleotide biosynthesis I Regulation of cellular mechanics by calpain protease Acute phase responses signaling Sertoli cell-Sertoli cell junction signaling	TO-901317 Cipro fibrate Diethyl nitrosamine HNF4A ACOX1	



Top Canonical Pathways and Upstream Regulators from Proteomic Data via IPA			
Condition	Top 5 Canonical Pathways	Top Upstream Regulators	Other interesting dysregulated proteins & pathways
12 mo Fe C57	Acute phase response signaling Mechanisms of viral exit from host cells Wnt/beta catenin signaling Endothelin-1 signaling Endometrial cancer signaling	HNF4A Let-7a-5p (and other miRNAs w/seed GAGGUAG) 1,2-dithiol-3-thione Methylprednisolone miR-30c-5p (other miRNAs w/seed GUAAACA)	Sirtuin signaling pathway
1 mo Si C57	Huntington's Disease signaling Stearate Biosynthesis I (animals) FAT10 signaling pathway D-myo-inositol (1,4,5,6)-tetrakisphosphate biosynthesis D-myo-inositol (3,4,5,6)-tetrakisphosphate biosynthesis	HNF4A Glucagon Desmopressin CALCA BCAN	Acyl-CoA hydrolysis
2 mo Si C57	Acute phase response signaling Fcy receptor mediated phagocytosis in macrophages and monocytes stearate biosynthesis I (animals) Caveolar-mediated endocytosis signaling Leukocyte extravasation signaling	HNF4A miR-1-3p (and other miRNAs w/seed GGAAUGU) ACOX1 ESR1 Fulvestrant	

Top Canonical Pathways and Upstream Regulators from Proteomic Data via IPA			
Condition	Top 5 Canonical Pathways	Top Upstream Regulators	Other interesting dysregulated proteins & pathways
4 mo Si C57	Huntington's Disease Signaling 3-phosphoinositide degradation D-myo-inositol-5-phosphate metabolism Superpathway of inositol phosphate compounds 3-phosphoinositide biosynthesis	HNF4A miR-30c-5p(and other miRNAs w/seed GUAAACA) PPARA KLF3 SREBF1	
9 mo Si C57	Remodeling of epithelial adherens junctions Caveolar-mediated endocytosis signaling Clathrin-mediated endocytosis signaling Paxillin signaling Integrin signaling	HNF4A ERBB3 IL4 RHOJ Cipro fibrate	
12 mo Si C57	Aldosterone signaling in epithelial cells Protein ubiquitination pathway stearate Biosynthesis I (animals) Acute phase response signaling FAT10 signaling pathway	Pirinixic acid ELL2 HNF4A CYP2E1 ciprofibrate	sirtuin signaling pathway
1 mo 1Gy C57	Sirtuin signaling pathway Antigen presentation pathway Phagosome maturation Remodeling of epithelia adherens junctions Molybdenum cofactor biosynthesis	HNF4A POR SREBF1 SCAP ESR1	PTEN signaling, sumoylation, death receptor signaling

Top Canonical Pathways and Upstream Regulators from Proteomic Data via IPA			
Condition	Top 5 Canonical Pathways	Top Upstream Regulators	Other interesting dysregulated proteins & pathways
2 mo 1Gy C57	stearate Biosynthesis I (animals) 3-phosphoinositide degradation Clathrin-mediated endocytosis signaling 3-phosphoinositide biosynthesis D-myo-inositol (1,4,5,6)-tetrakisphosphate biosynthesis	CFTR TO-901317 Pirinixic acid HNF4A PPARA	
4 mo 1Gy C57	NAD Salvage Pathway II Cholesterol Biosynthesis I Cholesterol Biosynthesis II (via 24,25-dihydrolanosterol) Cholesterol Biosynthesis III (via Desmosterol) TWEAK signaling	HNF4A Methylprednisolone miR-155-5p (miRNAs w/seed UAAUGCU) PML DMD	
9 mo 1Gy C57	Glycine Betaine Degradation Clathrin-mediated endocytosis signaling Methionine salvage II (mammalian) L-serine degradation Caveolar-mediated endocytosis signaling	Diethyl nitrosamine miR-155-3p (miRNAs w/seed UCCUACC) RORA TP53 NCOA6	Sirtuin signaling pathway, superoxide radicals degradation
12 mo 1Gy C57	stearate Biosynthesis I (animals) Acyl-CoA hydrolysis Acetone Degradation I (to methylglyoxal) Clathrin-mediated endocytosis signaling Sirtuin signaling pathway	NKX2-2-AS1 HNF4A Pirinixic acid Ciprofibrate di(2-ethylhexyl) phthalate	mitochondrial L-carnitine shuttle pathway

Top Canonical Pathways and Upstream Regulators from Proteomic Data via IPA			
Condition	Top 5 Canonical Pathways	Top Upstream Regulators	Other interesting dysregulated proteins & pathways
1 mo 3Gy C57	Remodeling of epithelial adherens junctions Clathrin-mediated endocytosis signaling Systemic lupus erythematosus signaling Fcγ receptor-mediated phagocytosis in macrophages and monocytes Caveolar-mediated endocytosis signaling	HNF4A SREBF1 TLE3 miR-30c-5p (and other miRNAs w/seed GUAAACA) COMMD1	Insulin receptor signaling, sirtuin signaling pathway, mTOR signaling, PPAR signaling, PI3K/AKT signaling, ceramide signaling (sphingomyelin phosphodiesterase 4 (up)), PTEN Signaling
2 mo 3Gy C57	Acute phase response signaling Clathrin-mediated endocytosis signaling tRNA charging RhoGDI signaling Death Receptor signaling	Monobutyl phthalate HNF4A CST5 OGA 2,4,5,2',4',5'-heachlorobiphenyl	
4 mo 3Gy C57	JAK/Stat signaling IL-7 signaling pathway Reelin Signaling in Neurons Clathrin-mediated endocytosis signaling Systemic lupus erythematosus signaling	HNF4A Glucagon SREBF1 Insulin PPARGC1B	Sirtuin signaling, sphingosine-1-phosphate signaling, ubiquinol-10 biosynthesis (coenzyme Q3, methyltransferase up & cytochrome P450 family 46 subfamily A member 1 (down))
9 mo 3Gy C57	Actin cytoskeleton signaling Acute phase response signaling Integrin signaling Signaling by Rho Family GTPases Remodeling of Epithelial Adherens Junctions	Desmopressin HNF4A Levodopa PPARA Gcg	Sirtuin signaling pathway, sphingosine-1-phosphate signaling

Top Canonical Pathways and Upstream Regulators from Proteomic Data via IPA			
Condition	Top 5 Canonical Pathways	Top Upstream Regulators	Other interesting dysregulated proteins & pathways
12 mo 3Gy C57	Tight Junction Signaling RhoGDI Signaling Huntington's Disease Signaling Mechanisms of Viral Exit from Host cells LXR/RXR activation	HNF4A CST5 SREBF1 D-glucose IPMK	
1 mo O C3H	PXR/RXR activation Melatonin degradation I Superpathway of melatonin degradation NER pathway Nicotine Degradation III	HNF4A NPC1 nR1I3 Pirinixic acid PXR ligand	Sirtuin signaling pathway
2 mo O C3H	Tight Junction Signaling Glucocorticoid Receptor Signaling BAG2 Signaling pathway Integrin signaling Remodeling of epithelial adherens junctions	HNF4A Methylprednisolone XBP1 D-glucose TP53	Sirtuin signaling pathway
4 mo O C3H	Estrogen Biosynthesis ILK signaling Tetrahydrobiopterin biosynthesis I Tetrahydrobiopterin biosynthesis II Acetone degradation I (to methylglyoxal)	CST5 Oxaliplatin Folic acid KLF1 PNN	Sirtuin signaling pathway, ceramide signaling
9 mo O C3H	Urate Biosynthesis/Inosine 5'-phosphate degradation Apelin Adipocyte Signaling pathway PXR/RXR activation Stearate Biosynthesis I (animals) LPS/IL-1 mediated inhibition of RXR function	HNF4A Carbohydrate TO-901317 NR1I2 SREBF1	Sirtuin signaling pathway

Top Canonical Pathways and Upstream Regulators from Proteomic Data via IPA			
Condition	Top 5 Canonical Pathways	Top Upstream Regulators	Other interesting dysregulated proteins & pathways
12 mo O C3H	Acute Phase Response Signaling Gα12/13 signaling Huntington's Disease Signaling AMPK Signaling Salvage Pathways of Pyrimidine Ribonucleotides	HNF4A HSF1 TGFB1 PTP4A1 Cyclosporine A	Sirtuin signaling pathway
1 mo Fe C3H	Actin cytoskeleton signaling Clathrin-mediated endocytosis signaling Mechanisms of viral exit from host cells RhoA signaling Tight Junction Signaling	HNF4A Ciprofibrate NPC1 Clofibrate CFTR	
2 mo Fe C3H	Remodeling of epithelial adherens junctions ILK signaling Sirtuin Signaling pathway PXR/RXR activation Fcy Receptor-mediated phagocytosis in macrophages and monocytes	HNF4A XBP1 Methylprednisolone Nitrofurantoin Latrunculin B	Ceramide signaling
4 mo Fe C3H	Acetone degradation I (to methylglyoxal) Tetrahydrobiopterin biosynthesis I Tetrahydrobiopterin biosynthesis II RhoA signaling NER pathway	HNF4A TO-901317 ACOX1 Ciprofibrate ZNF106	Sirtuin signaling pathway, ubiquinol-10 biosynthesis
9 mo Fe C3H	Acetone Degradation I (to methylglyoxal) Nicotine Degradation III Melatonin Degradation I Nicotine Degradation II Superpathway of Melatonin Degradation	PPARA TO-901317 Pirinixic acid POR HNF4A	Sirtuin signaling pathway, ubiquinol-10 biosynthesis

Top Canonical Pathways and Upstream Regulators from Proteomic Data via IPA			
Condition	Top 5 Canonical Pathways	Top Upstream Regulators	Other interesting dysregulated proteins & pathways
12 mo Fe C3H	Complement system ILK signaling Adenosine Nucleotides Degradation II Role of JAK2 in Hormone-like cytokine signaling Acute phase response signaling	HNF4A TO-901317 D-glucose CST5 Levodopa	Sirtuin signaling pathway, ubiquinol-10 biosynthesis, ceramide signaling
1 mo Si C3H	Death receptor signaling Phagosome maturation Actin cytoskeleton signaling Signaling by Rho family GTPases RhoGDI signaling	miR-155-5p (miRNAs w/seed UAAUGCU) Methylprednisolone HNF4A Gentamicin Interferon beta-1a	Sirtuin signaling pathway
2 mo Si C3H	Glycine degradation (creatine biosynthesis) NER pathway Mechanisms of Viral exit from host cells Acute phase response signaling Acetone degradation I (to methylglyoxal)	HNF4A miR-155-5p (miRNAs w/seed UAAUGCU) TO-901317 RAB1B 1,2-dithiol-3-thione	Phosphatidylcholine biosynthesis I, sirtuin signaling
4 mo Si C3H	PXR/RXR activation Acetone degradation I (to methylglyoxal) FXR/RXR activation Nicotine degradation III LXR/RXR activation	HNF4A Ciprofibrate TO-901317 Pregnenolone carbonitrile PXR ligand-PXR-retinoic acid RXR $\alpha$	Sirtuin signaling pathway, ubiquinol-10 biosynthesis
9 mo Si C3H	Acute phase response signaling LXR/RXR activation FXR/RXR activation Bupropion Degradation PXR/RXR activation	DYSF Pirinixic acid PPARA HNF4A POR	Sirtuin signaling pathway

Top Canonical Pathways and Upstream Regulators from Proteomic Data via IPA			
Condition	Top 5 Canonical Pathways	Top Upstream Regulators	Other interesting dysregulated proteins & pathways
12 mo Si C3H	Clathrin-mediated endocytosis signaling Phagosome maturation Autophagy Intrinsic prothrombin activation pathway Urate biosynthesis/inosine 5'-phosphate degradation	Metribolone IL4 CEBPA Methylprednisolone miR-1-3p (and other miRNAs w/seed GGAAUGU)	Sirtuin signaling pathway, 3-phosphoinositide degradation, ubiquinol-10 biosynthesis
1 mo 1Gy C3H	Phagosome maturation Remodeling of epithelial adherens junctions Tight junction signaling PXR/RXR signaling Superpathway of melatonin degradation	HNF4A D-glucose Collagen(s) Nitrofurantoin NR3C1	P13K/AKT signaling
2 mo 1Gy C3H	PXR/RXR activation Huntington's Disease Signaling Remodeling of Epithelial Adherens Junctions SAPK/JNK signaling Tumoricidal Function of Hepatic Natural Killer cells	HNF4A Mercuric chloride Nitrofurantoin XBP1 Bromobenzene	ceramide signaling, sirtuin signaling pathway, sphingosine-1-phosphate signaling
4 mo 1Gy C3H	Acetone Degradation I (to methylglyoxal) PXR/RXR activation Death receptor signaling Mechanisms of viral exit from host cells Estrogen biosynthesis	HNF4A NR1I2 PXR ligand-PXR-Retinoic acid-RXR $\alpha$ NKX2-3 oltipraz	Sirtuin signaling pathway
9 mo 1Gy C3H	Acute phase response signaling Nicotine degradation III Nicotine degradation II Bupropion Degradation Melatonin Degradation I	HNF4A Pregnenolone carbonitrile 1,2-dithiol-3-thione OBSCN TO-901317	mTOR



Top Canonical Pathways and Upstream Regulators from Proteomic Data via IPA			
Condition	Top 5 Canonical Pathways	Top Upstream Regulators	Other interesting dysregulated proteins & pathways
12 mo 1Gy C3H	Acute Phase Response signaling FAK signaling Autophagy Remodeling of epithelial adherens junctions Regulation of eIF4 and p70S6K	HNF4A ACOX1 Methylprednisolone DYSF PPARA	Sirtuin signaling pathway, ubiquinol-10 biosynthesis, ceramide signaling
1 mo 3Gy C3H	Sirtuin signaling pathway Clathrin-mediated endocytosis signaling Melatonin degradation I Superpathway of Melatonin Degradation FAT10 signaling pathway	HNF4A MAPT Pirinixic acid Glucagon XBP1	mTOR, glycolysis I
2 mo 3Gy C3H	Lipoate Biosynthesis and Incorporation II PFKFB4 signaling pathway Glycogen degradation II L-serine degradation Glycogen Degradation III	HNF4A PNPT1 MAP1S (-)-norephedrine RAB1B	Glucose & glucose-1-phosphate degradation, phosphatidylglycerol biosynthesis II
4 mo 3Gy C3H	NAD Salvage Pathway II Guanosine Nucleotide Degradation III Urate Biosynthesis/Inosine 5'phosphate degradation Adenosine nucleotides degradation II Purine nucleotides degradation II (aerobic)	HNF4A CST5 miR-30c-5p (and other miRNAs w/seed GUAAACA) PGR tazarotene	
9 mo 3Gy C3H	Acute phase response signaling Actin cytoskeleton signaling Integrin signaling Clathrin-mediated endocytosis signaling RhoA signaling	HNF4A Pirinixic acid TP53 Nitrofurantoin MAPT	Sirtuin signaling pathway, ubiquinol-10 biosynthesis, ceramide signaling, glycolysis I

Top Canonical Pathways and Upstream Regulators from Proteomic Data via IPA			
Condition	Top 5 Canonical Pathways	Top Upstream Regulators	Other interesting dysregulated proteins & pathways
12 mo 3Gy C3H	Acute phase response signaling Clathrin-mediated endocytosis signaling IL-7 signaling DNA double strand break repair by non-homologous end joining Endometrial cancer signaling	HNF4A SIRT1 Methylprednisolone TO-901317 tretinoin	Sirtuin signaling pathway

Table 11: Top canonical pathways and upstream regulators from proteomics data via IPA

As mentioned earlier, some of the mitochondria sirtuins are seen in the proteomic data set including SIRT 3 & 5. The NAD<sup>+</sup> dependence of sirtuins lead to the belief that they are metabolic sensors as their levels are high when NAD<sup>+</sup> is in abundance as they are in times of nutrient stress. Hepatic SIRT3 levels have been found to be increased during times of fasting. SIRT3 activates hepatic lipid catabolism. *Sirt3*<sup>-/-</sup> mutants show decreased fatty acid oxidation, low ATP production, develop fatty liver and show defects in thermogenesis and hypoglycemia during cold test. SIRT3 has also been shown to interact with and deacetylate Complex I subunits and succinate dehydrogenase in Complex II. In proteomic studies, SIRT3 has been shown to bind ATP synthase. It also regulates mitochondrial translation which affects electron transport. SIRT3 is heavily involved in deacetylation and numerous TCA cycle enzymes are modified by acetylation. SIRT3 interacts with succinate dehydrogenase and isocitrate dehydrogenase 2, and influences the TCA cycle indirectly via deacetylation and activation of AceCS2 and glutamate dehydrogenase. Changes in SIRT3 expression have been associated with ROS production and scavenging. There is also support for SIRT3

in a pro-apoptotic role and as a tumor suppressor. However, some studies have also found it to be anti-apoptotic.<sup>19</sup> SIRT 3 was found to be upregulated in 9 mo <sup>28</sup>Si C57, and 12 mo <sup>56</sup>Fe and 1Gy gamma C3H. It was downregulated in 1 & 2 mo 1Gy gamma C3H, 2 mo 3Gy gamma and <sup>16</sup>O C57, 2 mo <sup>16</sup>O C3H, 9 mo <sup>56</sup>Fe C3H, 9 mo <sup>16</sup>O, <sup>28</sup>Si & 3Gy gamma C57, 12 mo 1Gy gamma C57, and 12 mo <sup>56</sup>Fe & 1Gy gamma C3H.

SIRT5 is known to physically interact with cytochrome C, but the significance of this interaction is still unknown. It also regulates carbamoyl phosphate synthetase which is the rate-limiting and first step in the urea cycle. Thus, SIRT5 coordinates with the detoxification of hepatic by-products of amino acid catabolism.<sup>19</sup> SIRT5 was upregulated in 1 mo <sup>16</sup>O C57, 9 mo <sup>56</sup>Fe C57 and 12 mo <sup>28</sup>Si C57. It was downregulated in 1 mo <sup>28</sup>Si C3H, 4 mo <sup>16</sup>O C3H, 9 mo <sup>16</sup>O, <sup>28</sup>Si & 1Gy gamma C57, and 9 mo <sup>28</sup>Si C3H.

The process of endocytosis begins with the packing of biological materials into vesicles that are then sent to the early endosome for sorting. These vesicles are typically targeted back to the plasma membrane or to the late endosome and/or the lysosome for degradation. Endosomes can also interact with the Golgi apparatus and ER. Evidence has also shown that they can be directly trafficked to the mitochondria by clathrin-mediated endocytosis as well. It is thought this could be another possible way of importing lipids into the mitochondria.<sup>54</sup>

Pathogen-associated molecular patterns (PAMPs), damage-associated molecular patterns (DAMPs), and cytokines have been recognized to have both direct and indirect impacts on phagosome maturation. These signals can accelerate or delay phagosome maturation to enhance microbial killing or antigen presentation<sup>55</sup>. DAMPs are capable of

initiating an inflammatory response that is very similar to that caused by PAMPs, but they are able to do so without the presence of any microbial infections. Studies performed by Zhang et al.<sup>56</sup> have shown that mitochondria can release DAMPs following severe injury. In their study, correlating the fact that mitochondria evolved from bacteria, Zhang et al. looked for DNA and formylated peptides both of which are known bacterial PAMPs in the blood of trauma patients. In trauma patients, they found high levels of mitochondria DNA and DAMPs circulating in the blood compared with healthy control volunteers. They even detected high levels in bones after fractures that had been repaired by orthopedists.

The mitochondria DAMPs have maintained their evolutionarily conserved similarities to bacterial PAMPs.<sup>57</sup> When injury occurs, typically so does cell lysis, degradation, and tissue breakdown (necrosis) which causes the release of cellular content including disrupted mitochondria. Since each cell contains dozens of mitochondria and there are thousands of cells comprising our tissues, it is no surprise that when severe trauma occurs that large amounts of mitochondrial DAMPs are poured out into the circulatory system which activates an immunological cytokine storm.

In the ILK signaling pathway, ILK acts on PKB/Akt. It is involved in cell progression and promotes the nuclear translocation and activation of  $\beta$ -catenin. It is also involved in glycogen metabolism as it is able to inhibit the activity of glycogen synthase kinase-3(GSK-3).<sup>58</sup>

Leukocyte extravasation signaling is the movement of leukocytes from the blood vessels towards the site of inflammation, damage or infection with the most common cells being T lymphocytes, natural killer cells, neutrophil granulocytes and monocytes<sup>59</sup>.

While this pathway is not directly linked to mitochondria, this pathway is likely being activated due to the damage and inflammation that is occurring both from the irradiation itself as well as from the resulting ROS. Cancer cells are also very similar to leukocytes in that they do not randomly leave the blood vessels but are guided by certain signals that are delivered by the vascular endothelium. It is believed that they might use similar localization signals<sup>59</sup>. Thus, this pathway could also be seen due to the activation of carcinogenesis. The data also identifies some heme related pathways. Mitochondria are also involved in heme biosynthesis as they are responsible for synthesizing the precursor for heme groups<sup>49</sup>.

## **LIPIDOMICS**

As part of the integrated omics approach, comprehensive lipidomics was one of the key aspects in this project. Lipids are a very diverse group of molecules that are classified into 8 different groups: fatty acyls (fatty acids (FA), wax, hydroxyl-fatty acids, etc.), glycerolipids (di- & triacylglycerides (DAG/TAG), mono- and digalactosyldiacylglycerides, etc.), glycerophospholipids (phosphatidic acids (PA), phosphatidylethanolamines (PE), phosphatidylserines (PS), phosphatidylinositols (PI), phosphatidylglycerols (PG), cardiolipins), sphingolipids (sphingosines, sphingosine-1-phosphates, ceramides, sphingomyelins, ganglioside mannoside 3 (GM3), etc.), sterols (cholesterols, cholesteryl esters, cholesteryl sulfates, etc.), prenol lipids (isoprenoids, quinones, etc.), saccharolipids, and polyketides<sup>60</sup>. These molecules have several different functions, and are involved in a wide variety of processes such as energy homeostasis, membrane structure and dynamics along with cellular signaling.

Glycerophospholipids, sphingolipids, and sterols such as cholesterol are crucial constituents of the membrane whereas groups such as the steroid hormones and eicosanoids including prostaglandins are responsible for communication between cells. Sphingosines also occur in blood and plasma membranes of nearly all cells, but their highest concentrations are found in the white matter of the central nervous system. Other lipids are also enriched in certain areas such as cardiolipins in the mitochondria, and phosphoinositides and bis(monoacylglycero)phosphate in endosomes<sup>61</sup>. Because these molecules are not genetically encoded, but are instead generated and metabolized by enzymes, they are greatly influenced by the environment of the biological system<sup>61</sup>. Lipid composition is highly dynamic because it depends upon several factors such as diet, circadian rhythms, and cell cycle.<sup>62</sup> Thus, lipids are key indicators of change in the cellular environment.

Lipid homeostasis has been known to be fundamental to health maintenance, and thus, an imbalance in lipid metabolism often contributes to disease states. Dysregulation of lipid metabolism has been seen to play an important role in several human diseases such as neurodegenerative diseases, metabolic syndromes, cancer, and infectious diseases. Due to their involvement in signaling pathways, there have been an expanding number of drugs aimed at these molecules, such as the statins and cyclooxygenase inhibitors<sup>60,61</sup>.

The liver plays a vital role in lipid metabolism. It is responsible for the synthesis of plasma apolipoproteins, endogenous lipids, and lipoproteins along with being a site for  $\beta$ -oxidation. When hepatic damage occurs, these processes are impaired leading to alternations in lipid and lipoprotein production and degradation<sup>63,64</sup>. Because of this

organ's role in lipid metabolism and the dysregulation of these molecules that have been exhibited in other cancers, it is believed these elements will also play a crucial role in the formation and progression of HCC. We believe that because of their structural and signaling roles, lipids can act as a window for micro-environmental changes induced by HZE.

With the advancements that have been made in mass spectrometry (MS) over the last decade, high resolution MS has become the key technique for studying this diverse group of molecules. Advancements in both liquid chromatography and MS have increased sensitivity, when paired with highly selective analysis, LC-MS has allowed for the identification of lipids with diverse chemical compositions in complex mixtures<sup>60,61</sup>. Currently there are five generic types of MS which include quadrupole, magnetic sector, ion trap, time of flight (TOF), and Fourier transform (FT). The FT instruments are the highest resolution instruments available, and include instruments such as the FT-ICR MS and Orbitrap. The FT-ICR MS has the highest resolution, and the highest mass accuracy currently available<sup>65</sup>. Mass accuracy is crucial when dealing with masses that are isobaric. For example, one acetylation is 42.0373 Daltons (D) and three methylations are 42.0807D, a difference of 0.0434 D. If an instrument is not equipped with high mass accuracy, there will be no way to distinguish between these common modifications. The same is true for a phosphorylation at 79.9799 D and sulfonation at 80.0642 D with a difference of only 0.0843 D. These studies were performed with a Bruker Solarix FT-ICR MS equipped with a 12 tesla superconducting magnet, making it the highest performance MS in the South Central US. This instrument has mass accuracy that is routinely better than 500 parts per billion (ppb), which allows for masses such as

143.04288 and 143.04516 to be easily distinguished from each other. With its high resolution capabilities, the FT-ICR MS can also detect isotopic fine structure, isotope abundances, and aid in analysis of complex mixtures which is vitally important for making correct identification in complex biological samples.

Figures 17-21 show the lipids that exhibited the most changes in the C57 mice throughout the time course. There are two graphs for each species. The second of the two shows the variability within the samples. At 1 month post irradiation (Figure 17), two lipids changed, Sterol Ester (27:1/20:5) and PA (36:3). Sterol Ester was not present in the any of the non-irradiated samples and was the highest in <sup>56</sup>Fe irradiated mouse livers. PA (36:3) was decreased in the HZE irradiated. It should be noted that very little variability was seen for this species in the HZE animals. A study conducted in yeast, identified 17 genes that are required for efficient uptake and/or transport of sterols as sterols are synthesized in the ER and need to efficiently transported to the plasma membrane which harbors ~90% of the free sterol pool of the cell. When sterols are taken up from the environment, they are transported from the plasma membrane to the ER where they are esterified to sterol esters. Of these 17 genes, many were required for mitochondria function. Thus, it is thought there is a possible connection between mitochondrial biogenesis and sterol biosynthesis and uptake.<sup>66</sup> Also, sterol contents in organelle membranes is typically strictly controlled, and a fraction of excess sterols is esterified by acyl-CoA: sterol acyltransferases and stored as sterol ester in lipid droplets (LDs).<sup>67</sup> Thus, sterol esters are typically in low abundance and stored in lipid droplets. An increase in sterol ester within the mitochondria will result in mitochondria dysfunction.<sup>67</sup> Esterification of sterols will also interfere with cholesterol biosynthesis which is a pathway that was identified in the transcriptomic and proteomic data. Phosphatidic acid (PA) is a second messenger lipid that has many signaling functions such as cell growth, proliferation, reproduction and responses to hormones and stress.<sup>68</sup> PA also has a



connection to the mitochondria as it inhibits mitochondrial division and stimulates mitochondrial outer membrane fusion. Mitochondrial fusion and division play important roles in mitochondrial size, number, distribution, function and turnover.<sup>69</sup> PA is essential for controlling mitochondrial morphology as it results in curvature of the membrane that is necessary for mitochondrial interaction with the ER.<sup>70</sup> PA is also the precursor for the synthesis of cardiolipins.<sup>69</sup> Thus, if PA decreases so will the cardiolipins. It is, however, important to note that while these lipid species have connections to the mitochondria, these studies were conducted on whole cells. Thus, it could be very beneficial to look at just the lipids from isolated mitochondria in the future.

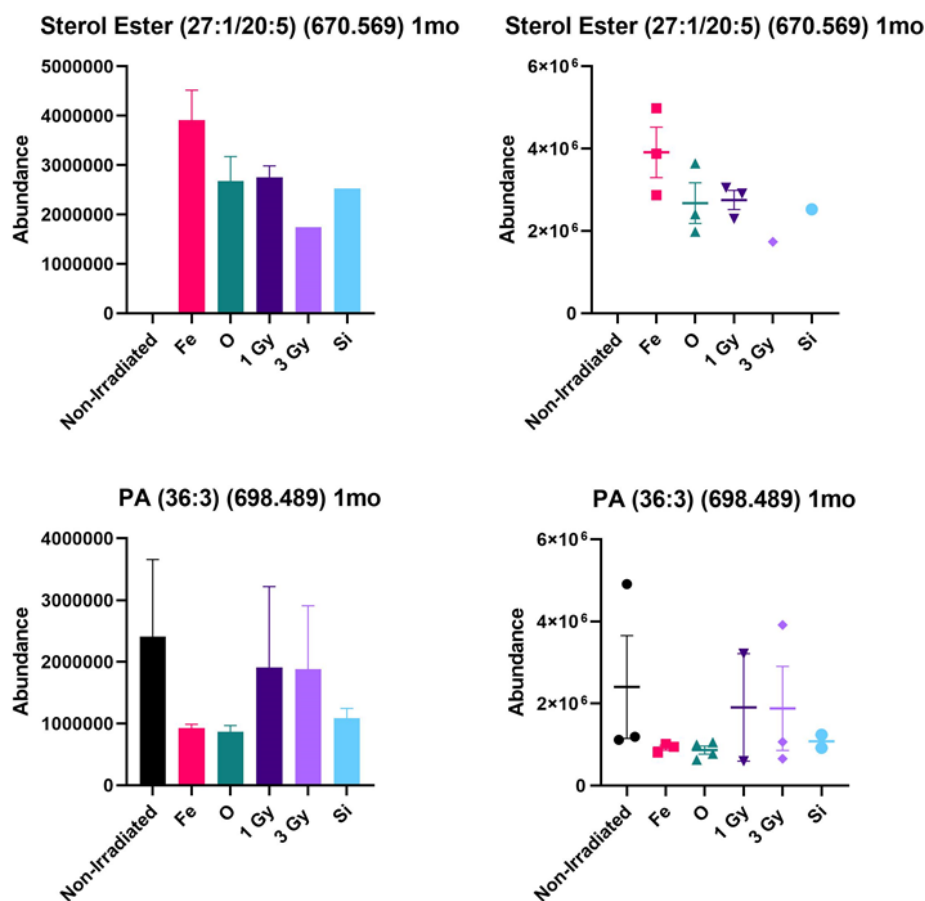


Figure 17: 1 month lipids of interest in C57 mice

At month 2 (Figure 18), only two species exhibited interesting trends as both lysophosphatidylethanolamine (LPE) (14:1) and PE(20:0) were only seen in the

irradiated samples. LPE was only seen in one of the 1Gy samples so if that data point was removed the levels would be the highest in  $^{56}\text{Fe}$  and  $^{16}\text{O}$  irradiated.

Phosphatidylethanolamine (PE) is synthesized by four different pathways, three of which are found in the ER and the remaining pathway is dependent on phosphatidylserine decarboxylase (Psd1) which is embedded in the mitochondrial membrane. The Psd pathway utilizes phosphatidylserine (PS) as a substrate. When Psd1 is deleted, it decreases cellular growth, impairs oxidative phosphorylation, alters mitochondrial morphology and diminishes PE levels both within the cells and the mitochondria. The PE that is made outside of the mitochondria cannot compensate for the absence of Psd1. However, it has been seen to improve oxidative phosphorylation in Psd1 deficient yeast.<sup>71</sup> Lysophospholipids are the products of the activity of phospholipase A2 (PLA2) on phospholipids.<sup>72</sup> They are more hydrophilic and versatile than their corresponding phospholipids. These lipids can act as extracellular mediators by activating specific G-protein coupled receptors (GPCR).<sup>73</sup> They have emerged as second-messenger molecules that can regulate intracellular signaling pathways that are involved in several physiological and pathological functions. Some of these functions include inflammation, angiogenesis, nervous system regulation, atherosclerosis and tumorigenesis.<sup>72</sup> LPE along with oleoylethanolamide, palmitoylethanolamide and oleoyethylamide are known to activate GPR119 that is expressed primarily in islet  $\beta$ -cells and the K and L cells of the gastrointestinal tract. This receptor has been strongly implicated in the regulation of energy balance as well as body weight.<sup>74</sup> Lysophosphatidylcholine (LPC) and LPE have also been found to be increased in individuals with Type 2 diabetes.<sup>75</sup> Accumulation of lysophospholipids can also have

harmful effects on the structure and function of mitochondria, and high blood levels of lysophospholipids is known as an indicator of mitochondria dysfunction.<sup>67</sup>

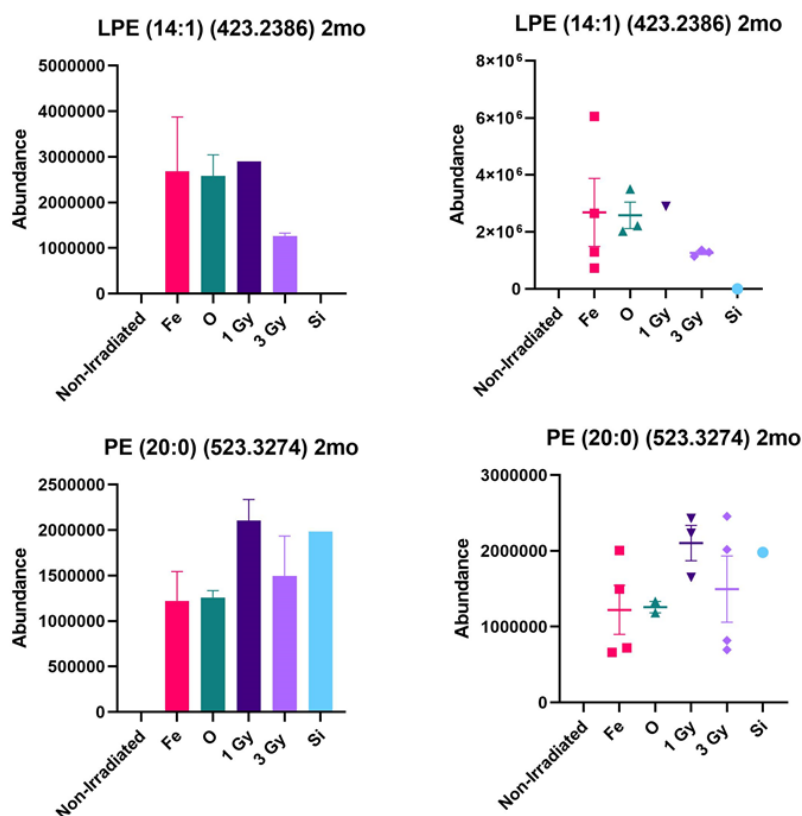
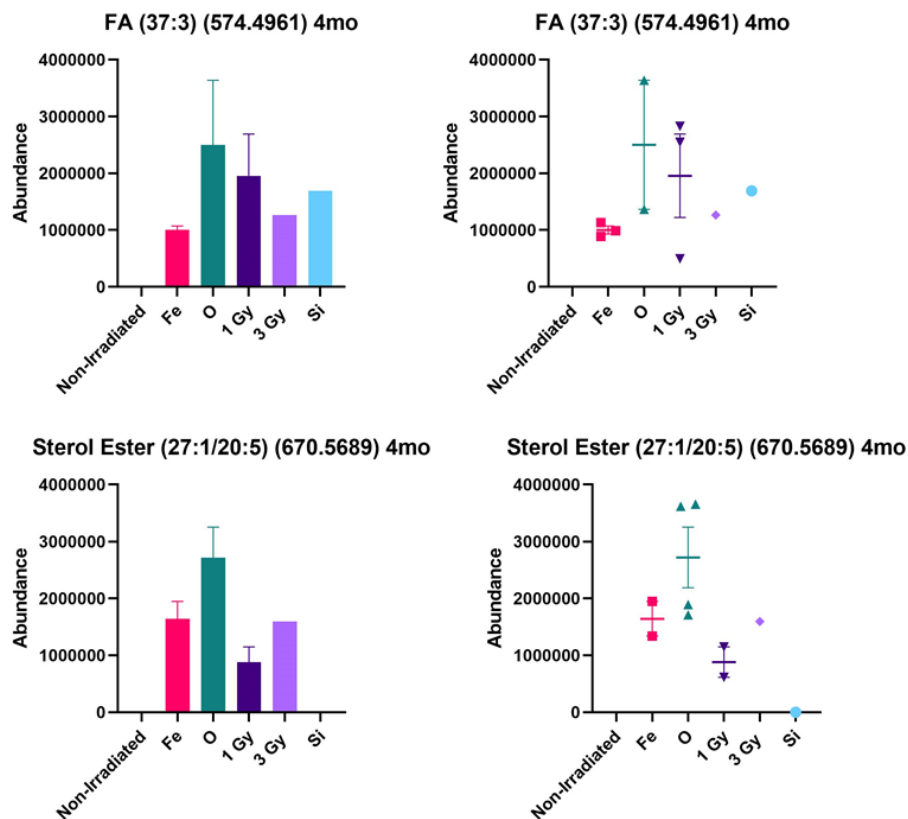


Figure 18: 2 month lipids of interest in C57 mice

At month 4 (Figure 19), three species were impacted, FA(37:3), Sterol ester (27:1/20:5), and PS(44:8). Both FA and Sterol were only present in the irradiated mice. Sterol ester was highest in  $^{16}\text{O}$  followed by  $^{56}\text{Fe}$  having the next highest levels. On the other hand, PS was basically only present in the non-irradiated control samples as it was only found in one  $^{16}\text{O}$  and 1Gy gamma irradiated sample. PS is synthesized on the mitochondrial-associated membrane of the ER by phosphatidylserine synthase. In order for the Psd1 pathway to function, it must then be imported into the mitochondria to synthesize PE.<sup>71</sup> Lipids are not randomly distributed among biological membranes. In

the plasma membrane PC, sphingolipids and glycolipids tend to be enriched on the exoplasmic leaflet of the membrane whereas PS, PE and PI are primarily confined to the cytoplasmic leaflet. Membranes of cellular organelles such as the Golgi, secretory vesicles and endosomes also show a similar asymmetric distribution. This distribution helps with a number of cellular processes that take place at the membrane such as budding, trafficking, membrane protein regulation, and cell signaling. It also helps determine the shape, stability and impermeability.<sup>62,76</sup> Many lipids also recruit proteins with lipid-binding domains to specific membrane compartments or membrane subdomains. The best understood lipids that engage in this type of protein recruit are the PIs. PA, DAG and PS are also known to recruit proteins. PS is also involved in intracellular trafficking.<sup>62</sup>



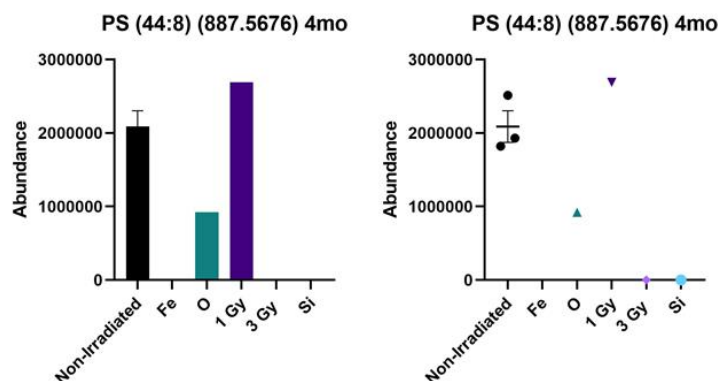


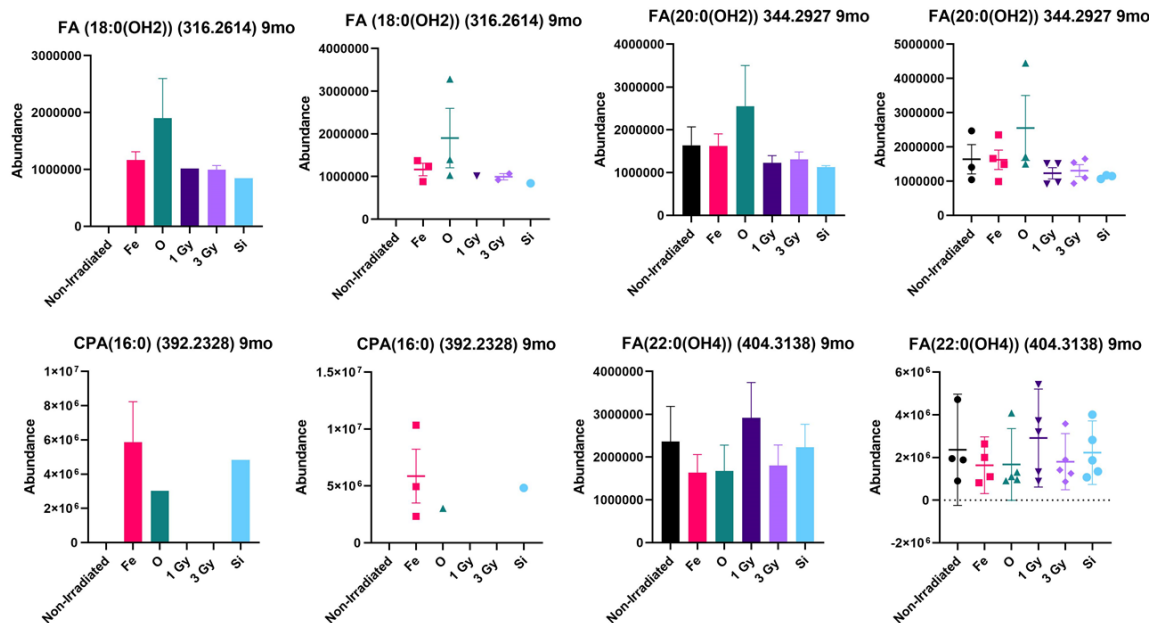
Figure 19: 4 month lipids of interest in C57 mice

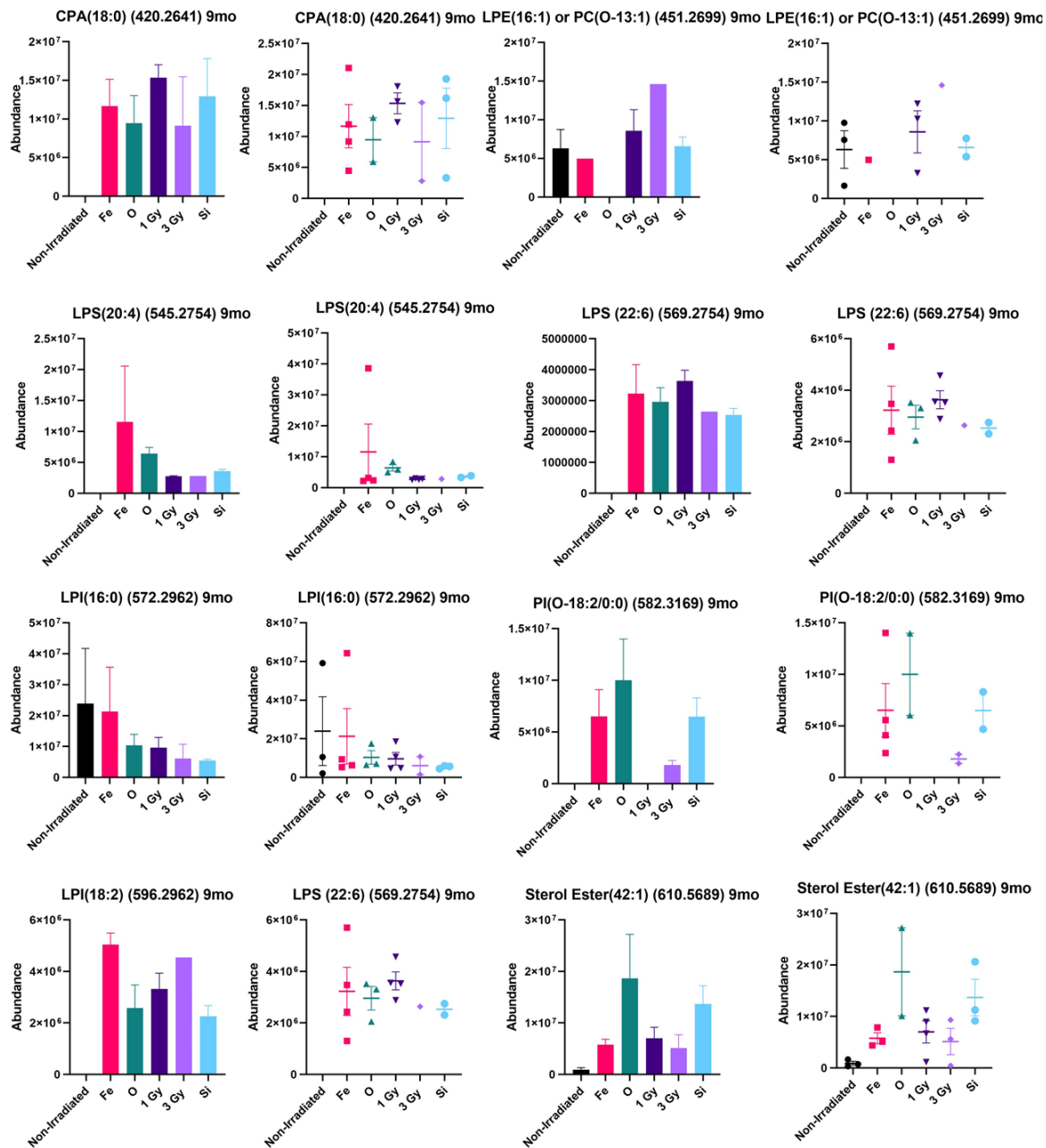
In month 9 (Figure 20), there were 22 species of lipids that are impacted including: FA(18:0(OH<sub>2</sub>)), FA(20:0(OH<sub>2</sub>)), cyclic phosphatidic acid CPA(16:0), FA(22:0(OH<sub>4</sub>)), CPA(18:0), LPE (16:1) or PC(O-13:1), lysophosphatidylserine (LPS) (20:4), LPS(22:6), LPI (16:0), PI(O-18:2/0:0), lysophosphatidylinositol (LPI) (18:2), Sterol ester (42:1), LPI (20:4), LPI(20:3), Sterol ester (27:1/16:0), LPI (22:6), Cholesteryl stearate, PI(34:2), phosphatidylglucose (Glc-GP) (38:4) or PI(38:4), PI(38:3), PI(40:6), GalNAcβ1-4(NeuGcα2-3)Galβ1-4Glcβ-Cer (d18:1/22:0), a glycosphingolipid which is the mouse analog of Ganglioside GM2 (t18:0/22:1) (13Z). Of these, only three statistically significant differences occur. These include Sterol ester 42:1 <sup>56</sup>Fe irradiated compared to non-irradiated (p=0.0127) and <sup>28</sup>Si irradiated compared to non-irradiated (p=0.0230), and Sterol ester (27:1/16:0) <sup>28</sup>Si irradiated compared to non-irradiated (p=0.0026). However, several of these species are only found in irradiated groups. Thus, while they are not statistically significant they may still hold important biological relevance. FA(18:0(OH<sub>2</sub>)) was only present in the irradiated samples and is quite high in one of the <sup>16</sup>O irradiated. FA(20:0(OH<sub>2</sub>)) was also elevated in one of the <sup>16</sup>O samples and was down in the gamma and <sup>28</sup>Si. CPA(16:0) was only present in HZE irradiated samples. FA(22:0(OH<sub>4</sub>)), with the exception of one sample, was lower in the

<sup>16</sup>O irradiated. CPA(18:0) also only found in irradiated samples. LPE (16:1) or PC(O-13:1) was not found in <sup>16</sup>O and only one of the 3Gy and <sup>56</sup>Fe. LPS(20:4) was only in the irradiated and quite high in one of the <sup>56</sup>Fe samples. LPS(22:6) was also only in irradiated samples. PI(O-18:2/0:0) was only in irradiated as well and highest in HZE and not in 1Gy gamma irradiated. LPI(18:2) was also only in irradiated and LPI(20:3) was not present in <sup>16</sup>O irradiated. Although Sterol ester (27:1/16:0) was only significant in <sup>28</sup>Si irradiated, it was also high in all the irradiated. There was simply too much variability in the other conditions to obtain significance with the small n number. LPI (22:6) was not present in the control samples and was the highest in HZE irradiated. Cholesteryl stearate was highest in the <sup>16</sup>O irradiated and PI(34:2) was basically only in the <sup>56</sup>Fe irradiated. Glc-GP(38:4) or PI(38:4) was only present in <sup>56</sup>Fe & <sup>16</sup>O. PI(38:3) and PI(40:6) were only found in the <sup>56</sup>Fe and <sup>28</sup>Si irradiated. Last but possibly the most interesting, mouse analogue of Ganglioside GM2 (t18:0/22:1) (13Z) was found in <sup>56</sup>Fe and <sup>16</sup>O and only one of the 3Gy gamma and <sup>28</sup>Si.

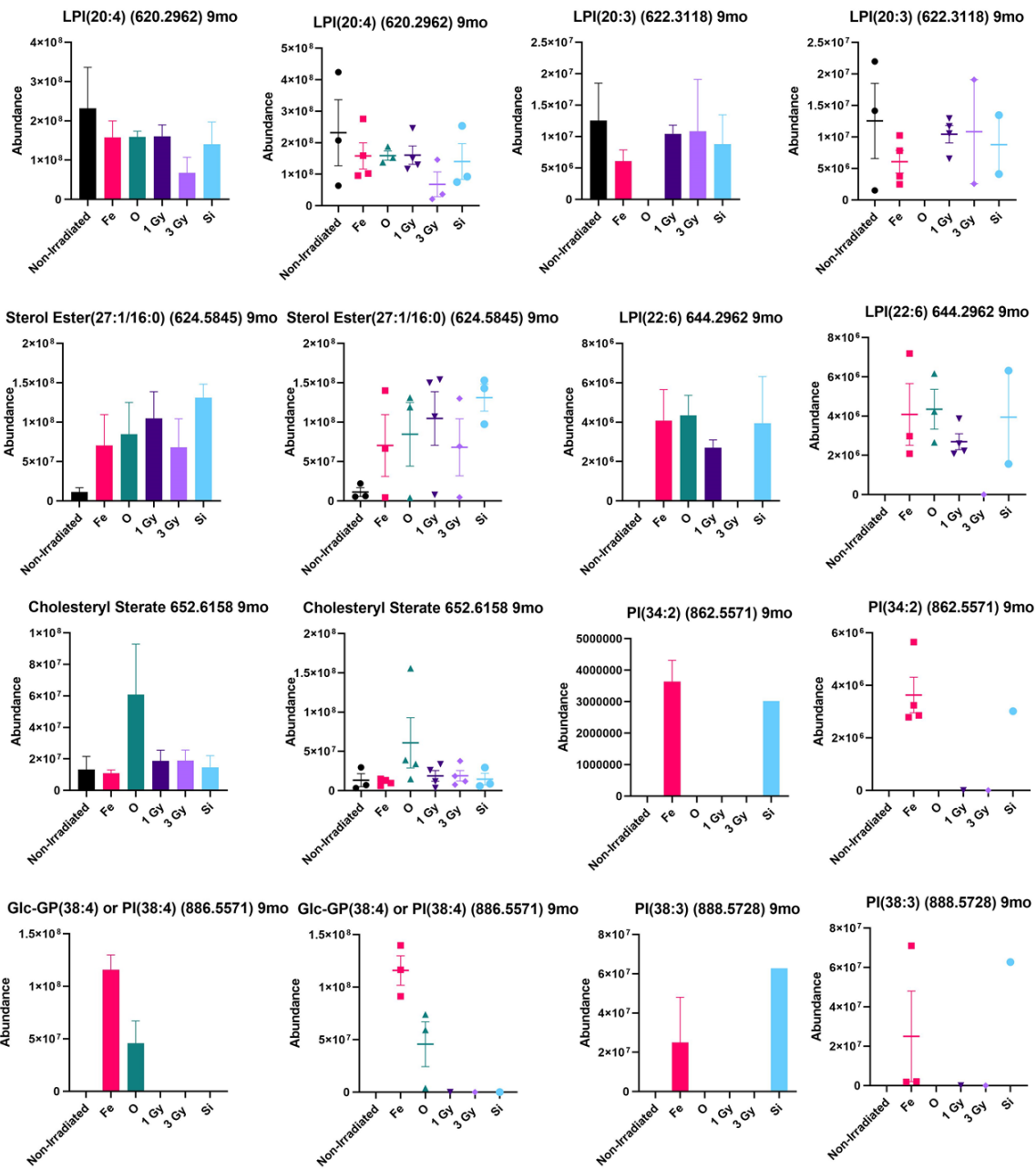
CPA is a cyclic phosphatidic acid. It has been shown to have specific biological functions such as antimitogenic regulation of cell cycle, regulation of actin stress fiber formation and rearrangement, inhibition of cancer cell invasion and metastasis, and mobilization of intercellular calcium.<sup>77</sup> CPA is also an antagonist at the peroxisome proliferator-activated receptor  $\gamma$  (PPAR $\gamma$ ). The PPAR $\gamma$  binds to the retinoid X receptors (RXR) which then acts as a transcription factor to initiate cell proliferation and inflammation.<sup>78</sup> Lysophospholipids and leukotrienes are agonists at the PPAR $\gamma$  receptor.<sup>78</sup> Thus, the increase in CPA infers a compensatory mechanism to shut down the effects of the proliferation and immune response from irradiation. Activation of the

PPAR $\gamma$  and RXR pathways are also in the transcriptomics and proteomics data. LPS is known to enhance histamine release and result in eicosanoid production. It has also been seen to promote the phagocytosis of apoptotic cells. For example, it has been shown to enhance the clearance of activated or aged apoptotic neutrophils by macrophages through the macrophage G-protein coupled receptor G2. Thus, it plays a key role in promoting timely resolution of inflammation.<sup>79</sup> LPI has been shown to be involved in cell growth, differentiation, and motility. It has also been shown to play a role in metabolism and glucose homeostasis.<sup>72</sup> Previous studies conducted in our lab at 6 months post <sup>56</sup>Fe irradiation, showed an upregulation of mouse analogue of GM2 in samples of irradiated livers. GM2 has been reported to be highly elevated (20-100 fold) in serum of human patients with HCC. These serum changes were reported in 1987 and there have been no follow up studies<sup>80</sup>.









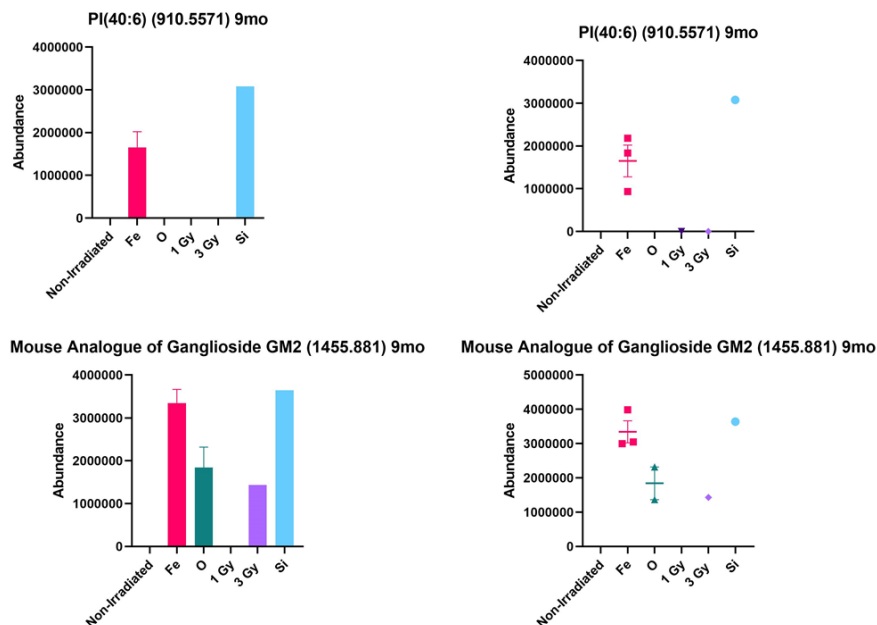


Figure 20: 9 month lipids of interest in C57 mice

At 12 month (Figure 21), we saw four species including CPA(18:0), LPS(16:0), LPS(20:4), and LPS(22:6). CPA(18:0) was only seen in irradiated and was highest in  $^{56}\text{Fe}$ . LPS(16:0) was particularly high in one non-irradiated sample but not present in the rest of the samples in that group. It was also only present in one of the 1Gy gamma samples and very high in one of the 3Gy gamma samples. There was less variability in the HZE irradiated samples. LPS(20:4) and LPS(22:6) were also only present in the irradiated samples. LPS(22:6) was highest in  $^{56}\text{Fe}$  and one of the  $^{28}\text{Si}$  samples.

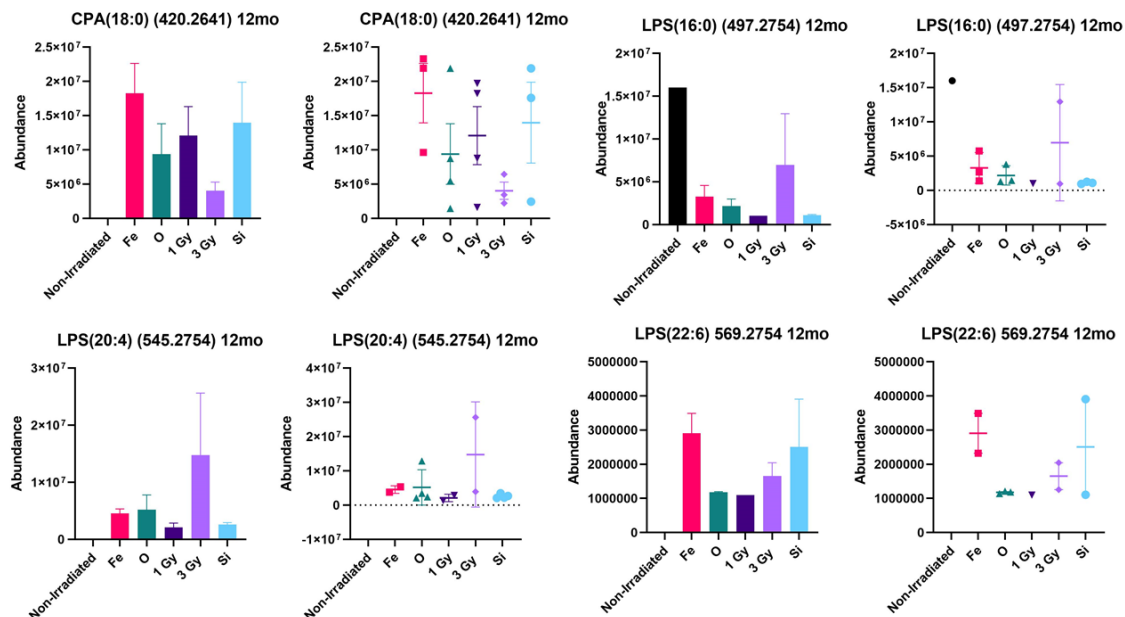


Figure 21: 12 month lipids of interest in C57 mice

## METABOLOMICS

Metabolomics was not included in the original plans, but an opportunity was presented to collect metabolomics data to add to our omics platform. The goal was to determine if the metabolomics data further supported the mitochondria dysfunction induced by low-dose HZE. Metabolomics data was collected on caudate liver from C57 non-irradiated, 1Gy gamma,  $^{56}\text{Fe}$  and  $^{16}\text{O}$  irradiated at all time points and  $^{28}\text{Si}$  irradiated data was collected on the 1, 2 and 4 month samples. It was decided to focus on these conditions because 3Gy gamma is a much harsher dose of irradiation and we wanted to see more of the distinct differences between gamma and HZE. Also of the HZE irradiated,  $^{56}\text{Fe}$  and  $^{16}\text{O}$  seem to be the most similar as we saw greater mitochondria effects in these samples. Data was collected on the  $^{28}\text{Si}$  irradiated samples for the first three time points (1, 2 & 4 months) so that data is included in Figures 23-25. The mitochondria effects were also much clearer in the C57 mice compared to the C3H. The

C3H strain's genetic makeup confounds the pathway analysis to determine irradiation effects in these animals. Since metabolomics also provides data on some of the TCA cycle metabolites, it was determined it would be best to focus on these conditions. Table 12 shows the total number of differentially expressed metabolites for each condition relative to control as well how many are up and down regulated. The lists of differentially expressed metabolites at each time point was compared using Venn diagrams (Figure 22). The most similarity was noted between  $^{56}\text{Fe}$  and  $^{16}\text{O}$  in months 1, 2 and 4 with 63, 11, and 45 metabolites in common respectively. Then at 9 months there was 0 in common between  $^{56}\text{Fe}$  and  $^{16}\text{O}$ , but 5 in common between  $^{16}\text{O}$  and 1Gy gamma. At 12 month there was 18 in common between to the two HZE irradiations but 54 in common between 1Gy gamma and  $^{16}\text{O}$  and 26 in common between 1Gy gamma and  $^{56}\text{Fe}$ .

Conditions	# of changed metabolites	up	down
1Gy 1mo	197	93	104
Fe 1mo	263	33	230
O 1mo	484	92	392
1Gy 2mo	27	12	15
Fe 2mo	124	11	113
O 2mo	467	160	307
1Gy 4mo	123	62	61
Fe 4mo	147	46	101
O 4mo	95	31	64
1Gy 9mo	64	23	41
Fe 9mo	10	4	6
O 9mo	325	187	138
1Gy 12mo	740	405	335
Fe 12mo	112	38	74
O 12mo	143	58	85

Table 12: Shows the number of differentially expressed metabolites for each condition. Filtering was based on  $\text{FDR} \geq .1$  and a  $\geq 1.5$  fold change.

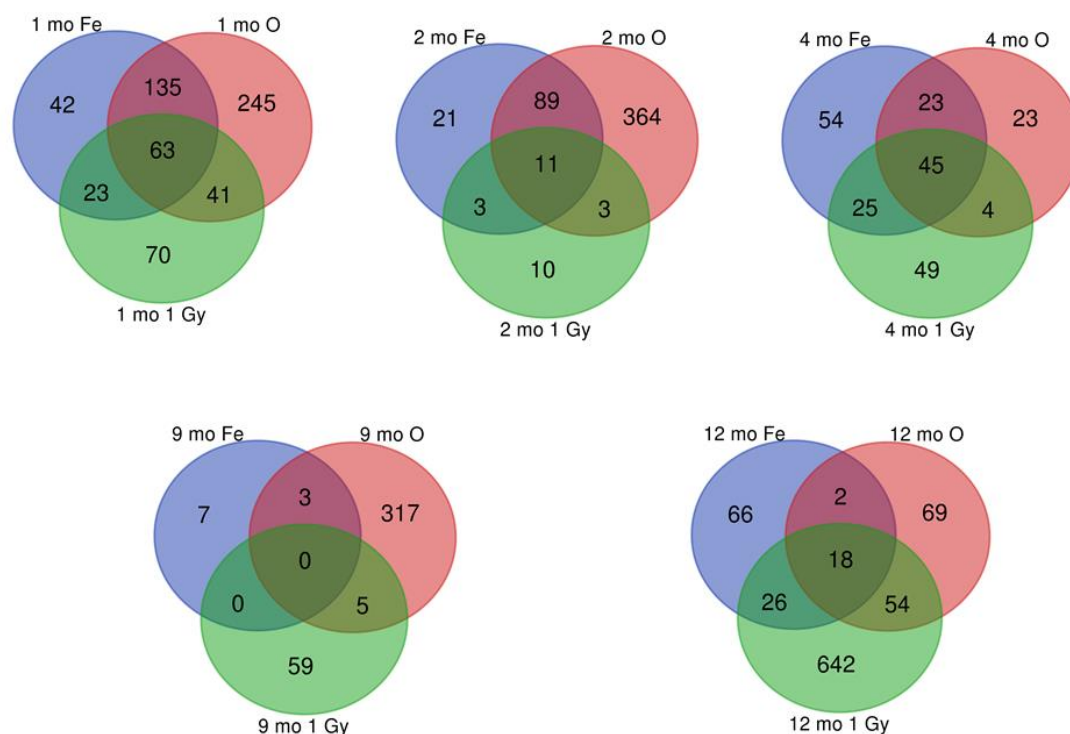
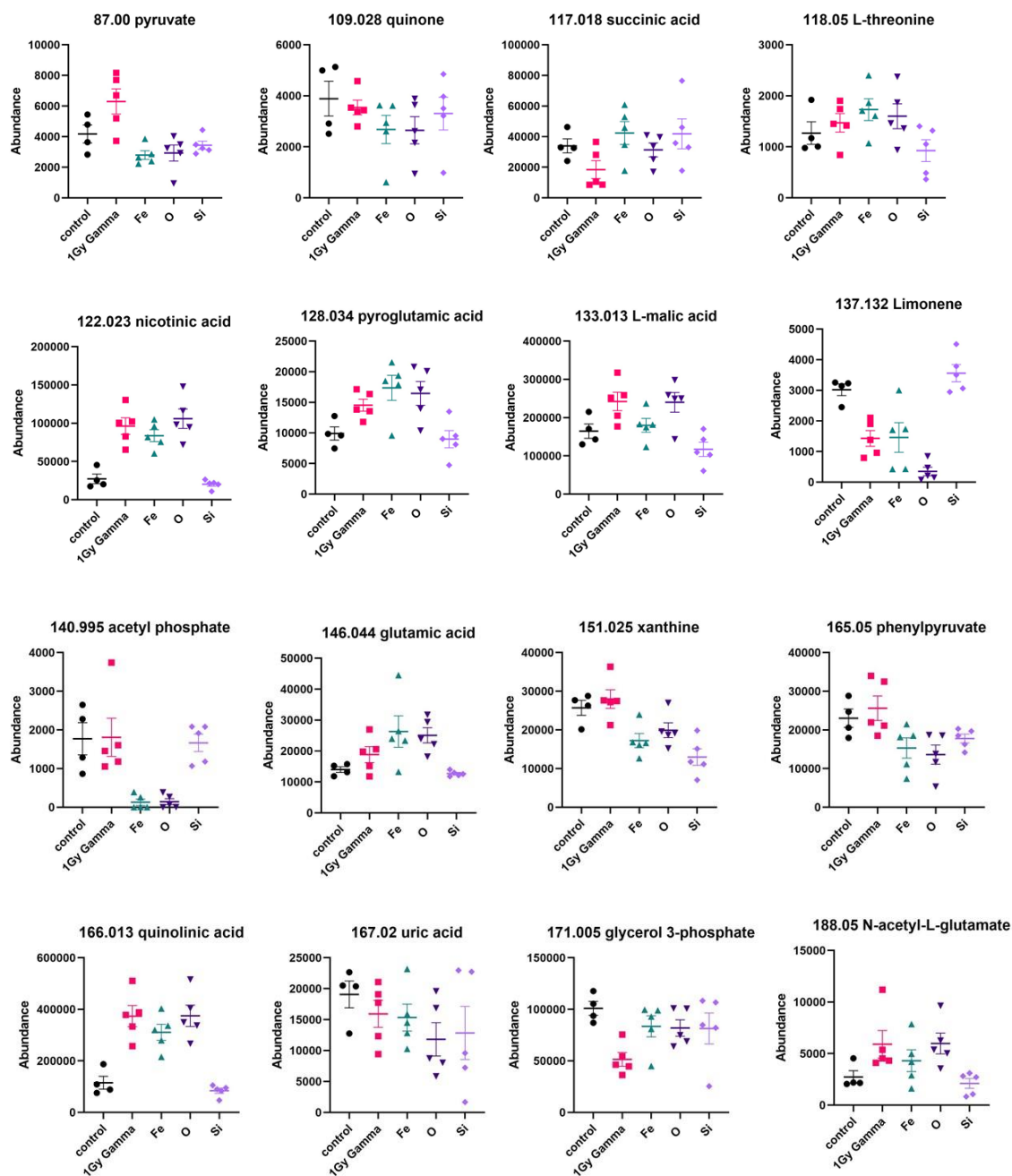
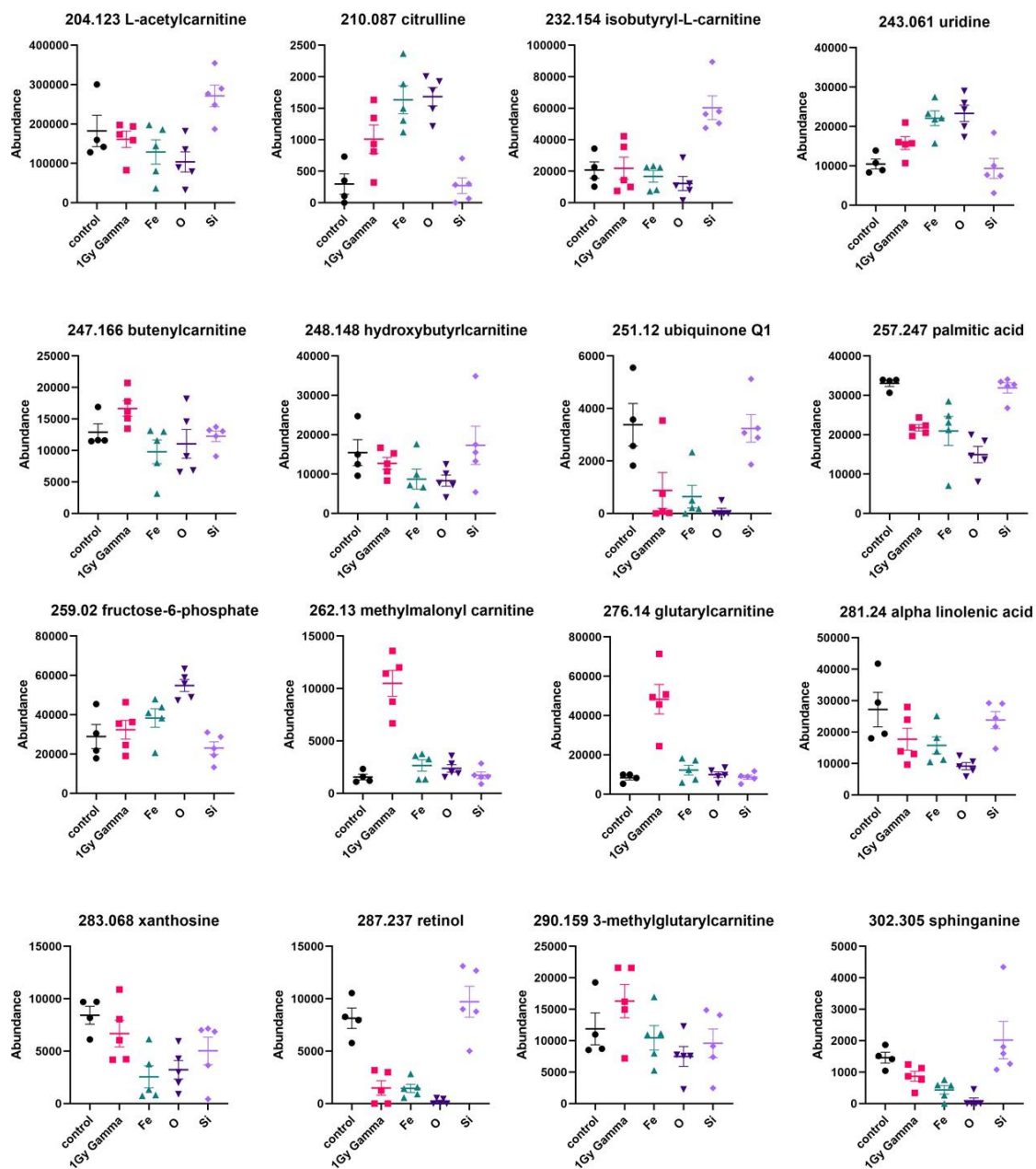


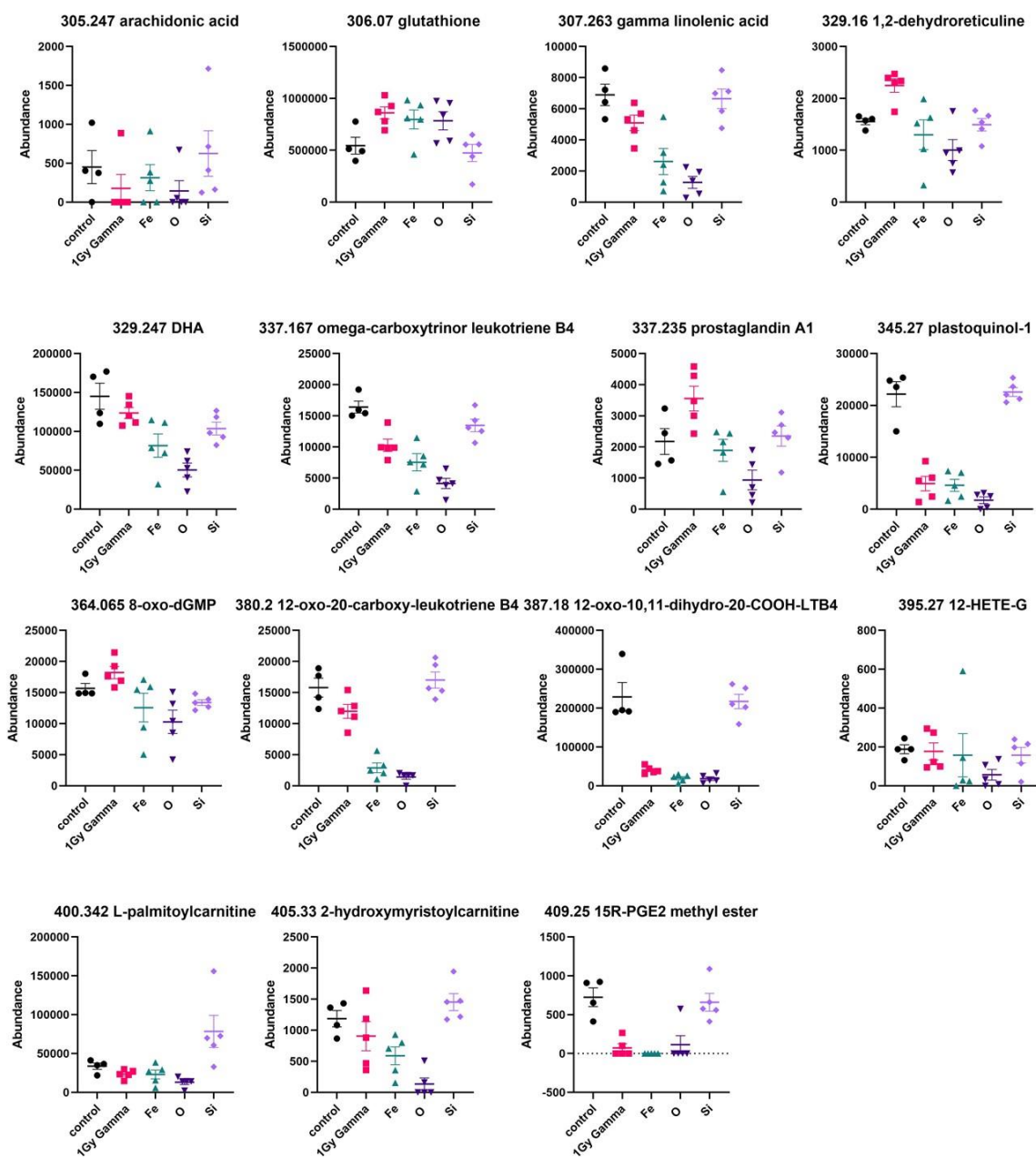
Figure 22: Venn diagrams show differentially expressed metabolites in common for each condition in the C57 mice throughout the time course.

Analysis was then performed on the specific levels of some of these changed metabolites as shown in Figures 23-27. As mentioned previously, focus was aimed at metabolites that were involved in the TCA cycle and metabolites with known relationship with mitochondria. At month 1 (Figure 23), we monitored 58 changed metabolites. Of these 47 contained statistically significant changes. At month 2 (Figure 24), 56 changed metabolites were monitored of which 39 were statistically significant. At month 4 (Figure 25), 41 changed metabolites were observed of which 24 were significantly altered. At 9 months (Figure 26), 32 metabolites were observed of which 17 were significantly altered. At 12 months (Figure 27), 28 changed metabolites were observed of which 14 were significantly altered. A description of the all changes seen

throughout the time course can be found in Table 13. P values are only noted if change was significant ( $p < 0.05$ ).









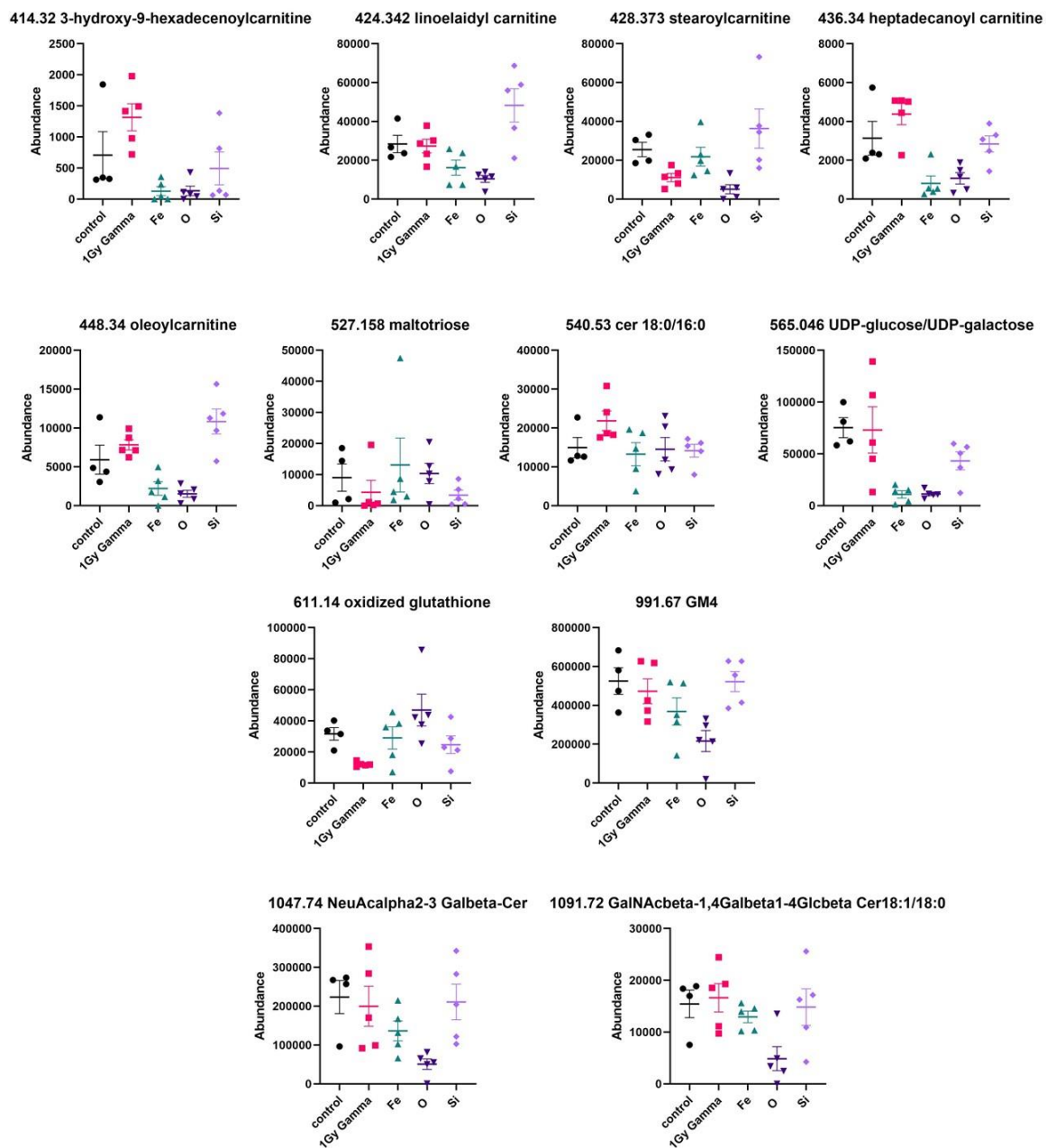
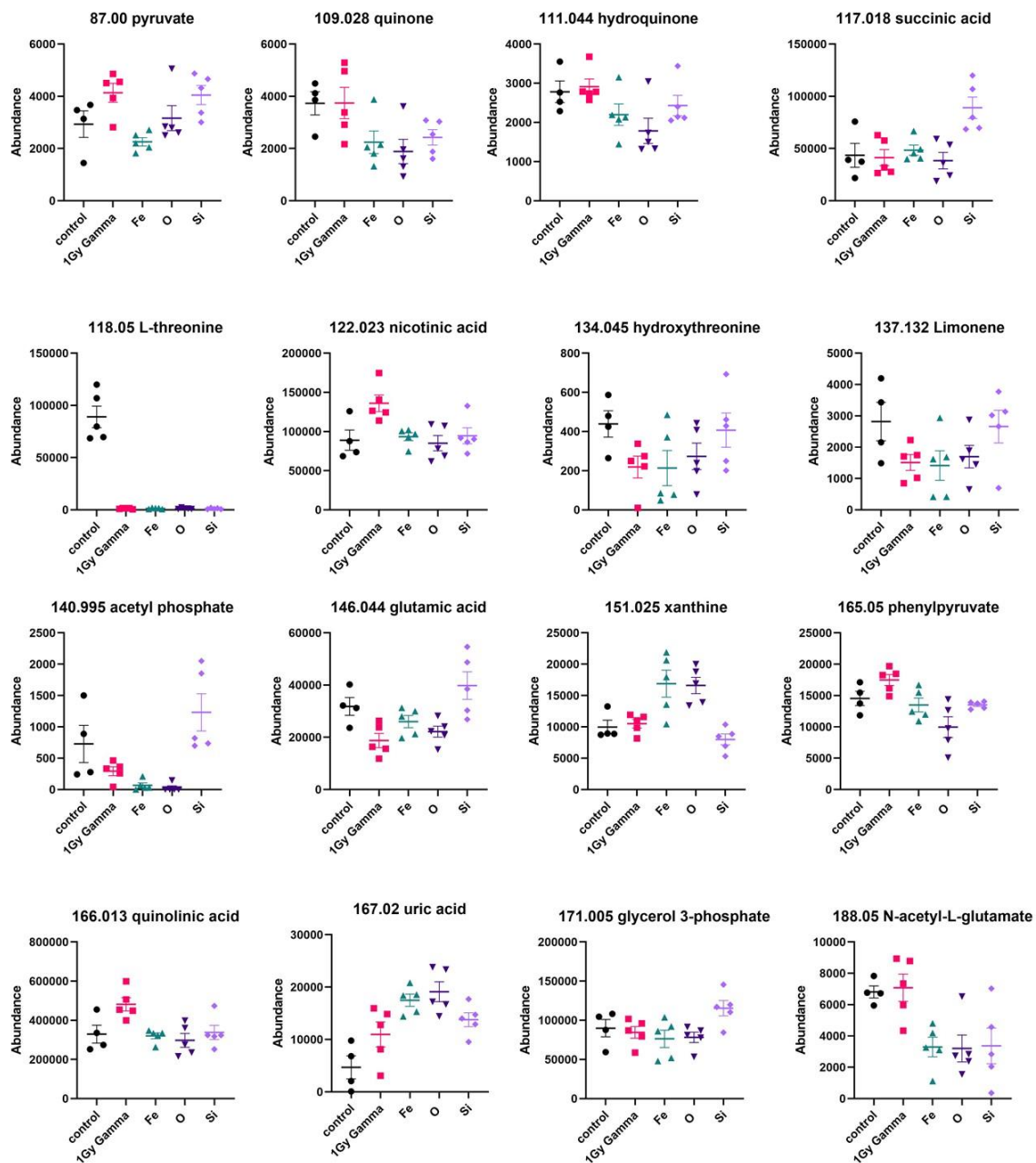
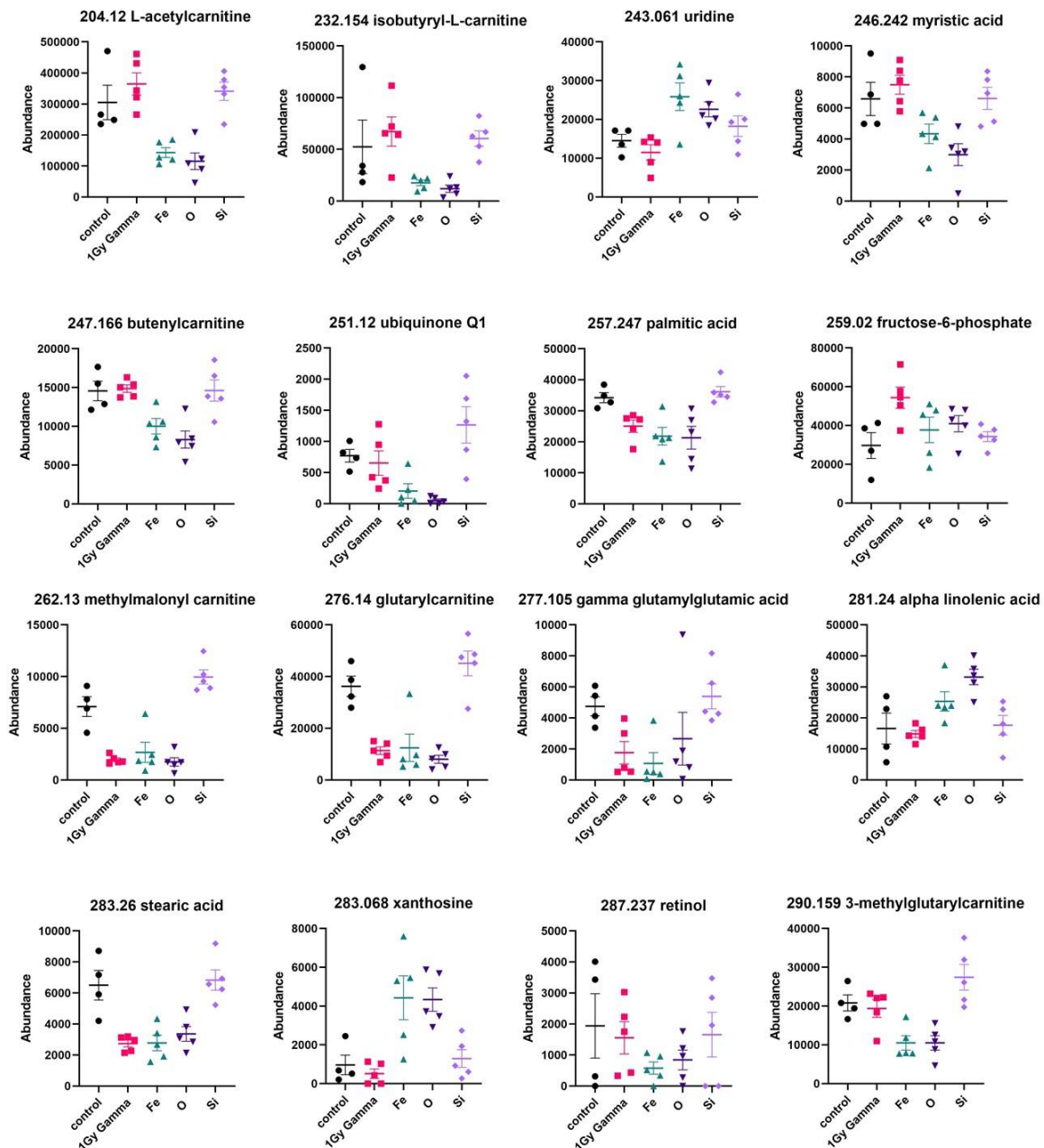
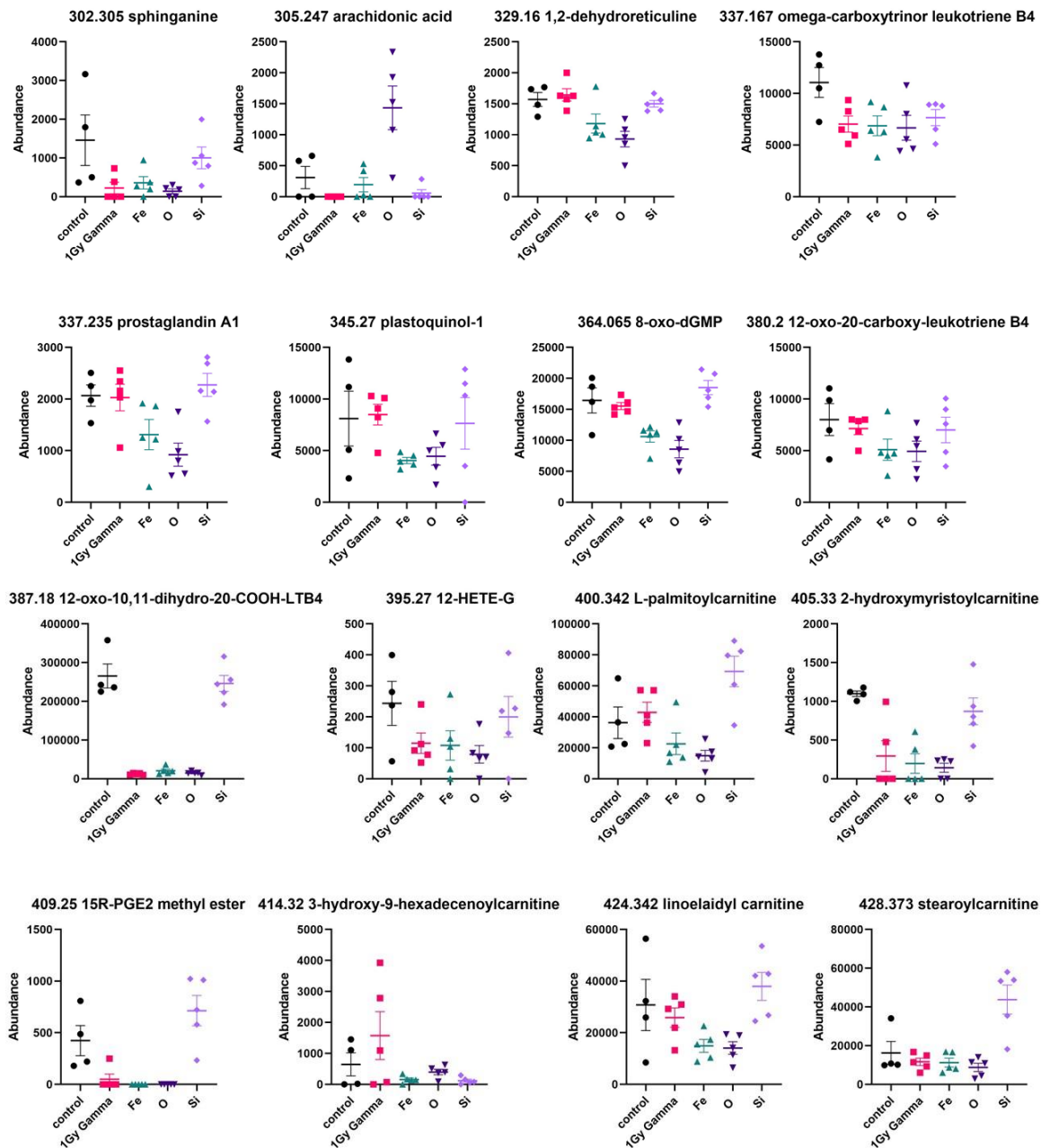


Figure 23: 1 month metabolomics graphs







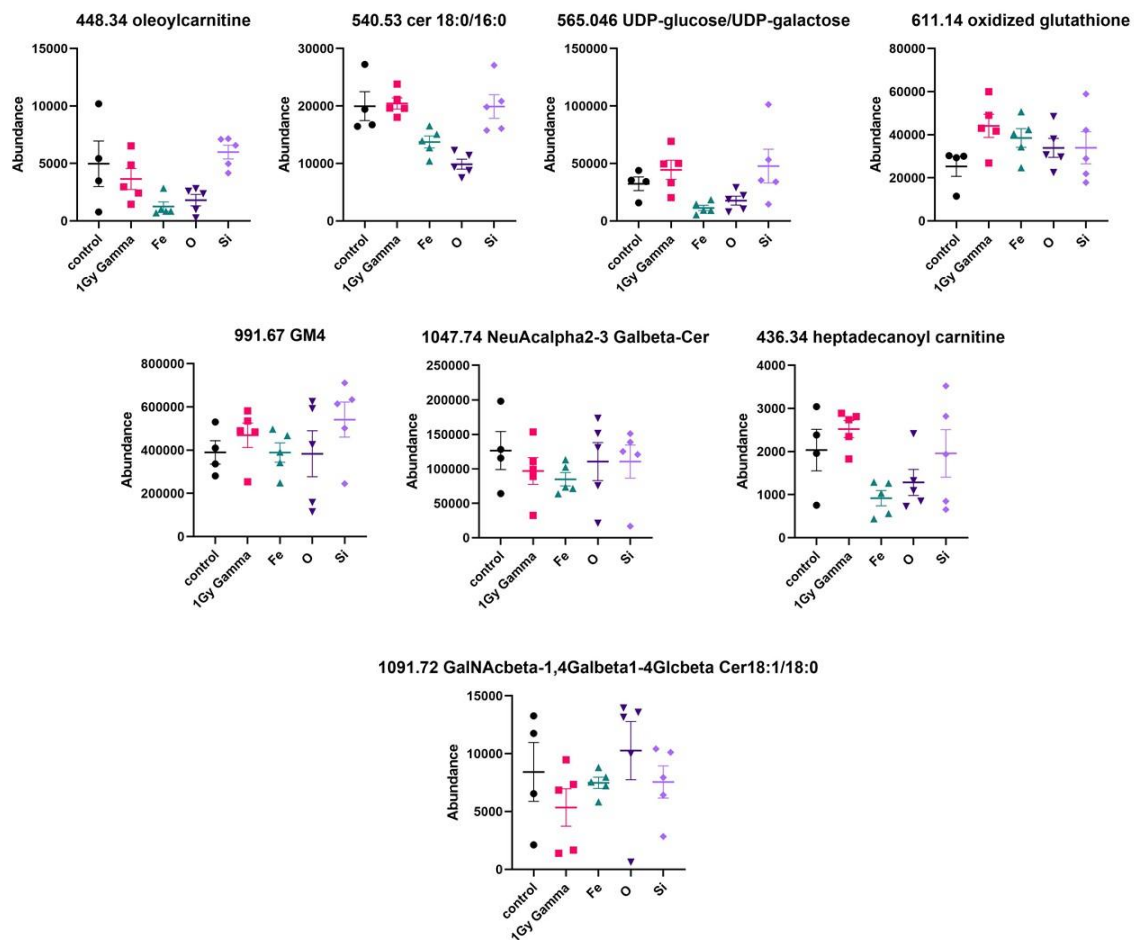
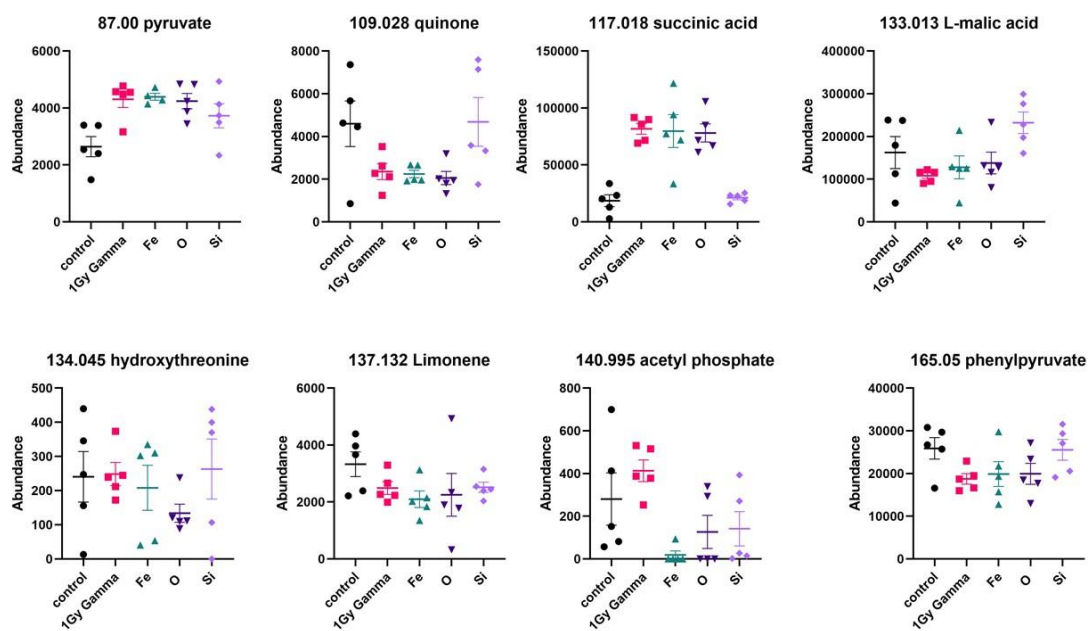
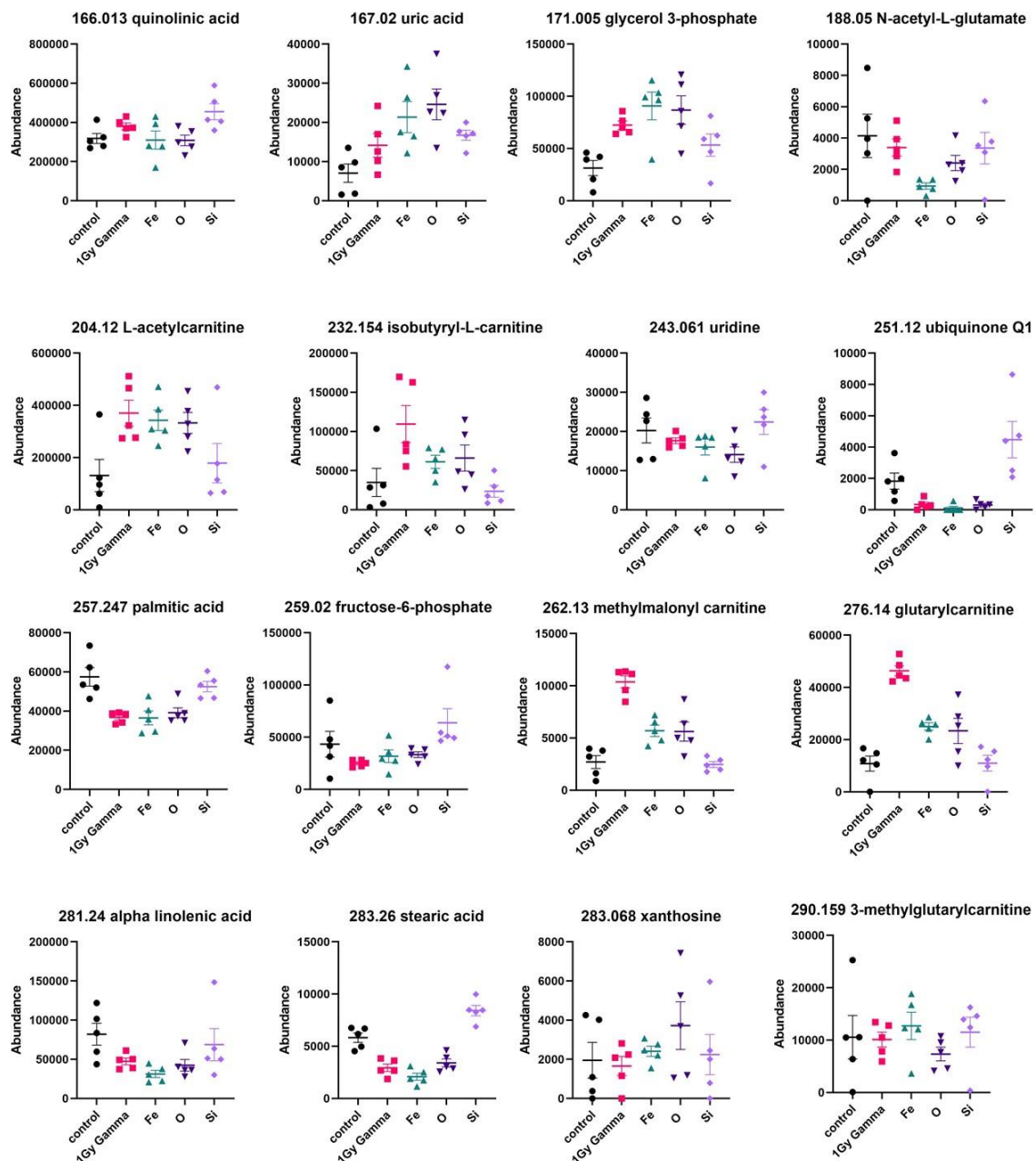


Figure 24: 2 month metabolomics graphs







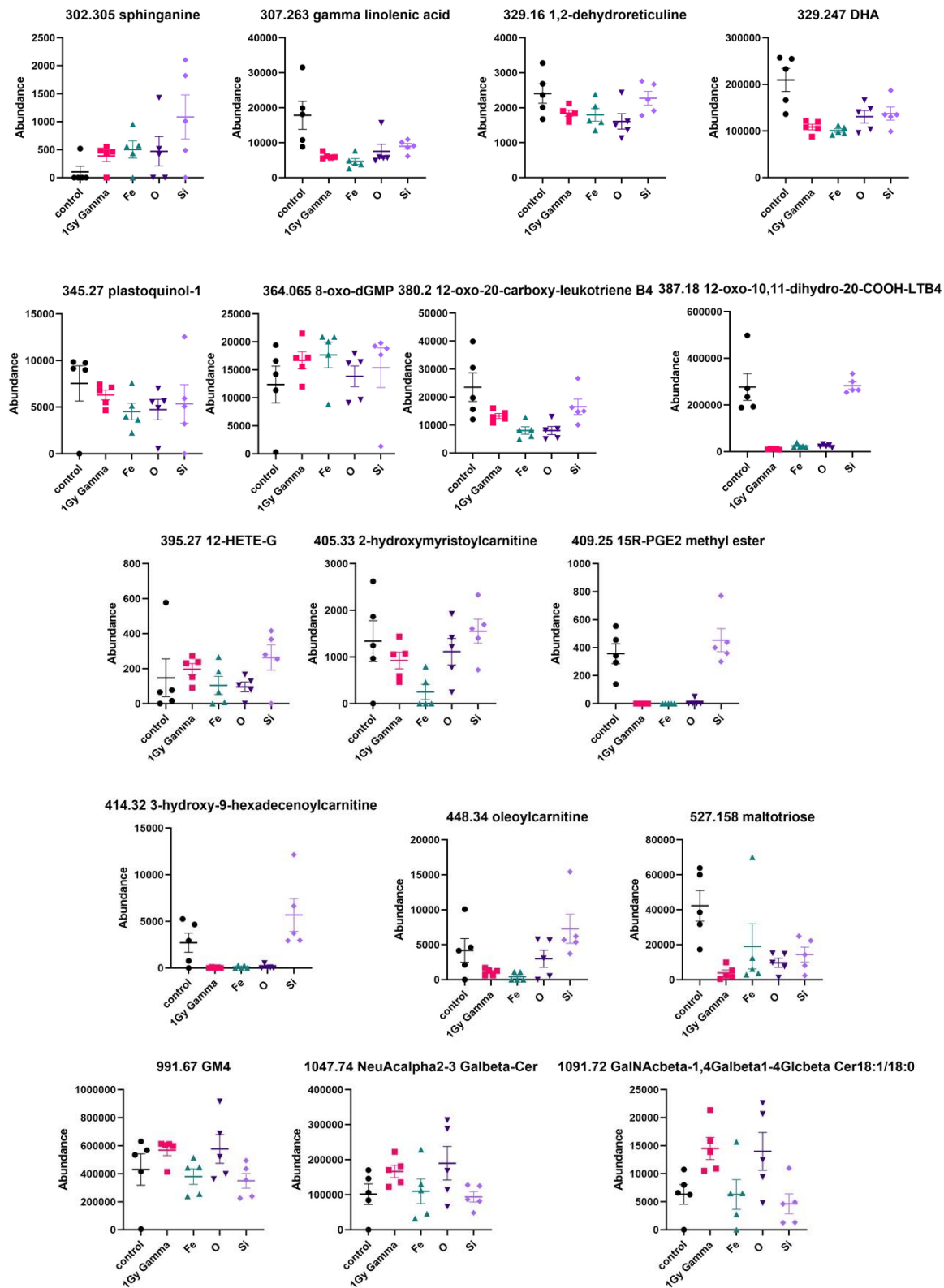
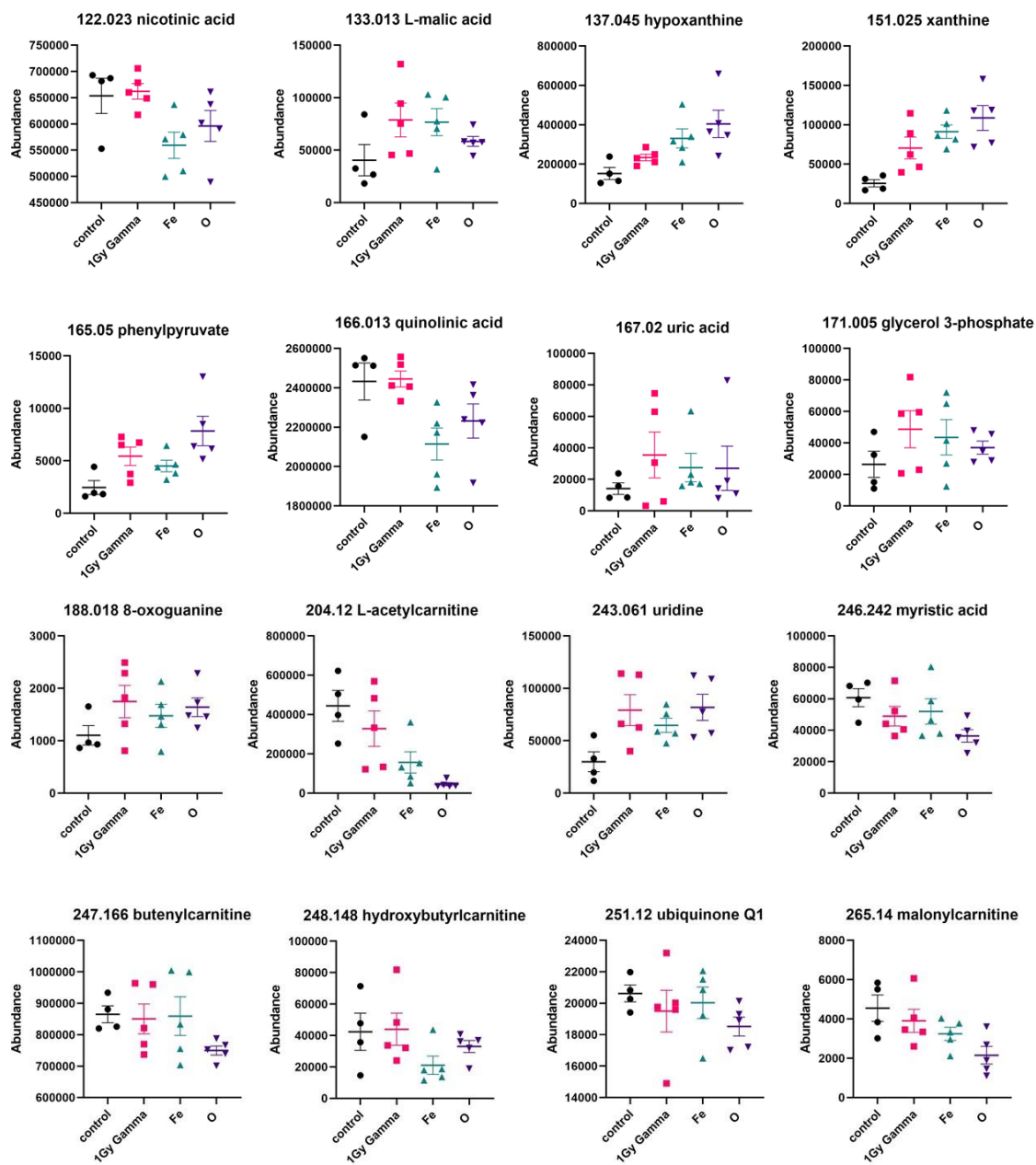


Figure 25: 4 month metabolomics graphs





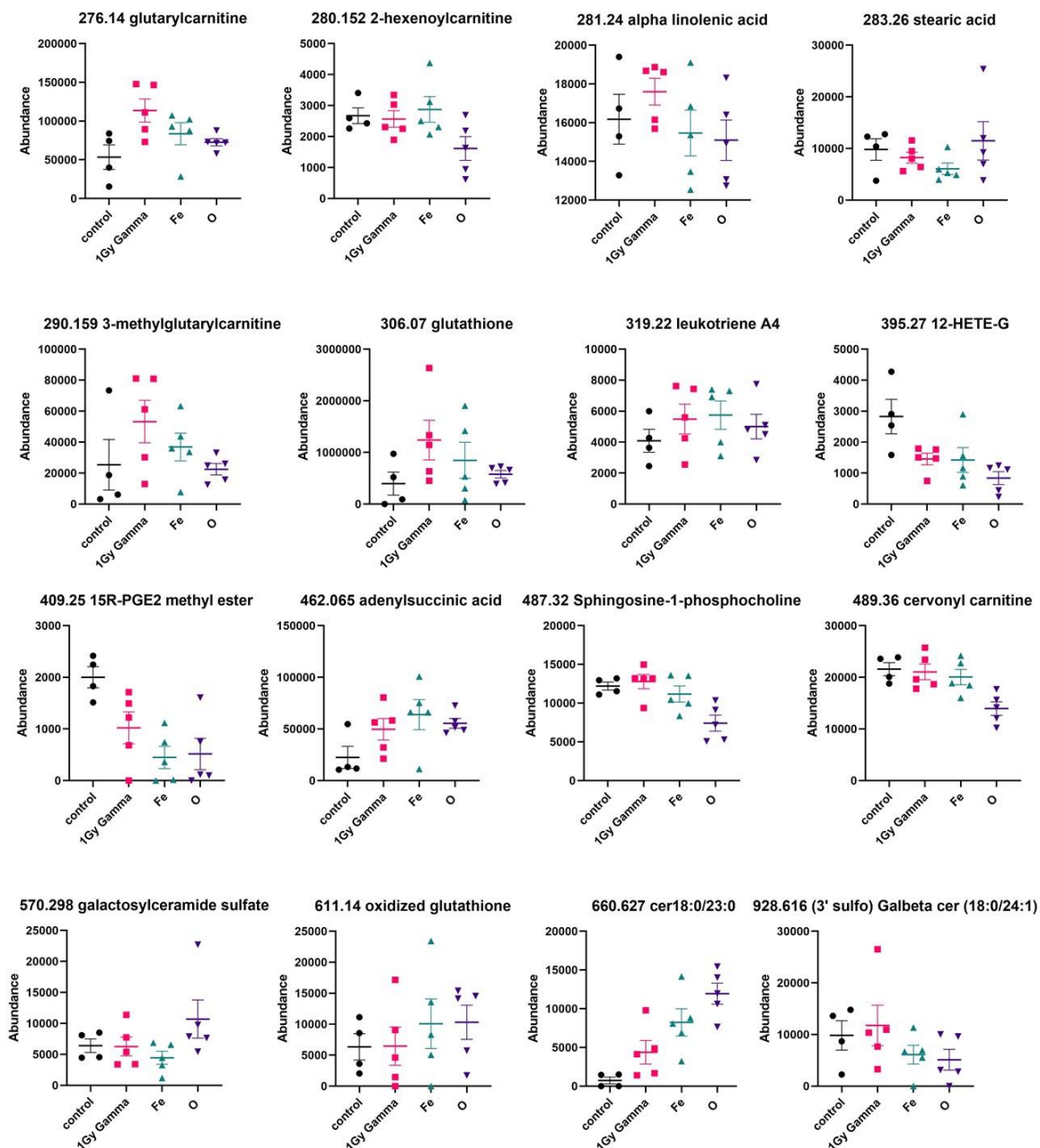
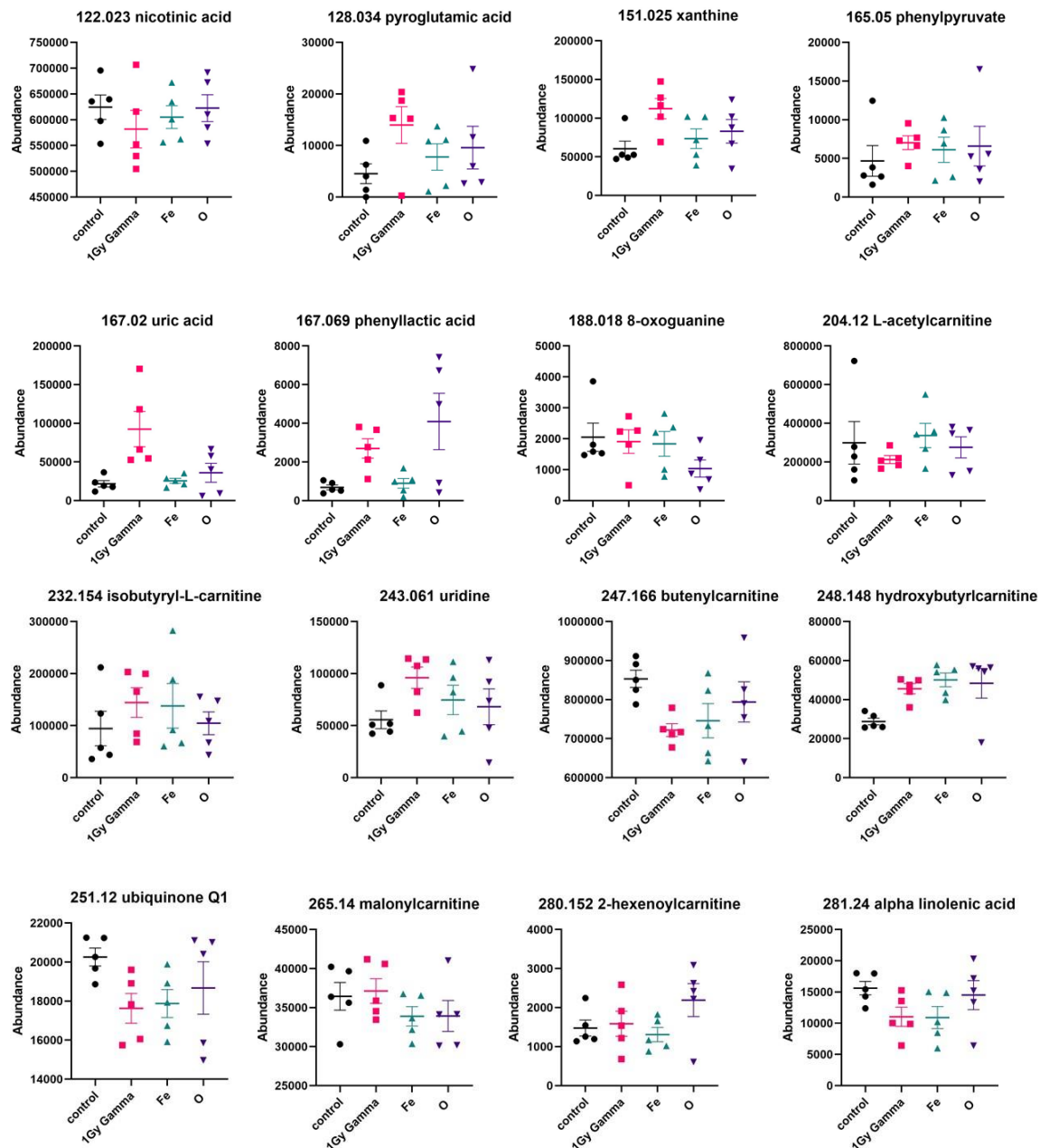


Figure 26: 9 month metabolomics graphs



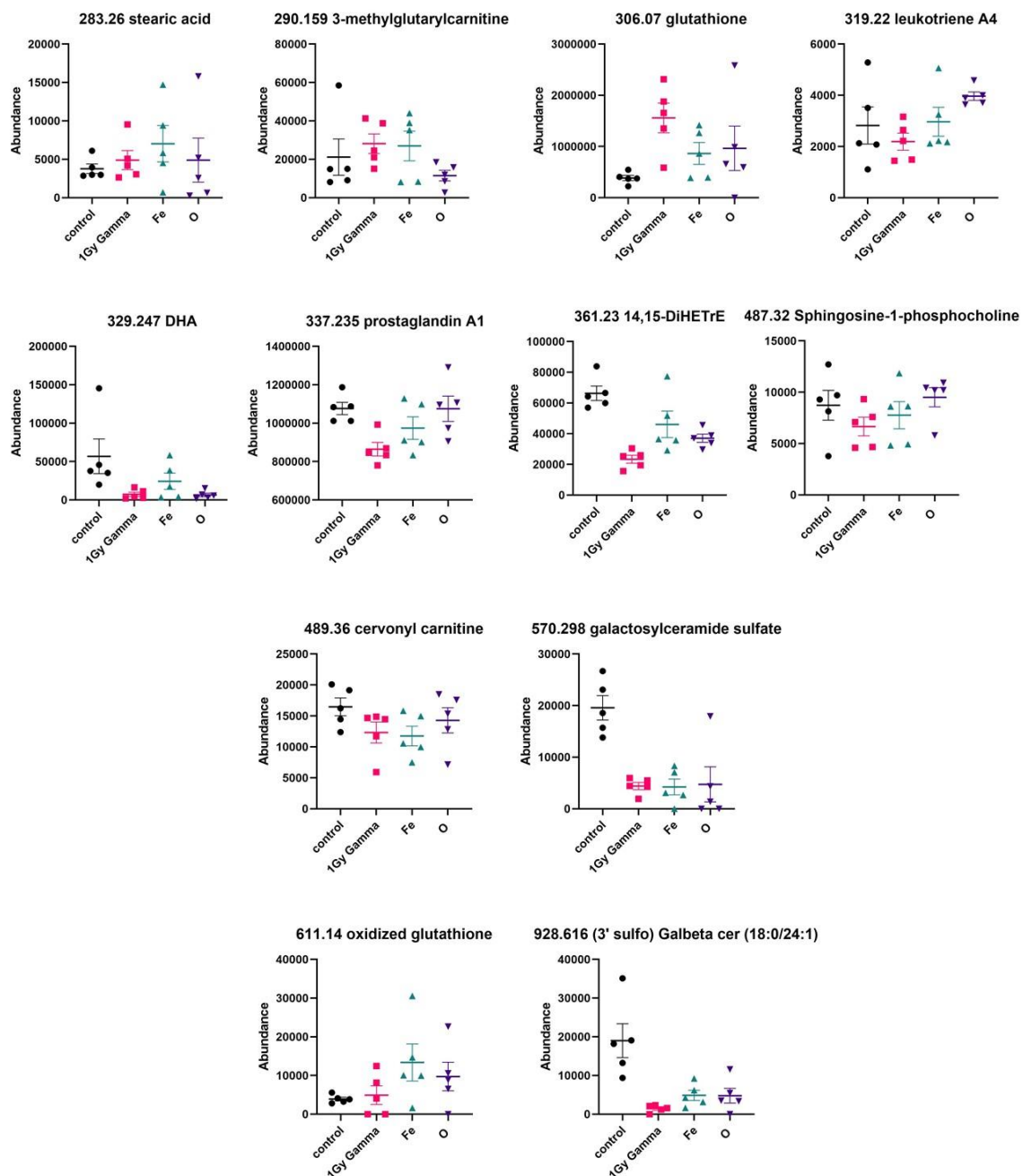


Figure 27: 12 month metabolomics graphs

Description of Metabolite Changes throughout Time Course (including P Values if Significant)					
Metabolite Name	1 month	2 month	4 month	9 month	12 month
pyruvate	down in HZE irradiated	down in $^{56}\text{Fe}$ and up in 1Gy and $^{28}\text{Si}$	up in all irradiated (1Gy ( $p=0.0067$ ), $^{56}\text{Fe}$ ( $p=0.0041$ ), $^{16}\text{O}$ ( $p=0.0072$ ))		
quinone	slightly down in $^{56}\text{Fe}$ and $^{16}\text{O}$	down in HZE ( $^{56}\text{Fe}$ ( $p=0.0492$ ), $^{16}\text{O}$ ( $p=0.0259$ ), $^{28}\text{Si}$ ( $p=0.0397$ ))	down in 1Gy, $^{56}\text{Fe}$ and $^{16}\text{O}$		
hydroquinone		slightly down in $^{56}\text{Fe}$ and $^{16}\text{O}$ ( $p=0.0574$ )			
succinic acid	up in $^{56}\text{Fe}$ and slightly down in 1Gy	elevated in $^{28}\text{Si}$ ( $p=0.0217$ )	up in 1Gy ( $p<0.0001$ ), $^{56}\text{Fe}$ ( $p=0.0040$ ) and $^{16}\text{O}$ ( $p=0.0002$ )		
L-threonine	down in $^{28}\text{Si}$ slightly up in $^{56}\text{Fe}$ and $^{16}\text{O}$	very low in all irradiated (1Gy ( $p<0.0001$ ), $^{56}\text{Fe}$ ( $p<0.0001$ ), $^{16}\text{O}$ ( $p<0.0001$ ), $^{28}\text{Si}$ ( $p<0.0001$ ))			
nicotinic acid	up 1Gy ( $p=0.0014$ ), $^{56}\text{Fe}$ ( $p=0.0010$ ), and $^{16}\text{O}$ ( $p=0.0014$ )	high in 1Gy ( $p=0.0250$ )		down in $^{56}\text{Fe}$ and $^{16}\text{O}$	down in 1Gy
pyroglutamic acid	up 1Gy ( $p=0.0158$ ), $^{56}\text{Fe}$ ( $p=0.0207$ ),				increased in 1Gy ( $p=0.0478$ )

Description of Metabolite Changes throughout Time Course (including P Values if Significant)					
Metabolite Name	1 month	2 month	4 month	9 month	12 month
	and $^{16}\text{O}$ (p=0.0294)				
L-malic acid	up in 1Gy (p=0.0459) and $^{16}\text{O}$ and down in $^{28}\text{Si}$		slightly up in $^{28}\text{Si}$	elevated in irradiated	
hydroxythreonine		slightly down in 1Gy (p=0.0380), $^{56}\text{Fe}$ and $^{16}\text{O}$	down in $^{16}\text{O}$		
hypoxanthine				elevated in irradiated highest $^{16}\text{O}$ (1Gy (p=0.0413), $^{56}\text{Fe}$ (p=0.0224), $^{16}\text{O}$ (p=0.0191))	
Limonene	down in 1Gy(p=0.00 21), $^{56}\text{Fe}$ (p=0.0294) and $^{16}\text{O}$ (p=<0.0001) and up in $^{28}\text{Si}$	down in 1Gy (p=0.0688), $^{56}\text{Fe}$ and $^{16}\text{O}$	slightly down in all irradiated $^{56}\text{Fe}$ (p=0.0463)		
acetyl phosphate	down $^{56}\text{Fe}$ (p=0.0034) and $^{16}\text{O}$ (p=0.0035)	low in $^{56}\text{Fe}$ (p=0.0412) and $^{16}\text{O}$ (p=0.0328)	up in 1Gy and slightly down in $^{56}\text{Fe}$ and part of the $^{16}\text{O}$ and $^{28}\text{Si}$ samples		
glutamic acid	up in $^{56}\text{Fe}$ and $^{16}\text{O}$ (p=0.0064)	down in 1Gy (p=0.0188), $^{56}\text{Fe}$ and $^{16}\text{O}$ (p=0.0395)			
xanthine	down in HZE ( $^{56}\text{Fe}$ (p=0.0161) and $^{28}\text{Si}$ (p=0.0036))	up in $^{56}\text{Fe}$ (p=0.0337) and $^{16}\text{O}$ (p=0.0070)		elevated in irradiated highest in $^{16}\text{O}$ (1Gy (p=0.0285), $^{56}\text{Fe}$	increased in 1Gy (p=0.0134)

Description of Metabolite Changes throughout Time Course (including P Values if Significant)					
Metabolite Name	1 month	2 month	4 month	9 month	12 month
				(p=0.0004), <sup>16</sup> O (p=0.0027))	
phenylpyruvate	down in HZE ( <sup>16</sup> O (p=0.0310))	down in <sup>16</sup> O	down in 1Gy (p=0.0338) and <sup>56</sup> Fe	elevated in irradiated especially <sup>16</sup> O (1Gy (p=0.0362), <sup>56</sup> Fe (p=0.0468), <sup>16</sup> O (p=0.0154))	slightly increased in irradiated
quinolinic acid	up in 1Gy (p=0.0016), <sup>56</sup> Fe (p=0.0022) & <sup>16</sup> O (p=0.0016)	up in 1Gy (p=0.0286)	up in <sup>28</sup> Si (p=0.0227)	decreased in <sup>56</sup> Fe (p=0.0371) and <sup>16</sup> O	
uric acid	down in HZE	up in HZE ( <sup>56</sup> Fe (p=0.0009), <sup>16</sup> O (p=0.0016), <sup>28</sup> Si (p=0.0076))	up in <sup>56</sup> Fe (p=0.0144), <sup>16</sup> O (p=0.0048) and <sup>28</sup> Si (p=0.0066)	increased in 1Gy	increased in 1Gy (p=0.0160)
Phenyllactic acid					elevated in 1Gy (p=0.0045) and part of the <sup>16</sup> O samples (p=0.0481)
glycerol 3- phosphate	slightly down in HZE and down in 1Gy (p=0.0013)	slightly up in <sup>28</sup> Si	up in 1Gy (p=0.0011), <sup>56</sup> Fe (p=0.0042) and <sup>16</sup> O (p=0.0071)	increased in irradiated especially some of the 1Gy and <sup>56</sup> Fe samples	

Description of Metabolite Changes throughout Time Course (including P Values if Significant)					
Metabolite Name	1 month	2 month	4 month	9 month	12 month
8-oxoguanine				slightly increased in irradiated	slightly down in $^{16}\text{O}$
N-acetyl-L-glutamate	up in 1Gy and $^{16}\text{O}$ (p=0.0375)	down in HZE ( $^{56}\text{Fe}$ (p=0.0029), $^{16}\text{O}$ (p=0.0100), $^{28}\text{Si}$ (p=0.0365))	down in $^{56}\text{Fe}$ and $^{16}\text{O}$		
L-acetylcarnitine	down in $^{56}\text{Fe}$ and $^{16}\text{O}$ and up in $^{28}\text{Si}$	down in $^{56}\text{Fe}$ (p=0.0170) and $^{16}\text{O}$ (p=0.0130)	up in 1Gy (p=0.0165), $^{56}\text{Fe}$ (p=0.0197) and $^{16}\text{O}$ (p=0.0250)	decreased in $^{56}\text{Fe}$ (p=0.0169) and $^{16}\text{O}$ (p=0.0007)	increased in part of the $^{56}\text{Fe}$ and $^{16}\text{O}$ samples
citrulline	up in 1Gy (p=0.0455), $^{56}\text{Fe}$ (p=0.0025) and $^{16}\text{O}$ (p=0.0004). Highest in $^{56}\text{Fe}$ and $^{16}\text{O}$				
isobutyryl-L-carnitine	up in $^{28}\text{Si}$ (p=0.0046)	too much variability in control but levels are low and tight in $^{56}\text{Fe}$ and $^{16}\text{O}$ and higher in 1Gy and $^{28}\text{Si}$	up in 1Gy (p=0.0370), $^{56}\text{Fe}$ and $^{16}\text{O}$		not much difference too much variability
uridine	up in $^{56}\text{Fe}$ (p=0.0019) and $^{16}\text{O}$ (p=0.0017) and slightly up in 1Gy (p=0.0427)	up in HZE ( $^{56}\text{Fe}$ (p=0.0328), $^{16}\text{O}$ (p=0.0173))	slightly down in $^{16}\text{O}$	elevated in irradiated (1Gy (p=0.0334), $^{56}\text{Fe}$ (p=0.0179), $^{16}\text{O}$ (p=0.0157))	elevated in irradiated (1Gy (p=0.0160))
myristic acid		down in $^{56}\text{Fe}$ (p=0.0986) and $^{16}\text{O}$ (p=0.0226)		slightly down in $^{16}\text{O}$ (p=0.0089)	

Description of Metabolite Changes throughout Time Course (including P Values if Significant)					
Metabolite Name	1 month	2 month	4 month	9 month	12 month
butenylcarnitine	down in HZE	down in $^{56}\text{Fe}$ (p=0.0240) and $^{16}\text{O}$ (p=0.0075)		down in $^{16}\text{O}$ (p=0.0050)	down in irradiated (1Gy (p=0.0014)
hydroxybutyrlcarnitine	down in $^{56}\text{Fe}$ and $^{16}\text{O}$			down in $^{56}\text{Fe}$	elevated in irradiated (1Gy (p=0.0007), $^{56}\text{Fe}$ (p=0.0006), $^{16}\text{O}$ (p=0.0364))
ubiquinone Q1	down 1Gy (p=0.0482), $^{56}\text{Fe}$ (p=0.0155) and $^{16}\text{O}$ (p=0.0026)	down in $^{56}\text{Fe}$ (p=0.0091) and $^{16}\text{O}$ (p=0.0075) and up in $^{28}\text{Si}$	slightly down in 1Gy (p=0.0230), $^{16}\text{O}$ (p=0.0195) and $^{56}\text{Fe}$ (p=0.0112) and up in $^{28}\text{Si}$	slightly down in $^{16}\text{O}$ (p=0.0393)	down in 1Gy (p=0.0183) and $^{56}\text{Fe}$ (p=0.0232)
palmitic acid	down in 1Gy (p=<0.0001), $^{56}\text{Fe}$ (p=0.0241) and $^{16}\text{O}$ (p=0.0002)	down in 1Gy (p=0.0107), $^{56}\text{Fe}$ (p=0.0094) and $^{16}\text{O}$ (p=0.0217)	down in 1Gy (p=0.0029), $^{56}\text{Fe}$ (p=0.0074) and $^{16}\text{O}$ (p=0.0091)		
fructose 6-phosphate	up in $^{16}\text{O}$ (p=0.0047)	up in 1Gy (p=0.0240)	up in $^{28}\text{Si}$		
methylmalonyl carnitine	up in 1Gy (p=0.0004)	down in 1Gy (p=0.0006), $^{56}\text{Fe}$ (p=0.0149) and $^{16}\text{O}$ (p=0.0008) up in $^{28}\text{Si}$ (p=0.0399)	up in 1Gy (p=<0.0001), $^{56}\text{Fe}$ (p=0.0066), and $^{16}\text{O}$ (p=0.0298). Very high in 1Gy	down in $^{16}\text{O}$ (p=0.0180)	
malonylcarnitine					down in $^{56}\text{Fe}$ and $^{16}\text{O}$
glutarylcarnitine	up in 1Gy (p=0.0022)	down in 1Gy (p=0.0003), $^{56}\text{Fe}$ (p=0.0108) and $^{16}\text{O}$ (p=0.0002)	up in 1Gy (p=<0.0001), $^{56}\text{Fe}$ (p=0.0023), and $^{16}\text{O}$ . Very high in 1Gy	increased in 1Gy (p=0.0287) and $^{56}\text{Fe}$	



Description of Metabolite Changes throughout Time Course (including P Values if Significant)					
Metabolite Name	1 month	2 month	4 month	9 month	12 month
gamma glutamylglutamic acid		down in 1Gy (p=0.0186), <sup>56</sup> Fe (p=0.0063) and <sup>16</sup> O			
2-hexenoylcarnitine				slightly down in <sup>16</sup> O	elevated in <sup>16</sup> O
alpha linolenic acid	down in 1Gy, <sup>56</sup> Fe and <sup>16</sup> O (p=0.0087)	up in <sup>56</sup> Fe and <sup>16</sup> O (p=0.0154)	slightly down in <sup>56</sup> Fe (p=0.0088) and <sup>16</sup> O (p=0.0370)	slightly elevated in 1Gy gamma	decreased in 1Gy (p=0.0408) and <sup>56</sup> Fe
xanthosine	down in HZE ( <sup>56</sup> Fe (p=0.0042), <sup>16</sup> O (p=0.0042))	up in <sup>56</sup> Fe (p=0.0380) and <sup>16</sup> O (p=0.0045)	too much variability in control. Up in part of the <sup>16</sup> O samples		
stearic acid		down in 1Gy (p=0.0036), <sup>56</sup> Fe (p=0.0080) and <sup>16</sup> O (p=0.0161)	down in 1Gy (p=0.0011), <sup>56</sup> Fe (p=0.0002) and <sup>16</sup> O (p=0.0034) and up in <sup>28</sup> Si (p=0.0048)	slightly decreased in <sup>56</sup> Fe	slightly down in some of the <sup>16</sup> O
retinol	down in 1Gy (p=0.0007), <sup>56</sup> Fe (p=0.0002) and <sup>16</sup> O (p=<.0001)	down in <sup>56</sup> Fe and <sup>16</sup> O but too much variability in control			
3-methylglutaryl carnitine	slightly up in 1Gy	down in <sup>56</sup> Fe (p=0.0074) and <sup>16</sup> O (p=0.0072)	slightly up in <sup>56</sup> Fe and <sup>28</sup> Si	high in 1Gy and <sup>56</sup> Fe	elevated in 1Gy and <sup>56</sup> Fe
sphiganine	down in 1Gy (p=0.0390), <sup>56</sup> Fe (p=0.0020) and <sup>16</sup> O (p=0.0001) especially <sup>56</sup> Fe and <sup>16</sup> O	down in 1Gy, <sup>56</sup> Fe and <sup>16</sup> O but too much variability in control	up in 1Gy, <sup>56</sup> Fe, <sup>16</sup> O and <sup>28</sup> Si (p=0.0430)		

Description of Metabolite Changes throughout Time Course (including P Values if Significant)					
Metabolite Name	1 month	2 month	4 month	9 month	12 month
arachidonic acid	too much variability	up in $^{16}\text{O}$ (p=0.0341)			
glutathione	up in 1Gy (p=0.0141), $^{56}\text{Fe}$ and $^{16}\text{O}$			slightly elevated in 1Gy and $^{56}\text{Fe}$	elevated in irradiated especially 1Gy (1Gy (p=0.0040))
gamma linolenic acid	down in $^{56}\text{Fe}$ (p=0.0066) and $^{16}\text{O}$ (p=0.0001)		down in all irradiated (1Gy (p=0.0202), $^{56}\text{Fe}$ (p=0.0123))		
leukotriene A4				not clear difference	elevated in $^{16}\text{O}$
1,2-dehydroreticuline	down in $^{16}\text{O}$ and up in 1Gy (p=0.0030)	down in $^{56}\text{Fe}$ and $^{16}\text{O}$ (p=0.0078)	slightly down in $^{16}\text{O}$		
DHA	down in $^{56}\text{Fe}$ (p=0.0259) and $^{16}\text{O}$ (p=0.0011)		down in all irradiated (1Gy (p=0.0040), $^{56}\text{Fe}$ (p=0.0024), $^{16}\text{O}$ (p=0.0227), & $^{28}\text{Si}$ (p=0.0345))		down in irradiated
omega-carboxytrior leukotriene B4	down in 1Gy (p=0.0033), $^{56}\text{Fe}$ (p=0.0016) and $^{16}\text{O}$ (p=<0.001). Lowest in $^{16}\text{O}$	down in all HZE (1Gy (p=0.0351), $^{56}\text{Fe}$ (p=0.0403))			
prostaglandin A1	down in $^{16}\text{O}$ (p=0.0462) and up in 1Gy (p=0.0494)	down in $^{56}\text{Fe}$ and $^{16}\text{O}$ (p=0.0082)			down in 1Gy (p=0.0022) and part of the $^{56}\text{Fe}$

Description of Metabolite Changes throughout Time Course (including P Values if Significant)					
Metabolite Name	1 month	2 month	4 month	9 month	12 month
plastoquinol-1	down in 1Gy (p=0.0003), <sup>56</sup> Fe (p=0.0002) and <sup>16</sup> O (p=<0.0001)	down in <sup>56</sup> Fe and <sup>16</sup> O	down in all irradiated		
14, 15-DiHETrE					down in irradiated (1Gy (p=<0.0001), <sup>16</sup> O (p=0.0006)
8-oxo-dGMP	slightly up in 1Gy and down in <sup>16</sup> O (p=0.0476)	down in <sup>56</sup> Fe (p=0.0255) and <sup>16</sup> O (p=0.0132)	slightly up in 1Gy and <sup>56</sup> Fe		
12-oxo-20-carboxy-leukotriene B4	down in <sup>56</sup> Fe (p=<0.0001) and <sup>16</sup> O (p=<0.0001)	down in <sup>56</sup> Fe and <sup>16</sup> O	down in <sup>56</sup> Fe (p=0.0193) and <sup>16</sup> O (p=0.0196)		
12-oxo-10,11-dihydro-20-COOH-LTB4	down in 1Gy (p=0.0007), <sup>56</sup> Fe (p=0.0004) and <sup>16</sup> O (p=0.0004)	very low in 1Gy (p=<0.0001), <sup>56</sup> Fe (p=<0.0001) and <sup>16</sup> O (p=<0.0001)	down in 1Gy (p=0.0016), <sup>56</sup> Fe (p=0.0023) and <sup>16</sup> O (p=0.0023)		
12-HETE-G	slightly down in <sup>56</sup> Fe and <sup>16</sup> O (p=0.0096)	down in 1Gy, <sup>56</sup> Fe and <sup>16</sup> O	up in <sup>28</sup> Si and slightly up in 1Gy	down in irradiated (1Gy (p=0.0373) <sup>16</sup> O (p=0.0082))	
L-palmitoylcarnitine	up in <sup>28</sup> Si and down <sup>16</sup> O (p=0.0040)	down in <sup>56</sup> Fe and <sup>16</sup> O, up in <sup>28</sup> Si			
2-hydroxymyristoylcarnitine	down in <sup>56</sup> Fe (p=0.0202) and <sup>16</sup> O (p=0.0003)	down in <sup>56</sup> Fe (p=0.0005), <sup>16</sup> O (p=<0.0001) and 1Gy (p=0.0093)	down in <sup>56</sup> Fe (p=0.0484)		

Description of Metabolite Changes throughout Time Course (including P Values if Significant)					
Metabolite Name	1 month	2 month	4 month	9 month	12 month
15R-PGE2 methyl ester	down in 1Gy (p=0.0010), <sup>56</sup> Fe (p=0.0002) and <sup>16</sup> O (p=0.0084)	down in 1Gy (p=0.0315), <sup>56</sup> Fe (p=0.0127) and <sup>16</sup> O (p=0.0127)	down in 1Gy, <sup>56</sup> Fe and <sup>16</sup> O	down in irradiated especially <sup>56</sup> Fe and <sup>16</sup> O (1Gy (p=0.0414), <sup>56</sup> Fe (p=0.0014), <sup>16</sup> O (p=0.0065))	
3-hydroxy-9-hexadecenoylcarnitine	down in HZE and up in 1Gy	up in 1Gy	down in 1Gy (p=0.0010), <sup>56</sup> Fe (p=0.0362), & <sup>16</sup> O (p=0.0375)		
linoelaidyl carnitine	down in <sup>56</sup> Fe and <sup>16</sup> O (p=0.0048), up in <sup>28</sup> Si	down in <sup>56</sup> Fe and <sup>16</sup> O and up in <sup>28</sup> Si			
stearoylcarnitine	down 1Gy (p=0.0092) and <sup>16</sup> O (p=0.0018)	up in <sup>28</sup> Si (p=0.0279)			
heptadecanoyl carnitine	down in <sup>56</sup> Fe (p=0.0333) and <sup>16</sup> O (p=0.0429)	down in <sup>56</sup> Fe (p=0.0484) and <sup>16</sup> O			
oleoylcarnitine	slightly down in <sup>56</sup> Fe and <sup>16</sup> O (p=0.0374) and slightly up in 1Gy and <sup>28</sup> Si	down in <sup>56</sup> Fe and <sup>16</sup> O and slightly up in <sup>28</sup> Si	slightly down in 1G and <sup>56</sup> Fe and slightly up in <sup>28</sup> Si		
adenylsuccinic acid				elevated in irradiated ( <sup>16</sup> O (p=0.0189))	
Sphingosine-1-phosphocholine				down in <sup>16</sup> O (p=0.0068)	down in 1Gy and <sup>56</sup> Fe
cervonyl carnitine				down in <sup>16</sup> O (p=0.0045)	slightly down in 1Gy

Description of Metabolite Changes throughout Time Course (including P Values if Significant)					
Metabolite Name	1 month	2 month	4 month	9 month	12 month
					gamma & <sup>56</sup> Fe
maltotriose	too much variability		down in all irradiated (1Gy (p=0.0026), <sup>16</sup> O (p=0.0073), <sup>28</sup> Si (p=0.0208)		
cer 18:0/16:0	up 1Gy	down in <sup>56</sup> Fe (p=0.0418) and <sup>16</sup> O (p=0.0042)			
UDP-glucose/UDP-galactose	down in HZE ( <sup>56</sup> Fe (p=0.0002), <sup>16</sup> O (p=0.0001), <sup>28</sup> Si (p=0.0422)	slightly down in <sup>56</sup> Fe (p=0.0088) and <sup>16</sup> O			
galactosylceramide sulfate				down in <sup>56</sup> Fe	down in all irradiated (1Gy (p=0.0003), <sup>56</sup> Fe (p=0.0006), <sup>16</sup> O (p=0.0071))
oxidized glutathione	down in 1Gy (p=0.0010) & up in <sup>16</sup> O	up in all irradiated (1Gy (p=0.0367))		slightly increased in <sup>56</sup> Fe and <sup>16</sup> O	elevated in irradiated especially <sup>56</sup> Fe and <sup>16</sup> O
cer18:0/23:0				high in <sup>56</sup> Fe (p=0.0079) and <sup>16</sup> O (p=0.0002) and slightly elevated in 1Gy	

Description of Metabolite Changes throughout Time Course (including P Values if Significant)					
Metabolite Name	1 month	2 month	4 month	9 month	12 month
(3' sulfo) Gal $\beta$ cer (18:0/24:1)				slightly down in $^{56}\text{Fe}$ and $^{16}\text{O}$	down in irradiated (1Gy (p=0.0040), $^{56}\text{Fe}$ (p=0.0151), $^{16}\text{O}$ (p=0.01 79))
GM4	down $^{16}\text{O}$ (p=0.0088) and $^{56}\text{Fe}$	too variability but up in 1Gy & $^{28}\text{Si}$	slightly down in $^{56}\text{Fe}$ and $^{28}\text{Si}$		
NeuAcalpha2-3 Gal $\beta$ -Cer	down in $^{56}\text{Fe}$ and especially $^{16}\text{O}$ (p=0.0037)	slightly down in 1Gy and $^{56}\text{Fe}$	slightly up in 1Gy and $^{16}\text{O}$		
GalNAcbeta- 1,4Galbeta1- 4Glcbeta Cer18:1/18:0	down in $^{16}\text{O}$ (p=0.0196)	too much variability in control	elevated in 1Gy (p=0.0149) and $^{16}\text{O}$		

Table 13: Description of Metabolite Changes throughout Time Course (including P Values if Significant)

#### BIOLOGICAL SIGNIFICANCE OF METABOLITES

In this data set, distinct differences in the metabolic profiles were noted in the irradiated samples vs control. Changes are seen in several metabolites that are related to the TCA cycle such as pyruvate, malic acid (ionized form is malate which is involved in the TCA cycle), and succinic acid (anion is succinate that is part of TCA cycle). We also see glycerol-3-phosphate, fructose-6-phosphate, maltotriose and UDP glucose/UDP galactose all of which are involved in energy metabolism. UDP glucose/UDP galactose and maltotriose are involved in glycogenesis. Both glycerol-3-phosphate and fructose-6-phosphate are intermediates in glycolysis.

Several acylcarnitines are being affected which as mentioned previously are a marker of radiation exposure and is involved in the bi-directional transport of acyl moieties from the cytosol to the mitochondria and vice versa. This allows them to play a fundamental role tuning the switch between glucose and fatty acid metabolism.<sup>21</sup> Acylcarnitine chain length is determined based on whether it resulted from fatty acid or amino acid  $\beta$ -oxidation. Even-chain acylcarnitines are increased due to incomplete fatty acid  $\beta$ -oxidation whereas odd-chain ones are produced during amino acid catabolism. Butyrylcarnitine (C4:0-CN) is the one exception in that it can be generated via either of these pathways.<sup>20</sup> The other chain lengths are as follows: acetylcarnitine (C2:0-CN), propionylcarnitine (C3:0-CN), valerylcarnitine (C5:0-CN), hexanoylcarnitine (C6:0-CN), Heptanoylcarnitine (C7:0-CN), octanoylcarnitine (C8:0-CN), nonanoylcarnitine (C9:0-CN), and decanoylcarnitine (C10:0-CN).

Several metabolites were changed that are involved in amino acid metabolism that are connected to the mitochondria. These metabolites include: phenylpyruvate (an intermediate or catabolic byproduct of phenylalanine metabolism), L-threonine, glutamic acid, pyroglutamic acid (cyclic lactam of glutamic acid), N-acetyl-L-glutamate (one of the amine hydrogens is substituted by an acetyl group) citrulline, and quinolinic acid (downstream product of the kynurenine pathway which metabolizes tryptophan). 8-oxoguanine, a common base lesion, accumulation in mitochondrial DNA is known to result in mitochondrial dysfunction. The level of 8-oxoguanine is typically kept low by two enzymes: MTH1 and OGG1. MTH1 hydrolyses 8-oxo-dGTP to 8-oxo-dGMP which prevents it from being incorporated into the DNA.<sup>81</sup> Changes in uridine indicates perturbed nucleotide metabolism. As you may recall, the mitochondria are also

required to synthesize uridine which is used to produce UTP for RNA synthesis as well as UTP glucose that is needed for both the synthesis of glycogen and complex carbohydrates. Xanthine is considered a universal base as it is a purine but it is large enough to interact with both purines and pyrimidines.<sup>82</sup> The nucleosides inosine and guanosine are converted into hypoxanthine and guanine. Hypoxanthine is then oxidized to form xanthine and guanine is deaminated to also form xanthine. Xanthine is oxidized again to form the final product of purine catabolism, uric acid. Thus, these metabolites indicate perturbed nucleotide metabolism. Typically uric acid is excreted through the kidneys. Of course, kidney dysfunction can result in hyperuricemia which is when uric acid begins to crystalize in the joints and kidneys, but it can also result from increased generation of uric acid. Uric acid has also been shown to induce gene expression of chemokines and growth factors. It can activate pro-inflammatory pathways and stimulate cell proliferation. However, acute increases in plasma uric acid levels may also be beneficial as it can act as a free radical scavenger and help stabilize vitamin C in the serum. The pro-inflammatory response could be due to the consequent accumulation of ROS which occurs as a result of the conversion of xanthine dehydrogenase to xanthine oxidase during the production of uric acid.<sup>83</sup>

Previous studies have shown upregulation of prostaglandin biosynthesis and eicosanoid signaling in <sup>56</sup>Fe irradiation.<sup>8</sup> Arachidonic acid, omega-carboxytrieninor leukotriene B<sub>4</sub>, leukotriene A<sub>4</sub>, prostaglandin A<sub>1</sub>, 12-oxo-20-carboxy-leukotriene B<sub>4</sub>, 12-oxo-10,11-dihydro-20-COOH-LTB<sub>4</sub>, 12-HETE-G and 15R-PGE<sub>2</sub> methyl ester (also known as prostaglandin E<sub>2</sub> methyl ester) all fall within the prostaglandin and eicosanoid pathways. Eicosanoids are known to be extremely potent immune-stimulants and able to



produce profound physiological effects at very low concentrations.<sup>84,85</sup> Both prostaglandins and leukotrienes can modulate tumor cell proliferation, differentiation and apoptosis through several signaling pathways. They have also been known to affect the migration and invasion of carcinoma cells. Chronic inflammation can result in the production of pro-inflammatory mediators which include eicosanoids, cytokines and chemokines which ultimately results in a shift in the micro-environment of the tissue. These changes in the leukocyte profile can result in the initiation of epithelial cell transformation as well as promote tumor growth, angiogenesis and metastasis. These molecules are also key in mediating the crosstalk between epithelial cells and their surrounding stromal cells.<sup>84</sup> Gamma linolenic acid is also the first intermediate in the metabolic conversion of linoleic acid to arachidonic acid.<sup>86</sup> Myristic acid has been shown to activate NFκB and other inflammatory genes in adipocytes, and TLR-4 to induce an inflammatory response in macrophages.<sup>87</sup> Saturated fatty acids in general especially palmitic acid (C16:0) are harmful to the body because they can elevate LDL cholesterol and increase atherosclerosis risk. Stearic acid (C18:0), however, does not increase atherosclerosis risk and increased levels of circulating stearic acid have been seen to reduce blood pressure, improve heart function and reduce the risk of cancer. In *Drosophila* as well as human cells, stearic acid has been shown to regulate mitochondrial morphology and function. When levels are low, the Transferrin Receptor TfR1 activates JNK signaling that ultimately leads to ubiquitination and inhibition of Mitofusin 2. This results in mitochondrial fragmentation and reduced oxygen consumption. When levels are high enough, stearic acid is covalently attached to TfR1 which leads to reduced JNK activation and mitochondrial fusion, with the final result being elevated oxygen

consumption. In these mentioned studies, dietary supplementation with stearic acid was able to partially rescue the impaired locomotion and reduced lifespan resulting from mitochondrial dysfunction.<sup>88</sup> DHA is well known for being essential for growth and functional brain development in infants as well as normal brain function in adults. However, it has also been shown to have profound effects on mitochondria function and membrane composition.<sup>89</sup> It has also been found to be depleted in cirrhotic liver. DHA was found to inhibit fibrosis more intensely than other omega-3 fatty acids and was shown to block TGF $\beta$  and NF $\kappa$ B pathways.<sup>90</sup> DHA can be obtained directly from the diet or can be synthesized in the body from  $\alpha$ -linolenic acid which is also obtained via the diet.<sup>91</sup> Thus, the decrement of DHA may be able to be overcome through the use of supplements. Sphinganine is biosynthesized by a decarboxylating condensation of serine with palmitoyl-CoA to form a keto intermediate that is reduced by NADPH. Sphinganine is acylated followed by a dehydrogenation to form ceramide.<sup>92</sup> Besides sphinganine we also see changes in some of the ceramides. The ceramides are potent regulators of cellular growth and death.<sup>93</sup> Ceramide is also the precursor of all sphingolipids including the gangliosides. GM4 is seen in the metabolite data and the mouse analogue of GM2 was seen in the lipid data set.

Glutathione is one of the most abundant antioxidants in aerobic cells. It is critical to help protect from oxidative stress by acting as a free radical scavenger and inhibiting lipid peroxidation. It also works to detoxify hydrogen peroxide. The ratio of reduced glutathione to oxidized glutathione is often used as an indicator of cellular health. Under normal conditions 98% of glutathione should be in the reduced state.<sup>94</sup>

## RESULTS

### **Chapter 4 MITOCHONDRIAL DYSFUNCTION VALIDATION BY BIOLOGICAL ASSAYS**

#### **MITOCHONDRIAL COMPLEX I ASSAY**

As mentioned before, studies have shown significant decreases in Complex I activity and dysfunction of this particular complex is the main cause of several mitochondrial diseases and disorders.<sup>15</sup> To validate the mitochondrial dysfunction, functional mitochondrial assays for Complex I of the electron transport chain were performed on mitochondria isolated from the same liver tissues. Complex I catalyzes the first step in the electron transport chain. An enzyme oxidizes NADH transferring an electron to Ubiquinone which is an electron carrier embedded in the lipid bilayer of the inner mitochondrial membrane. In the Complex I assay, capture anti-bodies specific for Complex I coat the wells of the plate so that Complex I is selected from the mitochondria extract. The assay works by measuring the oxidation of NADH to NAD<sup>+</sup> with simultaneous reduction of the provided dye. The more NAD<sup>+</sup> that is produced the more yellow the dye will be resulting in an increase in absorbance. Results from this assay for the C57 are shown in Figure 28 and indicate a decrease in activity of Complex I in both the <sup>56</sup>Fe and <sup>16</sup>O irradiated samples compared to non-irradiated control throughout the time course. Complex I activity was not altered in 1Gy and 3Gy gamma irradiated until the 4-month time point. At 9 months, there was no longer a decrease in function of the 1Gy gamma, but the decrease returned at 12 months. <sup>28</sup>Si also showed a

decrease at 9 months and it continued through the final time point. It has been thought that premature aging could potentially be an effect of HZE irradiation<sup>95</sup>. Mitochondria have been increasingly recognized as important players in the aging process and most aging related diseases have mitochondrial involvement<sup>96</sup>. Aging in general is known to result in biochemical and functional alterations within the mitochondrial electron transport chain resulting in reduced efficiency of electron transport as well as reduction in anti-oxidant activity, and an increase in oxidative stress<sup>53</sup>. In particular, the catalytic activity of complexes I, III, and IV have all been seen to decline with age in liver as well as brain, heart, and skeletal muscle<sup>17</sup>. This data seems to support that idea of premature aging as at 1-month post-irradiation there is a large gap between Complex I function for <sup>56</sup>Fe and <sup>16</sup>O compared to the other groups. However, at 9 months this gap begins to lessen as the activity of Complex I begins to drop in the non-irradiated control mice as well. According to abcam, Complex I dysfunction is thought to contribute to diabetes as well as several neurological disorders, including Parkinson's and schizophrenia. This is a very interesting thought as Fontaine believes Metformin to be inducing mitochondrial Complex I inhibition<sup>97</sup>. This is also particularly interesting because there was data presented at this year's NASA meeting that also proposed Metformin as a potential countermeasure for space flight.<sup>98</sup> All of this definitely begs for more investigation into Metformin's involvement with mitochondria especially in regards to complex I and if it would actually be beneficial or result in more harm based on our findings.

Results obtained for this assay for the C3H mice were quite different which was expected since the omics data is rather different for this strain than the C57. As seen in Figure 29, at 1 month post-irradiation a decrease in Complex I activity was seen for  $^{56}\text{Fe}$ , 3Gy gamma & 1Gy gamma. Then at 2 months all irradiations were slightly increased except for  $^{16}\text{O}$  irradiated. At 4 months, a decrease was seen in all HZE irradiated, and in all irradiation groups at 9 mo. At 12 months a decrease in activity was only seen in  $^{56}\text{Fe}$  and  $^{28}\text{Si}$  irradiation. A study in 2012 using human lung carcinoma looking at the effects of 10Gy X-ray 12 hours after irradiation found that Complex I was not affected. The only complex that showed effects were seen in Complex II and it was upregulated. However, they also note that this finding was inconsistent with reports showing that IR either caused no change or reduced electron transport chain enzymes.<sup>14</sup> It's also important to note that our study is examining more long term irradiation effects as well as we are looking at HZE and gamma irradiation although the gamma irradiation is at a much lower dose.

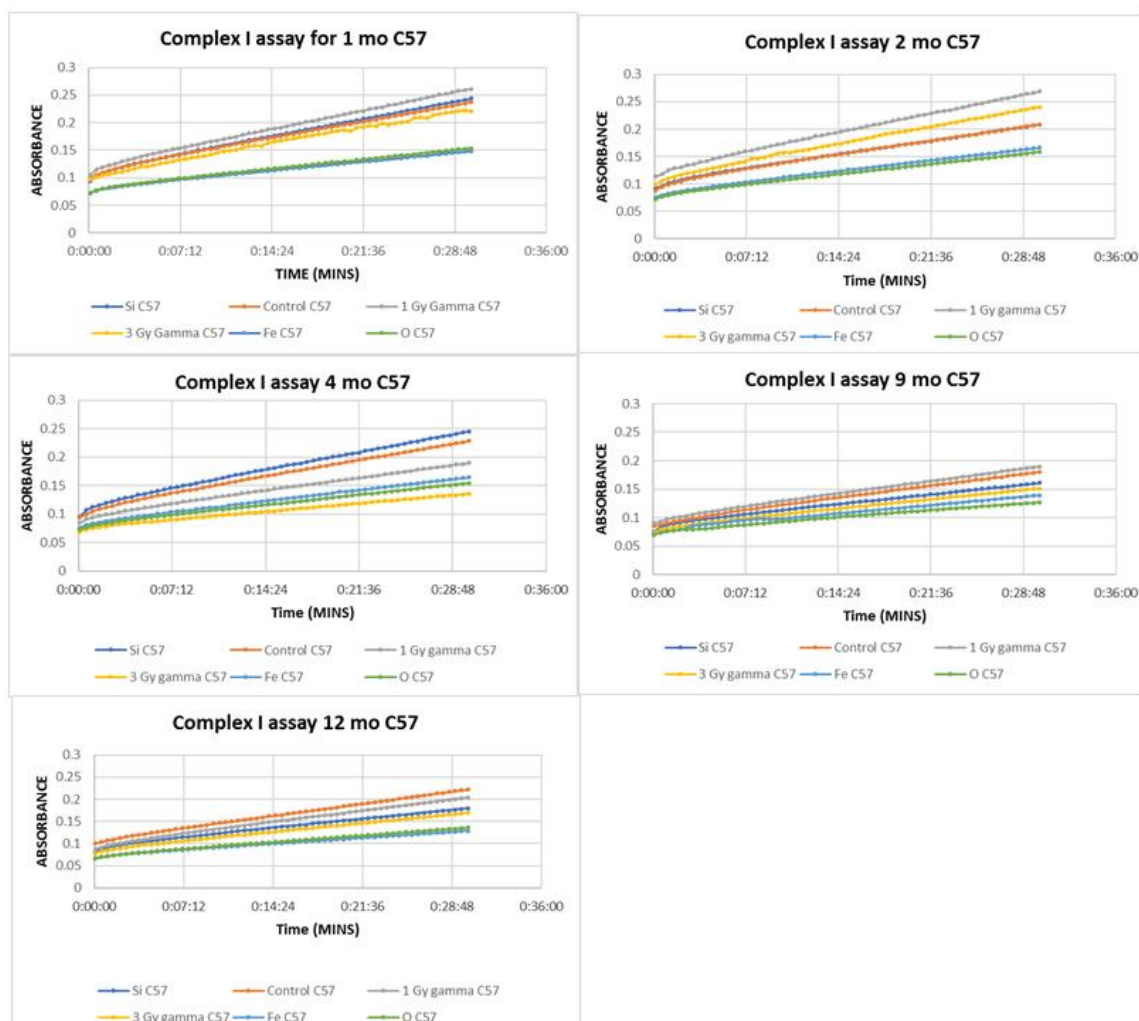


Figure 28: Mitochondria Complex I activity of C57 mice at 1 mo. post-irradiation exhibited a decrease in  $^{16}\text{O}$  and  $^{56}\text{Fe}$  irradiated compared to non-irradiated. All slopes are significantly different except for  $^{28}\text{Si}$  and non-irradiated as well as  $^{56}\text{Fe}$  and  $^{16}\text{O}$ . At 2 mo. a similar decrease in  $^{16}\text{O}$  and  $^{56}\text{Fe}$  irradiated compared to non-irradiated is seen. All slopes are significantly different except for  $^{28}\text{Si}$  and non-irradiated. At 4 mo. post-irradiation a decrease was seen in  $^{16}\text{O}$ ,  $^{56}\text{Fe}$ , 1Gy gamma & 3Gy gamma compared to non-irradiated. All slopes are significantly different. At 9 mo. a decrease was seen in all irradiation types compared to non-irradiated except for 1Gy gamma. All slopes are significantly different. At 12 mo. post-irradiation a decrease was seen in all irradiation types when compared to non-irradiated. All slopes are significantly different.

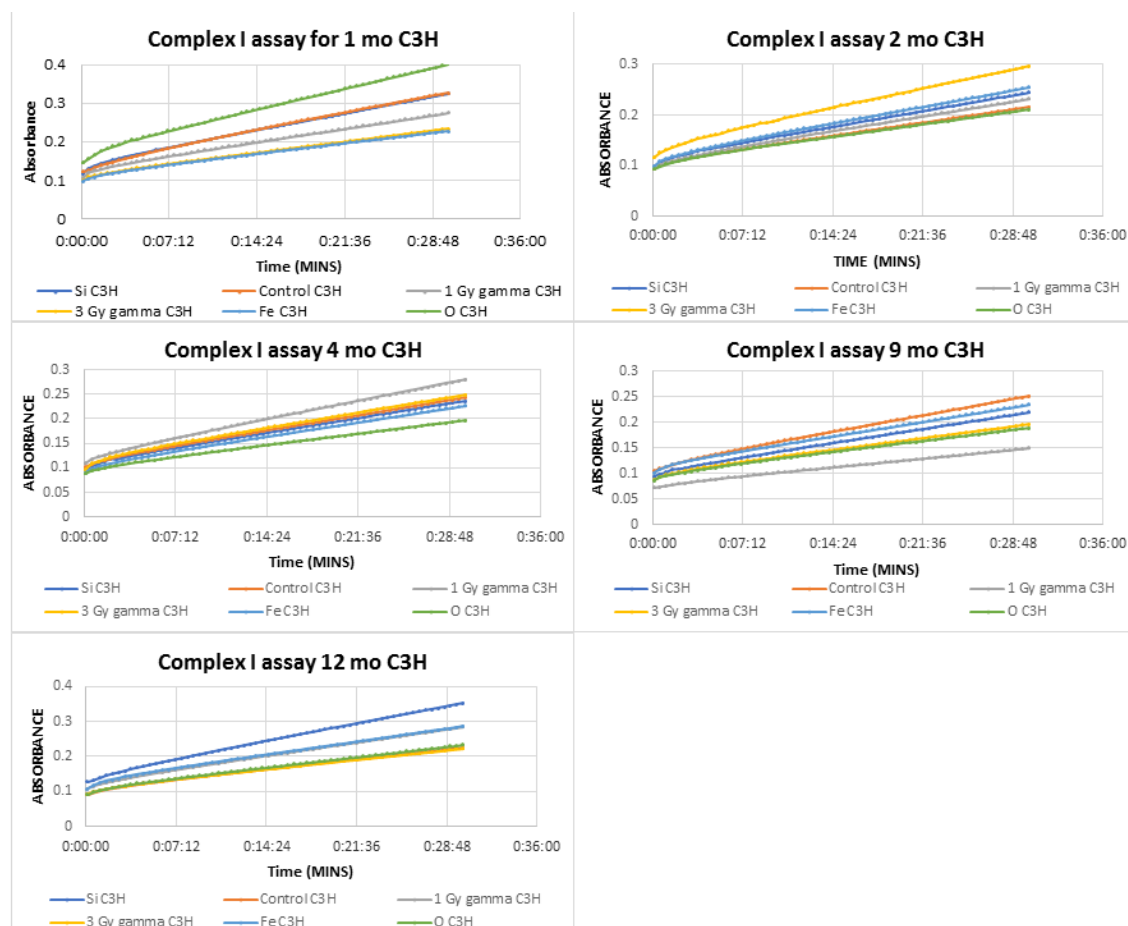


Figure 29: Mitochondria Complex I activity of C3H mice at 1 mo. post-irradiation exhibited a decrease in  $^{56}\text{Fe}$ , 3Gy gamma & 1Gy gamma compared to non-irradiated. All slopes were significantly different except for  $^{28}\text{Si}$  and non-irradiated as well as  $^{56}\text{Fe}$  and 3Gy gamma. At 2 mo. post-irradiation no decreases were seen compared to non-irradiated but instead all irradiations were slightly increased except for  $^{16}\text{O}$  irradiated. All slopes are significantly different except for non-irradiated and  $^{16}\text{O}$ . At 4 mo. post-irradiation a decrease was seen in  $^{16}\text{O}$ ,  $^{56}\text{Fe}$ , &  $^{28}\text{Si}$  compared to non-irradiated. All slopes were significantly different. At 9 mo. post-irradiation a decrease was seen in all irradiation groups compared to non-irradiated. All slopes are significantly different. At 12 mo. post-irradiation a decrease was seen in  $^{56}\text{Fe}$  and  $^{28}\text{Si}$  irradiation. All slopes were significantly different except for 1Gy gamma and  $^{56}\text{Fe}$ , 3Gy gamma and non-irradiated, and  $^{16}\text{O}$  and non-irradiated.

## MITOCHONDRIA COPY NUMBERS VIA QT-PCR

Mitochondrial dysfunction has been known to include declined mtDNA copy numbers as well as reduced mRNA concentration of genes encoding mitochondrial proteins and decreased antioxidant capacity<sup>18</sup>. To address this, mitochondrial copy numbers were measured via qt-PCR. While there were trends in this data that showed slight decreases in <sup>56</sup>Fe, <sup>16</sup>O and 1Gy gamma at 1 month for both strains (Figure 30) they were not statistically significant from non-irradiated control. The decreases likely did not reach significance due to the individual variability shown in Figure 31. In order to fully determine if the copy numbers were being affected this experiment would require a greater n number. To try to reduce the variability within the samples, we tried combining the qt-PCR data with the data from the Complex I where the functional slope was divided by the mtDNA copy number. As shown in Figure 32, variability for C57 was reduced when combining the two datasets but was not for C3H. For example, at 9 and 12 months it actually increased the variability for C3H dataset.

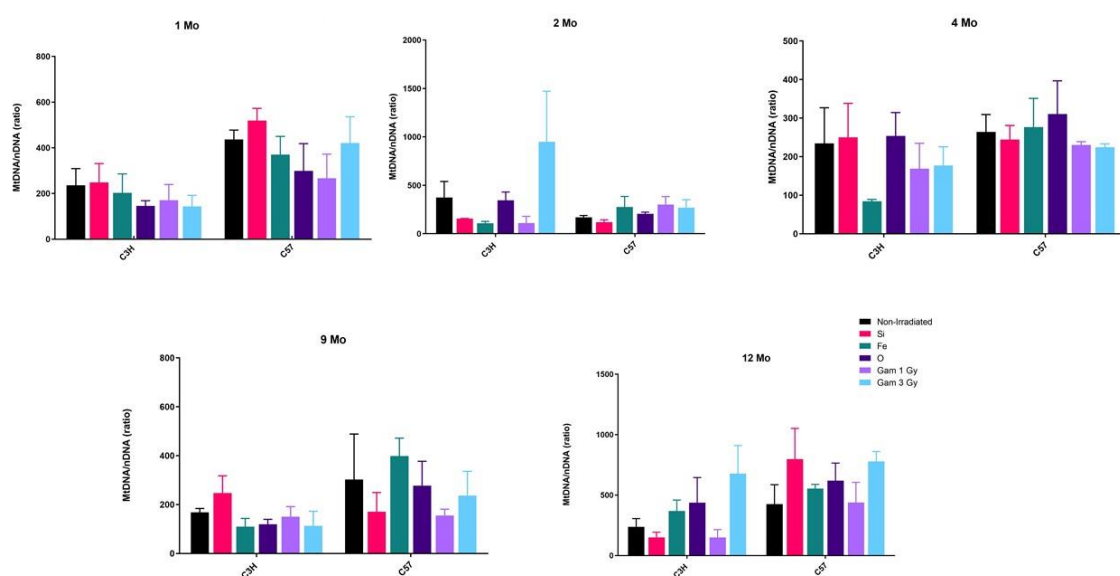




Figure 30: mtDNA copy number determined via PCR for each time point post-irradiation. Changes were not statistically significant.

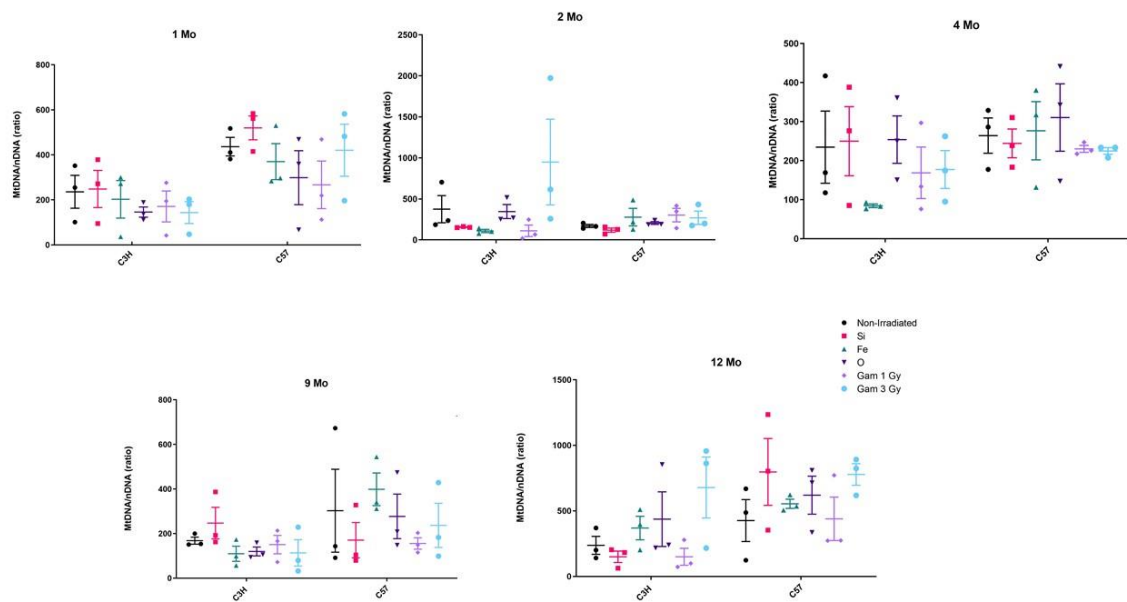


Figure 31: Data from Figure 30 graphed to show each individual sample

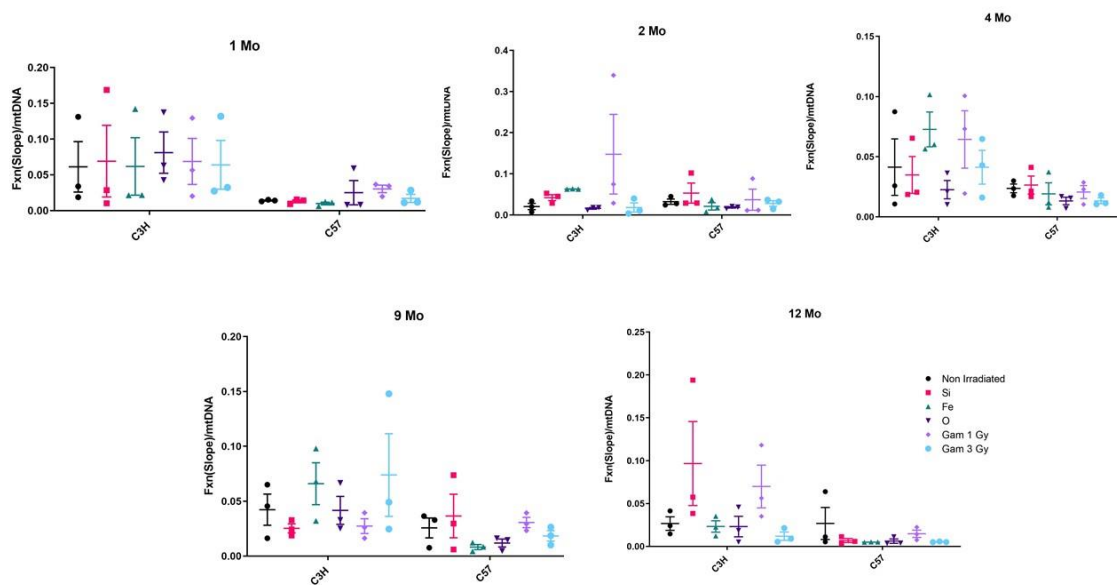


Figure 32: mtDNA copy number results from Figure 30 and 31 were also compared against mitochondria Complex I activity for all time points. Changes were not statistically significant.

## CARDIOLIPINS

Cardiolipins are known to be primarily found in the inner mitochondria membrane and are required for optimal mitochondrial function<sup>99</sup>. This gives it a conical structure that makes them particularly important for cristae formation<sup>17</sup>. They are involved in maintaining membrane potential and architecture and are also known to provide essential structure and functional support to several proteins that are involved in mitochondrial bioenergetics. Loss of cardiolipin content, alterations in its acyl chain composition, and or cardiolipin peroxidation have been previously associated with mitochondrial dysfunction.<sup>99</sup> Changes in cardiolipins cannot only alter fluidity and the folding of the inner mitochondrial membrane, but they can also alter organization and function of the respiratory complexes. These molecules help organize the respiratory complexes into supercomplexes in order to facilitate optimal electron transfer among redox partners. Many of the complexes as well as carrier proteins require this species for proper assembly and function. Loss of these lipids and their peroxidation have been associated with both aging and several metabolic and degenerative diseases.<sup>17</sup> Since our lipidomics platform was focused on global lipid levels in the whole liver instead of being focused on mitochondrial specific lipids, we utilized a fluorescence cardiolipin assay to obtain information on this vital class of lipids in isolated mitochondria. Studies have shown a decrease in cardiolipin levels in relation to age in mitochondria from brain, liver and heart<sup>17</sup>. Slight decreases in cardiolipin levels were seen at 1 month post HZE irradiation, at 9 months for <sup>56</sup>Fe & <sup>16</sup>O irradiation, and all radiation types at 12 months post irradiation, but none of these changes were statistically significant (Figure 33). Although the changes were not statistically significant this could potentially be due

to the small n number (n=3). If future mitochondria studies are completed, it could be interesting to repeat this experiment with a higher n number as well as with seeing if there is a difference in cardiolipin levels after treatment with mitochondria therapeutics which will be discussed in greater detail in the future directions chapter. It is also important to note that this assay detects both regular cardiolipins as well as in their oxidized state. Thus, we are looking at total cardiolipin levels in the dataset.

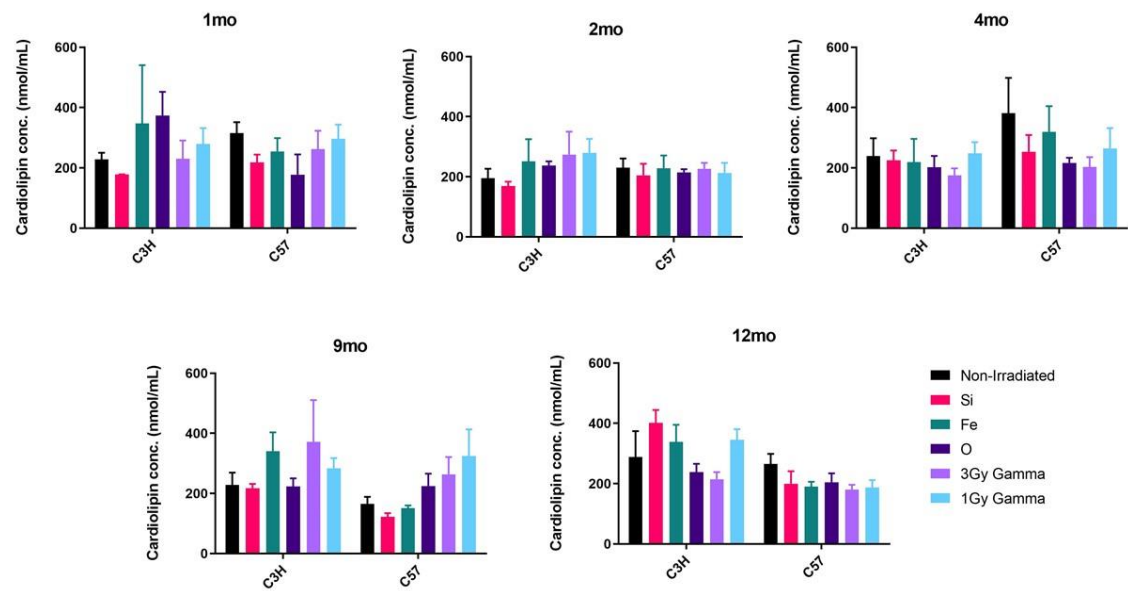


Figure 33: Cardiolipin Levels

# WEIGHTS

Mitochondrial dysfunction is known to contribute to the pathogenesis of metabolic disorders. Affected tissues include those that participate in nutrient metabolism such as adipose, liver and skeletal muscle. Abnormal mitochondrial function is known to result in lipid accumulation as well as insulin resistance. Also growth and transcription factors that regulate mitochondrial gene expression have been seen to contribute to the pathophysiology of obesity, insulin resistance, and type-2 diabetes.<sup>100</sup> Because

metabolism basically comes down to being able to convert food into energy, and mitochondria are the energy factories of the body, we thought that the ability to maintain a healthy weight may also be dependent on having healthy mitochondria. Therefore, the weights of the mice in this study were compared. As shown in Figure 34, no significant differences were found within the weights for the C57 mice with the exception for 1 month  $^{16}\text{O}$  irradiated which is decreased relative to control non-irradiated ( $p=0.046$ ). It also may be important to determine how much the mice are consuming because they could also potentially be eating more to compensate for the dysfunctional mitochondria that aren't producing energy as efficiently.

As for the C3H mice weights shown in Figure 35, there were some significant differences compared to their respective non-irradiated control. At 1 month there was a significant difference between  $^{16}\text{O}$  and non-irradiation ( $p=0.0161$ ). At 2 months there was a significant difference between 1Gy gamma and non-irradiation ( $p=0.0161$ ). At 9 months there was a significant difference between 3Gy gamma ( $p=0.0058$ ),  $^{56}\text{Fe}$  ( $p=0.0327$ ), and  $^{16}\text{O}$  ( $p=0.0358$ ).

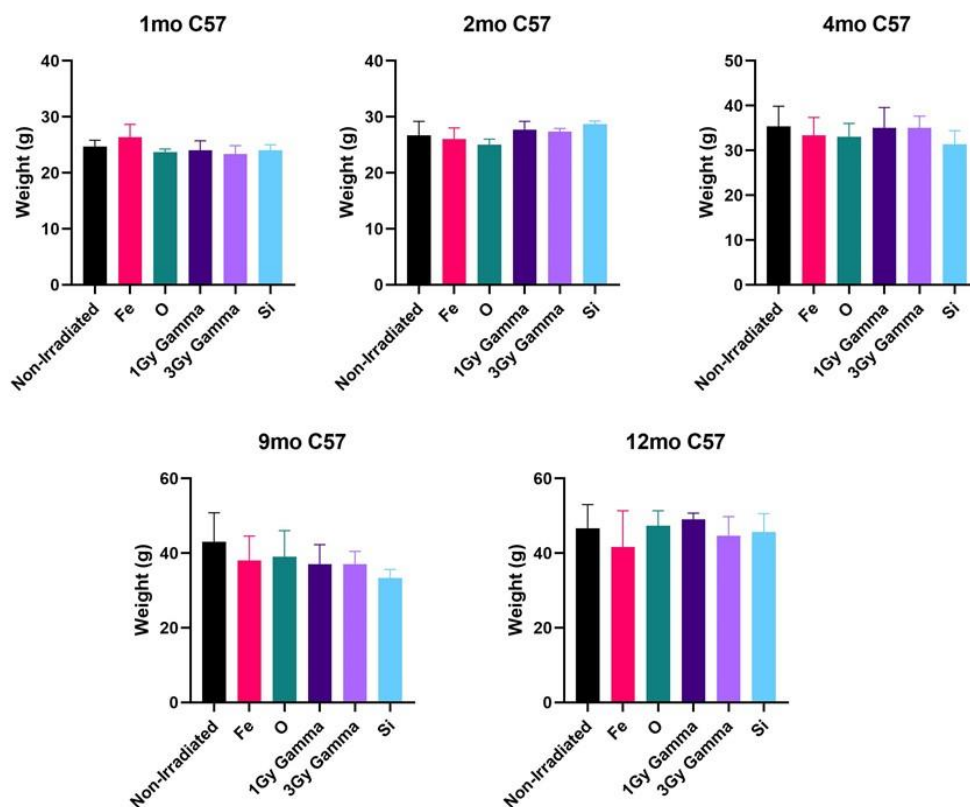


Figure 34: Weights for C57 mice at each time point. Differences within each time point were not significant. All p values were  $\geq 0.05$  by t-test compared to non-irradiated control except for 1 month  $^{16}\text{O}$  ( $p=0.046$ )

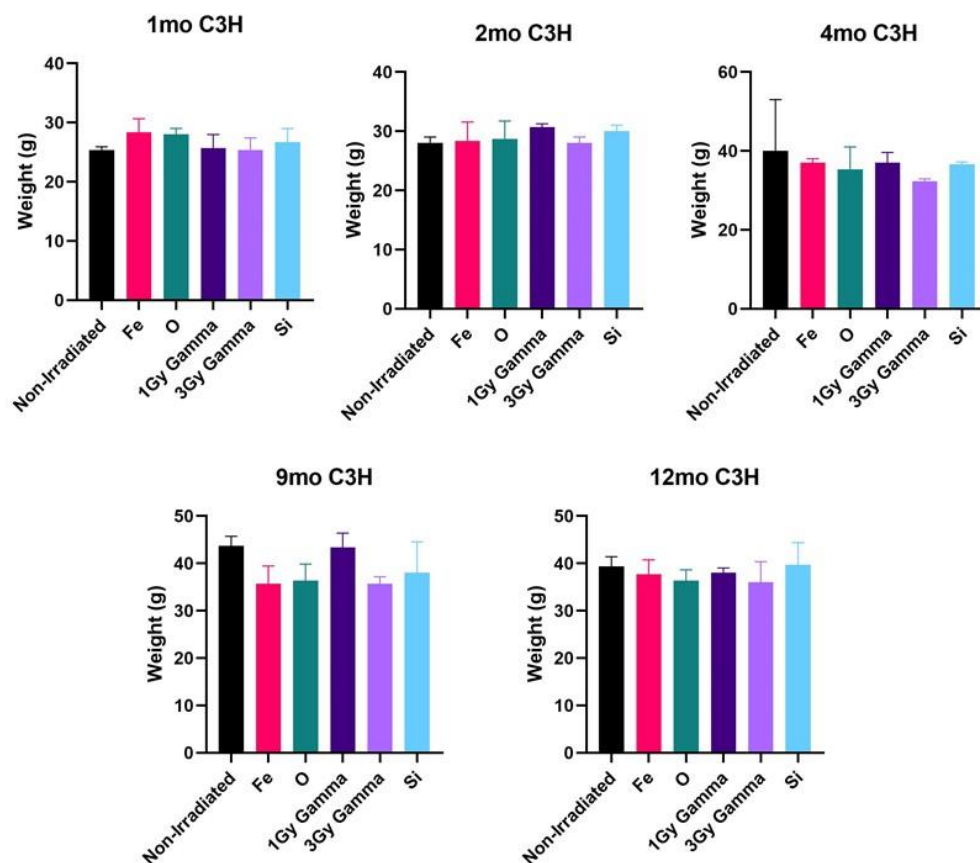


Figure 35: Weights for C3H mice at each time point. At 1 month there was a significant difference between  $^{16}\text{O}$  and non-irradiation ( $p=0.0161$ ). At 2 months there was a significant difference between 1Gy gamma and non-irradiation ( $p=0.0161$ ). At 9 months there was a significant difference between 3Gy gamma ( $p=0.0058$ ),  $^{56}\text{Fe}$  ( $p=0.0327$ ), and  $^{16}\text{O}$  ( $p=0.0358$ ) all in relation to non-irradiated by t-test comparison.

## CONCLUSIONS AND FUTURE DIRECTIONS

### **Chapter 5 WHAT DOES IT ALL MEAN AND WHERE DO WE GO FROM HERE?**

The data from our integrated omics study clearly shows that mitochondria dysfunction is one of the most prominent effects from HZE radiation in particularly in the C57 wild type mice. Since we also see mitochondria effects in the gamma irradiated mice at later time points, we believe that these effects could be due to premature aging. It is well known that mitochondria dysfunction begins to occur as part of the aging process and ultimately leads to several aging related diseases. Therefore, since we see these changes in the mitochondria occurring much sooner than in the gamma irradiated animals, it is believed that HZE is causing the animals to age more rapidly than their gamma irradiated and non-irradiated counterparts.

In the future, we would like to conduct more deep space irradiation studies to delve deeper into mitochondria effects. For starters, it would be very beneficial to have an earlier time point such as a day or a week post-irradiation. This would give us a better understanding of the early ROS pathways that are being activated and allow us to see if arachidonic acid is potentially going up directly following irradiation and being turned over into leukotrienes, etc. It would also be very insightful to measure mitochondria respiration via a seahorse system that measures the oxygen consumption rate and can quantify multiple parameters of mitochondria respiration. One problem with this though is these experiments are very low throughput and very time consuming, so they would have to be done with a small n number and it is unclear if an n number that is high enough to reach statistical power would physically be possible to do.

Utilizing mitochondria specific proteomics may also be useful as the protocol used in these studies was not enhanced for membrane bound proteins, and the signal from other non-mitochondria proteins could have swamped out some of the mitochondria specific proteins, thus we could not detect very small changes. It would also be very useful to collect mitochondria specific lipidomics as lipids play an important role in regulating the mitochondria membranes.

A positron emission tomography (PET) scan system would also be very useful to monitor for potential tumor growth, so we would not be relying simply on our eyes when the animals are euthanized to identify if there is a tumor present. This would also be useful in assessing the metabolic rate in the animals. It is also important to note that there are several environmental factors that an astronaut will encounter that could potentially also result in mitochondrial effects.

At the 2020 NASA meeting Dr. Laiakis presented data on the effects of mice exposed to microgravity conditions on the ISS.<sup>101</sup> Mitochondria dysfunction was one of the main findings of her data. It is also possible that hypoxia conditions encountered in the space craft could have also contributed to these findings as it could also contribute to effects on the mitochondria. As you may recall, astronauts on the ISS are not exposed to HZE irradiation as these ions are only a problem in deep space travel. Mental stress is also another factor that could contribute to the effects as astronauts are confined to small living quarters and limited communication with loved ones. This will be even more of an issue on a trip to Mars as the living quarters will be drastically smaller and they will have no communication with anyone back on Earth. Some “stress” conditions are also encountered by the mice in the ISS study because the mice have to learn how to climb and hold onto to ladders in order to retrieve their food which is very different compared to a normal lab environment that they have experienced on Earth. Bodily functions are also an issue for the animals as their urine and feces will float in their cages until it meets an absorbent material. Another area of concern is the astronauts’ diet. On the ISS fresh fruits and



vegetables can be delivered on a somewhat regular basis. However, on a trip to Mars this will not be possible. All of these factors could potentially have compounding mitochondrial effects and thus, create an even worse scenario for the astronauts.

We believe the best means of potentially mitigating the risk of serious mitochondrial effects from deep space travel is through mitochondria centered therapeutics. The next steps in this project should incorporate some of the currently known therapeutics and focus on studying their effects following deep space radiation. The majority of drugs focus on reducing mitochondria ROS by using mitochondria targeted antioxidants that are based on delivery of known redox agents to the mitochondria matrix by conjugation to delocalized cations such as triphenylphosphonium ion (TPP<sup>+</sup>). Although these compounds can reduce ROS, studies have now found that they can actually inhibit mitochondrial bioenergetics.<sup>17</sup>

One of the more promising drugs is Elamipretide (SS-31, D-Arg-Dmt-Lys-Phe-NH<sub>2</sub>).<sup>102</sup> It is important to note that Elamipretide is comprised of D amino acids which prolongs the stability and function in a biological environment because the D-analogues are much less susceptible to enzymatic processing as L-amino acids are typically found in nature and used by the cell.<sup>103</sup> It is a novel mitochondria targeted antioxidant peptide that has protective effects against mitochondria dysfunction and oxidative stress. Its dimethyltyrosine residue allows for scavenging of oxyradicals as well as inhibiting linoleic acid and low-density lipoprotein oxidation<sup>102</sup>. It ultimately eliminates ROS and increases ATP production by maintaining membrane potential. By reducing ROS, it is able to prevent the opening of the mitochondria permeability transition pore, prevent mitochondria swelling and reduce cytochrome c release in response to high Ca<sup>2+</sup> overload. This drug has previously been used as a strategy to protect against neurodegenerative diseases, inflammatory diseases and ischemia reperfusion injury in animal models<sup>102</sup>. This compound is also known to selectively target the inner mitochondrial membrane by binding cardiolipins selectively via electrostatic and hydrophobic interactions. As

mentioned previously, cardiolipins play an important structural role in cristae formation and organization of the respiratory complexes into supercomplexes for optimal oxidative phosphorylation. Interaction between cardiolipins and cytochrome c determines whether cytochrome c acts as an electron carrier or peroxidase<sup>17</sup>. By interacting with cardiolipins, SS-31 prevents them from converting cytochrome c into a peroxidase thus protecting its electron carrying function which in turn protects the structure of the mitochondria cristae and promotes oxidative phosphorylation<sup>17</sup>. Unfortunately, in a study published early this year while the drug was generally well tolerated, it failed to meet its primary endpoint. The study evaluated the effect of the compound on exercise performance in adults with primary mitochondrial myopathy. Patients with this disease possess genetic defects that impair normal mitochondrial function that primarily affects their skeletal muscle. While their study did show meaningful improvements in various outcome measures, it did not reach statistical significance. However, authors did note that they support the initiation of a Phase 3 trial to investigate the long-term dosing in a larger patient population.<sup>104</sup> This also doesn't discount the possibility of use of this drug for a potential countermeasure or possibly even a radio protectant. It will have to be studied in animal models to determine if it could potentially be used.

It is also possible that ubiquinol-10 supplementation could be used as it has been shown to activate mitochondria functions to decelerate senescence in senescence-accelerated mice. In this study, they reported decreases in expression of sirtuin gene family members that result in the activation of peroxisome proliferator-activated receptor  $\gamma$  coactivator 1 $\alpha$  that helps control mitochondrial biogenesis and respiration as well as the upregulation of superoxide dismutase 2 and isocitrate dehydrogenase 2 which are mitochondrial antioxidants. Supplementation with Ubiquinol-10 was also found to increase activity in mitochondrial complex I<sup>50</sup>. In addition to its major role in the electron transport chain, it also has an important anti-oxidant role which helps stabilize the plasma membranes as well as protect membrane phospholipids from peroxidation. Decreased

levels in aging likely help contribute to membrane peroxidation injury. Chronic inflammation is also a common problem in relation to aging. By reducing the free radicals, it also helps reduce NF- $\kappa$ B which ultimately reduces the release of pro-inflammatory cytokines in particularly tumor necrosis factor alpha (TNF- $\alpha$ ) and interleukin 6 (IL-6)<sup>53</sup>. Since decreases in ubiquinol-10 are thought to be age related and it seems that HZE induces a premature aging component, supplementation with this may also be of great benefit to help protect against space irradiation.

ROS accumulation could also result in insulin resistance<sup>100</sup>. Since excess insulin due to insulin resistance can result in weight gain, it could be possible that the mice with ROS accumulation have become insulin resistant and are gaining weight due to insulin resistance. This in turn could compensate for weight loss that was expected to be seen if the animals were unhealthy and were starting to form HCC. In the liver, when insulin resistance occurs insulin fails to suppress gluconeogenesis, but will continue to stimulate fatty acid synthesis. mTORC plays an important role in hepatic lipogenesis. It along with other mechanisms downstream of Akt2 may be responsible for the uncoupling of glucose and lipid metabolism in the insulin signaling pathway that ultimately results in hyperglycemia and hyper-triglyceridemia.<sup>105</sup> In order to know for sure if insulin resistance is playing a role in these animals, glucose, A1C levels and triglycerides would need to be monitored. However, we did notice upon collecting liver samples from these animals that several of the mice seemed to have what looked to be fatty livers as fatty livers are more blunt and yellowish/white in color whereas the healthy livers are dark red with sharp edges. In future studies, it would be a good idea to thoroughly assess the livers for fatty liver and prior to tissue collection monitor their glucose, A1C, triglycerides etc. It is also important to note that typically astronauts are very physically fit so it may be very important in future studies to exercise a group of mice and see how their results compare to those who did not receive extra physical training.

## Bibliography/References

1. Cucinotta, F. A. & Durante, M. Cancer risk from exposure to galactic cosmic rays: implications for space exploration by human beings. *Lancet Oncol.* **7**, 431–435 (2006).
2. Alpen, E. L., Powers-Risius, P., Curtis, S. B. & DeGuzman, R. Tumorigenic Potential of High-Z, High-LET Charged-Particle Radiations. *Radiat. Res.* **136**, 382 (1993).
3. Datta, K., Suman, S., Kallakury, B. V. S. & Fornace, A. J. Heavy Ion Radiation Exposure Triggered Higher Intestinal Tumor Frequency and Greater  $\beta$ -Catenin Activation than  $\gamma$  Radiation in APCMin/+ Mice. *PLoS One* **8**, e59295 (2013).
4. Datta, K., Suman, S., Kallakury, B. V. S. & Fornace, A. J. Exposure to Heavy Ion Radiation Induces Persistent Oxidative Stress in Mouse Intestine. *PLoS One* **7**, e42224 (2012).
5. Weil, M. M. *et al.* Incidence of Acute Myeloid Leukemia and Hepatocellular Carcinoma in Mice Irradiated with 1 GeV/nucleon  $^{56}\text{Fe}$  Ions. *Radiat. Res.* **172**, 213–219 (2009).
6. Weil, M. M. *et al.* Effects of  $^{28}\text{Si}$  Ions,  $^{56}\text{Fe}$  Ions, and Protons on the Induction of Murine Acute Myeloid Leukemia and Hepatocellular Carcinoma. *PLoS One* **9**, e104819 (2014).
7. Durante, M. & Cucinotta, F. A. Heavy ion carcinogenesis and human space exploration. *Nat. Rev. Cancer* **8**, 465–472 (2008).
8. Cheema, A. K. *et al.* Long-Term Differential Changes in Mouse Intestinal Metabolomics after  $\gamma$  and Heavy Ion Radiation Exposure. *PLoS One* **9**, e87079 (2014).
9. Laiakis, E. C. *et al.* Metabolomic profiling of urine samples from mice exposed to protons reveals radiation quality and dose specific differences. *Radiat. Res.* **183**, 382–90 (2015).
10. Azzam, E. I., Jay-Gerin, J.-P. & Pain, D. Ionizing radiation-induced metabolic oxidative stress and prolonged cell injury. *Cancer Lett.* **327**, 48–60 (2012).
11. Desouky, O., Ding, N. & Zhou, G. Targeted and non-targeted effects of ionizing radiation. *J. Radiat. Res. Appl. Sci.* **8**, 247–254 (2015).
12. Reisz, J. A., Bansal, N., Qian, J., Zhao, W. & Furdul, C. M. Effects of Ionizing Radiation on Biological Molecules—Mechanisms of Damage and Emerging Methods of Detection. *Antioxid. Redox Signal.* **21**, 260–292 (2014).
13. Wall:MSFC, J. NASA - Space Radiation Health Project.
14. Yamamori, T. *et al.* Ionizing radiation induces mitochondrial reactive oxygen species production accompanied by upregulation of mitochondrial electron transport chain function and mitochondrial content under control of the cell cycle checkpoint. *Free Radic. Biol. Med.* **53**, 260–270 (2012).
15. Nugent, S. *et al.* International Journal of Radiation Biology Altered mitochondrial function and genome frequency post exposure to  $\gamma$ -radiation and bystander factors. *Int. J. Radiat. Biol.* **86**, 829–841 (2010).
16. Suzuki, C., Venkatesh, S., Jayapalraja, T., Azzam, E. TISSUE SHARING PROJECT: EFFECTS OF SPACE RADIATION ON BIOMARKERS OF THE MITOCHONDRIAL STRESS AND ENERGY METABOLISM [#20487]. in *NASA Human Research Program Investigators' Workshop* (2020).
17. Szeto, H. H. First-in-class cardiolipin-protective compound as a therapeutic agent to restore mitochondrial bioenergetics. *Br. J. Pharmacol.* **171**, 2029–2050 (2014).
18. Bhatti, J. S., Kumar, S., Vijayan, M., Bhatti, G. K. & Reddy, P. H. *Therapeutic Strategies for Mitochondrial Dysfunction and Oxidative Stress in Age-Related Metabolic Disorders. Progress in Molecular Biology and Translational Science* vol. 146 (2017).
19. Verdin, E., Hirschey, M. D., Finley, L. W. S. & Haigis, M. C. Sirtuin Regulation of

- Mitochondria - Energy Production. **35**, 669–675 (2011).
20. Vera, N. B. *et al.* Quantitation of Urinary Acylcarnitines by DMS-MS/MS Uncovers the Effects of Total Body Irradiation in Cancer Patients. *J. Am. Soc. Mass Spectrom.* **31**, 498–507 (2020).
21. Melone, M. A. B. *et al.* The carnitine system and cancer metabolic plasticity review-article. *Cell Death Dis.* **9**, (2018).
22. Monn, M., Voza, A., Lasorsa, F. M., Porcelli, V. & Palmieri, F. Mitochondrial Carriers for Aspartate, Glutamate and Other Amino Acids : A Review. (2019).
23. Guda, P., Guda, C. & Subramaniam, S. Reconstruction of Pathways Associated with Amino Acid Metabolism in Human Mitochondria. *Genomics Proteomics Bioinforma.* **5**, 166–176 (2007).
24. Aravalli, R. N., Cressman, E. N. K. & Steer, C. J. Cellular and molecular mechanisms of hepatocellular carcinoma: an update. *Arch. Toxicol.* **87**, 227–247 (2013).
25. Marra, M. *et al.* Molecular targets and oxidative stress biomarkers in hepatocellular carcinoma: an overview. *J. Transl. Med.* **9**, 171 (2011).
26. Lin, S., Hoffmann, K. & Schemmer, P. Treatment of Hepatocellular Carcinoma: A Systematic Review. *Liver Cancer* **1**, 144–158 (2012).
27. Cucinotta, F. A. & Chappell, L. J. Non-targeted effects and the dose response for heavy ion tumor induction. *Mutat. Res. Mol. Mech. Mutagen.* **687**, 49–53 (2010).
28. Festing, M. F. W. & Blackmore, D. K. Life span of specified-pathogen-free (MRC category 4) mice and rats. *Lab. Anim.* **5**, 179–192 (1971).
29. Lichti, C. F. *et al.* Integrated Chromosome 19 Transcriptomic and Proteomic Data Sets Derived from Glioma Cancer Stem-Cell Lines. *J. Proteome Res.* **13**, 191–199 (2014).
30. Mastro, R. & Hall, M. Protein Delipidation and Precipitation by Tri-n-butylphosphate, Acetone, and Methanol Treatment for Isoelectric Focusing and Two-Dimensional Gel Electrophoresis. *Anal. Biochem.* **273**, 313–315 (1999).
31. Almeida, R., Pauling, J. K., Sokol, E., Hannibal-Bach, H. K. & Ejsing, C. S. Comprehensive Lipidome Analysis by Shotgun Lipidomics on a Hybrid Quadrupole-Orbitrap-Linear Ion Trap Mass Spectrometer. *J. Am. Soc. Mass Spectrom.* **26**, 133–148 (2015).
32. Rupasinghe, T. W. T. Lipidomics: Extraction Protocols for Biological Matrices. in *Methods in molecular biology (Clifton, N.J.)* vol. 1055 71–80 (2013).
33. He, H. *et al.* Method for Lipidomic Analysis: p53 Expression Modulation of Sulfatide, Ganglioside, and Phospholipid Composition of U87 MG Glioblastoma Cells. *Anal. Chem.* **79**, 8423–8430 (2007).
34. Sud, M. *et al.* LMSD: LIPID MAPS structure database. *Nucleic Acids Res.* **35**, D527–D532 (2007).
35. Team, R. RStudio: Integrated Development for R. (2020).
36. Searle, S. R., Speed, F. M. & Milliken, G. A. Population marginal means in the linear model: An alternative to least squares means. *Am. Stat.* **34**, 216–221 (1980).
37. Anthor, H. *et al.* Lack of myostatin results in excessive muscle growth but impaired force generation. *Proc. Natl. Acad. Sci.* **104**, 1835–1840 (2007).
38. Guo, W., Jiang, L., Bhasin, S., Khan, S. M. & Swerdlow, R. H. DNA extraction procedures meaningfully influence qPCR-based mtDNA copy number determination. *Mitochondrion* **9**, 261–265 (2009).
39. Terfve, C. *et al.* System-Wide Quantitative Proteomics of the Metabolic Syndrome in Mice: Genotypic and Dietary Effects. *J. Proteome Res.* **16**, 831–841 (2017).
40. Gao, Y. *et al.* Quantitative proteomics by SWATH-MS reveals sophisticated metabolic reprogramming in hepatocellular carcinoma tissues. *Sci. Rep.* **7**, 1–12 (2017).
41. Manzoni, C. *et al.* Genome, transcriptome and proteome: The rise of omics data and their integration in biomedical sciences. *Brief. Bioinform.* **19**, 286–302 (2018).

42. Haider, S. & Pal, R. Integrated Analysis of Transcriptomic and Proteomic Data. *Curr. Genomics* **14**, 91–110 (2013).
43. Hack, C. J. Integrated transcriptome and proteome data: the challenges ahead. *Brief. Funct. Genomic. Proteomic.* **3**, 212–219 (2004).
44. Kasai, S., Shimizu, S., Tatara, Y., Mimura, J. & Itoh, K. Regulation of Nrf2 by mitochondrial reactive oxygen species in physiology and pathology. *Biomolecules* vol. 10 (2020).
45. Xia, M. F. *et al.* Communication between mitochondria and other organelles: a brand-new perspective on mitochondria in cancer. *Cell Biosci.* **9**, 1–19 (2019).
46. Schenkel, L. & Bakovic, M. Formation and Regulation of Mitochondrial Membranes. *Int. J. Cell Biol.* (2014) doi:10.1155/2014/709828.
47. Yoshida, H. Critical Review ER Stress Response , Peroxisome Proliferation , Mitochondrial Unfolded Protein Response and Golgi Stress Response. **61**, 871–879 (2009).
48. Rainbolt, T. K., Atanassova, N., Genereux, J. C. & Wiseman, R. L. Stress-Regulated Translational Attenuation Adapts Mitochondrial Protein Import through Tim17A Degradation. (2013) doi:10.1016/j.cmet.2013.11.006.
49. Mitochondria in Liver Disease - Google Books.  
[https://books.google.com/books?id=XynSCgAAQBAJ&pg=PA387&lpg=PA387&dq=acute+phase+response+and+mitochondria&source=bl&ots=w0ab-NbIFD&sig=ACfU3U2ZJF-qi3oH5elOJLcQ\\_Xxh0hp7AQ&hl=en&sa=X&ved=2ahUKEwi1u7m78cDpAhUS7awKHZhbAEAQ6AEwEnoECAsQAQ#v=onepage&q=acute phase response and mitochondria&f=false](https://books.google.com/books?id=XynSCgAAQBAJ&pg=PA387&lpg=PA387&dq=acute+phase+response+and+mitochondria&source=bl&ots=w0ab-NbIFD&sig=ACfU3U2ZJF-qi3oH5elOJLcQ_Xxh0hp7AQ&hl=en&sa=X&ved=2ahUKEwi1u7m78cDpAhUS7awKHZhbAEAQ6AEwEnoECAsQAQ#v=onepage&q=acute%20phase%20response%20and%20mitochondria&f=false).
50. Tian, G. *et al.* Ubiquinol-10 supplementation activates mitochondria functions to decelerate senescence in senescence-accelerated mice. *Antioxidants Redox Signal.* **20**, 2606–2620 (2014).
51. Han, C. Y. Update on FXR biology: Promising therapeutic target? *International Journal of Molecular Sciences* vol. 19 (2018).
52. Zelcer, N. & Tontonoz, P. Liver X receptors as integrators of metabolic and inflammatory signaling. *Journal of Clinical Investigation* vol. 116 607–614 (2006).
53. De Barcelos, I. P. & Haas, R. H. Coq10 and aging. *Biology (Basel)*. **8**, (2019).
54. Wei, Z., Su, W., Lou, H., Duan, S. & Chen, G. Trafficking pathway between plasma membrane and mitochondria via clathrin-mediated endocytosis. *J. Mol. Cell Biol.* **10**, 539–548 (2018).
55. Pauwels, A. M., Trost, M., Beyaert, R. & Hoffmann, E. Patterns, Receptors, and Signals: Regulation of Phagosome Maturation. *Trends in Immunology* vol. 38 407–422 (2017).
56. Zhang, Q. *et al.* Circulating mitochondrial DAMPs cause inflammatory responses to injury. *Nature* **464**, 104–107 (2010).
57. Vargas-parada, B. L. Mitochondria and the Immune Response The Origin of Mitochondria as Cellular Organelles : Endosymbiotic Theory A Mystery in the Emergency Room : Mitochondria and the Inflammatory Response. **135**, 1–5 (2012).
58. Persad, S. Inhibition of integrin-linked kinase (ILK) suppresses activation of protein kinase B/Akt and induces cell cycle arrest and apoptosis of PTEN-mutant prostate cancer cells. *Proc. Natl. Acad. Sci.* **97**, 3207–3212 (2000).
59. Strell, C. & Entschladen, F. Extravasation of leukocytes in comparison to tumor cells. *Cell Communication and Signaling* vol. 6 10 (2008).
60. Lam, S. M. & Shui, G. Lipidomics as a Principal Tool for Advancing Biomedical Research. *J. Genet. Genomics* **40**, 375–390 (2013).
61. Wenk, M. R. Lipidomics: New Tools and Applications. *Cell* **143**, 888–895 (2010).
62. Harayama, T. & Riezman, H. Understanding the diversity of membrane lipid

- composition. *Nat. Rev. Mol. Cell Biol.* **19**, 281–296 (2018).
63. Jiang, J., Nilsson-Ehle, P. & Xu, N. Influence of liver cancer on lipid and lipoprotein metabolism. *Lipids Health Dis.* **5**, 4 (2006).
  64. Nguyen, P. *et al.* Liver lipid metabolism. *J. Anim. Physiol. Anim. Nutr. (Berl.)* **92**, 272–283 (2008).
  65. Di Girolamo, F., Lante, I., Muraca, M. & Putignani, L. The Role of Mass Spectrometry in the “Omics” Era. *Curr. Org. Chem.* **17**, 2891–2905 (2013).
  66. Schneider, R. Intracellular sterol transport in eukaryotes, a connection to mitochondrial function? *Biochimie* **89**, 255–259 (2007).
  67. Tian, S., Ohta, A., Horiuchi, H. & Fukuda, R. Evaluation of sterol transport from the endoplasmic reticulum to mitochondria using mitochondrially targeted bacterial sterol acyltransferase in *Saccharomyces cerevisiae*. *Biosci. Biotechnol. Biochem.* **79**, 1608–1614 (2015).
  68. Wang, X., Devaiah, S. P., Zhang, W. & Welti, R. Signaling functions of phosphatidic acid. *Progress in Lipid Research* vol. 45 250–278 (2006).
  69. Kameoka, S., Adachi, Y., Okamoto, K., Iijima, M. & Sesaki, H. Phosphatidic Acid and Cardiolipin Coordinate Mitochondrial Dynamics. *Trends in Cell Biology* vol. 28 67–76 (2018).
  70. Yang, C. Y. & Frohman, M. A. Mitochondria: Signaling with phosphatidic acid. *Int. J. Biochem. Cell Biol.* **44**, 1346–1350 (2012).
  71. Calzada, E. *et al.* Phosphatidylethanolamine made in the inner mitochondrial membrane is essential for yeast cytochrome bc 1 complex function. *Nat. Commun.* **10**, 1–17 (2019).
  72. Arifin, S. A. & Falasca, M. Lysophosphatidylinositol signalling and metabolic diseases. *Metabolites* vol. 6 (2016).
  73. Heringdorf, D. M. zu. Lysophospholipids - Encyclopedia of Molecular Pharmacology. in (eds. Offermanns, S. & Rosenthal, W.) 710–716 (Springer Berlin Heidelberg, 2008). doi:10.1007/978-3-540-38918-7\_90.
  74. Atanes, P. & Persaud, S. J. GPCR targets in type 2 diabetes. in *GPCRs: Structure, Function, and Drug Discovery* 367–391 (Elsevier, 2019). doi:10.1016/B978-0-12-816228-6.00018-0.
  75. Pallares-Méndez, R. & Fernández-Reynoso, C. The microbiome and metabolome in metabolic syndrome. in *Microbiome and Metabolome in Diagnosis, Therapy, and other Strategic Applications* 215–225 (Elsevier, 2019). doi:10.1016/B978-0-12-815249-2.00022-1.
  76. P-type ATPases in Health and Disease - Google Books.  
<https://books.google.com/books?id=NzCDDwAAQBAJ&pg=PA76&lpg=PA76&dq=Although+PC+%26+PE+are+the+most+abundant+phospholipids+found+within+cells+from+yeast+to+mammalian+cells,+lipids+are+not+randomly+distributed+among+biological+membranes.&source=bl&ots=YjVSsd5Dyp&sig=ACfU3U0DUkmp2A3uJKpGf-Vkrl3AdEkOLA&hl=en&sa=X&ved=2ahUKEwjTh93cqubpAhWGrp4KHRt-DB4Q6AEwCnoECAsQAQ#v=onepage&q=Although+PC+%26+PE+are+the+most+abundant+phospholipids+found+within+cells+from+yeast+to+mammalian+cells%2C+lipids+are+not+randomly+distributed+among+biological+membranes.&f=false>
  77. Murakami-Murofushi, K. *et al.* Biological functions of a novel lipid mediator, cyclic phosphatidic acid. *Biochimica et Biophysica Acta - Molecular and Cell Biology of Lipids* vol. 1582 1–7 (2002).
  78. Oishi-Tanaka, Y. & Glass, C. K. A new role for cyclic phosphatidic acid as a PPAR $\gamma$  antagonist. *Cell Metab.* **12**, 207–208 (2010).
  79. Frasch, S. C. & Bratton, D. L. Emerging roles for lysophosphatidylserine in resolution of inflammation. *Progress in Lipid Research* vol. 51 199–207 (2012).
  80. Higashi, H., Hirabayashi, Y., Hirota, M., Matsumoto, M. & Kato, S. Detection of

- ganglioside GM2 in sera and tumor tissues of hepatoma patients. *Jpn. J. Cancer Res.* **78**, 1309–13 (1987).
81. Leon, J. *et al.* 8-Oxoguanine accumulation in mitochondrial DNA causes mitochondrial dysfunction and impairs neuritogenesis in cultured adult mouse cortical neurons under oxidative conditions. *Sci. Rep.* **6**, (2016).
  82. Revankar, G. R. & Sudhakar Rao, T. DNA with Altered Bases. in *Comprehensive Natural Products Chemistry* 313–339 (Elsevier, 1999). doi:10.1016/b978-0-08-091283-7.00064-3.
  83. Maiuolo, J., Oppedisano, F., Gratteri, S., Muscoli, C. & Mollace, V. Regulation of uric acid metabolism and excretion. *Int. J. Cardiol.* **213**, 8–14 (2016).
  84. Wang, D. & Dubois, R. N. Eicosanoids and cancer. *Nature Reviews Cancer* vol. 10 181–193 (2010).
  85. Jiang, X., Nicolls, M. R., Tian, W. & Rockson, S. G. Lymphatic Dysfunction, Leukotrienes, and Lymphedema. *Annu. Rev. Physiol.* **80**, 49–70 (2018).
  86. FATTY ACIDS | Gamma-linolenic Acid. 2308–2311 (2003) doi:10.1016/B0-12-227055-X/00448-X.
  87. Da Silva, M. S. & Rudkowska, I. Macro Components in Dairy and Their Effects on Inflammation Parameters: Preclinical Studies. in *Nutrients in Dairy and Their Implications for Health and Disease* 287–302 (Elsevier, 2017). doi:10.1016/B978-0-12-809762-5.00022-X.
  88. Senyilmaz-Tiebe, D. *et al.* Dietary stearic acid regulates mitochondria in vivo in humans. *Nat. Commun.* **9**, 1–10 (2018).
  89. Stanley, W. C., Khairallah, R. J. & Dabkowski, E. R. Update on lipids and mitochondrial function: Impact of dietary n-3 polyunsaturated fatty acids. *Current Opinion in Clinical Nutrition and Metabolic Care* vol. 15 122–126 (2012).
  90. Enguita, M. *et al.* The cirrhotic liver is depleted of docosahexaenoic acid (DHA), a key modulator of NF- $\kappa$ B and TGF $\beta$  pathways in hepatic stellate cells. *Cell Death Dis.* **10**, 1–13 (2019).
  91. Domenichiello, A. F., Kitson, A. P. & Bazinet, R. P. Is docosahexaenoic acid synthesis from  $\alpha$ -linolenic acid sufficient to supply the adult brain? *Progress in Lipid Research* vol. 59 54–66 (2015).
  92. Benjamins, J. A., Murphy, E. J. & Seyfried, T. N. Lipids. in *Basic Neurochemistry* 81–100 (Elsevier, 2012). doi:10.1016/B978-0-12-374947-5.00005-5.
  93. Wenk, M. R. The emerging field of lipidomics. *Nat. Rev. Drug Discov.* **4**, 594–610 (2005).
  94. Owen, J. B. & Allan Butterfiel, D. Measurement of oxidized/reduced glutathione ratio. in *Methods in Molecular Biology* vol. 648 269–277 (Humana Press Inc., 2010).
  95. Poulouse, S. M., Bielinski, D. F., Carrihill-Knoll, K., Rabin, B. M. & Shukitt-Hale, B. Exposure to 16 O-Particle Radiation Causes Aging-Like Decrements in Rats through Increased Oxidative Stress, Inflammation and Loss of Autophagy. *Radiat. Res.* **176**, 761–769 (2011).
  96. Haas, R. H. Mitochondrial dysfunction in aging and diseases of aging. *Biology (Basel)*. **8**, (2019).
  97. Fontaine, E. Metformin-Induced Mitochondrial Complex I Inhibition: Facts, Uncertainties, and Consequences. *Front. Endocrinol. (Lausanne)*. **9**, 23–28 (2018).
  98. Siteni, S. RADIOPROTECTIVE EFFECT OF THE ANTI-DIABETIC DRUG METFORMIN [#20469]. in *NASA Human Research Program Investigators' Workshop* (2020).
  99. Chicco, A. J. & Sparagna, G. C. Role of cardiolipin alterations in mitochondrial dysfunction and disease. *Am. J. Physiol. - Cell Physiol.* **292**, (2007).
  100. Bournat, J. C. & Brown, C. W. Mitochondrial dysfunction in obesity. *Current Opinion in*



- Endocrinology, Diabetes and Obesity* vol. 17 446–452 (2010).
101. Laiakis, E., Kwok, A., Delp, M., Zawieja, D., Mao, X., Livingston, E., Bateman, T., Willey, J. METABOLOMIC ALTERATIONS ASSOCIATED WITH SPACEFLIGHT AND MICROGRAVITY IN GASTROCNEMIUS AND QUADRICEPS MUSCLE MURINE SAMPLES. [#20337]. in *NASA Human Research Program Investigators' Workshop* (2020).
  102. Zhao, W. *et al.* Elamipretide (SS-31) improves mitochondrial dysfunction, synaptic and memory impairment induced by lipopolysaccharide in mice. *J. Neuroinflammation* **16**, 1–19 (2019).
  103. Melchionna, M., E. Styan, K. & Marchesan, S. The Unexpected Advantages of Using D-Amino Acids for Peptide Self- Assembly into Nanostructured Hydrogels for Medicine. *Curr. Top. Med. Chem.* **16**, 2009–2018 (2016).
  104. Karaa, A., Haas, R., Goldstein, A., Vockley, J. & Cohen, B. H. A randomized crossover trial of elamipretide in adults with primary mitochondrial myopathy. *J. Cachexia. Sarcopenia Muscle* (2020) doi:10.1002/jcsm.12559.
  105. Hardy, O. T., Czech, M. P. & Corvera, S. What causes the insulin resistance underlying obesity? *Current Opinion in Endocrinology, Diabetes and Obesity* vol. 19 81–87 (2012).

## Vita

Brooke Lawson Barnette was born on the 13<sup>th</sup> day of December 1989 in Norton, VA to her parents Randy and Lisa Lawson. She attended the University of Virginia's College at Wise in her hometown of Wise, VA where she earned her Bachelor of Science degree in Biochemistry and a minor in Business Administration. While completing her undergraduate studies, Brooke completed a fellowship in the Natural Sciences where she worked to isolation and purify calmodulin from *Euglena gracilis* that could then be used for functional studies. She also served as teaching assistant in the general chemistry lab and was a Napoleon Hill Scholar who conducted seminars for area high school students on Napoleon Hill's principles of success. She also worked part time at the Napoleon Hill Foundation. Brooke went on to obtain her master's degree in Life Science Research from Lincoln Memorial University working under the advisement of Dr. Paul L. Wood. Her work focused on determining changes in the lipidome in relation to Alzheimer's Disease. While at LMU, she also worked as an assistant for the Chemistry Department. Prior to relocating to Galveston, TX for her doctoral work Brooke married her loving husband, Josh Barnette. During her time at UTMB, Brooke has been an active department citizen serving as co-chair of the Biological Chemistry Student Organization and chair of the journal club committee. She has sought out several teaching opportunities and played a vital role in the curriculum development and teaching of the Molecular Mechanisms of Disease course for the summer Joint Admission Medical Program (JAMP) students. She has also had the privilege of mentoring three high school students through the Bench Mentorship and was awarded Drs. Giovanni and Maria Grazia Micci Award for Mentoring Excellence for her efforts. Brooke also received the NASA/Texas Space Grant Consortium Fellowship for three consecutive years during the duration of her dissertation work.

## CURRICULUM VITAE

**NAME:** Brooke Lawson Barnette

Date: 07/2020

### PRESENT POSITION AND ADDRESS:

Predoctoral Research Fellow  
University of Texas Medical Branch at Galveston  
Department of Biochemistry and Molecular Biology  
Medical Research Building  
301 University Blvd.  
Galveston, TX 77555-1074  
Email: brlawson@utmb.edu

### BIOGRAPHICAL:

Birthplace: Norton, VA  
Current status: US citizen  
Languages: English

### EDUCATION:

09/2014 to present	<b>Predoctoral Research Fellow</b> Graduate Program Department of Biochemistry and Molecular Biology The University of Texas Medical Branch, Galveston, TX Mentor: Mark R. Emmett
08/2013-12/2014	Master of Science in Life Science Research, Lincoln Memorial University, Harrogate, TN Mentor: Paul L. Wood
08/2008-05/2012	Bachelor of Science in Biochemistry and Minor in Business Administration, University of Virginia's College at Wise, Wise, VA

### PROFESSIONAL AND TEACHING EXPERIENCE:

#### Professional Experience:

09/2014-Present	<b>Predoctoral Research Fellow</b> , Department of Biochemistry and Molecular Biology, University of Texas Medical Branch, Galveston, TX Mentor: Mark Emmett
-----------------	---

Project: An Integrated Omics Approach to Define the Molecular Mechanisms of Low Dose, High-Energy, High Charge (HZE) Irradiation in Liver

08/2013-05/2014	<b>Graduate Assistant</b> , Department of Science, Lincoln Memorial University, Harrogate, TN
12/2007-06/2013	<b>Student Assistant</b> , Napoleon Hill Foundation, Wise, VA
08/2009-12/2009	<b>Lab Assistant</b> , Department of Natural Science, UVA-Wise, Wise, VA

**Teaching Experience:**

08/2019-10/2019	<b>Adjunct Faculty</b> , Biology 1011, UVA-Wise, Wise, VA
05/2019-06/2019	<b>PBL Facilitator/Curriculum Developer</b> , Molecular Mechanisms of Disease-summer Joint Admission Medical Program (JAMP), UTMB, Galveston, TX
05/2018-06/2018	<b>PBL Facilitator/Curriculum Developer</b> , Molecular Mechanisms of Disease-summer Joint Admission Medical Program (JAMP), UTMB, Galveston, TX
05/2017-06/2017	<b>PBL Facilitator/Curriculum Developer</b> , Molecular Mechanisms of Disease-summer Joint Admission Medical Program (JAMP), UTMB, Galveston, TX
01/2017-04/2017	<b>Lab Facilitator</b> , BBSC 6222 Biostatistics, UTMB, Galveston, TX
3/28/2017	<b>Guest Lecturer</b> , BBSC 6222 Biostatistics, UTMB, Galveston, TX
09/2016-12/2016	<b>Small Group Facilitator</b> , BBSC 6401 Biochemistry, UTMB, Galveston, TX

**Training and Supervision of Undergraduate, Graduate and Medical Students**

09/2016-05/2017	Daniil Weaver, Ball High School (Bench Mentorship Program)
09/2017-05/2018	Rianna Larios, Ball High School (Bench Mentorship Program)
09/2017-05/2019	Alexandra Tan, Ball High School (Bench Mentorship Program)

**Trainees Awards Pertaining to Project**

Alexandra Tan-1<sup>st</sup> place in Earth and Space Category and 3<sup>rd</sup> place overall in County Science Fair; Grand Award for Physical Sciences, 1st place Earth and Space Senior Division, Jacobs Science Explorer Award by NASA, The Aspire Award Society of Women Engineers, Excellence Award from the State of Texas Chapter- Health Physics Society, and Best Radiation or Radiation-Related Project in Regional Science Fair; State of Texas Chapter-Health Physics Society Science and Engineering Fair Excellence Award for Best Radiation or Radiation-Related Project State (TX) Science Fair; 2019 Intel International Science and Engineering Fair Second Place Award on behalf of NASA

Alexandra Tan-1<sup>st</sup> place 2019 Research & Design “Bench” Tutorials Year-End Symposium

**GRANT SUPPORT:**

09/2018-05/2019	NASA/Texas Space Grant Consortium Fellowship
09/2017-05/2018	NASA/Texas Space Grant Consortium Fellowship

09/2016-05/2017	NASA/Texas Space Grant Consortium Fellowship
05/2011-01/2012	UVA-Wise Fellowship in the Natural Sciences

## **MEMBERSHIPS IN SCIENTIFIC SOCIETIES & ORGANIZATIONS:**

### ***National:***

07/2017-present	Member, Sigma Alpha Pi (National Society of Leadership & Success)
05/2015-12/2018	Member, American Society of Mass Spectrometry (ASMS)
09/2010-present	Member, Sigma Zeta (Math & Science Honor Society)
04/2011-present	Member, Omicron Delta (Leadership Honor Society)

### ***Local:***

03/2020-present	Member, UTMB Graduate School of Biomedical Sciences Associates
09/2014-present	Member, Biological Chemistry Student Organization
09/2009-05/2012	Napoleon Hill Scholar

### ***Leadership:***

07/2017-present	Graduate Student Organization Board of Ambassadors
07/2016-07/2017	Co-Chair, Biological Chemistry Student Organization
01/2016-08/2018	Chair of BMB Journal Club Committee

## **HONORS AND AWARDS:**

2019	GSBS Associates Travel Award
2019	Bench Tutorials: Scientific Research & Design Mentorship Award, UTMB
2018	Drs. Giovanni and Maria Grazia Micci Award for Mentoring Excellence, UTMB
2018	Irma Mendoza Graduate Student Award, UTMB
2018	Travel stipend, ASMS
2017	Katherina Siebert Award for Excellence in Oncologic Research, UTMB
2017	BCSO Award, UTMB
2017	Travel stipend, ASMS
2015	Shirley Patricia Parker Scholarship, UTMB
2012	Who's Who Award, UVA-Wise
2019-2012	Coeburn Medical Center Scholarship, UVA-Wise
2009-2012	C. Paul and Ida Banner Fugate Memorial Scholarship, UVA-Wise
2009-2012	Martha Ann Roberts Holyfield & James Holyfield Scholarship, UVA-Wise
2011-2012	Lettie P. Whitehead Foundation Medical, UVA-Wise
2008-2012	Slemp Foundation Scholarship, UVA-Wise

## COMMUNITY SERVICE AND ACTIVITIES:

12/2019	Holiday Toy Drive, UTMB
11/2019	Children's Fall Carnival Volunteer
09/2019	UVA-Wise Girl's Day in STEM-H
03/2019	Convoy of Hope Community Event-Texas City
12/2018	Holiday Toy Drive, UTMB
12/2017	Holiday Toy Drive, UTMB
10/2017	Walk to End Alzheimer's Participant
10/2017	Children's Fall Carnival Volunteer
03/2017	United to Serve Volunteer
03/2017	Society for Neuroscience Brain Fair Volunteer
12/2016	Holiday Toy Drive, UTMB
10/2016	Children's Fall Carnival Volunteer & Booth Organizer
10/2016	Walk to End Alzheimer's Participant/Team Leader
09/2016	Organizer & Volunteer at Ice Cream Social for Ronald McDonald House
12/2015	Holiday Toy Drive, UTMB
10/2015	Children's Fall Carnival Volunteer
12/2014	Holiday Toy Drive, UTMB
10/2014	Walk to End Alzheimer's Participant
10/2014	Children's Fall Carnival Volunteer
03/2014	United to Serve Volunteer
11/2013	Feeding America Food Distribution Volunteer
06/2013	Brown Bag Lunch Project Volunteer
06/2012	Brown Bag Lunch Project Volunteer
06/2011	Brown Bag Lunch Project Volunteer
07/2012	Relay for Life Participant
07/2010	Relay for Life Participant
10/2010	Jazzin' for a Cure Participant
04/2009	Autism Walk-A-Thon Participant

## BIBLIOGRAPHY:

### Publications

Wood PL, **Barnette B**, Kaye JA, Quinn JF, Woltjer RL. Non-targeted lipidomics of CSF and frontal cortex grey and white matter in control, mild cognitive impairment, and Alzheimer's disease subjects. *Acta Neuropsychiatrica*, **2015**, DOI: 10.1017/neu.2015.18.

Anna M. Nia, Tianlong Chen, **Brooke L. Barnette**, Kamil Khanipov, Robert L. Ullrich, Suresh K. Bhavnani, Mark R. Emmett. Efficient Identification of Multiple Pathways: RNA-Seq Analysis of Livers from <sup>56</sup>Fe Ion Irradiated Mice. *BMC Bioinformatics*, 2020, 21:118-129. DOI: 10.1186/s12859-020-3446-5.

Anna M. Nia, Kamil Khanipov, **Brooke L. Barnette**, , Robert L. Ullrich, George Golovko, Mark R. Emmett. Comparative RNA-Seq transcriptome analyses reveal

dynamic time-dependent effects of  $^{56}\text{Fe}$ ,  $^{16}\text{O}$ , and  $^{28}\text{Si}$  irradiation on the induction of murine hepatocellular carcinoma. *BMC Genomics*, 2020, 21:453. Published on-line 7-3-20. DOI:10.1186/s12864-020-06869-4.

### **Poster Presentations**

**Barnette, B.**, Strain, S., Lichti, C., Yu, Y., Ullrich, R., and Emmett, M. Induction of Hepatocellular Carcinoma By Space Radiation: A Systems Biology Study of Causative Mechanisms, 27<sup>th</sup> Annual NASA Human Research Program, Investigators' Workshop Integrated Pathways to Mars, February 9, 2016, Galveston, TX.

**Barnette, B.**, Strain, S., Lichti, C., Yu, Y., Ullrich, R., and Emmett, M. The application of lipidomics to the study of Hepatocellular Carcinoma (HCC) Induced by low dose, high-energy, high charge ions (HZE), 64<sup>th</sup> ASMS Conference on Mass Spectrometry, June 8, 2016. San Antonio, TX.

**Barnette, B.**, Strain, S., Lichti, C., Yu, Y., Ullrich, R., and Emmett, M. An integrated omics approach to the study of Hepatocellular Carcinoma (HCC) induced by low dose, high-energy, high charge ions (HZE), 28<sup>th</sup> Annual NASA Human Research Program, Investigators' Workshop Integrated Pathways to Mars, January 24, 2017, Galveston, TX.

**Barnette, B.**, Strain, S., Lichti, C., Yu, Y., Ullrich, R., and Emmett, M. Systems Biology Approach to Define the Molecular Mechanisms of Galactic Cosmic Ray Induced Hepatocellular Carcinoma, 65<sup>th</sup> ASMS Conference on Mass Spectrometry, June 5, 2017. Indianapolis, Indiana.

Folorunso, O., **Barnette, B.**, and Barral, J. Flipped learning to enhance pre-medical education amongst underrepresented undergraduates, Texas Academies Collaborative for the Health Professions-Southeast Educational (TEACH-S) Symposium, May 11, 2018.

**Barnette, B.**, Nia, A., Strain, S., Lichti, C., Yu, Y., Ullrich, R., and Emmett, M. An Integrated Omics Approach to Define the Molecular Mechanisms of Galactic Cosmic Ray Induced Hepatocellular Carcinoma, 66<sup>th</sup> ASMS Conference on Mass Spectrometry, June 6, 2018. San Diego, California.

**Barnette, B.**, Nia, A., Strain, S., Lichti, C., Yu, Y., Ullrich, R., and Emmett, M. An Integrated Omics Approach to Define the Molecular Mechanisms Induced by Low Dose, High Energy, High Charge Ions (HZE) in Relation to Hepatocellular Carcinoma, 30<sup>th</sup> Annual NASA Human Research Program, Investigators' Workshop Human Exploration and Discovery: the Moon, Mars and Beyond! January 24, 2019. Galveston, Texas.

**Barnette, B.**, Yu, Y., Ullrich, R., and Emmett, M. Mitochondrial Effects in Liver of C57 Mice by Low Dose, High-Energy, High Charge (HZE) Irradiation. 2020 NASA Human Research Program Investigators' Workshop. January 28, 2020. Galveston, Texas.

Yu, Y., **Barnette, B.**, Watson, Z., Ullrich, R., Weil, M., and Emmett, M. Lipid Profiling of Liver and Serum from C3H and Balb/c mice irradiated with  $^{28}\text{Si}$ . 2020 NASA Human Research Program Investigators' Workshop. January 28, 2020. Galveston, Texas. (not presenter)

Nia, A., Chen, T., **Barnette, B.**, Khanipov, K., Ullrich, R., Bhavnani, S. and Emmett, M. Application of Modularity Maximization Algorithm for RNA-Seq Analysis of Livers from  $^{56}\text{Fe}$  Ion Irradiated Mice. 2020 NASA Human Research Program Investigators' Workshop. January 28, 2020. Galveston, Texas. (not presenter)

### **Oral Presentations**

**Barnette, B.**, Nia, A., Strain, S., Lichti, C., Yu, Y., Ullrich, R., and Emmett, M. An Integrated Omics Approach to Define the Molecular Mechanisms of Hepatocellular Carcinoma (HCC) Induced by Low Dose, High-Energy, High Charge Ions (HZE), 29<sup>th</sup> Annual NASA Human Research Program, Investigators' Workshop The Gateway to Mars, January 22, 2018, Galveston, TX.



Permanent address: 6212 Stephens Rd., Wise, VA 24293

This dissertation was typed by Brooke L. Barnette.